AUMENTANDO O DESEMPENHO DO ENLACE DIRETO DE REDES UMTS FDD ATRAVÉS DE CONCEITOS AVANÇADOS DE ANTENAS
– UMA ANÁLISE SISTÊMICA –

Luis Guilherme Uzeda Garcia

DISSERTAÇÃO SUBMETIDA AO CORPO DOCENTE DA COORDENAÇÃO DOS PROGRAMAS DE PÓS-GRADUAÇÃO DE ENGENHARIA DA UNIVERSIDADE FEDERAL DO RIO DE JANEIRO COMO PARTE DOS REQUISITOS NECESSÁRIOS PARA A OBTENÇÃO DO GRAU DE MESTRE EM CIÊNCIAS EM ENGENHARIA ELÉTRICA.

Aprovada por:

Prof. Marcello Luiz Rodrigues de Campos, Ph.D.

Prof. Luiz Wagner Pereira Biscainho, D.Sc.

Prof. Paulo Sergio Ramirez Diniz, Ph.D.

Prof. José Antonio Apolinário Jr., D.Sc., IME.

RIO DE JANEIRO, RJ - BRASIL

FEVEREIRO DE 2006

GARCIA, LUIS GUILHERME UZEDA

Aumentando O Desempenho Do Enlace Direto De Redes UMTS FDD Através De Conceitos Avançados De Antenas -- Uma Análise Sistêmica -- [Rio de Janeiro] 2006

XVI, 239 p. 29,7 cm (COPPE/UFRJ, M.Sc., Engenharia Elétrica, 2006)

Dissertação - Universidade Federal do Rio de Janeiro, COPPE

1.WCDMA 2.*Smart-Antennas*

3.Diversidade 4.Simulações

I.COPPE/UFRJ II.Título (série)

Agradecimentos

Muitas pessoas ajudaram-me a concluir esta caminhada. Primeiramente, gostaria de agradecer a meus orientadores na Dinamarca, Dr. Preben E. Mogensen (Universidade de Aalborg) e Dr. Klaus I. Pedersen (*Nokia Networks*), por compartilharem seus vastos conhecimentos e pelas inúmeras sugestões durante esta pesquisa. Sem o auxílio técnico e financeiro da Nokia, esta tese de mestrado não existiria. Assim, gostaria de expressar minha gratidão à Nokia por conceder-me esta oportunidade extraordinária de realizar minha pesquisa de mestrado e estar simultaneamente em contato com o dinâmico mundo da indústria.

Um agradecimento especial ao amigo Mangesh A. Ingale pelas inúmeras discussões frutíferas e pela excelente atmosfera de trabalho. Sou muito grato aos demais colegas na Nokia, em especial Per-Henrik e Allan Rasmussen, por seu incrível apoio com o simulador sistêmico.

Agradeço também ao Prof. Marcello Luiz R. de Campos, meu orientador de tese na COPPE, e ao Prof. Luiz Wagner P. Biscainho por sua amizade e orientação na fase inicial do mestrado. Trabalhar com ambos foi um prazer e uma honra. Não poderia deixar de agradecer à CAPES por financiar parte de meus estudos.

Meus agradecimentos estariam incompletos caso não me lembrasse dos meus amigos do Laboratório de Processamento de Sinais (LPS) e daqueles que fiz em Aalborg. Especial gratidão à Sra. Lisbeth S. Larsen por facilitar sobremaneira minha vida na Dinamarca, sempre tendo uma solução para todo tipo de problema prático, e ao amigo Tadeu F. Nagashima, por me manter informado e realizar a minha inscrição nas disciplinas no Brasil.

Quero aqui expressar minha gratidão sincera à Sandra, minha noiva. Sem nossas conversas diárias através da Internet, tudo teria sido muito mais difícil.

Por fim, mas não menos importante, agradeço a minha família inteira pelo fantástico apoio durante os últimos 26 anos. Devo tudo o que sou a sua orientação, apoio e amor incondicional.

Resumo da Dissertação apresentada à COPPE/UFRJ como parte dos requisitos necessários para a obtenção do grau de Mestre em Ciências (M.Sc.)

AUMENTANDO O DESEMPENHO DO ENLACE DIRETO DE REDES UMTS FDD ATRAVÉS DE CONCEITOS AVANÇADOS DE ANTENAS – UMA ANÁLISE SISTÊMICA –

Luis Guilherme Uzeda Garcia

Fevereiro/2006

Orientadores: Marcello Luiz Rodrigues de Campos
Preben E. Mogensen
Klaus I. Pedersen

Programa: Engenharia Elétrica

O crescimento previsto dos sistemas de comunicação sem-fio tem estimulado esforços de pesquisa visando a aumentar a capacidade desses sistemas. Diferentemente do mundo das comunicações "com fio", sistemas de rádio simplesmente não podem criar mais largura de banda através da adição de novos recursos físicos (cabo, fibras, etc), pois o espectro disponível é extremamente escasso e caro.

Esta tese é o resultado de um ano de trabalho de pesquisa executado no Departamento da Tecnologia de Comunicação na Universidade de Aalborg em cooperação com a *Nokia Networks R&D*, Aalborg.

O autor estuda, apresenta e avalia, por meio de extensas simulações dinâmicas, vários métodos para aumentar a capacidade sistêmica do padrão de 3^a geração para comunicações móveis conhecido como *Universal Terrestrial Radio Access Frequency Division Duplex (UTRA FDD)*. O enfoque está no uso de arranjos de antenas (AA), mais especificamente, sistemas de chaveamento de feixes, terminais com duas cadeias de recepção, e a combinação de ambas as técnicas, com o intuito de se aumentar o desempenho do enlace direto. A análise engloba a transferência de dados tanto por comutação de circuitos quanto por comutação de pacotes.

Abstract of Dissertation presented to COPPE/UFRJ as a partial fulfillment of the requirements for the degree of Master of Science (M.Sc.)

PERFORMANCE ENHANCING ANTENNA SOLUTIONS FOR UMTS FDD DOWNLINK
– A SYSTEM LEVEL ANALYSIS –

Luis Guilherme Uzeda Garcia

February/2006

Advisors: Marcello Luiz Rodrigues de Campos
Preben E. Mogensen
Klaus I. Pedersen

Department: Electrical Engineering

The anticipated growth of wireless communication systems has fueled research efforts investigating methods to increase system capacity. In contrast to the "wired" communication world, wireless systems can not simply create more bandwidth by adding new physical resources (cables, fibers, etc), for the radio spectrum available for wireless services is extremely scarce.

This thesis report is the result of an one-year long research project carried out at the Department of Communication Technology at Aalborg University in close co-operation with Nokia Networks R&D, Aalborg.

The author studies, presents and assesses by means of extensive *dynamic system level simulations* various methods for improving the system level capacity of the 3^{rd} generation standard for mobile communications denoted Universal Terrestrial Radio Access Frequency Division Duplex (UTRA FDD). The focus is on the use of antenna arrays (AA) techniques, more specifically, switched beam systems, dual antenna receivers at the terminals, and both features combined, in order to enhance the performance in the downlink direction The analysis encompasses both circuit- and packet-switched traffic.

Sumário

Lista de Figuras

Lista de Tabelas

Capítulo 1

Introdução

Se o tempo fosse um recurso infinito, as inúmeras questões relacionadas ao aumento de desempenho das tecnologias de sistemas celulares poderiam ser abordadas. Uma vez que este não é o caso, é imperativo reduzir e definir precisamente o escopo da pesquisa. É exatamente isto o que este capítulo inicial se propõe a fazer. Inicialmente, o problema que motivou esta pesquisa é apresentado, seguido por uma curta elucidação sobre por que certos tópicos foram investigados nesta tese de mestrado, enquanto outros foram omitidos. Uma breve visão geral do sistema UMTS é apresentada, uma vez que este é o objeto de estudo deste projeto. Posteriormente, os objetivos deste trabalho são apresentados. Finalmente, um resumo daquilo que os leitores encontrarão no resto do relatório encerra o capítulo.

1.1 Motivação e Definição do Problema

Pode-se dizer que a meta final da comunicação móvel pessoal é permitir que as pessoas, e por que não máquinas, também, troquem qualquer forma de informação de forma confiável, o mais rápidamente possível, e sem qualquer restrição à mobilidade. Sistemas de terceira geração como o *Universal Mobile Telecommunication System (UMTS)* foram projetados de forma a dar mais um passo em direção a um sistema de comunicação ubíquo.

A terceira geração (3G) sistemas celulares foi cuidadosamente talhada para suportar uma grande variedade de taxas de bits e serviços, ao passo que os atuais sistemas de segunda geração foram projetados principalmente para a transmissão de voz e serviços com baixas taxas de dados. A introdução de serviços que requeiram altas taxas de transferência reforça a importância de soluções que ampliem a capacidade dos novos sistemas.

Diferentemente do mundo das comunicações "com fio", sistemas móveis simplesmente não podem criar largura de banda indefinidamente através da adição de novos recursos físicos (cabo, fibras, etc), pois espectro de freqüências disponível é escasso e caro.

Embora ainda não haja muitos assinantes utilizando serviços 3G, acredita-se que o número de usuários e a demanda por serviços digitais móveis de alta qualidade aumentarão rapidamente em todo o mundo. Com esse crescimento, haverá a necessidade de se estender a capacidade das redes UMTS inicialmente instaladas.

Conseqüentemente, o engenheiro de sistemas de comunicações móveis é posto diante do conflito entre a escassez do espectro eletro-magnético e a crescente demanda por serviços que exigem cada vez mais largura de banda. A fim de se resolver esse dilema, uma miríade de tecnologias diferentes foi projetada. Nesta tese, o ganho de capacidade sistêmica fornecido por antenas inteligentes [1] é investigado.

1.2 Por que Antenas Inteligentes?

Em áreas densamente povoadas, os sistemas móveis são normalmente *limitados por interferência*. A interferência co-canal (CCI, da expressão inglesa *co-channel interference*) é o maior fator restritivo à capacidade de sistemas de co-

[1] A expressão Antenas Inteligentes (AI), da forma inglesa *Smart-Antennas*, é usada neste capítulo como um "guarda-chuva", que abrange diferentes técnicas de AA. O Capítulo 2 abre este "guarda-chuva", abordando cada técnica separadamente.

municação sem fios. Ela resulta da reutilização dos recursos (p. ex., espectro) por um número de usuários, tornando os sinais transmitidos por (para) outros usuários na principal fonte de interferência no sistema.

Evidencia-se assim, que para aumentar a capacidade de um sistema, deve-se reduzir de alguma forma os níveis de interferência. O modo mais direto de se fazer isso em sistemas celulares é a divisão de células existentes em setores menores (três a seis) à medida que a quantidade de clientes em uma região cresce, tal técnica é conhecida como setorização.

O padrão UMTS inclui estruturas hierárquicas de células, onde os *hotspots*, regiões com muito tráfego, são servidos por micro-células. Caso as células pudessem ser subdivididas infinitamente, dificilmente haveria qualquer estímulo para se projetar interfaces aéreas mais eficientes. Embora em muitas áreas geográficas ainda haja muito potencial para novas subdivisões, células muito pequenas nem sempre são desejáveis, tanto por aspectos econômicos quanto por questões de engenharia. O preço de novas estações-base e de sua conexão à espinha dorsal da rede é também uma consideração importante [1].

Uma alternativa relativamente simples é uso de portadoras extras, ou seja, novas freqüências, mas deve-se ter em mente os altos custos associados a esta solução, devido à falta de espectro disponível mencionada anteriormente.

Há ainda as técnicas de detecção multi-usuário, entretanto, até mesmo os algoritmos sub-ótimos [2] implicam uma enorme complexidade no receptor. Além disso, a própria natureza desses algoritmos reduz significativamente sua aplicabilidade ao enlace direto ou *downlink (DL)*, devido ao fato de a informação a ser utilizada pelos algoritmos muitas vezes não ser fornecida pelo sistema. Contudo, no enlace reverso ou *uplink (UL)*, toda a informação necessária pode ser obtida, o que torna essas técnicas aplicáveis [3].

As Antenas Inteligentes (AI) são vistas como uma das mais promissoras

[2] O algoritmo ótimo foi apresentado por Verdú [2], mas é excessivamente complexo para sistemas reais.

tecnologias para redução da interferência co-canal, possibilitando o aumento da *capacidade* e (ou) *cobertura* das redes UMTS. Elas permitem expandir significativamente a capacidade do sistema, ao explorarem o domínio espacial do canal de rádio móvel, através do uso de um arranjo de antenas e técnicas apropriadas de processamento de sinais na estação-base. A cobertura pode ser ampliada devido ao ganho elevado que tais antenas apresentam em determinadas direções.

Não obstante, nem tudo é perfeito. Devemos ter em mente que não há nenhuma solução definitiva para todos os ambientes de rádio e que a solução ótima depende do ambiente e das características do canal. O leitor interessado encontrará uma caracterização mais elaborada dos diversos tipos de canais no Apêndice C. Além disso, a utilização de AI também implica alguma complexidade extra no sistema (nada é grátis), contudo, espera-se que esta complexidade adicional seja menos cara do que a instalação de novos sítios ou a aquisição de faixas de freqüência extras.

1.3 Por que o Enlace Direto?

Nos primeiros dias dos sistemas CDMA, acreditava-se que o enlace reverso seria o gargalo na capacidade sistêmica [4]. Contudo, a experiência provou que esta hipótese não estava correta. A razão disso é o fato de que a potência total transmitida pela estação-base é compartilhada por todos os usuários do enlace direto, ou seja, quanto maior o número de usuários, menor é a potência destinada a cada um. Ademais, espera-se que no futuro próximo o tráfego de dados nas redes será altamente assimétrico devido à natureza dos serviços 3G oferecidos, por exemplo, *streaming* de áudio, os quais demandam transferências de grandes quantidades de dados no DL, e poucas requisições de serviço no UL, fazendo com que a situação se agrave.

1.4 UMTS – Uma Visão Geral

Entre os sistemas de terceira geração disponíveis, este trabalho se restringe ao WCDMA que foi padronizado pelo 3GPP (3^{rd} *Generation Partnership Project* [5]), um projeto conjunto dos corpos de padronização da Europa, do Japão, da Coréia, dos EUA e da China. O sistema WCDMA padronizado pelo 3GPP é conhecido como *Universal Terrestrial Radio Access (UTRA)*, e possui duas modalidades: *Frequency Division Duplex (FDD)* e *Time Division Duplex (TDD)*. Nesta tese de mestrado, apenas o sistema UTRA FDD é considerado. Por questão de simplicidade, no restante deste trabalho, esse sistema será denotado por *Universal Mobile Telecommunication System (UMTS)*.

O padrão UMTS é composto por centenas de documentos. Um conjunto completo de documentos é gerado a cada etapa da evolução *("Release")* do padrão. A primeira versão do UMTS foi o *Release'* 99, seguido pelos *Releases'* 4 e 5. Atualmente a funcionalidade dos *Releases'* 6 e 7 está em discussão dentro do 3GPP. Mais detalhes são dados no Apêndice B, e a análise completa do UMTS encontra-se em [6].

Esta seção é uma descrição curta da arquitetura básica e das características gerais do UMTS. Uma vez que uma enchente de informações deve ser evitada, somente os aspectos essenciais serão abordados, de modo que o leitor adquira os conhecimentos necessários à compreensão dos problemas específicos do sistema que surgirão ao longo desta tese. Depreende-se daí que o enlace direto receberá atenção especial.

Ao longo desta e das próximas seções, preferencialmente as abreviações inglesas serão utilizadas para referência aos elementos de rede e canais de tráfego, bem como aos algoritmos de gerenciamento, uma vez que somente essa forma é encontrada nas especificações [7]. Espera-se, assim, evidenciar de forma direta e clara a que elemento da norma a passagem de texto diz respeito.

1.4.1 Arquitetura do Sistema e Gerenciamento dos Recursos de Rádio

A arquitetura do sistema UMTS está esboçada na Figura 1.1, que apresenta os elementos lógicos de rede, os nomes das diferentes interfaces e a maneira na qual os algoritmos de gerenciamento dos recursos de rádio (RRM, do termo original em inglês *Radio Resource Management*) estão distribuídos entre os elementos de rede. Funcionalmente, o sistema pode ser dividido em 3 partes: o Núcleo de Rede (CN, do original *Core Network*), a Rede Terrestre de Acesso de Rádio UMTS (UTRAN, do original em inglês *UMTS Terrestrial Radio Access Network*) e o Equipamento do Usuário (UE, do termo original em inglês *User Equipment*), como o celular é conhecido na terminologia UMTS.

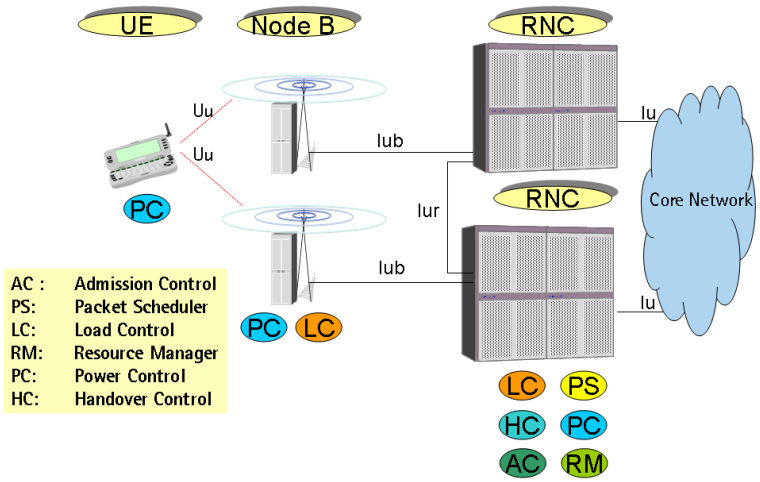

Figura 1.1: Arquitetura do sistema UMTS

O núcleo de rede do Release' 99 do UMTS é baseado no núcleo da rede GSM [8]. Esta é parte responsável pela comutação e encaminhamento das chamadas e conexões de dados às redes externas

A UTRAN é composta por um ou mais *Radio Network Controllers* (RNC) conectados a vários Nós-B. Na terminologia UMTS, o termo Nó-B (*Node-B*) refere-se ao que é normalmente chamado de estação-base. A sua tarefa principal é converter os dados recebidos do RNC para a camada física. Além disso, o Nó-B faz

medições necessárias para o gerenciamento dos recursos de rádio, posteriormente informadas ao RNC. O Nó-B é também responsável pelo controle rápido de potência do enlace reverso.

O RNC é o elemento de rede que equivale logicamente à BSC das redes GSM [8]. Quando um UE está ligado à rede UMTS, sua identidade é conhecida pelo RNC. Ademais, o RNC é a parte da UTRAN que interage com o núcleo de rede, sendo responsável, também, por grande parte dos algoritmos de RRM.

Os algoritmos de RRM são responsáveis pela utilização eficiente da interface aérea. Os principais objetivos destes são:

- Garantir a cobertura planejada.
- Assegurar a qualidade de serviço (QoS, *Quality of Service*) solicitada.
- Assegurar a capacidade planejada.

Como dito anteriormente, a localização típica dos algoritmos pode ser vista na Figura 1.1. Mais alguns detalhes sobre os princípios de funcionamento dos algoritmos de RRM são dados a seguir:

Controle de Carga: A missão principal do controle de carga (LC, do original *Load Control*) é garantir a estabilidade de sistema, assegurando-se de que ele não esteja sobrecarregado. Em um sistema corretamente planejado, sobrecargas serão raras, mas caso elas realmente ocorram, é tarefa do LC tomar as medidas apropriadas para fazer com que o sistema retorne a sua carga máxima planejada.

Gerente de Recursos: O gerente de recursos (RM, do termo *Resource Manager*) é a entidade que controla a alocação dos códigos de espalhamento (ver a Seção 1.4.2) entre os UEs de um modo ótimo.

Controle de Potência: O controle de potência (PC, da forma inglesa *Power Control*) mantém a qualidade do enlace de rádio de uma conexão através do ajuste das potências de transmissão tanto do enlace reverso quanto direto. A idéia é satisfazer os requisitos de qualidade estabelecidos para aquela conexão, utilizando

para isso potências mínimas de transmissão a fim de gerar menos interferência e aumentar a capacidade da rede de acesso de rádio. O PC também é fundamental para superar o conhecido problema *near-far* do enlace reverso das redes CDMA, isto é, caso os terminais não tenham suas potências de transmissão controladas, a estação-base receberá um sinal com muita potência daqueles celulares mais próximos dela, encobrindo os sinais mais fracos de terminais distantes.

Controle de *Handover*: O controle de *handover* (HC, abreviação de *Handover Control*) é necessário para permitir a mobilidade dos usuários dentro da rede, permitindo transições entre as células. O HC decide o conjunto de Nós-B aos quais o UE deve estar conectado. Tal decisão pode ser baseada em razões de cobertura e/ou carga, e é normalmente auxiliada por medições de qualidade do canal piloto conduzidas no terminal. No UMTS, um UE pode estar conectado a vários Nós-B ao mesmo tempo via *soft-handover* (SHO), isto é, a conexão do terminal a uma célula não precisa ser desfeita para que ele possa estabelecer uma conexão com outra célula. O SHO propicia ganhos de macro e micro- diversidades e garantias de uma transição suave entre células. O conceito de diversidade é explicado no Capítulo 2.

Controle de Admissão: O controle de admissão (AC, do termo *Admission Control*) é responsável por controlar a carga do sistema para que a capacidade disponível possa ser explorada sem comprometer a estabilidade do mesmo. Antes da admissão de um novo UE na rede ou modificação da conexão de um UE já admitido, o AC certifica-se se essas ações não sacrificarão a área de cobertura planejada ou a qualidade das conexões existentes. Quando um novo UE é admitido ou uma conexão existente é modificada, o AC também se encarrega de estabelecer os parâmetros da nova conexão, por exemplo, a potência inicial de transmissão do enlace direto.

Agendador de Pacotes: O agendador de pacotes (PS, do inglês *Packet Scheduler*) é o algoritmo encarregado de coordenar a alocação de recursos para o tráfego em tempo não-real (NRT), por exemplo, a leitura de correio eletrônico. As exigências de qualidade de serviço (QoS) dos diferentes UEs devem ser atendidas

fazendo um uso eficiente de recursos escassos. O grande objetivo do PS é utilizar eficientemente toda a capacidade restante da célula para as conexões NRT, mantendo o nível de interferência dentro dos valores planejados para que as conexões em tempo-real (RT), voz, por exemplo, não sejam afetadas [6].

Percebe-se que o assunto RRM é muito extenso, tendo sido (e ainda sendo) amplamente estudado. Os leitores podem encontrar uma discussão mais abrangente no Apêndice B.5 e muito material interessante em [6, 7, 9, 10, 11, 12].

1.4.2 Camada Física e Interface Aérea

O UMTS emprega o *Wide-band Code Division Multiple Access* (WCDMA) como técnica de acesso múltiplo. O WCDMA é uma técnica onde a informação a ser transmitida é "espalhada" através da multiplicação desta por uma seqüência pseudo-aleatória de bits (os *chips*), denominada código de espalhamento (*spreading code*), que ocupa uma banda freqüencial muito mais larga do que a mínima necessária para se transmitir a mesma informação.

A uma taxa de $3,84.10^6$ *chips* por segundo, a portadora WCDMA ocupa uma banda de 5 MHz. Bandas de freqüência separadas são usadas para os enlaces direto e reverso. A grande largura de banda (uma portadora GSM ocupa apenas 200 kHz), daí o nome *Wide-band* CDMA, permite o suporte a altas taxas de dados, e uma maior exploração da diversidade multi-percurso. A fim de possibilitar uma grande variabilidade das taxas de bits, são utilizados fatores de espalhamento [3] variáveis e conexões multi-código. Os princípios básicos de CDMA são descritos em [6, 13, 14].

A técnica CDMA permite que a mesma faixa de freqüências seja compartilhada simultaneamente por vários usuários. Como? O sinal de cada usuário é identificado unicamente por um código de espalhamento ortogonal a todos os demais códigos, caso haja uma perfeita sincronia. No enlace direto, por exemplo, os

[3] O fator de espalhamento, ou ganho de processamento, é definido como a razão entre a taxa dos *chips* e taxa de dados.

sinais transmitidos na mesma célula para diferentes usuários são diferenciados por seus códigos de espalhamento (também conhecidos como códigos de canalização) extraídos de uma árvore de códigos ortogonais com fator de espalhamento variável (OVSF, *Orthogonal Variable Spreading Factor*).

Em um canal de rádio sem dispersão temporal, ou seja, perfeitamente sincronizado, sinais transmitidos com códigos diferentes se mantêm totalmente ortogonais. Não obstante, em um cenário real, devido à propagação por multi-percursos (ver o Apêndice C.3 para detalhes) um terminal normalmente recebe múltiplas cópias do mesmo sinal com atrasos diferentes. Infelizmente, os códigos de canalização possuem propriedades de correlação cruzada relativamente pobres [15]. Em outras palavras, a dispersão temporal (falta de sincronismo) destrói parcialmente a ortogonalidade dos vários canais transmitidos pela estação-base e eles começam a interferir uns com os outros. Nesse caso, a parte não-ortogonal passa a ser vista como ruído pelos demais usuários, sendo somente atenuada pelo ganho de processamento quando o sinal desejado é recuperado no receptor [3]. Em sistemas CDMA, essa interferência é conhecida como *multiple-access interference* (MAI), ou interferência por acesso múltiplo. É importantíssimo ressaltar que, o número de códigos de canalização de uma árvore OVSF é limitado, obrigando a sua reutilização em outras células.

Nesse instante, os códigos de embaralhamento (*scrambling codes*), seqüências semelhantes a um ruído, tornam-se necessários. Eles embaralham (multiplicam) os sinais transmitidos em cada célula. Tais códigos possuem propriedades muito boas de auto-correlação e correlação cruzada [13, 15], permitindo assim a separação de sinais de fontes diferentes. No DL, por exemplo, eles separam os sinais de células distintas.

Segundo as especificações UMTS, somente uma árvore de códigos OVSF pode ser utilizada por código de embaralhamento, o que impõe um limite rígido à capacidade que pode ser alcançada em uma célula com apenas um código de embaralhamento. Obviamente, o sistema não poderá admitir uma nova conexão, mesmo que os níveis de interferência na interface aérea o permitam, caso não haja um

código disponível para essa conexão. Isto é um aspecto crucial que será retomado oportunamente.

1.4.3 Canais UTRA

A interface de rádio UMTS possui canais lógicos, que são mapeados para os canais de transporte, que por sua vez são mapeados nos canais físicos.

No *Release'* 99, há basicamente dois tipos de canais de transporte: o canal dedicado e os canais comuns. Como os nomes sugerem, o primeiro tipo é utilizado por um único usuário, ao passo que o segundo é compartilhado por todos ou por um grupo de usuários em uma célula. Há seis tipos de canais comuns: canal de transmissão (BCH, *Broadcast Channel*), o canal de acesso direto (FACH, *Forward Access Channel*), canal de paginação (PCH, *Paging Channel*), canal de acesso casual (RACH, *Random Access Channel*), canal reverso comum de pacotes (CPCH, UL Common Packet Channel) e canal compartilhado direto (DSCH, *Downlink Shared Channel*).

Há, ainda, alguns canais físicos que não possuem nenhum canal de transporte correspondente, dentre os quais o canal piloto, *Common Pilot Channel* (CPICH). Existem dois tipos de piloto, o primário e o secundário (P-CPICH e S-CPICH). Por enquanto, é suficiente saber que uma de suas funções é auxiliar o terminal a estimar o canal. Mais explicações sobre cada canal e detalhes sobre o mapeamento desses canais para a camada física podem ser encontrados no Apêndice B.4.

O Canal Dedicado (DCH, *Dedicated Channel*) é o único canal de transporte alocado exclusivamente para um UE. O DCH transporta todas as informações provenientes das camadas mais altas destinadas a um usuário. Na camada física, o DCH é mapeado no *Dedicated Physical Channel* (DPCH), o qual é composto por dois outros canais, o *Dedicated Physical Data Channel* (DPDCH), para dados do usuário, e o *Dedicated Physical Control Channel*, para sinalização e outras informações da camada física, por exemplo, um piloto dedicado.

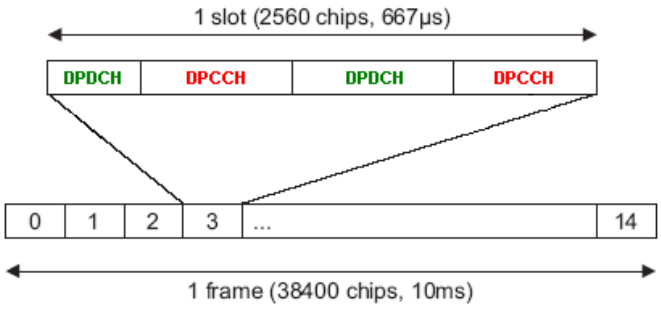

Figura 1.2: Estrutura do DCH no DL.

No enlace direto, os canais DPDCH and DPCCH são multiplexados temporalmente, como ilustrado na Figura 1.2. O esquema de modulação utilizado no enlace direto é o QPSK [13]. O DCH utiliza controle rápido de potência, 1500 comandos por segundo, e permite a adaptação da taxa de dados a cada quadro de rádio, ou seja, a cada 10 ms. Todos os resultados apresentados neste trabalho referem-se ao DCH.

1.5 Escopo e Objetivos

Durante as duas décadas passadas, foram publicados muitos trabalhos sobre o desenvolvimento de algoritmos em banda base para AA e estudos comparativos do desempenho de enlace de várias topologias de AA [16, 17]. Contudo, pouca atenção foi dada aos aspectos de nível de rede em sistemas WCDMA. Por exemplo, quais são as limitações impostas pelo sistema ao ganho de capacidade? Qual o ganho máximo alcançável em redes UMTS empregando AI?

Muitas vezes, simplesmente extrapolar os resultados e conclusões de estudos de nível de enlace não é o bastante, uma vez que há inúmeros mecanismos, como por exemplo, o efeito do agendador de pacotes no desempenho do sistema, que só podem ser totalmente entendidos conduzindo-se uma avaliação sistêmica completa.

Sob esta lógica, este trabalho se propõe a quantificar o ganho de desempenho

sistêmico obtido através da aplicação de antenas inteligentes em redes UMTS. O estudo contempla a investigação dos ganhos de capacidade das seguintes técnicas:

- Utilização de receptores Rake com duas antenas nos terminais para:
  - Diferentes características do canal de rádio móvel
  - Tráfego com taxa de bits fixa usando comutação de circuitos
  - Tráfego com taxa de bits variável usando comutação de pacotes
  - Velocidades baixa (3km/h) e mediana (50km/h) dos terminais
- Conformação de feixes utilizando arranjo de antenas na estação-base para:
  - Diferentes características do canal de rádio móvel
  - Tráfego com taxa de bits fixa usando comutação de circuitos
  - Tráfego com taxa de bits variável usando comutação de pacotes
  - Baixa velocidade (3km/h) dos terminais

As técnicas são estudadas tanto separadamente como combinadas a fim de se compreender sua interação. O estudo é baseado principalmente em resultados obtidos através de simulações de computador, porque a alta complexidade do UTRA FDD torna estudos puramente analíticos inadequados. Além dos resultados de simulações, análises teóricas simples são usadas, sempre que possível, para contextualizar os resultados.

1.6 Sinopse – Organização desta Tese

Esta tese está organizada da seguinte forma: o capítulo atual apresentou a motivação, definiu os objetos e metas da pesquisa, propondo-se a responder as perguntas – "*O que foi feito?*" e "*Por que foi feito*?"

No Capítulo 2, são apresentadas a ferramenta de simulação e suas configurações, juntamente com a modelagem e análise teórica das técnicas utilizadas, visando a responder a pergunta – "*Como foi feito?*"

Ao longo do Capítulo 3, os leitores encontram a resposta para a pergunta – "*Quais foram os resultados?*" A apresentação dos resultados é organizada em três partes. Primeiramente, a capacidade de uma rede UMTS padrão é avaliada. Em segundo lugar, o ganho fornecido por cada uma das soluções estudadas é avaliado separadamente. Finalmente, discutem-se os resultados alcançados quando ambas as técnicas apresentadas no Capítulo 2 são empregadas combinadas.

As conclusões da tese e propostas para trabalhos futuros são discutidas no Capítulo 4. O conteúdo do trabalho original do autor em inglês, do qual esta tese é uma síntese, está incluído nos Apêndices subseqüentes. Cada apêndice corresponde a um capítulo do trabalho original, logo, o Apêndice A corresponde ao Capítulo 1, o Apêndice B ao Capítulo 2 e assim sucessivamente. Os dois últimos Apêndices J e K são os apêndices originais do trabalho em inglês.

Em princípio, os capítulos podem ser lidos de forma independente, contudo, referências cruzadas foram feitas sempre que necessário para um melhor entendimento da discussão. Abreviações são explicadas antes de serem empregadas, não obstante, há uma lista com o significado de todas no final da tese.

Um dos compromissos do autor ao escrever este relatório foi o de fazê-lo tão autocontido quanto possível, mas sem poluir o texto com informações desnecessárias. Espera-se que os leitores refiram-se aos apêndices sempre que desejarem mais informações. As ilustrações apresentadas ao longo deste trabalho foram extraídas do trabalho original, daí o fato de conterem texto em inglês; e foram reproduzidas sempre que necessário, visando a facilitar a leitura e evitar referências excessivas aos apêndices, o que transformaria o texto em uma colcha de retalhos.

Estar familiarizado com conceitos fundamentais sobre sistemas de comunicações e propagação de sinais de rádio é essencial para a plena compreensão deste trabalho. Conhecimentos sobre processamento de sinais digitais e estatística também são de grande valia.

1.7 Publicações

Os seguintes trabalhos derivados desta tese já foram aceitos e serão publicados após o 63º VTC (*Vehicular Technology Conference*) a ser realizado em Maio de 2006 na Austrália.

- *Impact of the Pilot Signal per Beam on the Ideal Number of Beams and Capacity Gain of Switched Beam forming for WCDMA.*
- *Network Performance of Node-B Switched Beamforming and Dual Antenna User Equipment in WCDMA.*

Capítulo 2

Modelagem dos Sistemas e Análise Teórica

Este capítulo, do ponto de vista teórico, pode ser considerado o mais importante desta tese. Ele tenta transmitir aos leitores os conceitos essenciais que o autor teve que aprender a fim de realizar seu trabalho de pesquisa.

O capítulo começa apresentando os princípios básicos por trás dos diferentes tipos de simuladores de rede. A seguir, descreve-se a complexa ferramenta de simulação dinâmica de redes UMTS e a metodologia empregada para obtenção dos resultados apresentados no Capítulo 3.

Durante o curso de sua pesquisa de tese, o autor tentou não perder a "visão global"do problema. Este capítulo tenta refletir essa preocupação: o objetivo é tocar o cerne das questões mais relevantes. A ênfase está na compreensão intuitiva dos princípios. Referências para discussões detalhadas são dadas para aqueles leitores interessados.

2.1 O Simulador

Quando se trata da avaliação de desempenho de sistemas celulares, há uma grande variedade de abordagens, que incluem a análise teórica, simulações estáticas ou dinâmicas e os testes de campo. Cada um delas representa um compromisso entre o nível de detalhe e o custo associado, como mostrado na Tabela 2.1. A diferença entre os diferentes tipos de simulações será esclarecida oportunamente.

Abordagem	**Custo**	**Nível de detalhes**
Modelos teóricos	Baixo	Limitado
Simulações estáticas	Moderado	Bom
Simulações dinâmicas	Alto	Abrangente
Testes de campo	Muito alto	Realidade

Tabela 2.1: Métodos de avaliação do desempenho de redes celulares.

Avaliar analiticamente o desempenho de uma rede UMTS é uma tarefa árdua devido a sua alta complexidade. Por essa razão, recorremos às simulações de computador, as quais nos permitem incluir um alto nível de detalhes, poupando tempo e dinheiro, sobretudo quando comparadas aos testes de campo. Estes têm como principal vantagem a acurácia, simplesmente porque todos os aspectos práticos, inclusive implementações imperfeitas dos equipamentos, são automaticamente levados em conta. Contudo, além dos vultosos custos envolvidos, os resultados tendem a ser específicos àquela configuração de rede e ambiente, variando, portanto, de caso para caso.

Tipicamente, as simulações de redes de rádio podem ser divididas em duas partes: *enlace* e *sistema*. Naturalmente, a abordagem de um simulador único seria ideal, mas a complexidade de tal simulador seria proibitiva. Para o sistema UMTS, simular uma rede inteira com uma resolução temporal de *chips* ($260\,ns$), incluindo todos os detalhes da camada física, os modelos de tráfego e de mobilidade, inúmeros terminais e estações-base, seria absurdamente complexo. Por isso, a separação em simuladores de enlace e simuladores sistêmicos é necessária, *"dividir para conquis-*

tar". Nessa lógica, os simuladores sistêmicos podem ainda ser divididos em dois subgrupos: estáticos e dinâmicos. Diz-se que um simulador é estático quando não há processos variantes no tempo. O resultado é uma média dos resultados de um conjunto suficientemente grande de realizações ou "fotos" do sistema (Método de Monte Carlo). Por indução, uma ferramenta dinâmica inclui explicitamente a dimensão temporal, ou seja os usuários se movem, chamadas têm início e fim, pacotes são agendados, o desvanecimento é modelado, etc.

A ferramenta de simulação usada neste projeto é um simulador UMTS sistêmico e dinâmico sendo desenvolvido pela Nokia e conhecido como WALLU. Familiarizar-se com esta ferramenta realmente complexa, auxiliar no processo de implementação e depuração de código e testar as técnicas implementadas foi uma tarefa complexa e desafiadora. O simulador funciona com uma resolução temporal de $667\mu s$ (duração de um *slot*), a fim de capturar as constantes modificações no cenário de interferência causadas pelo controle de potência rápido. Os sofisticados algoritmos de RRM (ver Seção 1.4.1) – como *handovers*, controle de admissão, etc – também estão presentes. Com isso, logra-se uma modelagem bastante precisa do sistema.

Uma vez que a simulação foi dividida em duas partes, um método para interligar os dois simuladores deve ser definido. O simulador apresentado faz uso de uma tabela chamada de interface de valor real (AVI, *Actual Value Interface*) [18]. Tabelas AVI modelam de forma precisa variações rápidas de potência e representam a probabilidade da taxa de erro de blocos (BLEP, *block error rate probability*) versus a média geométrica da razão sinal-ruído (Eb/N_0) sob certas condições. A média é calculada ao longo da duração de um bloco de transmissão, o qual depende do tipo de dado transmitido. Maiores detalhes são dados no Apêndice E.3.3.

Tendo sido apresentados alguns dos aspectos relacionados a simuladores de redes celulares, vejamos agora como a propagação dos sinais de rádio e as demais técnicas consideradas foram modeladas no simulador.

2.1.1 Perdas de Propagação

Ao transmitirmos um sinal de rádio com uma determinada potência, apenas uma fração desta alcança o receptor porque os sinais transmitidos são atenuados pelas perdas de propagação e pelos fenômenos de sombreamento e desvanecimento causados pela propagação multi-percurso. Naturalmente, o grau de atenuação depende muito de diversos fatores ambientais.

No WALLU, todas as atenuações sofridas por um sinal de rádio transmitido pelo Nó-B até sua recepção no terminal, a uma distância de d km, são modeladas através de um modelo de três componentes. Expressa em decibéis, a perda total é dada por:

$$P(d) = P_L(d) + P_S + P_F, \tag{2.1}$$

onde $P_L(d)$ é a perda de propagação dependente da distância, P_S é uma variável aleatória descrevendo o sombreamento (desvanecimento de larga-escala), e P_F é outra variável aleatória que modela o desvanecimento de pequena-escala). Considera-se que P_S e P_F são descorrelacionadas e independentes da distância (d).

Durante este trabalho, o modelo conhecido como COST 231-Hata [19] foi utilizado para calcular-se as perdas $P_L(d)$, dependentes da separação entre transmissor e receptor.

Obstáculos, como colinas e edifícios, criam efeitos de sombreamento. Para o cálculo de P_S, adotou-se o modelo apresentado em [20]. Assume-se que a variável aleatória descrevendo o sombreamento é gaussiana com média zero e desvio padrão de 8 dB. Observa-se daí, que a variável P_S expressa em escala linear possui uma distribuição normal logarítmica.

O desvanecimento de pequena escala do canal de rádio móvel foi modelado através de perfis de atraso de potência (PDP, *Power Delay Profiles*). Assumiu-se que os multi-percursos estão separados temporalmente por ao menos um período de *chip*, de forma que as pernas do receptor Rake possam resolvê-los. Os perfis de atraso de potência utilizados foram selecionados de acordo com as recomendações *Vehicular-A* e *Pedestrian-A* da *International Telecommunication Union* (ITU) [21].

Considerações mais específicas encontram-se nos Apêndices C.3 e E.3.1.

2.1.2 Espalhamento Angular

Tratando-se de técnicas baseadas em arranjos de antenas, a caracterização convencional do canal de rádio não é suficiente, devemos considerar, também, as propriedades espaciais do canal. O espalhamento angular (AS, abreviação de *angle spread*) é quem nos dá informações sobre tais características.

O espalhamento angular no receptor diz respeito à gama de ângulos de chegada dos multi-percursos, ou seja, de quais direções eles vêm. Do mesmo modo, no transmissor, o AS refere-se à gama de ângulos de partida dos multi-percursos, isto é, para quais direções eles vão. Tal espalhamento faz com que os multi-percursos se combinem de maneira aleatória no receptor em função da posição da antena receptora. Daí, pode-se depreender que a correlação dos sinais recebidos por cada antena, mantendo-se fixa a separação entre as antenas, varia de acordo com o AS do canal. Uma discussão mais elaborada é apresentada no Apêndice C.3.3.

A dispersão angular do canal de rádio observada na estação-base não está modelada explicitamente no WALLU. Tal simplificação tem um efeito que pode ser negligenciado em uma rede convencional, porém o mesmo não é verdade quando incluímos AA no Nó-B e passamos a explorar as características espaciais do canal de rádio. A modelagem utilizada nesse caso é explicada na Seção 2.4.1.

2.2 Referência

Antenas são um meio de se transferir potência de uma linha de transmissão, por exemplo, um cabo coaxial para ondas eletromagnéticas que se propagam pelo ar ou espaço livre. Suas características físicas e complexidade podem variar muito, desde antenas omni-direcionais, muito simples, que irradiam e recebem igualmente bem em todas as direções, em um modelo que se parece com ondulações na água causadas pelo arremesso de uma pedra, até as chamadas Antenas Inteligentes,

passando por antenas diretivas, normalmente utilizadas em conjunto com técnicas de setorização. No entanto, cada assunto a seu tempo, aqui investigaremos um pouco mais sobre a técnica de setorização utilizada na rede UMTS de referência desta tese.

Sistemas setorizados são uma alternativa à redução do raio das células e à subseqüente adição de novas estações-base. Muito comumente, a área de cobertura de uma estação-base é dividida em três setores de 120 graus. Cada setor é iluminado por uma antena direcional. Operacionalmente, cada setor é tratado como uma célula independente. Mantendo-se as demais condições iguais, as antenas direcionais apresentam um ganho superior ao das antenas omni em uma faixa restrita de azimutes. É importante ressaltar que a aplicação de antenas direcionais reduz a quantidade de CCI, uma vez que as células transmitem e recebem sinais de uma forma ligeiramente mais diretiva. Uma desvantagem da setorização é o natural aumento na quantidade de *handovers*, já que ela reduz a área de cobertura das células. Isso deve ser considerado durante o dimensionamento da rede.

2.2.1 Modelagem no Simulador

A rede investigada é composta por 9 estações regularmente espaçadas com uma distância de base a base de $2,8$ km, como mostrado na Figura 2.1(a). A coleta de estatísticas é limitada às 4 células centrais (6, 7, 8 e 14), destacadas em azul. Os reduzidos níveis de interferência nas células exteriores polarizariam os resultados, daí sua exclusão.

Em todos os casos, a densidade de tráfego na rede é uniforme com respeito à área, isto é, não há *hotspots*, células com tráfego muito superior ao de suas vizinhas. Cada estação-base é equipada com 3 antenas diretivas, uma para cada setor. A orientação de cada antena é indicada na Figura 2.1(a) pela flecha preta apontando para fora da respectiva célula. O padrão de irradiação das antenas é apresentado na Figura 2.1(b), tendo sido gerado segundo [22].

Todos os UEs na rede utilizam um receptor Rake padrão. O valor da razão

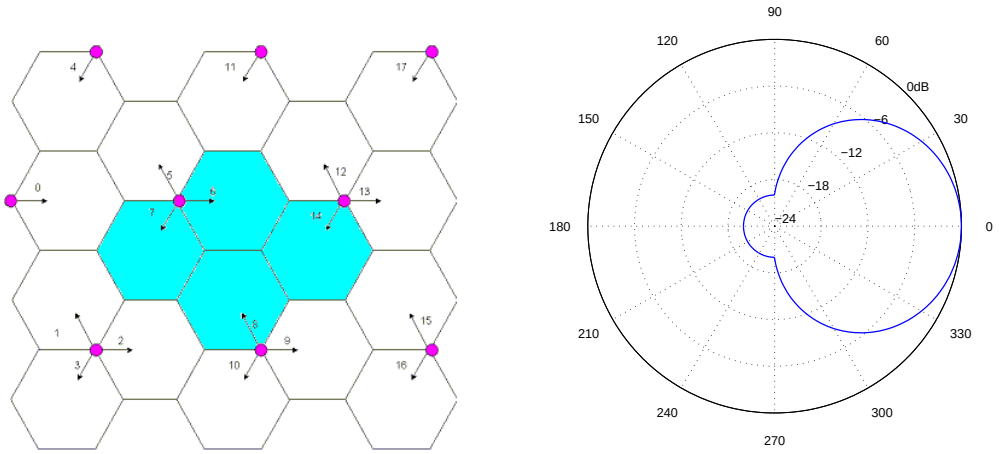

(a) Topologia da rede com as 4 células centrais em azul.

(b) Padrão de irradiação da antena diretiva

Figura 2.1: Organização da simulação.

E_b/N_0 para cada perna do receptor é computado a cada *slot*, intervalo correspondente a $667\mu s$, seguido pela combinação do tipo MRC (*Maximal Ratio Combining*, ver o Apêndice D.4.1) de todas as pernas. O efeito da utilização de códigos de canalização ortogonais esta incluído no cálculo da E_b/N_0 em cada perna, quando a parte sincronizada e, conseqüentemente, ortogonal da interferência intra-celular (P_{own}) é subtraída da interferência total no denominador. A expressão utilizada no cálculo d razão E_b/N_0 para o terminal i a cada *slot* é mostrada abaixo:

$$\frac{E_b}{N_0}(i)_{|slot} = \sum_{l=1}^{R} \frac{P_{\text{RxDPCH}}(s,i).h_{ff}(s,i,l)}{P_{\text{Noise}}^{\text{UE}} + P_{\text{RxTotal}}(i) - P_{\text{own}}(s,i).h_{ff}(s,i,l)} \,.\, G_p \,, \tag{2.2}$$

onde

$$P_{\text{RxDPCH}}(s,i) = P_{\text{TxDPCH}}(s,i).\, h(s,i) \,, \tag{2.3}$$

$$P_{\text{RxTotal}}(i) = \sum_{k=1}^{K} \left(P_{\text{TxTotal}}(k).\, h(k,i).\, \sum_{l=1}^{L} h_{ff}(k,i,l) \right) \,, \tag{2.4}$$

$$P_{\text{TxTotal}}(k) = \sum_{u=1}^{\text{Users}_k} P_{\text{TxDPCH}}(k,u) + P_{\text{P-CPICH}}(k) \,, \tag{2.5}$$

$$P_{\text{own}}(s,i) = P_{\text{TxTotal}}(s).\, h(s,i) \,, \tag{2.6}$$

e o restante da notação é dado na Tabela 2.2. Observe que (2.2) assume que a razão E_b/N_0 resultante na saída do receptor Rake pode ser computada como a soma das razões E_b/N_0 na saída de cada perna do receptor Rake. Isto é uma aproximação que assume que as componentes do ruído e da interferência em cada perna do receptor são totalmente descorrelacionadas, o que não é totalmente verdadeiro, mas uma boa aproximação. Todavia, como explicado no Apêndice E.3.3, o efeito de se ter ruído (e interferência) parcialmente correlacionados nas pernas do receptor está embutido nas tabelas de busca AVI, baseadas em detalhadas simulações de enlace. Contudo, tabelas específicas não foram empregadas para situações de SHO. Nesse caso, assume-se MRC ideal entre os diferentes ramos de SHO, assim, os valores de E_b/N_0 correspondentes a cada ramo são somados, de modo que (2.2) toma a forma:

$$\frac{E_b}{N_0}(i)_{|slot} = \sum_{s\in \mathbf{A}(i)} \sum_{l=1}^{R} \frac{P_{\mathrm{RxDPCH}}(s,i).h_{ff}(s,i,l)}{P_{\mathrm{Noise}}^{\mathrm{UE}} + P_{\mathrm{RxTotal}}(i) - P_{\mathrm{own}}(s,i).h_{ff}(s,i,l)} \cdot G_p \qquad (2.7)$$

Símbolo	**Definição**
G_p	Ganho de processamento da técnica (W)CDMA.
L	O número de componentes multi-percurso.
R	A quantidade de pernas Rake ($R \leq L$).
K	Número total de células na rede.
$\mathbf{A}(i)$	Células no conjunto ativo do terminal i durante SHO.
s	Célula servindo o usuário.
Users_k	Número total de usuários servidos pela *k-ésima* célula.
$h_{pl}(k,i)$	Representa a perda determinística e dependente da distância de propagação da *k-ésima* célula ao *i-ésimo* usuário.
$h_{sf}(k,i)$	Representa o sombreamento da *k-ésima* célula ao *i-ésimo* usuário.

Símbolo	Definição
$h(k,i)$	Ganho do percurso da *k-ésima* célula ao *i-ésimo* usuário. Inclui a perda de propagação determinística h_{pl}, a componente de sombreamento h_{pl}, e os ganhos das antenas de transmissão e recepção, G_{Tx} e G_{Rx} respectivamente.
$h_{ff}(k,i,l)$	Ganho do percurso descrevendo o desvanecimento de pequena escala para o *l-ésimo* percurso do enlace entre a *k-ésima* célula e o *i-ésimo* usuário.
$P_{\mathrm{Noise}}^{\mathrm{UE}}$	Potência do ruído térmico no UE.
$P_{\mathrm{TxTotal}}(k)$	A potência em banda larga total transmitida na *k-ésima* célula.
$P_{\mathrm{RxTotal}}(i)$	A potência em banda larga total recebida pelo *i-ésimo* terminal, incluindo a interferência intra e inter-celular, mas não o ruído térmico. Computada como a soma das potências totais recebidas de todas as células da rede.
$P_{\mathrm{own}}(s,i)$	Interferência intra-celular observada pelo *i-ésimo* UE na *s-ésima* célula de serviço excluindo o desvanecimento.
$P_{\mathrm{TxDPCH}}(k,u)$	A potência transmitida no canal DPCH para o *u-ésimo* usuário na *k-ésima* célula.
$P_{\mathrm{RxDPCH}}(s,i)$	Descreve a potência recebida no canal DPCH o *i-ésimo* usuário na *s-ésima* célula excluindo o desvanecimento.
$P_{\mathrm{P-CPICH}}(k)$	A potência alocada ao canal piloto primário da *k-ésima* célula.

Tabela 2.2: Notação para o cálculo da razão E_b/N_0.

2.3 Diversidade

No passo seguinte em direção às antenas inteligentes, temos a *diversidade*. A diversidade é um conceito bastante intuitivo e pode ser vista como uma maneira de se introduzir informação redundante. A idéia básica: se várias réplicas da mesma informação são transmitidas (ou recebidas) através de canais com desvanecimento

independente ou com baixa correlação, então há uma boa probabilidade de que pelo menos uma réplica não esteja severamente degradada pelo desvanecimento [13, 23].

Há várias formas de diversidade, sendo exemplos comuns: a freqüencial, a temporal e a espacial. Aqui daremos ênfase à diversidade espacial, também conhecida como a *diversidade de antenas*, um dos empregos mais populares em sistemas celulares. Quando um receptor é equipado com duas ou mais antenas suficientemente separadas (tipicamente vários comprimentos de onda) elas oferecem ramos úteis de diversidade. É importante ressaltar que baixa correlação pode ser obtida mesmo sem uma separação excessiva das antenas, caso o espalhamento angular do canal seja grande [24]. Além do ganho de diversidade propriamente dito, as técnicas de recepção que exploram a diversidade de antenas fornecem um ganho adicional de SINR, mesmo que os sinais dos ramos de diversidade sejam correlacionados. Por quê? A razão é o fato de que os sinais desejados de cada ramo podem ser combinados coerentemente, ou seja, construtivamente, ao passo que o ruído térmico recebido é combinado de forma não-coerente [6].

Tirar proveito da diversidade em um canal com desvanecimento Rayleigh reduz a potência média de transmissão exigida para a obtenção de uma determinada taxa de erro de bits (*bit-error rate, BER*) no receptor; conseqüentemente, aumenta-se a capacidade de ambos os enlaces, já que potências de transmissão mais baixas diminuem a quantidade de CCI [25]. Outro aspecto altamente positivo da diversidade de recepção, quando aplicada à estação base, é a redução do consumo de energia da bateria do celular.

Um ponto importante que se deve ter em mente é que a lei de "quanto mais, melhor" nem sempre vale aqui. Quanto maior for o grau de diversidade já disponível, seja ela temporal, freqüencial ou espacial, menor será o retorno da diversidade adicional fornecido pelo arranjo de antenas [6]. Isso significa que se o canal de rádio já possui um alto grau de diversidade de multi-percursos (*Vehicular A*, por exemplo), o emprego de muitos ramos adicionais de diversidade não trará muitos benefícios. Por outro lado, é extremamente vantajoso aumentar o número de ramos de diversidade, caso o canal possa ser caracterizado como aproximadamente

plano (*Pedestrian A*, por exemplo).

Muito embora técnicas de diversidade já sejam largamente utilizadas nas estações-base, o emprego de arranjos de antenas nos terminais móveis é uma área relativamente nova de pesquisa. Pesquisas recentes nessa direção indicaram ganhos de desempenho bastante significativos [26, 27]. O advento de processadores de sinais digitais de baixo custo, porém velozes, pode tornar a aplicação de múltiplas antenas no celular economicamente viável.

2.3.1 Modelagem no Simulador

A fim de realizar as simulações envolvendo terminais com duas cadeias completas de recepção, daqui em diante, denominados *2Rake*, os perfis de atraso de potência utilizados seguiram mais uma vez as recomendações da ITU, contudo, alguns fatores distintos não podem deixar de ser mencionados. A abordagem empregada é descrita a seguir. Neste caso, dois enlaces (canais) independentes de rádio foram simulados entre o Nó-B e cada terminal 2Rake. Os dois enlaces experimentam as mesmas perdas determinísticas de propagação e efeitos de sombreamento. Os perfis de atraso de potência são idênticos e perfeitamente alinhados no tempo em ambas as antenas, isto é, o mesmo número de percursos com os mesmos atrasos e potências médias. Não obstante, assume-se que o desvanecimento rápido observado em cada antena é descorrelacionado. A Figura 2.2 ilustra a discussão anterior.

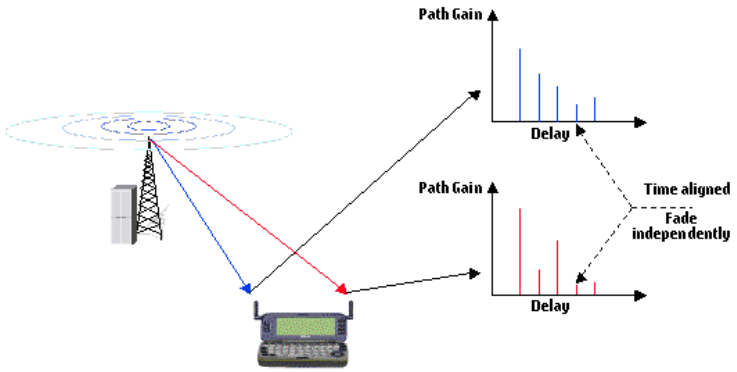

Figura 2.2: Os dois enlaces entre o Nó-B e o terminal.

Tais hipóteses são bastante razoáveis quando se trata de uma única antena com polarizações diferentes, ou de duas antenas suficientemente separadas espacialmente. A separação depende do espalhamento angular observado pelo receptor.

Semelhantemente ao material apresentado na Seção 2.2.1, mostra-se aqui a forma pela qual o valor de E_b/N_0 é calculado para os terminais com receptores 2Rake. O princípio das tabelas AVI continua sendo utilizado, na seqüência, introduz-se a expressão utilizada para o cálculo do valor de E_b/N_0 a cada *slot* para o terminal i:

$$\frac{E_b}{N_0}(i)_{|slot} = \sum_{m=1}^{M}\sum_{l=1}^{R} \frac{P_{\mathrm{RxDPCH}}(s,i).h_{ff,m}(s,i,l)}{P_{\mathrm{Noise}}^{\mathrm{UE}} + P_{\mathrm{RxTotal}}(m,i) - P_{\mathrm{own}}(s,i).h_{ff,m}(s,i,l)} \,.\, G_p, \qquad (2.8)$$

onde

$$P_{\mathrm{RxTotal}}(m,i) = \sum_{k=1}^{K}\left(P_{\mathrm{TxTotal}}(k).\, h(k,i).\sum_{l=1}^{L} h_{ff,m}(k,i,l)\right), \qquad (2.9)$$

$M = 2$ é o número de antenas no UE, $P_{\mathrm{RxTotal}}(m,i)$ é a potência total recebida pela *m-ésima* antena do *i-ésimo* UE, e $h_{ff,m}$ é o ganho descrevendo o desvanecimento rápido do *l-ésimo* percurso do enlace entre a *k-ésima* célula e a *m-ésima* antena receptora do *i-ésimo* usuário. O restante da notação foi apresentado na Tabela 2.2. No caso de SHO, assume-se MRC ideal dos diferentes ramos, e os valores de E_b/N_0 correspondentes a cada ramo são somados, de forma análoga ao que foi feito em (2.2).

Observe que esta expressão também assume que o valor de E_b/N_0 resultante na saída do receptor Rake pode ser computada através da soma dos valores de E_b/N_0 na saída de cada perna do receptor. Na expressão correspondente apresentada na Seção 2.2.1, foi ressaltado que tal cálculo assume que as componentes de ruído e interferência em cada perna do receptor são totalmente descorrelacionadas. Como já foi afirmado, isto não é totalmente verdadeiro para o caso em que combinamos as saídas das pernas do receptor Rake conectadas a uma única antena. Contudo, ao combinarmos as saídas de pernas conectadas a antenas diferentes, é justo afirmar que as componentes do ruído térmico são totalmente descorrelacionadas. Quanto à interferência, esta suposição também mantém-se verdadeira, caso

as antenas estejam suficientemente separadas, que é o caso neste estudo.

2.4 Conformação de Feixes

Em ambientes com níveis significativos de interferência, é altamente desejável que se possa transmitir os sinais aos numerosos usuários de forma mais eficiente, sem intensificar o problema da quantidade de interferência, o que nos conduz ao passo evolutivo seguinte dos sistemas de antenas e desta tese: Antenas-Inteligentes. Uma pergunta razoável seria – o que faz com que essas antenas sejam inteligentes? Nada, as antenas não são inteligentes, o sistema como um todo o é. A inteligência do sistema reside na combinação de um arranjo de antenas com técnicas de processamento de sinais, que pode ser empregada de forma a transmitir e receber sinais de forma sensível e adaptativa às características espaciais do canal de rádio móvel. Isto é, o sistema pode combinar de forma perspicaz os sinais de diferentes antenas, criando uma única antena efetiva, com ganho e características direcionais totalmente distintas daquelas de cada antena individual.

Atualmente, vários termos são usados para referir-se a diferentes aspectos da tecnologia de antenas inteligentes, como, por exemplo, processamento espacial, conformação digital de feixes, acesso ao meio por divisão espacial (*spatial division medium access*, SDMA) entre outros. Entretanto, os sistemas de antenas inteligentes são normalmente categorizados em duas classes: sistemas de feixes fixos ou sistemas de feixes adaptativos. Neste projeto o arranjo de antenas na estação-base é utilizado como um conformador de feixes fixos, que em resumo, filtra os usuários co-canal no domínio espacial.

A conformação de feixes fixos é considerada como uma alternativa simples, porém bastante eficaz, ao complexo sistema totalmente adaptativo. Ela normalmente envolve o uso de quatro a oito antenas por setor para criar um grupo de feixes sobrepostos, cujos lóbulos principais apontam para direções fixas diferentes, criando porções de célula que em conjunto cobrem a área da célula integralmente. O canal dedicado (DCH) de um usuário é transmitido em um único feixe, enquanto

o canal piloto primário (P-CPICH) e os demais canais comuns são transmitidos através do feixe setorial, já que devem ser recebidos em toda a área servida pelo setor. A escolha do feixe ao qual o terminal, quando ativo, estará conectado dá-se através do *chaveamento de feixes*; dentre todos os feixes, aquele onde a potência recebida no UL dos sinais de um determinado UE for maior, será o feixe utilizado para transmissão dos sinais destinados a esse mesmo UE no DL. Isto reduz drasticamente a CCI, uma vez que um feixe com um padrão de irradiação muito mais estreito que o do feixe setorial convencional serve aos usuários dentro da sua porção de célula, possuindo, ao mesmo tempo, ganho bastante reduzido em direções fora do lóbulo principal. A Figura 2.3 ilustra a discussão acima.

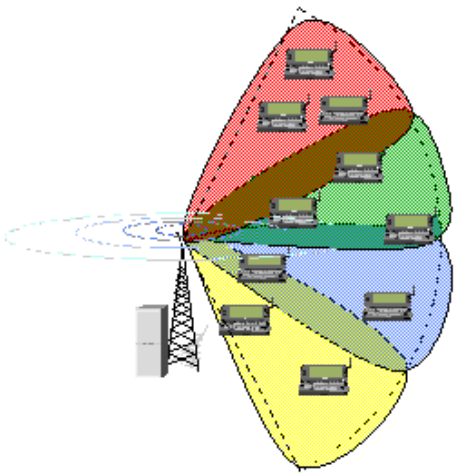

Figura 2.3: Setor de 120° servido por quatro feixes fixos.

Em um sistema UMTS convencional o P-CPICH é usado como referência pelos UEs para a estimação do canal. Entretanto, os sinais transmitidos através dos feixes e aqueles do canal piloto primário, transmitidos por uma antena convencional, muito provavelmente sofrem distorções distintas, assim o P-CPICH deixa de ser uma referência confiável. Ao empregarmos a conformação de feixes fixos é possível transmitir um canal piloto comum secundário (S-CPICH) em cada feixe e usá-lo para estimar o canal em vez do P-CPICH [6]. Uma outra possibilidade seria utilizar os símbolos piloto presentes no DCH. Contudo, o S-CPICH usado pelos UEs nesse caso tem duas vantagens: está sempre ativo e sua potência de transmissão não é

influenciada pelo controle de potência, permitindo uma melhor estimação do canal. Neste trabalho, o uso do piloto dedicado não é analisado.

2.4.1 Modelagem no Simulador

Os princípios básicos da conformação de feixes fixos foram discutidos brevemente na seção anterior. Do ponto de vista do simulador WALLU, as antenas inteligentes são modeladas através do uso de diferentes padrões de irradiação na estação-base, um para cada feixe, escolhidos de acordo com a posição do usuário. O padrão de irradiação de cada feixe foi pré-computado segundo o material apresentado no Apêndice D.5.1 e fornecido ao simulador como uma tabela de busca. Ressalta-se ainda que toda a modelagem foi realizada no domínio da potência, uma vez que a ferramenta não trabalha com números complexos.

O número de antenas no arranjo está intimamente ligado à largura (3dB) dos feixes sintetizados. Em princípio, quanto mais estreitos forem os feixes, maior será a supressão de CCI, o que pode ser mapeado em mais capacidade. Não obstante, devido a limitações do padrão UMTS, cada usuário só pode conectar-se a um único feixe dentro de uma mesma célula; assim, impõe-se a primeira restrição à largura do feixe. É importante que tal largura seja relativamente grande em comparação ao espalhamento angular (AS) esperado; do contrário, percursos com energias significantes podem deixar de ser capturados, o que degradaria o desempenho. Outros dois fatores restritivos práticos cruciais são o custo e a parte estética. O transceptor de AI é muito mais complexo e caro do que o convencional, devido à necessidade de cadeias completas de transcepção para cada antena do arranjo e calibração precisa das mesmas. Por fim, muitas antenas podem não ser bem vistas pela população. Optou-se, então por um AA com quatro elementos, capaz de enfrentar grande AS, fornecendo ganhos de capacidade substanciais a um custo razoável.

Em todas as simulações envolvendo AI o efeito do AS no padrão de irradiação efetivo dos feixes direcionais não pôde ser negligenciado, tendo sido mode-

lado segundo o material apresentado em [24] e [28] e descrito resumidamente no Apêndice G.2.1.

Ao tratarmos de conformação digital de feixes, uma vez que o número de antenas está definido, uma das primeiras questões a surgir é o número de feixes usados em um setor. Ao longo deste projeto, o autor desenvolveu um modelo analítico simples capaz de calcular o número ideal de feixes em função de várias características do ambiente investigado. Este estudo é apresentado no artigo *Impact of the Pilot Signal per Beam on the Ideal Number of Beams and Capacity Gain of Switched Beam forming for WCDMA*, citado na Seção 1.7.

Como nas seções anteriores, aqui é apresentado o cálculo da razão E_b/N_0 para o terminal i em uma rede que utiliza feixes fixos:

$$\frac{E_b}{N_0}(i)_{|slot} = \sum_{l=1}^{R} \frac{P_{\mathrm{RxDPCH}}(s,i).h_{ff}(s,i,l)}{P_{\mathrm{Noise}}^{\mathrm{UE}} + P_{\mathrm{RxTotal}}(i) - P_{\mathrm{own}}(s,i).h_{ff}(s,i,l)} \,.\, G_p \,, \tag{2.10}$$

onde

$$P_{\mathrm{RxDPCH}}(s,i) = P_{\mathrm{TxDPCH}}(s, \mathrm{beam(i)}, i).\, W_s(\phi_{\mathrm{beam(i)}}, \phi_i^s).\, h(s,i) \,, \tag{2.11}$$

$$P_{\mathrm{RxTotal}}(i) = \sum_{k=1}^{K} \left(P_{\mathrm{TxTotal}}(k).\, h(k,i).\, \sum_{l=1}^{L} h_{ff}(k,i,l) \right) \,, \tag{2.12}$$

$$P_{\mathrm{TxTotal}}(k) = \sum_{n=1}^{N(k)} \left(P_{\mathrm{beam(n)}}(k).\, W_k(\phi_{\mathrm{beam(n)}}, \phi_i^k) \right) + P_{\mathrm{P-CPICH}}(k).\, S_k(\phi_i^k) \,, \tag{2.13}$$

$$P_{\mathrm{beam(n)}}(k) = \sum_{u=1}^{\mathrm{Users}_{k,n}} P_{\mathrm{TxDPCH}}(k,n,u) + P_{\mathrm{S-CPICH}}(k,n) \,, \tag{2.14}$$

$$\begin{aligned} P_{\mathrm{own}}(s,i) \;\; = \;\; & \sum_{n \in \mathbf{OS}(i)} \left(P_{\mathrm{beam(n)}}(s).\, W_s(\phi_{\mathrm{beam(n)}}, \phi_i^s).\, h(s,i) \right) + \\ & + X(i).\, P_{\mathrm{P-CPICH}}(s).\, S_k(\phi_i^s).\, h(s,i) \,, \end{aligned} \tag{2.15}$$

Pode ser visto que os cálculos neste caso são significativamente mais complexos do que os apresentados nas duas seções precedentes, o que implica longas simulações envolvendo AI. Novamente, no caso de SHO, assume-se MRC dos diferente ramos e os valores de E_b/N_0 correspondentes são somados, de maneira

análoga ao que é feito em (2.2). A Tabela 2.3 complementa a notação introduzida na Tabela 2.2, não reproduzida aqui em favor da apresentação e organização do trabalho.

2.5 O Caso Combinado

O caso combinado é a continuação óbvia das seções anteriores. Ele estuda o ganho de capacidade quando 100% dos terminais possuem receptores 2Rake e a técnica de chaveamento de feixes fixos é empregada nas estações-base.

Ao fazermos uso de técnicas que reduzem os níveis de interferência na interface aérea, é possível que a capacidade do sistema fique limitada pela quantidade de códigos de canalização disponível. Esta limitação pode, em tese, ser superada com a utilização de códigos de embaralhamento secundários, o que disponibilizaria outras árvore de códigos OVSF, como descrito na Seção 1.4.2. Infelizmente, em muitos casos não há uma maneira simples de se introduzir códigos secundários em uma célula sem deteriorar severamente a ortogonalidade do enlace direto. Assim, caso o sistema atinja este limite rígido, não será possível explorar totalmente o ganho de capacidade fornecido por uma determinada técnica, mesmo que o nível de interferência não tenha alcançado seu limite.

Felizmente, a técnica de conformação de feixes permite dividir a célula em múltiplas zonas, o que não é possível no sistema padrão, ou mesmo com receptores 2Rake. Neste caso, a separação espacial entre feixes que utilizam códigos de embaralhamento diferentes ajuda a compensar a perda da ortogonalidade, permitindo que a falta de códigos de canalização seja superada. Tal conceito é discutido mais aprofundadamente no Apêndice G.2.3.

Agora, imaginemos um sistema que combine a conformação de feixes com terminais com receptores 2Rake. Embora ambas as técnicas sejam independentes, elas se complementam, já que este sistema poderá usufruir da filtragem espacial fornecida pelas AI e de todo potencial dos receptores avançados, pois o limite de

Símbolo	Definição
$W_k(\phi_{\text{beam(n)}}, \phi_i^k)$	O ganho de potência na direção ϕ_i^k do *n-ésimo* feixe da *k-ésima* célula apontado para $\phi_{\text{beam(n)}}$.
$S_k(\phi_i^k)$	O ganho de potência na direção ϕ_i^k do feixe setorial que cobre toda a área da *k-ésima* célula.
ϕ_i^k	Direção azimutal do *i-ésimo* UE, em relação à direção de *broadside* do arranjo de antenas na *k-ésima* célula.
beam(i)	Feixe servindo ao *i-ésimo* UE.
$\phi_{\text{beam(n)}}$	Direção azimutal para a qual o *n-ésimo* feixe aponta. A referência é a direção do *broadside* do AA correspondente.
$N(k)$	Número de feixes sintetizados em uma célula.
$\text{Users}_{k,n}$	Total de usuários servidos pelo *n-ésimo* feixe da *k-ésima* célula.
$h(k,i)$	Ganho do percurso da *k-ésima* célula ao *i-ésimo* usuário. Semelhante a definição encontrada na Tabela 2.2, excluindo-se o ganho da antena de transmissão, modelado explicitamente nas equações anteriores.
$P_{\text{beam(n)}}(k)$	Potência total transmitida através do *n-ésimo* feixe da *k-ésima* célula.
$P_{\text{TxDPCH}}(k,n,u)$	A potência transmitida no DPCH para o *u-ésimo* usuário através do *n-ésimo* feixe da *k-ésima* célula.
$P_{\text{S-CPICH}}(k,n)$	A potência alocada ao canal piloto secundário transmitido no *n-ésimo* feixe da *k-ésima* célula.
$X(i)$	Variável igual a um se o *i-ésimo* UE está sob o código de embaralhamento primário, caso contrário igual a zero.
$\mathbf{OS}(i)$	Conjunto de feixes empregando o mesmo código de embaralhamento usado pelo feixe servindo o *i-ésimo* UE.

Tabela 2.3: Notação complementar para o cálculo de E_b/N_0.

códigos de canalização deixa de ser tão rígido.

2.5.1 Modelagem no Simulador

Neste caso, a razão E_b/N_0 é obtida através da combinação das expressões introduzidas nas Seções 2.3.1 e 2.4.1. Em sua forma final, o cálculo de E_b/N_0 para cada slot para o *i-ésimo* terminal é dado por:

$$\frac{E_b}{N_0}(i)_{|slot} = \sum_{m=1}^{2}\sum_{l=1}^{R} \frac{P_{\text{RxDPCH}}(s,i).h_{ff,m}(s,i,l)}{P_{\text{Noise}}^{\text{UE}} + P_{\text{RxTotal}}(m,i) - P_{\text{own}}(s,i).h_{ff,m}(s,i,l)} \cdot G_p, \quad (2.16)$$

onde

$$P_{\text{RxTotal}}(m,i) = \sum_{k=1}^{K}\left(P_{\text{TxTotal}}(k).\, h(k,i).\sum_{l=1}^{L} h_{ff,m}(k,i,l)\right), \quad (2.17)$$

e $h_{ff,m}$ é é o ganho descrevendo o desvanecimento rápido do *l-ésimo* percurso do enlace entre a *k-ésima* célula e a *m-ésima* antena receptora do *i-ésimo* usuário.

Aparentemente a expressão é idêntica a (2.8). A diferença está nos cálculos de $P_{\text{RxDPCH}}(s,i)$, $P_{\text{TxTotal}}(k)$ e $P_{\text{own}}(s,i)$, que agora são feitos respectivamente de acordo com (2.11), (2.13), e (2.15).

Naturalmente, o princípio das tabelas AVI e os comentários feitos na Seção F.2.1 sobre o SHO e a combinação dos sinais segundo o princípio MRC continuam válidos aqui.

Por fim, pode-se observar nas equações acima que ao combinarmos as duas técnicas, o cálculo da razão E_b/N_0 para cada terminal implica efetuarmos todos os cálculos ligados à conformação de feixes o dobro de vezes, uma vez para cada antena de cada terminal. Isso torna a simulação de tal caso inacreditavelmente demorada.

2.6 Um Novo Conceito

Durante muito tempo a indústria de telefonia celular concentrou os seus esforços na garantia de cobertura ao ar livre, simplesmente porque a indústria

foi desenvolvida antes da explosão da Internet, enfocando os usuários móveis de serviços de voz, como pessoas dirigindo entre suas casas e o trabalho. Daí, a histórica dificuldade em oferecer altas taxas de bits com robustez em ambientes fechados como edifícios, onde há perdas extras de penetração [4].

Por outro lado, pode-se dizer que grande parte das aplicações que demandam altas taxas estão ligadas ao meio corporativo ou ao mundo do entretenimento digital, transferência de grandes arquivos pela Intranet ou Internet. Tais atividades são comumente realizadas em casa ou dentro de escritórios, justamente onde costumamos encontrar redes de computadores. Mesmo sendo imbatíveis em termos de taxas de transferência, as redes cabeadas convencionais também possuem algumas desvantagens, como, por exemplo, permitir pouquíssima ou nenhuma mobilidade, e exigir a passagem dos cabos pelo ambiente. Isso explica por que a redes sem fio *Wi-Fi* ou *WLANs* estão ganhando terreno muito rapidamente, apesar das taxas de transferência inerentemente menores.

Considerando este cenário, é evidente que as operadoras 3G precisarão de terminais e, principalmente, de redes celulares capazes de alcançar altas taxas de transferência, independentemente da localização do usuário final, ambientes fechados ou abertos. De outra maneira, outras tecnologias sem fio, como redes Wi-Fi terão uma grande vantagem na competição pelo mesmo nicho. Analisando a situação, uma questão intrigante surge: o que pode ser feito com esse objetivo?

Já há algum tempo, repetidores vêm sendo usados para aumentar a cobertura em sistemas GSM. Alguns estudos sobre a sua aplicabilidade a redes UMTS estão sendo executados no 3GPP. De fato, os repetidores asseguram sinais melhores, mas não aumentam necessariamente a capacidade de uma célula. Micro-células são uma boa opção, porém é muito importante considerar sempre os custos envolvidos. Além disso, a capacidade de uma macro-célula não está sendo realmente ampliada, simplesmente uma nova célula menor é criada dentro da célula já existente.

Nesta tese, a técnica de conformação de feixes recebeu atenção especial por ser capaz de ampliar significativamente a capacidade de uma célula. Além disso, resultados em [29] confirmam que a aplicação de um feixe específico para cada usuário

podem melhorar muito o desempenho da rede, mas a um custo computacional elevado. O rastreamento da posição de todos os usuários desejados é uma tarefa intensa; à parte isso, em sistemas FDD, o ganho de capacidade pode ser degradado devido a estimativas imperfeitas da posição do terminal. Essas razões explicam por que os trabalhos em [3, 9, 29], entre muitos outros, favoreceram sistemas de chaveamento de feixes, eles oferecem um bom compromisso entre complexidade e desempenho.

Por que nos preocuparmos, então? A *Conformação de Feixes Específicos a Repetidores* é um conceito elaborado pelo autor durante a realização da pesquisa de tese. Como ilustrado pela Figura 2.4, os repetidores estariam fixos e serviriam os usuários em ambientes fechados. Como os repetidores não se movem, os feixes poderiam ser apontados precisamente, proporcionando os ganhos de capacidade das técnicas de feixes específicos, mas sem implicar a complexidade adicional de se estimar e acompanhar a localização de cada usuário. Os terminais localizados em ambientes fechados se beneficiariam do sinal reforçado transmitido pelos repetidores, permitindo, desta forma, altas taxas de transferência de dados. A diferença fundamental entre a solução proposta e os repetidores convencionais é o fato de estarmos criando um enlace de alta qualidade entre a estação-base e o repetidor, concentrando a potência irradiada na direção deste, reduzindo a interferência co-canal.

O arranjo de antenas utilizado para gerar os feixes específicos poderia também sintetizar os feixes utilizados pela técnica "padrão" de comutação de feixes aplicada ao resto da rede. Tais repetidores seriam instalados em locais-chave escolhidos pelas operadoras, como grandes escritórios, aeroportos e edifícios residenciais dispostos a pagar pelo serviço, ou seja, trata-se claramente de uma questão de planejamento estratégico.

Outro aspecto positivo deste conceito é o fato de não depender de nenhuma colaboração ou alteração dos terminais; mais além, em vez de implementarmos a diversidade de recepção nos UEs, os repetidores poderiam fornecê-la através de duas ou mais antenas, pois tais repetidores não teriam as severas restrições de consumo

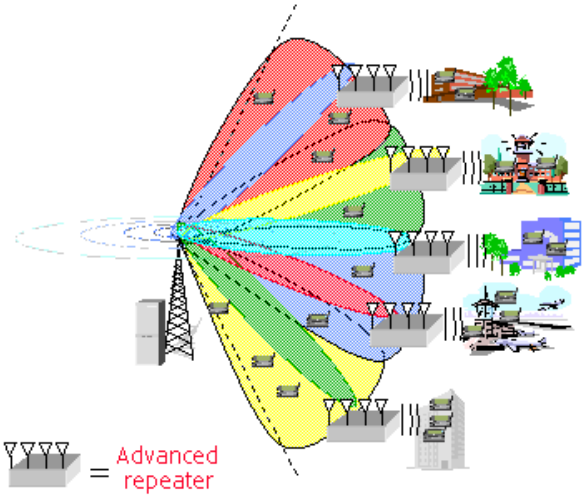

Figura 2.4: Feixes Específicos a Repetidores.

dos terminais móveis alimentados por baterias. Além disso, todo o processamento pode ser feito em RF; entretanto, caso estejamos interessados em aumentar a complexidade e realizar o processamento em banda base, os repetidores poderiam ser utilizados até mesmo para interconectar duas tecnologias de comunicações sem fio completamente distintas, por exemplo, um terminal Wi-Fi poderia conectar-se a uma rede UMTS através de um repetidor. Transformar-se-ia, assim, uma tecnologia potencialmente competidora em uma aliada complementar.

Conclui-se assim, que a utilização de repetidores e feixes específicos parece ser uma forma efetiva de se aumentar a capacidade do enlace direto, capaz de competir com a tecnologia WLAN com a vantagem adicional de oferecer em um único equipamento serviços de voz [1], altas taxas de transferência de dados e mobilidade.

Infelizmente, esse conceito não foi simulado, pois demandaria profundas modificações na estrutura da ferramenta de simulação. A idéia foi apresentada aqui como um complemento e como uma proposta para futuras investigações.

[1] WLANs não podem oferecer serviços de voz por comutação de circuitos, apenas serviços de Voz sobre IP (VoIP).

Capítulo 3

Resultados Obtidos

Este capítulo é dedicado à apresentação dos resultados da extensa campanha de simulações realizada durante o desenrolar deste projeto. A proposta é ressaltar os aspectos mais relevantes, propiciando uma visão geral dos resultados obtidos e guiar os leitores aos apêndices, onde encontrarão discussões mais específicas.

Em todas as simulações, a meta era operar a rede com carga máxima, a fim de se avaliar sistematicamente o aumento de desempenho em relação a uma rede padrão de referência proporcionado pelas diferentes técnicas sob condições controladas e reprodutíveis. Outro objetivo crítico era observar como os algoritmos de RRM convencionais distribuiriam a capacidade extra entre os usuários.

Não há simulações com modelos mistos de tráfego, ou seja, o tráfego oferecido é 100% comutado por circuito em tempo real (RT), ou 100% comutado por pacotes em tempo não-real (NRT). Sugere-se o caso mais realista como um possível estudo futuro.

3.1 Referência

Os resultados apresentados nesta seção para o sistema empregando três antenas diretivas, uma por setor, servirão como base de comparação para as demais

simulações na seções subseqüentes.

A carga oferecida (*Offered Traffic*) à rede foi progressivamente aumentada até que o tráfego transportado *(Carried Traffic)* saturasse, ou seja, novos usuários passassem a não ser admitidos pelo sistema. As simulações foram conduzidas para os dois perfis de atraso de potência recomendados pela ITU. No caso *Vehicular A*, (VehA), terminais movendo-se a velocidade de 50 km/h (VehA50) também foram simulados.

Analisando os resultados, percebemos que o perfil PedA alcançou a maior capacidade absoluta por célula. Tal resultado deve-se à menor dispersão temporal no perfil PedA, o que preserva melhor a ortogonalidade entre sinais sob um mesmo código de embaralhamento. O desempenho do perfil VehA foi ligeiramente inferior, apesar da diversidade de multi-percurso presente. A maior dispersão temporal deste perfil é a responsável pela menor capacidade. Os resultados do perfil VehA50 são os mais pobres, devido à natureza rapidamente variante do canal, que implica uma maior variação da potência recebida; tal variação resulta na exigência de E_b/N_0 maiores a fim de prover a mesma qualidade.

A Figura 3.1 ilustra o comportamento do sistema para o modelo de tráfego comutado por circuito (RT). Complementarmente, as vazões (*throughput*) médias das amostras na região plana (saturada) das curvas foram calculadas e empregadas como referência. A Tabela 3.1 resume os valores encontrados.

Os resultados das simulações para o caso comutado por pacotes (NRT) não são mostrados aqui, mas encontram-se no Apêndice E.5.2, juntamente com o restante das discussões sobre o caso RT. Não obstante, as principais observações são apresentadas a seguir.

Percebeu-se, tanto no modelo de tráfego RT como no modelo NRT, que o sistema estava limitado pela quantidade de interferência na interface aérea. No caso NRT, a capacidade alcançada, bem como a utilização de códigos de canalização, foram mais altas do que no caso RT. Uma explicação para isso consiste na liberdade de escolha das taxas de transmissão; o sistema pode acomodar usuários extras com

taxas de bits mais baixas quando não há "espaço" para um usuário demandando altas taxas de transferência. No caso RT, não há a tal liberdade, pois as taxas de transferência são fixas. O maior consumo de códigos deve-se à natureza intermitente (em rajadas) do tráfego comutado por pacotes.

Por fim, concluiu-se que em um cenário de macro-células a capacidade sistêmica do enlace direto varia de 550 kbps a 900 kbps por setor por 5 MHz em função das características de dispersão do canal e da natureza da informação transmitida.

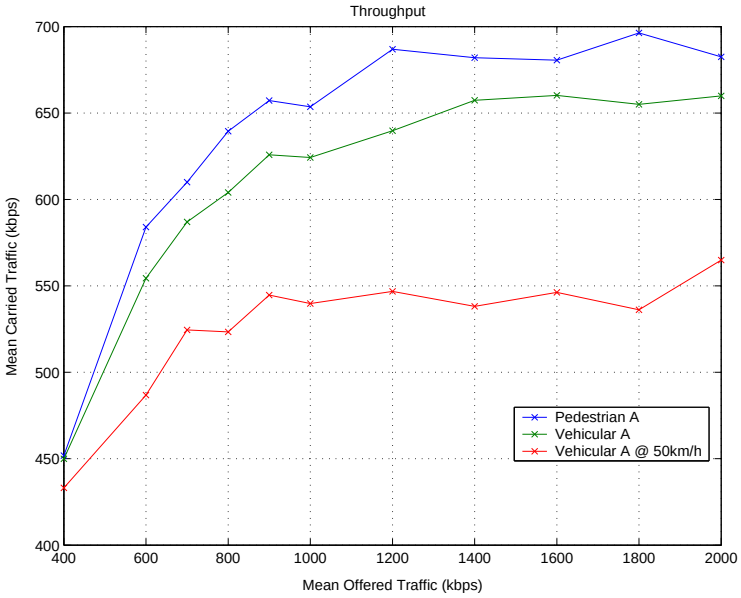

Figura 3.1: Vazão média das células centrais em função do tráfego oferecido.

PDP	$E\{$Tráfego Transportado$\}$ (kbps)
PedA	$685,4$
VehA	$658,1$
VehA50	$546,4$

Tabela 3.1: Valores de referência para comparações.

3.2 Diversidade

Esta seção retoma a discussão introduzida na Seção 2.3. O objetivo é medir os ganhos médios de capacidade em uma rede celular UMTS onde 100% dos terminais são equipados com receptores 2Rake. Uma análise teórica simples apresentada em [3] demonstra que em tais circunstâncias a capacidade pode ser pelo menos dobrada se não houver restrições quanto à quantidade de códigos de canalização.

Como antes, simulações foram executadas para diferente classes de tráfego e perfis de canal. A seguir são ilustrados e discutidos os principais resultados, a análise completa das peculiaridades encontra-se no Apêndice F.3.

As Figuras 3.2(a) e 3.2(b) representam os casos com e sem restrição ao número de códigos de canalização disponíveis em uma célula, respectivamente. As vazões médias na região plana de cada curva são apresentados na Tabela 3.2, em conjunto com os ganhos relativos. Considerando-se o cenário com apenas uma árvore OVSF por setor, observou-se um ganho médio de 86% em todos os cenários avaliados para tráfego comutado por circuitos.

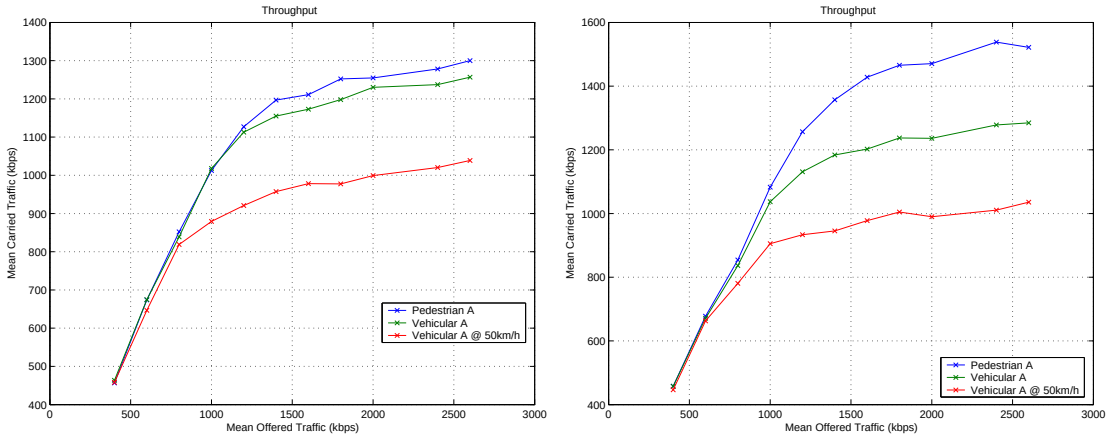

(a) Comparação da vazão média (*Ped A*). (b) Comparação da vazão média (*Veh A*).

Figura 3.2: Caso 2Rake versus referência.

Infelizmente, nesse caso não há uma maneira simples de se introduzir novos códigos de embaralhamento em cada célula sem que haja, ao mesmo tempo, uma severa degradação da ortogonalidade entre os sinais transmitidos com códigos de embaralhamento diferentes. Isso significa que o ganho está limitado pela falta de

Caso	**PDP**	$E\{$Tráfego Transportado$\}$ (kbps)	**Ganho** (%)
Restrito	PedA	1277,8	86,4
	VehA	1241,4	88,6
	VehA50	1019,4	86,5
Irrestrito	PedA	1530,0	123,23
	VehA	1281,4	94,71
	VehA50	1023,3	87,28

Tabela 3.2: Resultados 2Rake (RT)

códigos de espalhamento Ainda assim, simulando-se um caso hipotético, onde tal limite foi removido artificialmente, ou seja, "enganando-se" o simulador, ganhos de 123,23%, 94,71%, and 87,28% foram obtidos para os perfis de atraso de potência *Pedestrian A*, *Vehicular A*, (UEs a 3km/h) e *Vehicular A* (UEs a 50km/h), respectivamente.

A parte mais interessante diz respeito ao perfil PedA. Há uma grande diferença entre ambos os casos. A razão desta diferença é a pequena diversidade inerente. No caso do perfil VehA, como já há alguma diversidade devido aos múltiplos-percursos os receptores 2Rake não conseguem acrescentar ganhos substanciais de diversidade, limitando-se à combinação construtiva dos sinais recebidos. Tal efeito é ainda mais evidente no perfil VehA50, onde há ainda diversidade temporal devido às rápidas variações do canal.

Para o tráfego comutado por pacotes, a análise teve que ser um pouco mais cuidadosa, pois os ganhos obtidos tendem a ser camuflados. Os ganhos máximos de vazão tendem a ser marginais, bem inferiores aos apresentados anteriormente. À luz do que foi dito na seção anterior, é de se esperar que a limitação imposta pelo número de códigos de canalização seja mais severa no caso NRT, pois este modelo de tráfego demanda ainda mais códigos do que o modelo RT, que, por sua vez, já havia se tornado claramente limitado por códigos com o advento de receptores 2Rake.

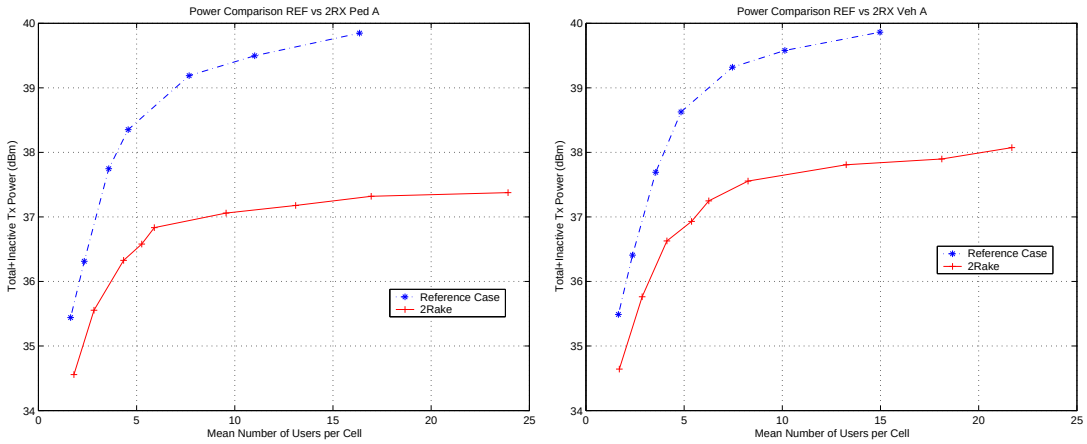

(a) Potências de transmissão (Ped A). (b) Potências de transmissão (Veh A).

Figura 3.3: 2Rake versus referência (Potências de transmissão).

Adicionalmente, analisamos a evolução da exigência das potências de transmissão à medida que a carga é aumentada e a comparamos com o caso de referência para ambos os perfis de atraso de potência. O resultado é apresentado na Figura 3.3. Aqui, a diferença é cristalina. O sistema de referência atinge sua potência de transmissão limite, ao passo que o sistema com receptores 2Rake não. O limite de códigos não deixa que isso que ocorra. Há uma diferença de pelo menos 2 dB em ambos os casos. Entretanto, os usuários não tiram proveito algum disto, por outro lado, as operadoras necessitariam de menos potência em suas estações-base para oferecer a mesma capacidade.

Por fim, as taxas médias de transferência observadas pelos usuários não sofrem nenhuma modificação significativa. Isto se deve à estratégia empregada pelo agendador de pacotes, que tenta servir o maior número possível de usuários obedecendo às restrições de potência e às taxas mínimas de transferência. Seria necessário a política de agendamento de pacotes a fim de permitir que usuários com terminais avançados pudessem beneficiar-se de alguma maneira.

3.3 Chaveamento de Feixes

O objetivo desta seção é investigar os ganhos no DL de uma rede UMTS provenientes da aplicação da técnica de chaveamento de feixes fixos nas estações-base. A fim de se avaliar o desempenho da técnica de conformação de feixes em um ambiente de simulação realista, incorporaram-se ao modelo de canal, os efeitos da dispersão angular.

A metodologia empregadas nas duas seções precedentes foi mantida. Contudo, devido à complexidade dos cálculos apresentados na Seção 2.4.1, as simulações envolvendo AI têm uma duração extremamente elevada. Reduzir o comprimento das simulações não era uma opção desejável, pois isso poderia prejudicar a confiabilidade estatística dos resultados. Conseqüentemente, optou-se por simular apenas o perfil *Vehicular A* – a alternativa pouco atraente era a exclusão das simulações com tráfego comutado por pacotes. A opção por um único perfil se justifica pelo fato de que diferentemente das simulações na Seção 3.2, o ganho fornecido pelo arranjo de antenas operando no modo de conformação de feixes independe da quantidade de diversidade já presente.

Todos os resultados apresentados aqui assumem um arranjo com quatro antenas e um espalhamento angular fixo de cinco graus. O número de feixes por setor é igual a quatro, tendo sido selecionado segundo os resultados do estudo analítico desenvolvido pelo autor e confirmado por simulações de teste. A separação espacial entre feixes permitiu que um código de embaralhamento secundário fosse disponibilizado, duplicando, assim, o número máximo de códigos de canalização.

Resultados (4 Feixes com S-CPICH)		
PDP	$E\{$Tráfego Transportado$\}$ (kbps)	**Ganho** (%)
VehA	1250,4	90

Tabela 3.3: Resultados do chaveamento de feixes (RT).

Observou-se um ganho de 90% com o modelo de tráfego RT ao consideramos uma configuração com 4 W, de um total de 10 W, dedicados aos canais piloto: 2

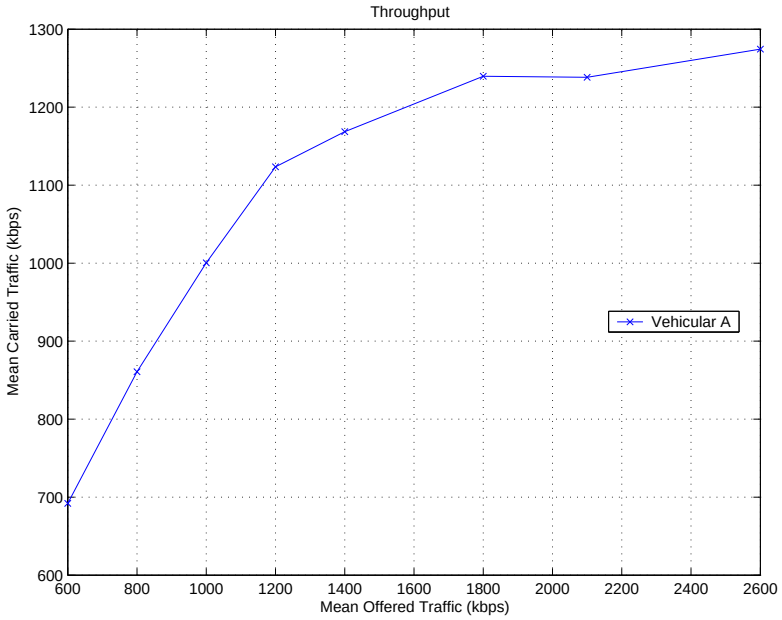

Figura 3.4: Vazão média das células centrais em função do tráfego oferecido.

W para o P-CPICH, e outros 2W no total para os quatro pilotos secundários. A Figura 3.4 ilustra o comportamento do sistema para o modelo de tráfego comutado por circuito. A Tabela 3.3 resume os valores encontrados. A presença de dois códigos de embaralhamento permitiu que o sistema alcançasse o limite imposto pelo nível de interferência, assim como no caso de referência, mas com um número muito maior de usuários por célula.

Ao avaliarmos o tráfego comutado por pacotes, observou-se que o ganho máximo de capacidade de vazão é de aproximadamente 58%. A Figura 3.5(a) apresenta a vazão das células em função da carga observada *a posteriori* (o número médio de usuários em uma célula) para os sistema de referência e aquele com AI. Uma pergunta intrigante é: por que este ganho é menor do que aquele alcançado com o modelo de tráfego RT? Desta vez, o bloqueio por falta de códigos não é a resposta, pois há dois códigos de embaralhamento e a Figura 3.5 comprova que o sistema atinge sua potência de transmissão limite.

A resposta reside no fato de que o ganho máximo da técnica de chaveamento de feixes só pode ser explorado caso a interferência seja espacialmente branca, isto

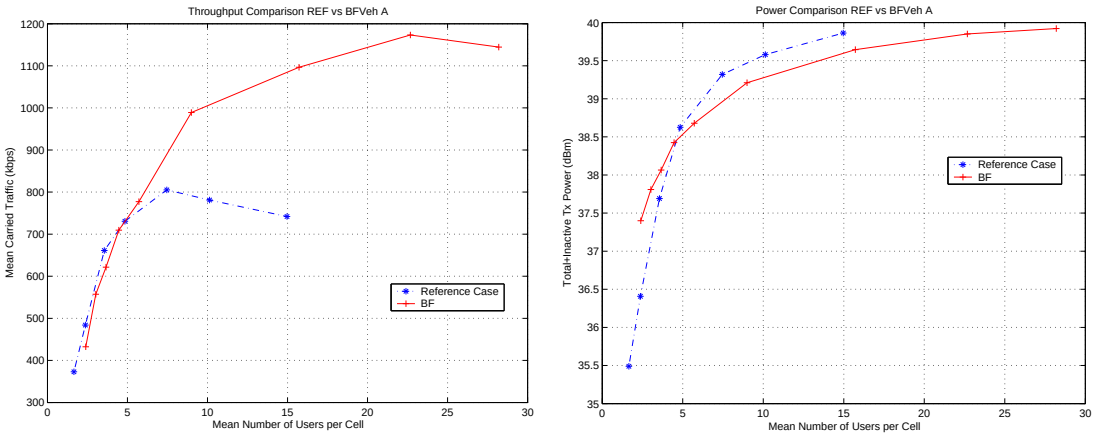

(a) Comparação da vazão média. (b) Comparação das potências de trasnmissão.

Figura 3.5: Chaveamento de feixes versus referência.

é, aproximadamente a mesma em todas as direções, ao passo que não haveria nenhum ganho de capacidade se todos os usuários estivessem posicionados na mesma direção, servidos por um mesmo feixe. Isso significa que o ganho de capacidade é muito sensível à distribuição espacial da interferência. Em sistemas com a distribuição de taxas de bits não-uniforme, usuários com taxas mais altas requerem mais potência de transmissão do que aqueles com taxas mais baixas, devido aos menores ganhos de processamento CDMA. Dessa forma é bastante provável que espacialmente a interferência se desvie da suposição ideal.

Por fim, os resultados mostraram apenas ligeiras melhoras nas taxas de dados observadas pelos usuários, para um mesmo número de usuários, em células com uma carga moderada. Em uma célula altamente carregada, os usuários não experimentam nenhuma melhora substancial na qualidade do serviço, quando comparada àquela de uma rede convencional carregada. A operadora fica com todo o ganho, já que a rede passa a ser capaz de acomodar mais usuários.

3.4 O Caso Combinado

Considerando as simulações incrivelmente longas devido à complexidade computacional exigida pelo caso combinado e que o comportamento de uma rede UMTS implementando individualmente as técnicas descritas anteriormente fora

cuidadosamente investigado com cargas gradualmente incrementadas, decidiu-se simular dois casos apenas, um para cada modelo de tráfego, com uma carga oferecida muito alta. O objetivo era avaliar a capacidade máxima absoluta fornecida pela combinação das duas técnicas.

Como apenas o perfil *Vehicular-A* foi simulado na Seção 3.3, para mantermos a coerência, somente esse perfil de canal foi empregado. Novamente, dois códigos de embaralhamento foram utilizados, dobrando o número de códigos de canalização disponíveis. A Tabela 3.4 apresenta os resultados obtidos resumidamente. O tráfego carregado médio superou os 2800 kbps, o que significa um ganho impressionante de 326%. As melhoras de capacidade seriam ainda mais substanciais para o perfil *Pedestrian-A* devido a sua menor diversidade inerente, como discutido na Seção 3.2, o que poderia fazer com que dois códigos de embaralhamento não fossem suficientes para evitar o bloqueio por falta de códigos de canalização.

Resultados (4 Feixes c/ S-CPICH + 2Rake)		
PDP	$E\{$Tráfego Transportado$\}$ (kbps)	*Ganho* (%)
VehA	2806,4	326%

Tabela 3.4: Resultados do caso combinado (RT).

O ganho de capacidade alcançado foi surpreendentemente superior ao produto dos ganhos alcançados por cada solução individualmente. Por quê? A combinação foi vantajosa para ambas as técnicas, pois introduziu uma maneira de se superar o limite rígido de códigos que afeta a solução de receptores 2Rake. Ademais, o grande número de usuários aproxima mais a interferência do caso ideal, espacialmente branca, o que é fundamental para se explorar totalmente o ganho da conformação de feixes.

Ao analisarmos o caso NRT, a situação se torna um pouco mais complicada. O ganho observado na vazão foi de aproximadamente 104%. Entretanto, mesmo com dois códigos de embaralhamento, o sistema estava severamente limitado pela falta de códigos, dificultando um julgamento balizado dos resultados. Tal análise permanece como uma tarefa futura.

Capítulo 4

Conclusão e Trabalhos Futuros

E chegamos ao fim. Ao relembrar todos os meus esforços para escrever esta tese, percebo quão longa foi a jornada que me trouxe até estas últimas linhas. Viver mais de um ano em uma pequena cidade no norte da Dinamarca, conhecer um pouco mais do fascinante mundo das comunicações móveis foram alguns dos aspectos mais desafiadores e, ao mesmo tempo, recompensadores deste trabalho. O desenrolar desta tese foi uma fascinante mistura de conhecimento técnico, planejamento, determinação, e por que não, criatividade.

Acima de tudo, acredito que a essência deste projeto pode ser resumida em uma palavra: pesquisa. Há a necessidade constante de se investigar, explorar e analisar. É preciso estar sempre motivado e trabalhar em direção a uma meta, superando os eventuais obstáculos.

Uma pergunta pertinente para este momento seria: "Quais foram as principais lições que aprendi com esta tese?" Responder esta questão e apresentar o caminho para possíveis futuros trabalhos é o objetivo deste capítulo.

4.1 Conclusões

Esta tese avaliou alguns métodos que utilizam estruturas avançadas de antenas para aumentar a capacidade de redes UMTS FDD. O desempenho do canal dedicado DCH no enlace direto foi analisado através de simulações sistêmicas dinâmicas, bem como modelos teóricos simples, sempre que possível.

O problema foi abordado de forma sistemática, construindo a cada capítulo a base de conhecimentos necessária para se alcançar os objetivos da pesquisa. A organização do texto que se segue tenta transmitir de forma sintética o processo de aprendizagem pelo qual o autor passou.

O Capítulo 1 foi o primeiro passo. A arquitetura do sistema UMTS foi apresentada, seguida por uma breve descrição de sua camada física. Em última forma, era essencial compreender o sistema considerado em todos os capítulos subseqüentes. Referências aos Apêndices B e C foram feitas freqüentemente, ou para apresentar mais detalhes, ou para lembrar aos leitores que o canal de rádio móvel impõe restrições e limites fundamentais.

O Capítulo 2, teve início com uma discussão acerca dos vários métodos existentes de avaliação do desempenho de redes celulares UMTS; na seqüência, descreveu-se a complexa ferramenta de simulação e a metodologia empregada para obtenção dos resultados. Finalmente, algumas soluções capazes de mitigar as limitações do canal de rádio móvel foram enumeradas em ordem crescente de "inteligência". Viu-se que os arranjos de antenas podem ser utilizados basicamente de duas formas, diversidade e conformação de feixes. Esta permite a supressão de interferência através da filtragem espacial, aquela oferece proteção contra o desvanecimento e um ganho médio na razão sinal-ruído.

O Capítulo 3 foi inteiramente dedicado à apresentação dos resultados obtidos. Primeiramente, os leitores encontraram os resultados referentes a uma rede UMTS convencional, isto é, sem nenhuma das técnicas mencionadas no capítulo antecedente. Tais resultados, indicaram que o sistema é claramente *limitado por interferência*, independentemente do tipo de tráfego; não obstante, a demanda por

códigos de canalização do tráfego NRT é muito maior do que a mesma quando se transporta apenas tráfego RT. O desempenho alcançado serviu de base de comparação para as demais simulações realizadas.

O passo seguinte foi a realização de simulações assumindo uma penetração de 100% dos terminais com duas antenas e receptores Rake (2Rake) e nenhuma alteração nas estações-base. Este estudo demonstrou que a utilização maciça de tais terminais torna o sistema *limitado por código*, o que ocorre quando os usuários servidos por uma célula requerem mais códigos de canalização do que o número máximo existente em uma árvore OVSF sob um único código de embaralhamento. Tal limitação é mais severa para o tráfego NRT, devido à maior exigência inerente por códigos.

Verificou-se ainda que os algoritmos de RRM também são capazes de capturar automaticamente os ganhos providos por receptores 2Rake no domínio da comutação de pacotes. Entretanto, isso não significou taxas de dados mais elevadas. Resumindo, o usuário adquire um terminal potencialmente mais caro que beneficia apenas a operadora. Seria necessário alterar a estratégia de agendamento de pacotes a fim de estimular os consumidores, ou então subsidiar tais aparelhos.

Na seqüência, investigou-se o desempenho do DL de uma rede UMTS com a aplicação da técnica de chaveamento de feixes nas estações-base. Aqui, toda a potência transmitida concentra-se no feixe estreito apontando para a direção que mais se aproxima daquela do usuário desejado, gerando muito menos interferência em outras direções.

Observou-se que o notório aumento de desempenho fornecido pela técnica de chaveamento pode tornar o sistema limitado pela falta de códigos de canalização. Nesse caso, devido às propriedades das AI de filtragem espacial anteriormente citadas, podem-se alocar de forma sistemática e organizada outro(s) código(s) de embaralhamento em uma mesma célula, disponibilizando, dessa forma, outra(s) árvore(s) de códigos de canalização.

Os algoritmos de RRM convencionais conseguiram explorar os ganhos pro-

porcionados pela conformação de feixes fixos. Em uma célula altamente carregada, os usuários não experimentam nenhuma melhora substancial na qualidade do serviço. A operadora é a grande favorecida.

A parte final tratou dos ganhos fornecidos pela combinação de ambas as técnicas, ou seja, terminais com receptores 2Rake e antenas inteligentes nas estações-base. Tal solução fará o problema da falta de códigos de canalização ainda mais severo sob condições que favoreçam uma capacidade absoluta maior, exigindo três ou mais códigos de embaralhamento. Os resultados para tráfego RT demonstraram um ganho extraordinário comparado ao caso de referência. Infelizmente os resultados para o caso de dados NRT não foram conclusivos. O artigo *Network Performance of Node-B Switched Beamforming and Dual Antenna User Equipment in WCDMA* a ser publicado investiga o caso combinado um pouco mais.

4.2 Trabalhos Futuros

Tópicos para estudos posteriores foram sugeridos ao longo de toda esta tese, contudo, eles são relembrados aqui a fim manter nossas mentes ocupadas.

Infelizmente, o conceito de Feixes Específicos a um Repetidor introduzido na Seção 2.6 não pôde ser simulado, porque exigia profundas modificações na estrutura do simulador. Apesar de ser bastante desafiante do ponto de vista da implementação, parece ser um tópico bastante interessante para futuras investigações.

Outro aspecto relevante que tange todas as campanhas de simulação é a ausência de simulações com tráfego misto, ou seja, serviços de voz e dados na rede simultaneamente. Tal cenário certamente se aproximará ainda mais da realidade de uma rede 3G, podendo, portanto, ser considerado como uma extensão natural deste projeto.

Uma das conclusões mais fortes apresentadas no Capítulo 3 e reforçadas na seção anterior é o fato de que atualmente as operadoras de redes de telefonia celular tiram todo o proveito das técnicas analisadas. Seria extremamente importante que

parte desta capacidade extra pudesse ser compartilhada com os usuários; para tal a política de agendamento de pacotes deve ser modificada. Tais alterações nos algoritmos de RRM são um campo estratégico de pesquisa, porque darão aos operadores uma liberdade muito maior para distribuir a capacidade adicional de acordo com suas necessidades.

Por último, mas não menos importante, o conceito apresentado na Seção 2.5 e simulado na Seção 3.4 merece muito mais atenção, especialmente no caso NRT. Para tal estudo, seria conveniente utilizar tabelas AVI específicas para terminais com receptores 2Rake.

Tese Original na Forma de Apêndices

Preface

This thesis report is the result of an one-year research project carried out at the Department of Communication Technology at Aalborg University in close co-operation with Nokia Networks R&D, Aalborg.

The author studies, presents and assesses the gains of various methods for improving the system level capacity of the 3^{rd} generation standard for mobile communications denoted Universal Terrestrial Radio Access Frequency Division Duplex (UTRA FDD).

One of the author's compromises was to make this report as self-contained as possible without polluting the text with unnecessary information. Even though a basic overview of UTRA FDD system level issues and radio propagation characteristics is provided for the sake of completeness, it is expected from the reader to have knowledge about these topics. Statistics as well as digital signal processing theory are also helpful to understand this work.

This thesis is divided into two parts and nine chapters. Although the chapters can be read in rather independent way, cross references are given when needed. The first part is mainly theoretical and composed by chapters A – D. The second part consists of chapters E– I. It details the simulator, the simulation methodology, presents and analyzes the results, and comprises this thesis.

Aalborg, Denmark — Luis Guilherme Uzeda Garcia

April 31, 2005

Part I

Structure & Concepts

Apêndice A

Introduction

If time was an infinite resource, the endless issues related to the performance enhancement of cellular system technologies could be approached. Since this is not the case, it is always necessary to narrow down and define precisely the scope of the research. This is exactly what this initial chapter does. First of all, the motivation behind this project is given, followed by an elucidation about why certain topics are being focused on in this Master's Thesis, while others have been left out. Subsequently, the objectives of this work are presented. Finally, an overview of what the readers will find in the rest of the report, closes the chapter.

A.1 Motivation

One could say that the ultimate goal of wireless personal communications is to allow people, and why not machines as well, to exchange any form of information reliably, as fast as possible and without mobility or location constraints. Third generation systems like the Universal Mobile Telecommunication System (UMTS) have been designed to take one step further towards this "any-time, anywhere" communication system.

The anticipated growth of wireless communication systems has fueled research efforts to investigate methods to increase system capacity [30]. One can say that recent progresses in radio technology, on the one hand, and the ever-growing

demand for efficient bandwidth-consuming high-quality digital wireless communication services, on the other hand, play a dramatic role in this trend. Although there are not many subscribers using 3G services right now, the number of users is expected to increase rapidly around the world. As the number of subscribers grows, there will be the need to extend the capacity of the initially deployed UMTS networks.

In contrast to the "wired" communication world, wireless systems can not simply create more bandwidth by adding new physical resources (cables, fibers, etc), for the radio spectrum available for wireless services is extremely scarce.

As a consequence, the wireless system engineer is faced with the conflict between the increasing demand for wireless services and the scarce electromagnetic spectrum. A number of different technologies have been designed to solve this dilemma. Sectorization, addition of extra carriers, and the application of smart antennas[1] are some of the possibilities. In this thesis, the system capacity gain provided by smart antennas is focused.

A.2 Why Smart Antennas?

In cellular systems, the most straightforward way to increase capacity is to partition cells as customer demand increases. UMTS includes hierarchical cell structures with hot spots served by micro cells. If cells could be subdivided *ad infinitum* there would be hardly any incentive to design more efficient air interfaces. Although in many geographical areas there is still much potential for further cell partitioning, very small cells are not always desirable due to both economical and engineering factors. The cost of base stations and their connection to the wired backbone is an important consideration too [1].

[1]Smart Antennas is used in this chapter as a big "umbrella" name, which stands for different antenna array (AA) technologies. Chapter D opens up this "umbrella" by approaching each technique separately.

Yet another possibility is to use extra carriers if they are available, but one has to keep in mind the very large licensing costs due to the aforementioned scarcity of available spectrum.

Smart antennas (SA) are foreseen as one of the most promising technologies for reducing interference and increasing *capacity* or *coverage* in UMTS WCDMA networks. Smart antennas can significantly boost the system capacity by exploiting the spatial domain of the mobile radio channel with the help of an antenna array and appropriate signal processing at the base station.

Not everything is perfect though. One has to bear in mind that there is no ultimate antenna solution for all radio environments, and that the optimal antenna solution depends on the local environment and the channel characteristics. Besides SA's utilization also involves some extra complexity in the system (nothing is for free), yet this added complexity is expected to be less expensive than the deployment of extra sites or additional carriers.

A.3 Why the Downlink?

In the early days of CDMA systems, it was believed that the uplink would be the bottleneck in system capacity [4]. However, experience has proven it to be the other way around. The reason for this is that the total transmitted power of the base station is shared by all downlink users, i.e. the more users, the less power assigned to each user. Besides, it is widely expected that in the near future the traffic in the networks will be highly asymmetric due to the nature of the 3G offered services with much larger requirements on the downlink, making the situation even worse.

A.4 Objectives of this Work

This work's main focus is on UTRA FDD downlink capacity enhancements in a macro cell scenario. The study comprises the investigation of the capacity gains of following features in UTRA FDD:

- Deployment of dual antenna Rake receivers at the terminals for:
  - Different radio channel characteristics
  - Fixed bit rate circuit switched traffic
  - Variable bit rate packet switched traffic
  - Low (3km/h) and medium (50km/h) mobile speeds
- Beamforming using antenna arrays at the base station for
  - Different radio channel characteristics
  - Fixed bit rate circuit switched traffic
  - Variable bit rate packet switched traffic
  - Low (3km/h) mobile speeds

The features are studied both separately and combined to understand how they interact with each other. The study is mainly based on results obtained from computer simulations, because the high complexity of UTRA FDD makes analytical studies cumbersome. In addition to the simulation results, simple theoretical analysis will be used whenever possible, to try and put the results into perspective.

A.5 Synopsis – How this Thesis Is Organized

This thesis is divided into two parts and nine chapters. Although chapters can be read independently, cross references are given when needed. The exception is Chapter 5, which is needed by all chapters in the second part. The first part is

composed by chapters 1 – 4 (Appendixes A– D). The main conceptual aspects are broached without getting lost in complicated maths and losing sight of the main goal. It can be seen as a tutorial, a preparation for things to come in the second part.

- Chapter 1 presents the motivation, states the research goals, and outlines the current work. It answers the questions –"*what was done?*" and "*why was it done*?"
- Chapter 2 presents the main aspects of the UMTS standard needed to understand this thesis. The answer to the question – "*where is it applicable?*" is given here and in the next chapter.
- Chapter 3 briefly discusses the mobile radio channel model and the different characteristics that impact the performance of a smart antenna system.
- Chapter 4 introduces the different advanced antenna strategies available to mitigate the limitations of the mobile radio channel. This chapter alongside the practical chapters answer –"*how was it done?*"

The second part consists of chapters 5 – 9 (Appendixes E– I). It details the simulator, the simulation methodology, presents the results and closes this thesis. Some deeper and less generical issues that would not fit in the previous conceptual chapters are also taken into consideration in the appropriate place. The chapters in this part respond the questions – "*how was it done?*" and "*what were the results?*". The writing style here is more straightforward, since the aim is to present and analyze the achieved results objectively, as opposed to the contextual character of the first part. Chapter 5 can be seen seen once more as the exception. It interfaces the two parts so that the transition is not so abrupt.

- Chapter 5 presents the basic principles behind different types of network simulators, and generically describes the complex dynamic network simulation tool used in order to obtain the results presented thereinafter. Additionally,

the simulation methodology and the default configuration of the simulator employed subsequently are introduced. Finally, achieved reference results are presented.

- Chapter 6 deals with the DL capacity gain that is obtained when deploying dual antenna Rake receivers at the mobile.

- Chapter 7 investigates the capacity gain when beam forming AAs are present at the base-station (Node-B). Additionally, specific topics such as the selected number of antennas, the utilized radiation patterns are discussed in this chapter.

- Chapter 8 can be seen as a mix of the two previous chapters, for the two techniques are simulated ("deployed") together.

- Chapter 9 concludes this work. The achieved results and the learned concepts are discussed, propositions for future work are also addressed here, answering the question "*what else can be done?*".

Apêndice B

The UMTS Standard

This chapter gives a generic overview of the FDD mode of UMTS. Since a flood of unnecessary information is to be avoided, only the features that are relevant to this thesis are considered. A thorough overview of UMTS is given in [6]. The UMTS standard consists of hundreds of documents. A complete set of documents is generated for each evolution stage ("Release") of the standard. The first release of UMTS was Release' 99, followed by Releases 4 and 5. Currently the functionality of Release 6 is under discussion within 3GPP (3^{rd} Generation Partnership Project) [5].

The chapter begins with a presentation of possible UMTS services followed by a short description of the UMTS physical layer and its basic architecture. This description is in line with the specifications for Release' 99.

B.1 UMTS Services

Second generation systems like GSM, were originally designed for efficient delivery of voice services, but the demand for more bandwidth consuming interactive multimedia services like video-on demand and internet access is growing rapidly around the world and this trend is likely to continue for several years. With that in mind UMTS networks, on the contrary, have been designed from the very beginning for flexible delivery of any type of service.

In general, applications and services can be divided into different groups depending on how they are considered. Specially, when a system is highly loaded, it becomes important to prioritize services according to their requirements, this prioritization is known as *Quality of Service* (QoS) differentiation. UMTS defines four traffic classes with different QoS requirements: *conversational*, *streaming*, *interactive* and *background*. The most important parameters distinguishing them are maximum delay sensitiveness, delay variation (jittering), and bit error rates.

The conversational and streaming classes are typically transmitted as *real-time* (RT) connections over the air interface, while the interactive and background services are transmitted as *non-real time* (NRT) packet data.

The conversational class is characterized by very low end-to-end delay and nearly symmetric traffic between UL and DL in person-to-person communications. Streaming class applications are very asymmetric and withstand more delay than the conversational services. They also tolerate more delay variation due to the presence of a dejitter buffer at the receiver. The interactive class is characterized by the request response pattern of the end user. At the message destination there is an entity waiting for a response within a certain time. The background class assumes that the destination is not expecting the data within a certain time [6]. In the last two classes, the messages should be transferred transparently, i.e with a low bit-error rate.

During the simulations carried out in chapters E, F, G and H the streaming and interactive classes have been used for the RT and NRT traffic respectively. Table B.1 summarizes the UMTS traffic classes.

Now, it is time to catch a glimpse of the system architecture that makes delivery of any type of service possible.

B.2 System Architecture

The system architecture of Release' 99 of UMTS is illustrated in Figure B.1. The UMTS system can be functionally divided into 3 parts: the core network, the UMTS Terrestrial Radio Access Network (UTRAN) and the User Equipment (UE). Throughout this report the terms "mobile","terminal" and UE are used interchangeably.

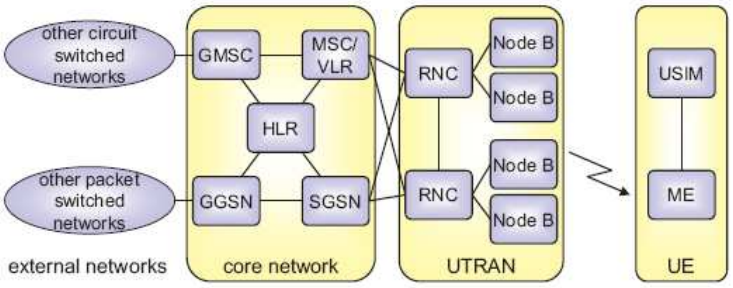

Figure B.1: UMTS system architecture. Extracted from [29]

Traffic Class	Example Applications	Traffic Characteristics
Conversational	Voice call Video call Video-gaming	Stringent and low delay Minimize delay variation Real time traffic
Streaming	Streaming video Streaming audio	Minimize delay variation Real time traffic
Interactive	Web/WAP browsing E-Commerce Server access	Request response pattern Minimize bit-error rate Non real-time
Background	File download SMS/MMS Mail download	Low time sensitivity Minimize bit-error rate Non real-time

Table B.1: UMTS Traffic Classes

B.2.1 Core Network

The core network of Release' 99 of UMTS is based on the GSM core network. It is responsible for switching and routing calls and data connections to external networks[1].

The main parts of the core network are the Home Location Register (HLR), the Mobile Switching Center/Visitor Location Register (MSC/VLR), the Gateway MSC (GMSC), the Serving GPRS (General Packet Radio Service) Support Node (SGSN) and the Gateway GPRS Support Node (GGSN). In Release 4 and 5 new entities have been added. Since the core network is out of the scope of this work, no further details are given, the interested reader can refer to [6] for more details.

B.2.2 UMTS Terrestrial Radio Access Network

The UMTS Terrestrial Radio Access Network (UTRAN) comprise one or several Radio Network Subsystems consisting of one *Radio Network Controller (RNC)* that is connected to several *Node- Bs*. Node-B is the acronym for base station in the UMTS specification. In order to improve the readability I will use the term base station (BS) throughout this thesis, except for this section.

Radio Network Controller

The RNC is the network element that is responsible for the control of the radio resources of UTRAN. When a UE is connected to the UMTS network (i.e., when it is not in idle mode [6]), its identity is known by its serving RNC [2]. Moreover it interacts with the core network and is responsible for the radio resource control protocol, e.g. scheduling of packet data, power control, handovers, code allocation,

[1]The external networks can be either circuit-switched, for example, the existing telephony system; or packet-switched, e.g. the Internet.

[2]The possibility of having a UE connected to several RNCs is out of the scope of this work and therefore is not addressed here.

etc [3].

Node-B

A Node-B can serve several sectors of a base station site. Its main task is to convert the data received from the RNC to the physical layer. Furthermore, the Node-B does measurements for radio resource management and reports them to the RNC. Additionally, the Node-B is also responsible for the fast power control.

B.2.3 User Equipment

The User Equipment (UE) consists of two parts: the Mobile Equipment (ME), which is the radio terminal used for communication over the radio interface, and the UMTS Subscriber Identity Module (USIM), a smart card that holds the subscriber identity, performs authentication algorithms, and stores authentication and encryption keys. Furthermore the USIM holds some subscription information that is needed at the terminal.

B.3 Physical Layer Aspects

B.3.1 Basic CDMA Concepts

In Code Division Multiple Access (CDMA) systems like UMTS, all data streams (users) share the same frequency at the same time, i.e. all data streams are transmitted continuously on the same frequency. Figure B.2 depicts this situation.

An obvious question is: how can they be separated? A code, which is orthogonal to all other codes, is assigned to each data stream. This code is used to spread the narrow band data in order to occupy the entire available bandwidth.

[3]Section B.5 deals with power control, packet scheduling, handovers, etc.

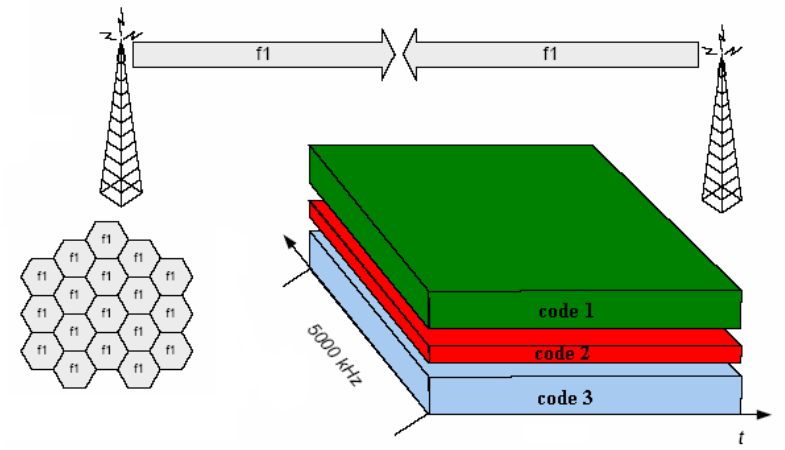

Figure B.2: Allocation of bandwidth in the time frequency space.

Spreading means that each data symbol is multiplied with a pseudo-noise[4] sequence (PN) of length

$$SF = \frac{R_c}{R_{data}}, \tag{B.1}$$

where SF, R_c and R_{data} represent the *spreading factor*, the *chip* [5] rate and the symbol rate. Basically, at the cost of bandwidth, we are obtaining a *processing gain*, which equals the spreading factor and represents the gain in SNR achieved by processing (despreading and integrating) a spread-spectrum signal over an non-spread (or spread with a different code) signal. Note, from (B.1), that for a fixed chip rate, the higher the symbol rate, the smaller the gain. More details about CDMA systems can be found in [6, 13, 14].

The chip rate in UMTS FDD is 3.84 Mchips per second, with a carrier bandwidth of 5 MHz. The wide bandwidth, hence the name WCDMA, allows the support of high user data rates, and opens for exploitation of multipath diversity. Separate 5 MHz frequency bands 190 MHz apart are used for the uplink and the downlink.

[4]A pseudo-noise sequence is a periodic binary sequence with a noise like waveform that is usually generated by means of a feedback shift register [13].

[5]Chip is the rectangular pulse which occupies the whole bandwidth.

B.3.2 Spreading and Scrambling

Strictly speaking, the spreading process includes two operations as shown in Figure B.3. First, the data is spread or channelized (increasing the bandwidth) with a *channelization code* taken from a Orthogonal Variable Spreading Factor (OVSF) code tree which is derived from the set of Walsh codes [31].

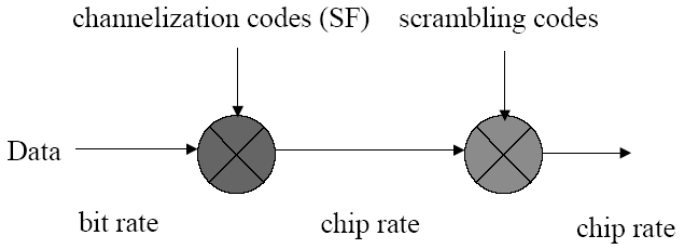

Figure B.3: Spreading and Scrambling.

The tree-structured codes are generated recursively according to the following equation,

$$c_{2n} = \begin{pmatrix} c_{2n,1} \\ c_{2n,2} \\ \vdots \\ c_{2n,2n} \end{pmatrix} = \begin{pmatrix} \begin{pmatrix} c_{n,1} & c_{n,1} \\ c_{n,1} & -c_{n,1} \end{pmatrix} \\ \vdots \\ \begin{pmatrix} c_{n,n} & c_{n,n} \\ c_{n,n} & -c_{n,n} \end{pmatrix} \end{pmatrix} \tag{B.2}$$

where c_{2n} is the orthogonal code set of size $2n$. Codes within the same layer constitute a set of orthogonal functions and are thus orthogonal. Furthermore, any two codes of different layers are also orthogonal except for the case that one of the two codes is a mother code of the other. For example, code $c_{4,4}$ is not orthogonal to codes $c_{1,1}$ and $c_{2,2}$. Figure B.4 depicts the OVSF code tree.

Each level in the code tree corresponds to a particular SF. *The number of codes in a particular level and the length of all the codewords in that level are both equal to the SF.* Hence, the number of available channelization codes is not fixed, it depends on the data rate and the SF of each physical channel.

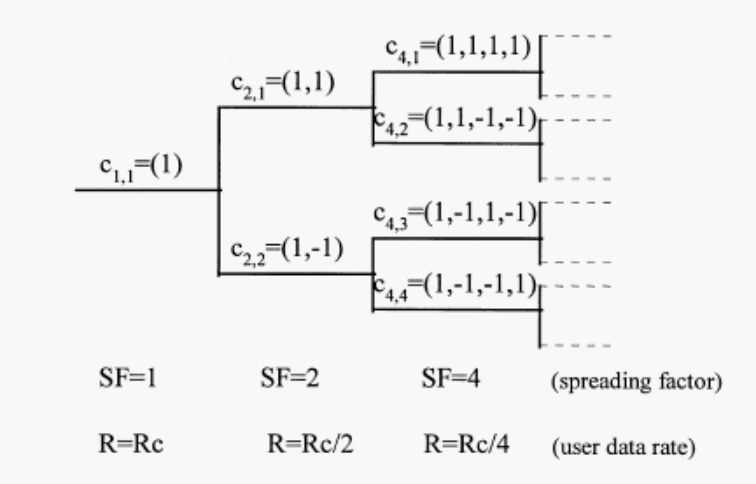

Figure B.4: OVSF code tree. Extracted from [6]

However, nothing is perfect, OVSF codes channelization codes have relatively poor correlation properties [15]. The codes exhibit a significant amount of auto-correlation at lags other than the zeroth lag. In a real world scenario due to multipath propagation (see section C.3 for details) a mobile usually receive multiple copies of the base station's signal with different delays. This implies that, such copies of the desired user signal will contribute with a significant amount of unwanted auto-correlation products to the desired correlator output on the receiver side [6]. Moreover, the cross-correlation of two OVSF codes also shows high correlation values at regular intervals. Thus, if two users separated by two OVSF codes are not perfectly time-synchronized, then the unwanted cross-correlation products will also be significant.

The previous discussion boils down to the fact that time dispersion (lack of synchronism), caused by multipath propagation, partially destroys the orthogonality of the different channels transmitted by the base station, i.e., they begin to interfere with each other. In this case, part of the interference that is not longer orthogonal is just attenuated with the processing gain when despreading the desired signal [3].

[6]See Section D.4.1 for a description of the CDMA Rake receiver, which includes several correlators.

This is where the scrambling codes mentioned in the beginning of this section come into picture. The complex-valued scrambling codes are obtained by I-Q multiplexing a Gold code and a delayed replica of the same Gold code [6, 13]. As expected, the scrambling codes have very good auto- and cross correlation properties [13, 15]. In the second step of Figure B.3, they are used to scramble the data stream. The scrambling operation does not increase the bandwidth of the signal but makes signals of different sources separable as different sources use different scrambling codes. This is the only code separating the asynchronous UL users. In the DL, the scrambling codes separates the cells. Due to its good auto-correlation property, the unwanted correlation products from the desired user's multipaths will also be very small.

According to the UMTS specifications, *only one* OVSF code tree per scrambling code is available, which *imposes a hard limit* on the cell capacity that can be achieved with one single scrambling code per cell. In order to overcome this limitation, one primary and 15 secondary scrambling codes are allocated to each cell. As spreading codes under different scrambling codes are not orthogonal to each other, the secondary scrambling codes are only used if another instance of the OVSF code tree is necessary to grant extra capacity. This is a very crucial point and will be the subject of some extra considerations later in this report.

B.4 UTRA Channels

Three separate channels concepts in the UTRA have been defined: logical, transport, and physical channels.

- Logical channels define what type of data is transferred.
- Transport channels define how and with which type of characteristics the data is transferred by the physical layer.
- Physical data define the exact physical characteristics of the radio channel.

One might wonder, what all these channels are. The logical channels can be seen as services that the Medium Access Control (MAC) protocol offers to the Radio Link Control (RLC) protocol. Both, MAC and RLC are sub-layers of the Data Link Layer (Layer 2). See [6] for details.

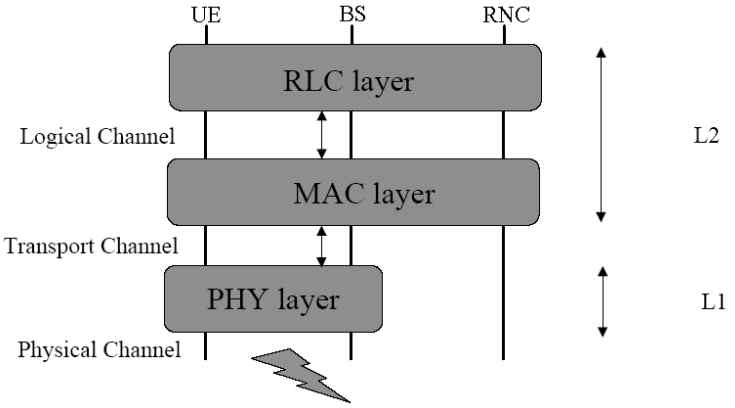

Figure B.5: Part of the UTRA-FDD radio interface protocol stack.

The transport channels, in turn, are services that the physical layer offers to the MAC layer. The physical layer is required to support variable bit rate transport channels in order to offer bandwidth-on-demand services, and to be able to multiplex several services to one connection. As one image is worth a million words, Figure B.5 depicts this structure in a clear way.

In Release' 99, there are basically two types of transport channels: dedicated transport channels and common transport channels. As the naming convention suggests, the former is reserved for a single user only, whereas the latter is shared by all or a group of users in a cell. A description of these channels is given next.

B.4.1 Dedicated Channels

The Dedicated Channel (DCH) is the only dedicated transport channel, i.e. it is exclusively allocated to one UE. The DCH carries all higher layer information intended for a given user including data for the actual service as well as higher layer control information (e.g. handover commands). The DCH uses fast power control

and fast data rate adaptation on a frame-by-frame [7] basis. In the physical layer, the DCH is mapped onto the Dedicated Physical Channel (DPCH) that consists of two channels, the Dedicated Physical Data Channel (DPDCH) that carries the actual data and the Dedicated Physical Control Channel (DPCCH) that carries physical layer information, e.g pilot sequence. As the modulation scheme is different in up- and downlink, the structure of the DCH is also different for the two link directions.

In the DL the DPDCH and DPCCH are time multiplexed forming a DL dedicated physical channel (DPCH), as shown in Figure B.6. The user specific DPCH is differentiated from the others by its channelization code. Finally, the modulation scheme used for the DL DPCH is quadrature phase shift keying (QPSK) [13].

For the sake of completeness, since the DCH is the channel used in all simulations of this thesis, the uplink slot structure of the DCH is shown in Figure B.7.

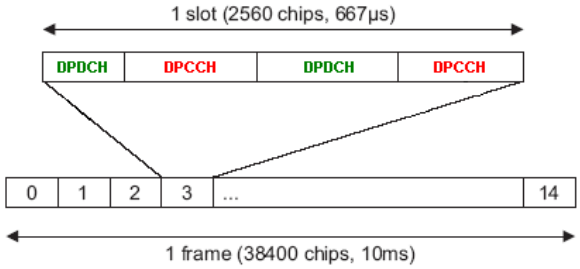

Figure B.6: Downlink dedicated channel structure.

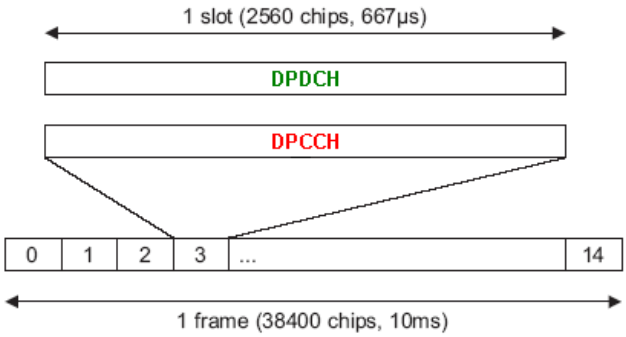

Figure B.7: Uplink dedicated channel structure.

[7] UTRA channels use a 10 ms radio frame structure.

In the UL, one scrambling code per UE is used. Channelization codes are used to separate different channels that are transmitted by a certain UE at the same time. Signals transmitted by different UEs use different scrambling codes. Furthermore, the DCH is mapped onto a DPCCH and one or more (up to six) DPDCHs, which are I-Q/code multiplexed.

The modulation scheme for the UL DPDCH and the UL DPCCH is binary phase shift keying (BPSK). It is worth mentioning that this modulation scheme has been chosen in the uplink direction because the normal time-multiplexed QPSK modulation used in the downlink would generate audible interference during discontinuous transmission (DTX) [8].

Finally, the DCH supports data interleaving and two different channel coding methods, convolutional and Turbo coding. The former is meant for relatively low data rates and the latter is applied for higher data rates. Channel coding adds extra bits (redundancy) to the data flow in order to allow detection or even correction of bit errors that might be introduced during transmission. Both coding schemes provide considerable *coding gains*, specially Turbo coding. Coding gain expresses how much more signal energy per data bit for the same level of noise (E_b/N_0) is needed by the uncoded signal. Interleaving mixes up bits of coded data blocks, spreading out adjacent bit over several data blocks, thus offering protection against error bursts by adding temporal diversity (see Section D.4). The interested reader can refer to [13, 31] for more information on these topics.

B.4.2 Common Channels

Six types of common transport channels have been defined in Release' 99: broadcast channel (BCH), forward access channel (FACH), paging channel (PCH) and downlink shared channel (DSCH) – all being DL channels. Random access channel (RACH) and uplink common packet channel (CPCH) – being UL channels.

[8]The audible interference is not an issue in the downlink since the common channels are transmitted continuously

Common channels do not have soft handover, but some can be power controlled. The main purpose of these channels is to transmit network or cell specific information (signalling). New channels for High-Speed Downlink Packet Access (HSDPA) are not considered here. Since the focus of this project is on the dedicated channels it suffices to say that it is also possible to use the RACH and FACH for transmitting small user data packets. Should readers wish a more detailed description, they can refer to the specialized literature [6].

B.4.3 Mapping the Transport Channels onto the Physical Channels

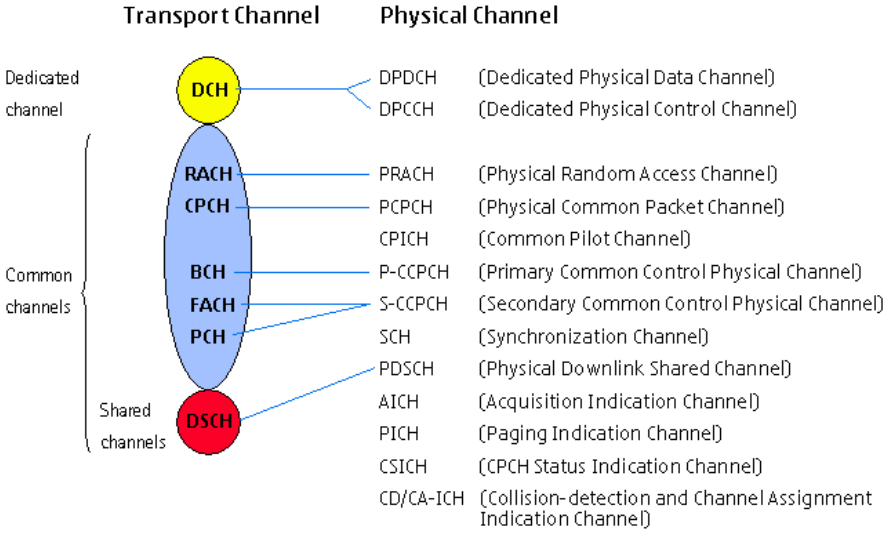

Figure B.8: Mapping of transport channels onto physical channels.

Figure B.8 shows the mapping of transport channels onto the physical channels. Besides, there exist a group of physical channels just for signaling purposes, those have no corresponding transport channels to carry.

Among these channels, the Common Pilot Channel (CPICH) deserves some extra clarifications, for reasons that will become clear in chapters D and G. For the moment, it is enough to know that the function of the CPICH is to aid the channel estimation at the terminal. Intra-mode handovers (see Section B.5.2) are also based

on measurements performed on the CPICH. There are two types of CPICHs, the Primary and the Secondary (P-CPICH and S-CPICH). The P-CPICH is always spread with a fixed channelization code with a spreading factor of 256 under the primary scrambling code, like most common channels, it is broadcasted over the entire cell area, and there can be only one P-CPICH per cell. The S-CPICH can be spread by any channelization code of length 256 and can be under either the primary or a secondary scrambling code. There maybe none, one or several S-CPICHs per cell. Moreover a S-CPICH may be transmitted over the entire cell or only a part of it.

A basic UMTS network requires the following common transport channels: BCH, FACH, PCH and RACH.

B.5 Radio Resource Management — RRM

Radio resource management (RRM) defines the algorithms responsible for an efficient utilization of the air interface. The family of RRM algorithms comprises the handover, power, admission and load control, plus the packet scheduling functionalities. The main goals of RRM are:

- Guarantee planned coverage.
- Ensure requested link quality (QoS).
- Ensure planned capacity.

RRM is a very extensive subject and has been (and still is) largely studied. Typical location of the algorithms are shown in Figure B.9. Readers can find very interesting and comprehensive material in [6, 7, 9, 10, 11, 12], in the following, the working principles of the main RRM algorithms are described:

Load Control

The main purpose of the load control (LC) is to guarantee system stability, making sure that it is not overloaded. If the system is properly planned, overloads will be rare, but if they do occur, it is the LC's task to take the appropriate measures to bring the system back to its desired load.

Resource Manager

The resource manager (RM) is the entity that manages the allocation of proper spreading codes among the UEs in an optimum way.

The other members of the RRM family are discussed separately in the next sessions because of their relevance to this project and inherent complexity.

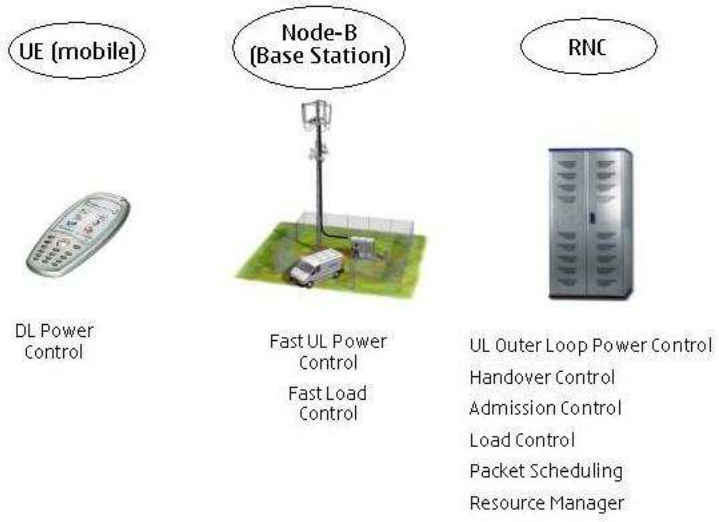

Figure B.9: Location of RRM algorithms.

B.5.1 What Is the Power Control Good for?

Tight and fast power control (PC) is probably the most important aspect in WCDMA. It is used to overcome the so-called CDMA *near-far problem*, i.e. if mobiles are not power-controlled the base station receives much more power from

a mobile close to it than from one far from it. Why is that so? The answer is straightforward, the farther the transmitter is from the receiver, the larger the path loss; more details on path loss can be found in Section C.2.

Moreover, link and system levels benefit from PC. At the link level, PC at a rate of 1.5 kHz is capable of mitigating fading, thus compensating rapid changes in propagation conditions for low to moderate mobile speeds [6]. At system level, it increases capacity, since it decreases interference from other users by keeping the signal at the minimal required level needed to achieve the quality requirements. Fading is described in Section C.3, while the relationship between interference level and system capacity is discussed in Section B.5.3.

Before leaving power control behind, outer loop power control should be mentioned. It adjusts the target Signal to Interference Ratio (SIR) of the link according to the service used and the achieved Block Error Rate (BLER). The SIR target is adjusted at a slower rate, $(10-100)$ Hz, and signaled via higher layers. By doing so, we let the SIR target float around the minimal value, instead of setting the SIR target for the worst case.

B.5.2 The Idea Behind Handovers

Mobility provides the possibility of being reachable anywhere and at any time for the end-user. In order to guarantee mobility, handovers (HOs) are needed; they ensure that, whenever a mobile is moving from one base station area/cell to another, the signal is handed over to the target base station.

In UMTS, this functionality is taken care of by the handover control (HC), which alongside power control, tries to maintain the radio link quality. The HC minimizes interference by optimum cell selection in HO. The following procedures are supported by the HC:

Soft/Softer handover: Intra-frequency handovers, which rely on pilot quality measurements conducted at the UE.

Hard handovers: Inter-system handovers, to UTRA TDD [9] mode (or to another system, such as GSM) and inter-frequency handovers, to a different WCDMA frequency carrier. They rely on measurements done in a special mode called compressed mode [6].

In this project, only the first type of HO is being considered. In UMTS, a mobile can be connected to several BSs at the same time, this is known as *soft handover* (SHO), as opposed to *hard handover*, where the terminal is connected to only one BS at a time. *Softer* HO, means that the terminal is connected to two sectors [10] of one BS. Among the advantages of soft/softer HOs is the provided macro and micro diversity [11], and the guarantee of a smoother and seamless transition between cells. The macro diversity gain stems from the fact that antennas from different BSs experience different shadowing (see Section C.2), and can be combined to offer a protection against large-scale fading. The micro diversity is due to the additional paths created when receiving the same signal from multiple antennas [9].

SHO decisions are based on wide band P-CPICH E_c/I_0 measurements done at the UE and fed back to the RNC via Layer-3 signalling. A new SHO leg is added to the UE's active set [12] if the ratio between the strongest P-CPICH in the active set and that of the new SHO candidate leg is below a certain threshold, denoted *Wadd* for some time (*Tadd*). A SHO leg is removed from the active set if the aforementioned ratio is above a threshold (*Wdrop*) over a certain period denoted *Tdrop*. Refer to [6], page 245, for details.

[9] Details can be found in [6, 5]

[10] Sectorization is introduced in Section D.3

[11] Diversity is discussed in Section D.4

[12] The UMTS standard requires mobiles to be able to be in soft handover with up to six different base stations [32]

B.5.3 Admission Control

The admission control (AC) is the RRM algorithm responsible for deciding whether a new Radio Access Bearer (RAB) is admitted or if a current RAB (connection) can be modified. The RAB can be seen as an illusional fixed communication path between the UE and the core network.

The admission process roughly consists of two parts, depending on the type of traffic supported. Remember that UMTS supports various types of traffic. For RT traffic it must be decided whether a RAB is allowed to enter the network. For NRT traffic, there is a second step, the proper scheduling of the packets must be determined after the RAB has been admitted, this task is handled by the *packet scheduler*, which is the subject of the next section. Now, let us return to the AC.

The principle behind the AC is intuitively simple, if the new connection, i.e. additional load, causes excessive interference to the system, jeopardizing the planned coverage area or the quality of the existing connections, access must be denied. Separate estimates are made for uplink and downlink directions. Only if both uplink and downlink admission criteria are fulfilled and a spreading code is available, is the bearer setup or modification request accepted. In what follows, we will be dealing with the power-based load estimation because it automatically gives us a *soft capacity* [6].

When the maximum capacity is limited by the amount of interference in the air interface, it is by definition a soft capacity, since there is no single fixed value for the maximum capacity. This can be explained as follows. The less interference coming from the neighboring cells, the more channels will be available in the middle cell. If there is extra capacity available in the neighboring cells, it can be "borrowed" from them [6].

The readers might reasonably ask themselves: why are interference in the air interface and capacity related? The answer leads us to one of the major impairments of wireless communication systems, namely, *co-channel interference* (CCI).

CCI arises in cellular systems when signals intended to other users using the same carrier frequency reach the receiver of the desired user. Signals that miss an intended user become interference to users sharing a carrier frequency in the same or adjoining cells. Putting it simple, if you want to hear what someone is saying but music is being played loud next to you, the music becomes interference to your ears and the other person will probably have to scream to be heard, increasing even further the noise level perceived by someone else who is interested neither in the music nor in your interlocutor's message. Therefore, it is crucial to manage CCI in order to maximize the capacity of a wireless system. In CDMA systems, which allow a frequency reuse of 1, CCI is frequently associated with *multiple-access interference* (MAI), which arises because of the deviation of DL spreading codes from perfect orthogonality. Recall from Section B.3.2, that if this occurs, own cell users sharing one scrambling code also interfere with each other. The orthogonality of own cell[13] interference plays a major role in the DL of UTRA FDD. Hence, differentiation between the types of interference is of paramount importance here, consequently the following naming conventions are introduced: *Intra-cell* interference denotes the interference coming from the user's own cell, while *Inter-cell* interference denotes the interference coming from all other cells. The main difference between them is explained next.

Inter-cell interference is non-orthogonal, due to the use of different scrambling and channelization codes and can be modelled as AWGN, thus this interference is simply scaled down by the SF in the despreading process. Intra-cell interference could, in theory, be completely removed during despreading if orthogonality between channelization codes were kept.

Considering that both kinds of interference have radically different natures, from a WCDMA system perspective it is interesting to introduce G, the *geometry factor* [6]. It is defined as the power ratio of the total wideband received power from the own cell to the total received wideband power from other cells plus the thermal noise. Its value indicates whether the user experienced interference is intra-

[13]Assuming one scrambling code per cell.

or inter-cell dominated and its impact is discussed further in Section E.3.3.

$$G = \frac{P_{own}}{P_{other} + P_{noise}} \tag{B.3}$$

Now, after having digressed a little, let us return to the AC itself. Since we are only dealing with the DL the AC algorithm for the UL will be omitted, it suffices to say that is very similar to the DL algorithm presented next.

The AC uses thresholds set during the radio network planning. A RT bearer will be admitted if the *non-controllable* DL load, $P_{TX|NC}$, fulfills the equation

$$P_{TX|NC} + \Delta P \leq P_{TX|\text{Target}},$$

and if the current total load[14], $P_{TX|\text{Total}}$, fulfills

$$P_{TX|\text{Total}} \leq P_{TX|\text{Target}} + P_{TX|\text{Offset}},$$

where $P_{TX|\text{Target}}$ defines the optimal operational point and $P_{TX|\text{Offset}}$ is an offset defining the maximum margin in which $P_{TX|\text{Target}}$ can be exceeded. The DL non-controllable load, $P_{TX|NC}$, consists of the load of real time users in the own cell, and the load of NRT users operating at the minimum bit rate. ΔP includes the power reserved for the new connection and the additional power rise of the existing connections due to the additional interference generated by the new connection. It can be estimated based on *a priori* knowledge of the required E_b/N_0, the requested bit rate and the pilot feedback report from the mobile [6].

If the first threshold, $P_{TX|\text{Target}}$, is exceeded the preventive LC actions are initiated. If $P_{TX|\text{Target}} + P_{TX|\text{Offset}}$ is exceeded, the cell is then overloaded, and, actions to bring it back to normal must be taken. We can thus see that AC and LC are intrinsically related.

[14] $P_{TX|\text{Total}}$ equals the sum of non-controllable plus controllable load. The latter is defined in the next section. Here the load is determined by the transmission power.

B.5.4 How Does the Packet Scheduler Work?

It was said in the previous section, that NRT radio access bearers need to be scheduled after being admitted. This task is the job of the packet scheduler (PS), which is located in the RNC. The PS functionality is divided into User-Specific and Cell-Specific packet scheduling. The User-Specific part controls the allocation of transport channels and bit rates to the users depending on their traffic volume. The Cell-Specific part periodically divides the NRT capacity between simultaneous users. The target of the scheduling is to use efficiently all remaining cell capacity for NRT connections, maintaining interference levels within planned values so that RT connections are not affected [6].

There are different approaches to divide the available capacity between the simultaneous users. They can be categorized into the following three classes: Fair Throughput, Fair Resource and C/I Scheduling.

The goal of fair throughput scheduling is to give all users the same throughput, independent of where they are. When dealing with the DCH, resources mean power. This scheduling method gives the most fair throughput distribution at the cost of a lower cell throughput.

Fair resource scheduling allocates the same amount of power to the different users, i.e. all users get the same amount of resources. This leads to a lower throughput at the cell border compared to close to the BS, so the user throughput is not fairly distributed. The cell throughput of this scheme is higher than the cell throughput of a cell using Fair Throughput scheduling.

When C/I scheduling is used, packets belonging to links with a good quality have higher priority than packets with a lower quality link. The C/I scheduler provides maximum system capacity at the expense of fairness, because all resources can be allocated to a single user with good channel conditions.

In this work, the first method is the one used; despite the higher capacity, C/I scheduling may not be acceptable due to its unfairness. Fair resource scheduling

does provide on average higher bit rates, but fair throughput is useful for guaranteed bit rates services because it supports more users with a given bit rate [6].

The principle of downlink [15] load distribution in a cell is depicted in Figure B.10(a); the non-controllable power has already been described, the controllable power is caused by the own-cell NRT traffic. The idea is simple, since $P_{TX|\text{Target}}$ is the optimal operating point of the system, the PS has to continuously control the NRT load, by either increasing or decreasing bit rates (high bit rate connections require more power than low bit rate ones), so that it fluctuates around this target. If the green area is big, capacity is being wasted.

Figure B.10(b) displays the meaning of the $P_{TX|\text{Allowed}}$, whose value is used at the beginning of the bit rate allocation algorithm. It is computed in the following way:

$$P_{TX|\text{Allowed}} = P_{TX|\text{Target}} - P_{TX|\text{Total}} - P_{TX|\text{NrtInactive}},$$

where $P_{TX|\text{NrtInactive}}$ is the the power reserved for inactive NRT traffic [16]. These reserved powers are the estimated powers needed if the inactive calls should become active.

The bit rate allocation is presented in Figure B.10(c), it includes the *Allocate bit rates* and the *Increase and Decrease loading* sub-algorithms which are not shown here, but are based on the fair throughput strategy. The $P_{TX|\text{Allowed}}$ value is used inside the *Increase Loading* sub-algorithm to determine if the bit rate increase can be accepted.

Basically, the instantaneous DL total transmitted power is measured by the BS, then if it is below the target, the PS can increase the amount of NRT bearers. If it is above the target, but within the allowed offset, the PS can not increase NRT load, but can still change NRT bit rates. Finally, if the instantaneous load exceeds the $P_{TX|\text{Target}} + P_{TX|\text{Offset}}$, the PS must decrease the bit rates of NRT bearers. In a well planned system, overloads would rarely occur and load would never be

[15] The principle for the uplink is the same, but the prefix P_{rx} has to be used instead of P_{tx}.

[16] NRT inactivity is further discussed in Section E.4.5

above the threshold. If this occurs users will start being dropped. It is also worth mentioning that minimum and maximum allowed bit rate values can be defined. In this work the allowed bit rates are 32, 64, 128, 256, 320 and 384 kbit/s.

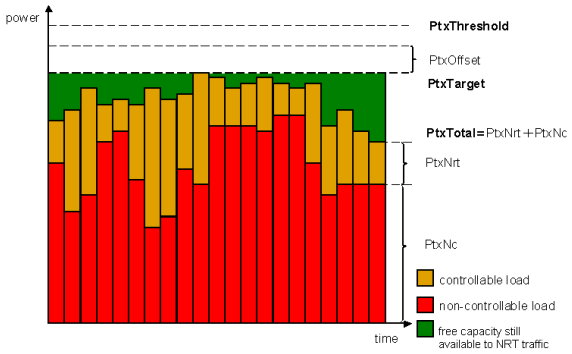

(a) Load distribution in a WCDMA cell.

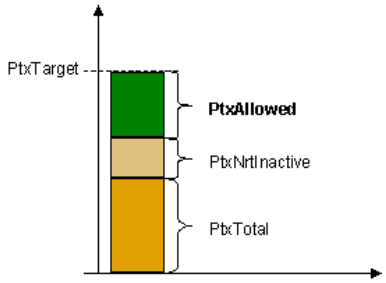

(b) $P_{TX|\text{Allowed}}$.

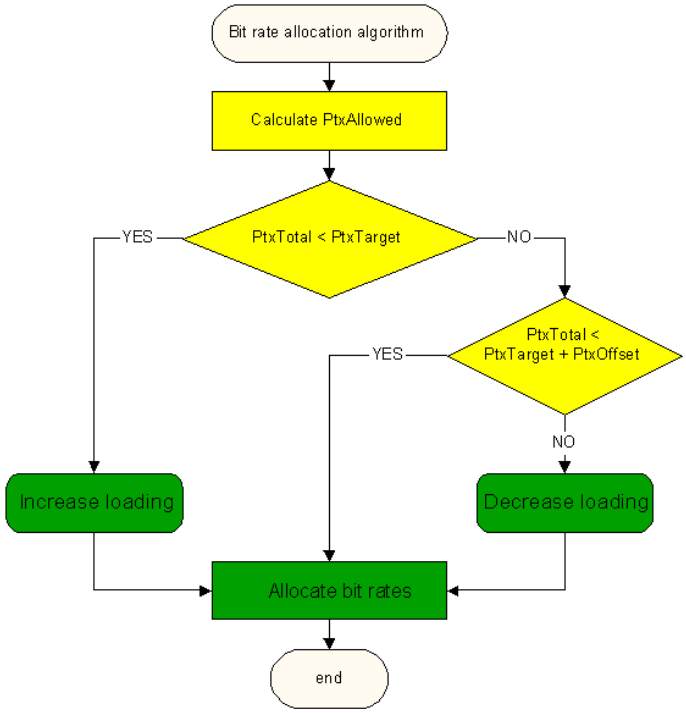

(c) PS bit rate allocation algorithm.

Figure B.10: PS basic structure.

Apêndice C

The Mobile Radio Channel

In this chapter we deviate our attention from the UMTS system and focus on the mobile radio channel. Why? Putting it simple, in order to evaluate the performance of smart antenna systems, it is necessary to understand the fundamental problems and limitations that are imposed by the mobile radio channel.

The author tried, during the course of this project, to not lose sight of the "big picture". This chapter, and for that matter, the next one are not intended to be too mathematical, the main aim is to get to the heart of what one needs to know in order to understand this thesis. Therefore, the next sections describe some of the most important characteristics of a mobile radio channel and the corresponding parameters used to measure the effects. The emphasis is on intuitive understanding of the principles, instead of getting lost in long mathematical expressions. The ultimate goal is to present the material in a way that is relevant to the thesis project. References to in-depth discussions are given for interested readers.

C.1 Important Aspects of Signal Propagation

Unlike wired channels that are stationary and predictable, radio channels are extremely random and hard to analyze. The transmission path between the transmitter and the receiver can vary from a simple line-of sight scenario to one that is severely obstructed by buildings, hills, etc. Modeling of the radio channel

is typically done in a statistical manner.

The mechanisms behind electromagnetic wave propagation are diverse. It can be said that a signal propagating through the wireless channel usually arrives at the destination along a number of different paths, referred to as *multipath propagation*. These paths generally arise from reflection, diffraction and scattering [33].

Reflection occurs when a propagating electromagnetic wave impinges upon an object with large dimensions when compared to the wavelength of the propagating wave. Examples are the surface of the earth, buildings, etc.

Diffraction happens when the path between the transmitter (Tx) and the receiver (Rx) is obstructed by a surface that has sharp irregularities (edges). The resulting secondary waves (wavelets) are present even behind the obstacle, giving rise to a bending of waves around the obstacle. This phenomenon can be explained by Huygen's principle [23].

Scattering occurs when the there is a big number of obstacles per unit volume whose dimensions are small compared to the wavelength. When a radio wave impinges on a rough surface, the reflected energy is spread out (diffused) in all directions due to scattering. Objects such as lamp posts, street signs and foliage tend to scatter the energy in all directions, thereby providing additional energy at the receiver.

Propagation models, which try to capture the effects of radio propagation on the transmitted signal, can be broadly divided into two main classes: *large- and small-scale propagation models*. Large-scale models try to predict the mean signal strength for an arbitrary separation between the transmitter and the receiver. Small-scale or *fading* models try to characterize the rapid fluctuations of the received signal strength over very short distances or short time durations. Both types of models may be described by the physics of the three basic propagation mechanisms [23].

C.2 Large-Scale Path Loss

The received power, or its reciprocal, the mean path loss, is highly dependent on the transmission distance and environment. Most radio propagation models are derived using a combination of analytical and empirical[1] methods. Over time, various classical propagation models have emerged, which are now used to estimate the received signal level as a function of distance.

The simplest model of all describes the attenuation of a radio signal in a free space propagation situation, i.e. there is a line-of sight path (LOS) between the transmitter (Tx) and the receiver (Rx) due to isotropic power spreading, and is given by the famous Friis' inverse square law:

$$P_r = P_t \left(\frac{\lambda}{4\pi d}\right)^2 G_t G_r \tag{C.1}$$

where P_r and P_t are the received and transmitted powers, λ is the radio wavelength, d is the distance between the Tx and the Rx, and G_t, G_r are the gains of the transmit and receive one-element antennas, respectively.

In cellular environments, the main path is often accompanied by reflected paths which may interfere with the primary path. Specific models have been developed to consider this effect, they usually also include Tx and Rx antenna heights. What most models have in common, both analytical and empirical, is the fact that they indicate that the average received signal power decreases logarithmically with distance. The average large-scale path loss for an arbitrary distance between the Tx and the Rx can be generically expressed by using a path loss exponent [23]:

$$\overline{PL}(\text{dB}) = \overline{PL}(d_0) + 10n \log_{10}\left(\frac{d}{d_0}\right) \tag{C.2}$$

where n is the path loss exponent which indicates the rate at which the path loss increases with distance, d_0 is the close-in reference distance determined from measurements close to the Tx, and d is the Tx–Rx separation. The bars in (C.2) denote the ensemble average of all possible path loss values for a given value of d.

[1]The empirical approach is based on fitting curves that recreate a set of measured data.

If one plots the modelled path loss in a log-log scale, the result is a straight line with a slope of $10n$ dB per decade. As said before, the loss is very dependent on the propagation environment. If we take a look at (C.1), we see that, in that case, n equals 2. When obstacles are present, n increases. In fact, it may vary from 1.6 to 6. Typical values can be found in [34].

C.2.1 Shadowing

There is, however, one last important issue to be considered. Namely, *shadowing*. The model in (C.2) completely ignores the fact that two different locations with the same Tx–Rx separation might have completely different surrounding environmental clutters. What happens then, is that measured signals may differ considerably from the ensemble *average* value calculated by (C.2), a generalization of which can be written as [34]:

$$PL(d)[\text{dB}] = \overline{PL}(d_0) + 10n \log_{10}\left(\frac{d}{d_0}\right) + X_\sigma \tag{C.3}$$

This equation, where X_σ is a zero-mean random variable, states that at any value of d, the path loss $PL(d)$ is a *random variable* with a *log-normal* distribution (normal in dB) around the mean distance dependent value with a standard deviation σ (also in dB). It describes the long-term random shadowing effects of buildings or natural features in the terrain. The probability density function of a log-normal distribution with a mean value μ and variance σ^2 is [31]:

$$f(x) = \begin{cases} \frac{1}{\sqrt{2\pi\sigma^2}x} \exp -(\ln x - \mu)^2/2\sigma^2 & \text{if } x \geq 0 \\ 0 & \text{otherwise} \end{cases}$$

Typical values of σ are in the range of 5 to 12 dB [25].

The spatial *auto-correlation* of shadowing and has been shown experimentally to be correlated with the standard deviation of the log-normal fading [20]. The spatial correlation distance [2] and the mobile speed have a significant impact

[2]The coherence distance is defined at the distance where the spatial auto-correlation equals $1/e \approx 0.37$.

on the capacity results since they influence the performance of the handover algorithm. The reason for this is that the shorter the distance or the higher the speed, the harder it is to track long term channel variations [9].

Obviously, it is impossible to mention all propagation models, but at least, the most relevant concepts regarding the large-scale path loss have been addressed. More details will be given in chapter E, where the propagation model used in the simulations is described. Once the concepts presented here and in the next section are fully apprehended, it becomes rather easy to understand how the propagation losses are modelled in the simulator.

C.3 Small-Scale Path Loss

The major propagation problems encountered in the use of cellular radio in built-up areas are due to the fact that the antenna of a mobile frequently lies well below or inside the surrounding buildings. To put it simple, there is no line-of-sight path to the base station. Instead, multipath propagation often takes place, hence, two or more versions of the signal reach the receiver at different times via multiple paths. Even when a line-of-sight exists, multipath propagation still occurs.

This kind of propagation gives rise to the so-called small-scale fading, short-term fading or simply *fading* phenomenon: rapid fluctuations of the amplitude over a short period of time or distance. The reason for this is that the received signal is the vectorial combination of these multipath wave components coming from different directions having randomly distributed amplitudes, phases and angles of arrival.

As the mobile moves, even over short distances, there is a continuous change in the amplitude, phase and angle of arrival of the components of the received signal; the net result is that the received amplitude (envelope) of the received signal varies with location in a complicated (random) fashion. These signal components might add either constructively or destructively at the receiver, resulting in a variation of

the power level of up to $20 - 30$ dB over a distance of 0.5λ. What is worse, even if the mobile is stationary, the received signal may fade due to the movement of the surrounding objects.

In mobile radio channels, the Rayleigh distribution [3] is commonly used to describe the statistical time varying nature of the received envelope of a flat-fading [4] signal, or that of an individual multipath component [23]. Signal fading is a *spatial phenomenon* that manifests itself in the time domain as the receiver moves [6, 13].

These concepts are illustrated in Figure C.1. The "Global mean" line in the figure represents the estimate average value predicted the large-scale model, whereas the "log-normal fading" line represents shadowing. One can notice that the signal fades rapidly as the receiver moves, but the local average signal values change much more slowly with distance.

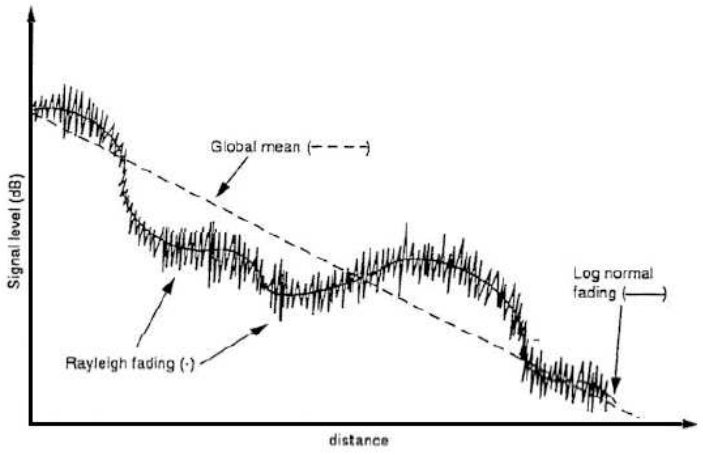

Figure C.1: Received signal level with log-normal and Rayleigh fading.

Propagation to or from a mobile in a multipath channel, causes the received signal energy to be spread (dispersed) in different domains: time (delay spread), frequency (Doppler Spread) and spatial (angle spread). These spreads have signif-

[3] If there is one dominant path (i.e. LOS condition), the envelope will have a Rician distribution with less severe fading.

[4] Defined later in Section C.3.1.

icant effects on the signal.

The mathematical details pertaining to the statistical characterization of channel dispersion will not be deeply addressed, yet some important concepts are touched. The interested reader can refer to [13, 31, 23] for more on these topics. Besides a simple concept, which describes the *severity* of fading in the time, frequency and spatial domains, is presented here, which leads to different channels characterizations, namely, time-, frequency, and space-selective channels. It is important to stress that these characterizations *are not mutually exclusive* and can be quantified in terms of the envelope correlation function defined as [33]:

$$\rho(\Delta f, \Delta t, \Delta \mathbf{z}) = \frac{< r_1 r_2 > - < r_1 >< r_2 >}{\sqrt{\left[< r_1^2 > - < r_1 >^2 \right] \left[< r_2^2 > - < r_2 >^2 \right]}} \tag{C.4}$$

where $< \cdot >$ denotes the ensemble average, r_1 is the received signal envelope measured at frequency f_1, time t_1 and spatial location $\mathbf{z}_1$, and with a corresponding definition for r_2. The arguments of the correlation coefficient are the frequency, time and spatial separations, $\Delta f, \Delta t, \Delta \mathbf{z}$, respectively. The next sections will try to shed some light upon these concepts. Section C.4 tries to summarize and put all these ideas in the same context.

C.3.1 Delay Spread

As stated earlier, multipath propagation is often characterized by several versions of the transmitted signal arriving at the receiver with different attenuation factors and delays. Before we proceed further, let us make two assumptions:

1. The channel under consideration is wide sense stationary [35].

2. The channel under consideration is a multipath channel where the propagation paths are statistically independent or at least uncorrelated.

The previous assumptions define the so-called wide sense stationary uncorrelated scattering (WSSUS) channels which are an important class of practical

channels. The radio propagation channel can be visualized as a system element that transforms the input signal into an output signal. It is therefore similar to a linear filter with the extension that the radio propagation channel is randomly time-variant.

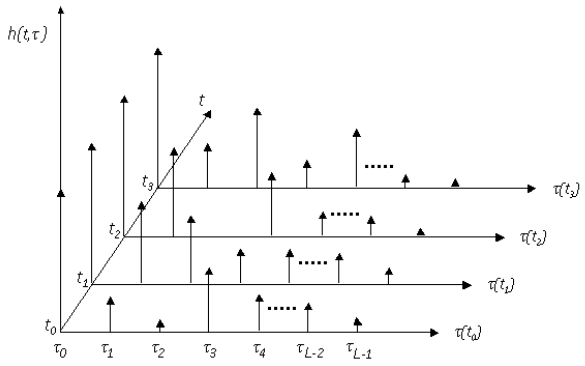

Figure C.2: An example of the time varying impulse response model for a multipath radio channel.

Let us observe Figure C.2 carefully. It illustrates an example of "snapshots" of the channel impulse response at different time instants $(t_0, t_1, \ldots, t_3)$, where t varies into the page. The multipath delay axis, τ, is segmented into *excess delay bins* ($\Delta\tau$). The excess delay is defined as the relative delay of the i-th multipath as compared to the first arriving component, τ_0, and is given by τ_i. All mutipath signals received within the i-th bin are represented by a single resolvable multipath component having delay τ_i. This quantization of the bins determines the time delay resolution of the channel model and is inversely related to the bandwidth of the transmitted signal. It is straightforward to understand that $(L-1)\Delta\tau$, where L is total number of equally-spaced multipath components, represents the *maximum excess delay* of the channel.

What the last figure is trying to tell us is that the channel can indeed be represented by its time-variant impulse response $h(t, \tau)$, also known as the channel *delay spread function* [31]. Mathematically, we denote $h(t, \tau)$ in complex equivalent

low-pass [5] signal domain in the form [31]:

$$h(\tau, t) = \sum_{l=0}^{L-1} \alpha_l(t) e^{-j2\pi f_c \tau_l(t)} \delta(\tau - \tau_l(t)), \tag{C.5}$$

where $\tau_l(t)$ is the propagation delay of the l^{th} path as a function of time, $\alpha_l(t)$ is the gain of the l^{th} path as a function of time, and f_c is the carrier frequency. The expression might seem complicated but the idea behind it is that $h(\tau, t)$ is a complex-valued Gaussian random process in the t variable. The Gaussian distribution stems from the central limit theorem, see [31, 35].

With the previous discussion in mind, let us move ahead and introduce the *power delay profile* concept which is deeply related to the delay spread function shown in (C.5). The autocorrelation of $h(\tau, t)$ is defined as

$$P_h(\tau, \Delta t) = E\{|h^*(\tau, t)h(\tau, t + \Delta t)\}.$$

Now, for $\Delta t = 0$, we may write $P_h(\tau) = E\{|h(\tau, t)|^2\}$. The function $P_h(\tau)$ describes the intensity (averaged over the fading fluctuations) of the scattering process at propagation delay τ and is called accordingly the *delay power spectrum* or *power delay profile* (PDP).

The PDP characterizes the multipath channel. The simplest profile model is the uniform PDP with L resolved paths having equal average powers. The sum of the average of the squared path gains of the uniform profile shape is given as $\sum_{l=1}^{L} E\{\xi_l\} = L$, where $\xi_l = \alpha_l^2$ is a random variable describing the power of the l^{th} path component. A more realistic profile, however, is the negative exponential PDP where the average power decays exponentially as the path delay increases. The average of the squared path gains is given as $E\{\xi_l\} = (1 - e^{-\epsilon})e^{-\epsilon l}$ with $l \geq 0$ and ϵ being the decay factor. Specific UMTS PDPs for different terrestrial environments exist and are presented in detail in Chapter E.

Many important channel parameters are derived from the power delay profile, which are usually represented as plots of relative received power as a function

[5] This representation removes the high-frequency variations caused by the carrier, making the signal more mathematically tractable [23].

of excess delay [23]. The two most important ones, often used to quantify the time dispersive properties of wide band multipath channels, are the *mean excess delay* (τ_{avg}) and the *delay spread* (σ_τ), which are defined, respectively, as the first moment and the square root of the second central moment of the power delay profile. Defining equations can be found in [13, 31, 23].

The previous conceptual analysis described the modeling of the time domain effects of the radio channel, i.e. how the channel spreads the signal in time. This spreading in the time domain is called delay spread and it is a natural phenomenon. However, sometimes it is more convenient to operate in the frequency domain, rather than in the time domain. Much like in filter theory, if we calculate $P_H(\Delta f, \Delta t) = \mathcal{F}\{P_h(\tau, \Delta t)\}$, where $\mathcal{F}\{.\}$ stands for the Fourier transform, we get a completely analogous characterization of the time-variant multipath channel in the frequency domain. If we do as before and set $\Delta t = 0$, we get the *frequency correlation function* $P_H(\Delta f)$. It provides us with a measure of the frequency coherence of the channel, the *coherence bandwidth* (B_c).

The coherence bandwidth is the delay spread's reciprocal in the frequency domain. It is a statistical measure of the maximum frequency separation for which the correlation of the signal amplitudes at two distinct frequencies becomes 0.5 and can be computed from (C.4) by setting Δt,and $\Delta \mathbf{z}$ to zero [33]. The coherence bandwidth and the delay spread are inversely proportional to each other.

This discussion can be summarized in the following way: if the transmission bandwidth of the signal is larger than coherence bandwidth, the signal will undergo *frequency selective fading*. It means that the different frequency components of the signal will experience different fading. In the time domain, this implies a large delay spread relative to the symbol duration. In this case, the channel induces intersymbol interference (ISI), loosely speaking, symbols "crashing" into one another, which severely degrades performance if not mitigated.

If the channel frequency response is approximately constant with a linear phase over a bandwidth larger than that of the transmitted signal, we speak of a *flat fading* channel. It means that the coherence bandwidth of the channel is much

larger than the bandwidth of the transmitted signal. Switching back to the time domain, the delay spread is very small when compared to the symbol period.

Now it is time to investigate other forms of channel selectivity. In the following, we focus our attention on the time varying nature of the channel.

C.3.2 Doppler Spread

The relative motion between the Tx and the Rx, also the relative motion of the obstacles in the radio channel causes random frequency modulation to the signal carrier frequency, since each multipath component has a different Doppler shift (phase change per time unit). The Doppler shift can be calculated as $\nu = \frac{v}{\lambda}\cos\alpha$, where v is the speed of the terminal, α is the angle between the direction of motion of the terminal and the direction of arrival of the wave, and λ is the RF wavelength. This means that when transmitting a sinusoidal wave at frequency f_c the received signal is shifted so that the apparent received frequency is $f_c + \nu$. If the mobile is moving towards the transmitter ν is positive, it becomes negative if the mobile is moving away from the transmitter.

Doppler shift causes a broadening of the received signal over a finite spectral bandwidth. In this case the *Doppler power spectrum* is defined as $P_D(\nu, 0) = P_D(\nu) = \mathcal{F}\{P_H(0, \Delta t)\}$, in which case we have set $\Delta f = 0$ and took the Fourier transform with respect to Δt. The function $P_D(\nu)$ gives us the signal intensity as a function of the Doppler frequency ν. In turn, the *Doppler Spread* (σ_ν) is a measure of this spectral broadening and can be defined as the range of frequencies over which the received Doppler Spectrum is essentially non-zero [31, 23]. It is worth of mention that σ_ν has been defined as the square root of the second moment of the Doppler Spectrum in [13], nevertheless both references agree on the definition of the Doppler Spectrum.

Doppler spread causes the channel characteristics to change rapidly in time, giving rise to the so-called *time selectivity*. As before, since $P_D(\nu)$ and $P_H(\Delta t)$ form a Fourier pair, the time domain dual of Doppler spread is called *coherence*

time (τ_c). It is a statistical measure of the time duration over which the received signal is essentially invariant, and quantifies the similarity of the channel response at different times [23]. In other words, it represents the time separation for which the correlation between the envelopes of the received signals at two time instants becomes 0.5 and can be computed from (C.4) by setting Δf,and $\Delta \mathbf{z}$ to zero [33]. Finally, τ_c is inversely proportional to σ_ν.

Depending on how quickly the transmitted baseband signal changes when compared to the changing rate of the channel, a channel may be classified either as *fast fading* or *slow fading* channel. Slow fading occurs if the coherence time of the channel is larger than the symbol time, i.e. the Doppler spread of the channel is much less than the baseband signal bandwidth, which is usually the case in WCDMA. In this case, the effects of the Doppler Spread are negligible at the receiver and the channel may be considered approximately static for some time, e.g. one slot.

Fast fading is just the opposite, it occurs if the coherence time of the channel is less than the symbol time, hence the channel impulse response will change during the transmission of a symbol, leading to *frequency dispersion/time selectivity*, which causes signal distortion. In the frequency domain, this means that the Doppler spread is larger than the baseband signal bandwidth. Understandably, this is associated with very low data rates (long symbol time) and and fast moving mobiles (low coherence time).

C.3.3 Angle Spread

We have not yet dealt with *angle spread*, (also known as *azimuth spread*) which gives us information about the spatial spreading of the signal.

Azimuth spread (AS or σ_a) at the receiver refers to the spread of the angles of arrival (AoA) of the incoming paths (i.e. from which direction). Likewise, AS at the transmitter refers to the spread of departure angle of the multipath (i.e. to which direction). AS will cause the paths to add up in a random manner at the

receiver as a function of the location of the receive antenna, hence it will be source of *space selective fading*. As with the definitions of coherence time and bandwidth of the channel, we can define the *coherence distance* (D_c) [6], which is inversely related to the AS, as the maximum spatial separation for which the correlation between the received signal amplitudes at two antennas becomes 0.5 and it can be computed from (C.4). As a result, two antennas spaced by more than the coherence distance tend to experience uncorrelated fading.

Nonetheless, one must also notice that there is a fundamental difference between azimuth dispersion observed at an elevated BS and a mobile station even though the propagation channel is assumed to be reciprocal. At an elevated BS, the incoming field is expected to be more concentrated in azimuth since the BS antenna is located well above surrounding scatterers [28]. Hence, the AoA at the base station is restricted to a smaller angular region, which leads to a larger coherence distance. This can be seen in Figure C.3. When the AS is large, which is usually the case on the terminal side in dense urban environments, a significant gain can be obtained from space *diversity*. Note that this usually conflicts with the possibility of using directional *beamforming*, which typically requires well defined and dominant signal directions, i.e. a low angle spread [33, 25].

What does it mean? It means that large angle spreads can be either beneficial or detrimental, depending on how antenna arrays are being operated, beamforming or diversity mode. This leads us to the next chapter, where these concepts are clarified, but before that, because getting a global view ("big picture", if you will) is an important issue to the author, an attempt is made in the next section to summarize the important concepts of the chapter and to show how they tie together. Of particular relevance is seeing how they each play a part in the general setting of this thesis project.

[6] This distance refers to the small-scale fading, not shadowing. Usually, D_c is in the order of 1λ to 10λ. An interesting analysis is found in [24].

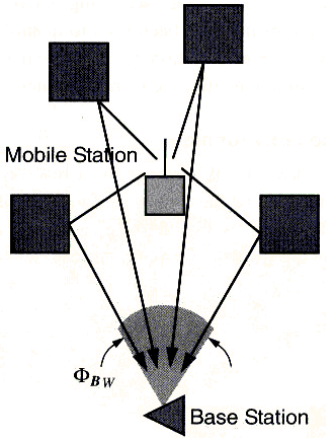

Figure C.3: AoA in a macro cell environment. Extracted from [14].

C.4 Contemplate

As was pointed out, there are two main kinds of propagation models: *large- and small-scale propagation models*. Large-scale models try to model the mean path loss, which is highly dependent on the transmission distance and environment. Shadowing and its modeling have also been broached. Small-scale or *fading* models which characterize the rapid fluctuations of the received signal are recapitulated and summarized here in Tables C.1 and C.2. In Table C.2, T_s and B_s represent, respectively, the transmitted signal's symbol period and baseband bandwidth.

Spread	**Time Domain**		**Frequency Domain**	
—	Parameter	Name	Parameter	Name
Delay	σ_τ	Delay Spread	B_c	Coherence Bandwidth
Doppler	τ_c	Coherence Time	σ_ν	Doppler Spread
—	**Angular Domain**		**Space Domain**	
Angle	σ_a	Angle Spread	D_c	Coherence Distance

Table C.1: Time, frequency and angular domain parameters

At this point, readers who got this far might ask themselves, what this all means from the WCDMA performance point of view. A very brief analysis which

	Fading	**Time**	**Frequency**	**Classification**
Delay Spread	Flat	$T_s >> \sigma_\tau$	$B_s << B_c$	Non-time dispersive and Frequency Flat
	Frequency Selective	$T_s < \sigma_\tau$	$B_s > B_c$	Time dispersive and Frequency Selective
	Fading	**Time**	**Frequency**	**Classification**
Doppler Spread	Fast	$T_s > \tau_c$	$B_s < \sigma_\nu$	Frequency dispersive and Time selective
	Slow	$T_s << \tau_c$	$B_s >> \sigma_\nu$	Non-frequency dispersive and Time-flat
	Fading	**Angle**	**Space**	**Remarks**
Angle Spread	Space Selective	Large σ_a	Small D_c	Close antennas may experience uncorrelated fading.
	Non-Space Selective	Small σ_a	Large D_c	Close antennas may experience correlated fading.

Table C.2: Channel characteristics.

tries to answer this question is presented in Table C.3, where T_{chip} and $T_{inteleaving}$ are respectively the chip and interleaving periods. Diversity concepts and the Rake receiver are mentioned, if needed the reader can refer to the next chapter.

Last but not least, a brief characterization of macro and micro cells and a qualitative description of the channel dispersion effects in these cells is given next.

A *macro cell* is characterized by a large cell radius (up to a few tens of kilometers) and a base station located above the roof top, i.e. above the surrounding scatterers, which generally leads to a scenario of small angle spreads. The Doppler spread can be quite large compared to a micro cell, since the macro cell is intended to serve both pedestrians and vehicular users. Due to the larger coverage area, the delay spread is also normally larger in a macro cell than in a micro cell.

Frequency Selective	**Frequency Flat**
$T_{chip} \ll \sigma_\tau \Rightarrow$ Interpath interference	$T_{chip} \gg \sigma_\tau \Rightarrow$ No interpath interference
Many resolvable paths $\Rightarrow$ Rake fingers	One resolvable path $\Rightarrow$ Rake finger
Good multipath diversity	Low multipath diversity
Poor orthogonality in WCDMA DL	Good orthogonality in WCDMA DL
Time Selective	**Time Flat**
$T_{inteleaving} \gg \tau_c \Rightarrow$ Efficient interleaving	$T_{inteleaving} \ll \tau_c \Rightarrow$ Inefficient interleaving
Good time diversity	Low time diversity
PC does not have a large effect	PC has a large effect
UE at high speeds	UE at low speeds

Table C.3: WCDMA and channel characteristics.

Micro cells are characterized by highly dense built-in areas, and by the user's terminal and base being relatively close (a few hundred meters). The base antenna has a low elevation and is typically below the roof top, causing significant scattering in the vicinity of the base leading to very high angle spreads. Small delay spreads are likely to occur in this situation due to the smaller coverage radius. The Doppler spread is generally smaller than that of the macro cell case, however it is possible to have relatively large Doppler spread if multipaths are caused by reflections from high-speed vehicles passing nearby.

We can clearly perceive now, based on what was mentioned earlier, that due to the generally smaller angle spreads, *beamforming* is suited to macro cells, whereas the gains from *diversity* will be larger in micro cells than in macro cells. Typical values for the delay, angular and Doppler spreads (at 1800 MHz) in different environments are presented in Table C.4, taken from [36].

Cell Type	Environment	Delay(rms)	Angle (AoA)	Doppler
Macro Cell	Flat	$0.5\mu s$	1°	190Hz
	Urban	$5\mu s$	20°	120Hz
	Hilly	$20\mu s$	30°	190Hz
Micro Cell	Urban	$0.3\mu s$	120°	10Hz
	Indoor	$0.1\mu s$	360°	5Hz

Table C.4: Typical spread values in cellular applications.

Apêndice D

Performance Enhancing Antenna Solutions for UMTS

Having dealt with the limitations imposed by the mobile radio channel in the last chapter, it is now time to focus our attention on advanced *antenna array* systems (also known as *smart antennas*) that can be used to mitigate the shortcomings of the channel, thus enhancing the performance of the UTRA FDD cellular system.

From a purely theoretical point of view this can be considered the most important chapter of this thesis, hence its length. It tries to present the concepts the author had to learn in order to carry out his work. As in the previous chapter, the emphasis is on intuitive concepts. As usual, references for further investigation are provided.

The chapter begins with an useful analogy which helps readers to grasp the intuitive idea behind smart antennas. The following sections summarize various antenna development stages in an increasing order of intelligence. The objective is to provide an overview of how antenna array technology can be used to improve digital cellular systems.

If readers are familiar with these concepts they might skip to the next chapters where the simulation results are presented. Nevertheless, this chapter is very important because it is in line with the aim of making this thesis as self-contained as possible.

D.1 Introduction – An Useful Analogy

A problem humans are familiar with is the determination of the position of a sound source. If we close our eyes while a sound source (a loudspeaker, someone talking or playing instrument, etc) is moving around us, we can tell with a remarkable accuracy where the sound is coming from. How can we do it?

We use our ears as an array of acoustic sensors. The sound waves impinge at each ear at different times, depending upon the direction from which the sound is coming. Then the brain, a very special signal processor, uses this information from both ears and computes the location of the source.

Not only does it find out the direction of the sound source, but it also combines the sounds from the selected direction in a constructive way. Sounds from other directions add together incoherently. The result is that we perceive sounds coming from the chosen direction as being twice as loud as anything else. We are able to focus on a speaker in the noisy environment of a cocktail party, despite the fact that the speech signal originating from that speaker is buried in a noisy background due to other interfering conversations in the room.

Antenna array (AA) – also known as *smart antenna* (SA) – systems do something very similar, using antennas instead of ears. More than that, they are not limited to only two "ears". There can be as many as $4, 6, 8, \ldots$ antennas. Besides, since antennas can also transmit signals, they can "talk" back in the same direction the signals came from. In sum, such an antenna system can both send and receive signals in a much more directed and efficient way. The main benefits that can be achieved with smart-antennas in mobile communications systems are: *coverage extension, capacity improvement, quality improvement, initial deployment cost reduction, spectrum efficiency increase and transmit power reduction* [25, 37, 38].

D.2 Antenna Systems

Radio antennas are a means of coupling radio frequency power from a transmission line (e.g., wire, coaxial cable, or waveguide) into free space. Physical designs can vary greatly. The simplest antennas radiate and receive equally well in all directions[1]. They are know as omnidirectional antennas. To find its users, this dipole antenna broadcasts in all directions in a pattern resembling ripples radiating outward in a pool of water.

One might then ask, why should anything different from this simple solution be used? The answer lies in the fact that this unfocused approach scatters the signals, reaching users with only a small percentage of the overall transmitted energy.

Given this limitation, the most straightforward strategy to increase the received power is to boost the power level of the signals broadcasted. In a setting of numerous users (and interferers), this makes a bad situation worse in that the signals that miss the intended user become interference for those in the same or adjoining cells [37].

How can antennas be made smarter? First, a single antenna can be constructed to have a fixed preferential transmission and reception direction. Second, multiple antennas can be used in combination with some clever signal-processing. As a matter of a fact, the smartness of such antenna system resides in the latter. Let us investigate further in the next sections.

D.3 Sectorized Systems

As an alternative to reducing the cell radius and adding new transmitter sites, many conventional antenna towers split, or *sectorize* cells. A BS coverage

[1]To be precise, when we speak of direction, we are generally referring to azimuth. It is also worth mentioning that it is impossible to build a truly omnidirectional antenna.

area is normally partitioned into three 120° sectors or six 60° sectors that are covered using *directional* antennas looking out from the same BS location. Operationally, each sector is treated as a different cell whose range is greater than the omnidirectional case. This results in a single antenna per cell and does not really qualify as an antenna array technique at the BS [39].

All else being equal, sector antennas provide increased gain over a restricted range of azimuths as compared to an omnidirectional antenna. Besides, by using directional antennas, CCI is reduced since a given cell will receive and transmit in a slightly less broadcast method. A penalty from sectorization is the larger number of handovers, since it reduces the coverage area of cells.

D.4 Diversity Systems

In the next step towards smart-antennas, we have diversity systems. Among the most common approaches to mitigate the fading and distortion effects mentioned in the previous chapter are diversity techniques. Diversity is a very intuitive concept and may be seen as a manner of introducing redundant information. The basic idea is as follows: if several replicas of the same information carrying signal are transmitted (or received) over multiple branches with comparable strengths, which fade independently, then there is a good probability that at least one replica will not be severely degraded by fading [13, 23, 25].

Applying diversity in a Rayleigh fading channel reduces the average transmit power required to maintain a particular bit-error rate (BER) level at the receiver, therefore, receive diversity at the BS can be traded for reduced power consumption and longer battery life at the user terminal, moreover, lower transmit powers decrease the amount of CCI, consequently, increasing system capacity [25]. There are several forms of diversity; *Frequency*, *Time* and *Space* diversity are common examples.

Frequency diversity is achieved by transmitting the message signal over more

than one carrier frequency. As seen in Section C.3.1, if the two frequencies are separated by more than the coherence bandwidth of the channel, their fading will be uncorrelated.

Time diversity is obtained if the information is sent repeatedly at time intervals longer than the coherence time of the channel, thus undergoing independent fading as explained in Section C.3.2. In UMTS, time diversity is linked to *interleaving* and *error-control coding*.

Space diversity, also known as *antenna diversity* is one of the most popular forms of diversity found in cellular systems. When a receiver is equipped with two or more antennas that are sufficiently separated (typically several wavelengths) they offer useful diversity branches. It is worth stressing that low correlation can be achieved *without excessive antenna separation* when the AS of the channel is large [24]. Furthermore, besides the diversity gain, receive antenna diversity techniques provide an additional SINR gain *even if* the diversity branches are correlated, the reason is that the desired signals from the branches can be combined coherently, while the received thermal noises are combined non-coherently [6].

In cellular systems we can speak of two types of antenna diversity, *microscopic* and *macroscopic*. Microscopic diversity is used in order to mitigate the effects of deep rapid (small-scale) fades; if you have two antennas separated by a fraction of a meter, one might receive a strong signal while the other is in a deep fade. The *Rake* receiver [2] also provides diversity, assuming the fading of the multipath components assigned to each finger is uncorrelated.

Diversity also helps to combat large-scale fading effects caused by shadowing from buildings or terrain features. However, antennas serving the same sector experience the same shadowing. Instead, antennas from different sectors can be combined to offer a protection against large-scale fading, this is called macro diversity [25].

The UMTS standard also supports the use of transmit diversity at the BS,

[2]The Rake receiver is discussed in Section D.4.1.

the target of which, is to move the complexity of antenna diversity in the downlink from the mobile reception to the BS transmission. Two different open-loop transmit diversity techniques are supported: time-switched transmit diversity (TSTD) and space-time transmit diversity (STTD) (the details can be found in [40]), the latter being a slightly modified version of the dual antenna space time block coding scheme proposed by Alamouti [41]. The closed-loop schemes (CLTD) rely on information fed back by the terminal. All these techniques have already been studied at system level for both, power controlled DCHs [9, 42] and HSDPA [3], thus they are no longer investigated here.

One last important point one has to bear in mind is that the more diversity already available through the different diversity schemes, the smaller is the additional diversity gain by the antenna array [6]. If the radio channel has a high degree of multipath diversity, employing many antenna diversity branches will not bring many benefits. However, if the radio channel can be approximately characterized as a flat Rayleigh fading channel, it is advantageous to increase the number of diversity branches.

D.4.1 Multiple Antennas at the UE

Although antenna diversity techniques are nowadays by default employed in the base station receiver, in terminal side the additional cost and complexity have so far prevented them to be adapted by the existing mobile systems [27].

The use of antenna arrays at the terminal is a new area of research. Nevertheless, some researchers have proposed diversity combining at the mobile stations which have shown significant performance improvements [27, 26]. The advent of very fast and low-cost digital signal processors (Moore's law) may soon render commercial applications of multiple antennas at the UE practical.

At this stage, a detour is necessary, since it is hard to imagine a (W)CDMA discussion without a description of the Rake receiver.

The Rake Receiver and MRC:

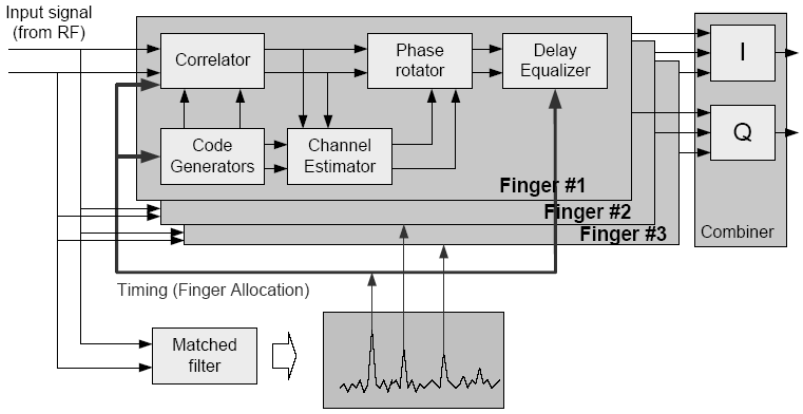

Figure D.1: Structure of the Rake receiver. Extracted from [6].

In conventional modulation schemes (non-spread-spectrum), if the baseband bandwidth of the transmitted signal is larger than the coherence bandwidth of the channel, ISI between adjacent symbols will occur and some form of channel equalization is required. That is not the case with CDMA systems, even though the bandwidth of the chip is much larger than the flat-fading bandwidth of the channel. This happens because the spreading and scrambling process described in Chapter B was designed to provide very low correlation between successive chips. In other words, the delay spread of the channel simply generates multiple versions of the transmitted signal at the receiver. If these versions are delayed by more than a chip duration they appear to be uncorrelated noise, but the processing gain makes uncorrelated noise negligible after despreading [23], thus the need for an equalizer is eliminated up to a certain extent (high bit rates excluded due to low processing gains).

However, it is intuitive to understand that the multipath components do carry useful information. Instead of disregarding them, why not use them in a constructive way? That is exactly what the Rake receiver does. It tries to capture the energy from each delayed version in order to improve the SINR. It provides a separate correlation receiver (*finger*) for each multipath component and then adds

them coherently. The signals from R branches are first co-phased to bring mutual coherence and then summed after weighting.

The code generator and correlator blocks show in Figure D.1 perform the de-spreading of the data, the channel estimator block normally uses the pilot symbols from the CPICH to estimate the channel impact which will, in turn, be removed from the received symbols by the phase rotator, besides an appropriate delay is introduced into each correlator output in order to ensure that all correlator outputs add constructively. Last but not least, the matched filter is used to detect the R strongest multipath components so that a Rake finger is assigned to them.

The weighting coefficients are calculated according to the *maximal ratio combining* principle, i.e. they are proportional to their pertinent SINR. After ideal [3] MRC of all the fingers the resulting SINR can be written as

$$\mathrm{SINR} = \sum_{r=1}^{R} \mathrm{SINR}_r, \tag{D.1}$$

where SINR_r is the SINR at the r^{th} finger. The Rake receiver shown in Figure D.1 is a CDMA diversity receiver, where the diversity stems from the fact that multipath components are virtually uncorrelated when their relative propagation delays is greater than the chip duration. It must be noted that this model can be easily extended to multiple receive antennas by adding additional fingers to the antennas. From the Rake receiver's perspective, there is no difference between the two forms of receive diversity. If we assume M antennas, (D.1) becomes

$$\mathrm{SINR} = \sum_{m=1}^{M} \sum_{r=1}^{R} \mathrm{SINR}_{r,m}, \tag{D.2}$$

where $\mathrm{SINR}_{r,m}$ is the SINR at the r^{th} finger of the m^{th} antenna.

UMTS and Multiple Antennas at the UE

For UMTS, the link level improvement from the deployment of dual antenna Rake receivers with MRC (as of now, referred to as 2Rake receivers) has been

[3] This implies perfect channel estimates, independent branch fading and equal mean branch powers.

reported to range between 3 and 4.5 dB for a block error rate (BLER) target of 10%, depending on the frequency selectivity of the radio channel [3, 27].

We will not be dealing with transmit diversity techniques, since no scheme has been standardized for UL transmission in UMTS. Therefore, in this study, the use of multiple antennas at the UE is restricted to DL signal reception. The use of antenna MRC at the UE is reasonable, since the correlation between the antenna elements is usually low [24] even for a small antenna separation. One must keep in mind that large mobiles are not desired, they probably will not sell. A discussion about why beamforming techniques are not employed at the UE is addressed at the end of Section D.5.1.

In order not to distract from the flow of the "thought process", in-depth discussion of dual antenna mobile specificities are put off until Chapter F.

D.5 Smart Antennas

Finally, it is time to start opening up the "big umbrella" title given to different antenna-array (AA) technologies in the motivation of this report. Antenna diversity and beamforming techniques are both AA technologies, but only the latter truly qualifies as a smart-antenna system. Diversity systems are useful in environments where fading is the dominant mechanism for signal degradation. In environments with significant interference, it is highly desired to transmit to numerous users more efficiently without compounding the interference problem, that leads us to the next evolutional step of antenna systems: smart-antennas [37].

A reasonable question is, what is it that make antennas smart? Nothing, the antennas are not smart, antenna systems are! The system intelligence is located in the digital signal-processing capability which may be used to receive and transmit signals in an adaptive spatially sensitive manner. That is to say, the system can combine in a keen way the outputs of the individual antennas in an array, creating a single effective antenna, with gain and directional characteristics that are very

different from those of the individual elements.

Today, several terms are used to refer to the various aspects of smart-antenna system technology, such as phased-arrays, spatial division medium access (SDMA), spatial processing, digital beamforming, among others [38], however, smart antenna systems are normally categorized as either *fixed beam systems* or *adaptive systems*. In this thesis the antenna array at the BS is operated as a *beamformer*, which in short, is a *spatial filter*, that aided by the appropriate analog or digital signal processing, and an array of M antenna elements is capable of pointing a narrow beam towards the desired user (or group of users), so that the power radiated (received) towards (from) other directions is attenuated, thus filtering the co-channel users in the spatial domain. In the next sections, beamforming and its most common variations are introduced. Simulation specific topics, such as the choice of the steering directions, optimal number of beams are discussed in Chapter G.

D.5.1 Beamforming

Beamforming has been used for many years in different radio applications such as communications, radar and, with different array sensors, in sonar and audio fields.

Traditional analog ways to perform beamforming, e.g. the Butler matrix [43], were very cheap but not flexible at all. Today, modern technology offers high-speed digital devices, whose performance is expected to increase even further in accordance with Moore's law, which implement the fundamental blocks of digital beamforming in an efficient and extremely flexible manner. Therefore, we will not address analog beamforming here.

The three most common arrangements of the antenna array elements are: linear, circular, or planar. The *linear equally spaced* (LES), also known as *uniform linear array* (ULA) is considered to be the simplest configuration for a basic beamforming implementation and is analyzed next. The analysis done here is for uplink reception, simply because it is more intuitive. Yet, it does not matter if the

weights are applied at the receiving or at the transmitting end, because the weight calculations is the same in both cases, rendering DL beamforming analogous.

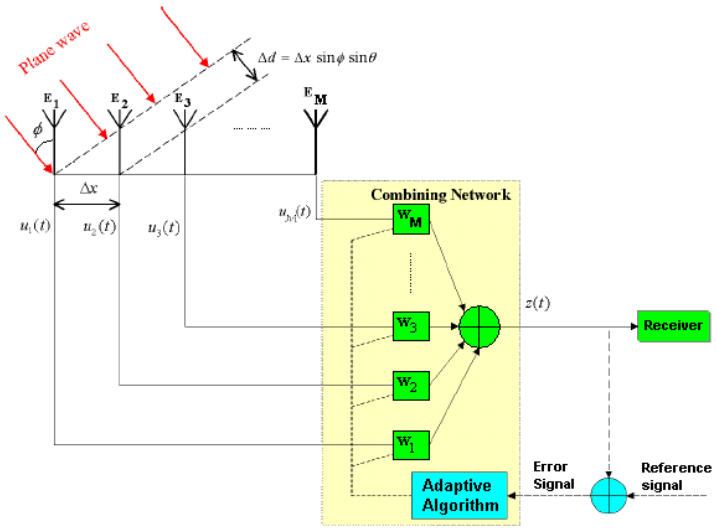

Figure D.2: Uniform Linear Array

Uniform Linear Array

Figure D.2 shows the baseband complex envelope representation of the ULA. It consists of an array of M identical isotropic elements spaced uniformly apart along the axis of the array. The adaptive algorithm block, dotted lines, error and reference signals are related to adaptive antenna systems, which are presented in Section D.5.5.

Before we continue, let us make certain assumptions: the spacing Δx between antenna elements is small enough, so that the M antenna elements operate coherently. There is no mutual coupling between elements. The bandwidth of the signal incident on the array is either limited or small compared with the carrier frequency and can be taken as f_m, allowing us to write $c = \lambda_m f_m$, where c is the speed of light, and λ_m is the corresponding wavelength.

Now, notice that the plane wavefront arrives at each of the antenna elements $1, 2, \ldots, M$ at different times, hence with different phase shifts, depending on the incidence angles (ϕ, θ). This angle pair is known as *Angle-of-Arrival* (AoA) of

the received plane wave. The first angle ϕ is the azimuth, measured respective to the broadside of the array, the second θ is the elevation. Consequently, we have multiple copies of the wavefront delayed by Δt seconds at each antenna. This delay corresponds to the time it takes the wave to cover the differential distance $\Delta d = \Delta x \sin\phi \sin\theta$ between the ray paths of elements m and $m+1$. But, if we then apply weights to the outputs of each antenna and sum everything, would it not be exactly a *FIR filter implemented as tapped delay line?* This explains our previous claim that an ULA is a spatial domain form of a temporal FIR filter.

The elevation angle can usually be assumed to be $\pi/2$ [14], which represents the horizon, thus, in this work, unless noted different, the AoA is completely described by the azimuth ϕ. We can then calculate the time delay (phase shift) for each element m as:

$$\Delta t = \frac{(m-1)\Delta x \sin\phi}{c} = \frac{(m-1)\Delta x \sin\phi}{\lambda_m f_m} \tag{D.3}$$

If the phase is set to zero at element 1, and $\Delta x = \lambda_m/2$ [4], the phase at element m, relative to element 1, will be given by: $\beta(m-1)(\lambda_m/2)\sin\phi$, where $\beta = 2\pi/\lambda_m$ is the phase propagation factor. We are now, ready to introduce the *steering vector*, which contains the information about the phase of the signal available at each antenna element relative to the phase of the signal at the reference element. Equations D.4 and D.5 define it. A set of steering vectors over all values of AoA ϕ is called the array *manifold*.

$$\mathbf{a}(\phi) = [1, a_2(\phi), \ldots, a_M(\phi)]^T, \tag{D.4}$$

where $a_m(\phi)$ is given by

$$a_m(\phi) = e^{-j(m-1)\pi \sin\phi} \quad \forall\, m \in \{1, 2, \ldots, M\} \tag{D.5}$$

[4]This value is chosen because it is expected to satisfy the coherence assumption in a typical urban macro cell environment. Moreover, if the element spacing exceeds $\lambda/2$ grating lobes can appear [6, 14, 43].

The most common method used to create directional beams is to introduce phase shifts for each element. The m^{th} element has a *weighting element* w_m, which has both a magnitude and phase associated with it. As already seen, these weights can be calculated similarly to the coefficients of a FIR filter. In working with arrays, it is convenient to use vector notation, we then define the weight vector as

$$\mathbf{w}(\phi) = [w_1(\phi), w_2(\phi), \ldots, w_M(\phi)]^H, \tag{D.6}$$

where the superscript H denotes Hermitian transpose. By adjusting the weight vector, it is possible to direct the maximum of the main beam in any desired direction [14]. In order to maximize the response in a given direction ϕ_{dir}, a constant phase offset between the elements shifts the radiation pattern, each weight is then given by

$$w_m(\phi_{dir}) = \frac{1}{\sqrt{M}} e^{j(m-1)\pi \sin\phi_{dir}} \quad \forall\, m \in \{1, 2, \ldots, M\}, \tag{D.7}$$

where $\sqrt{M}$ is simply a normalizing factor to ensure the same transmit power for the antenna array as an isotropic antenna. It can be noted that only phase weighting is considered here, all the weights have the same magnitude. In the sequel, this kind of beamforming is referred to as conventional beamforming (CBF) and is also known as *delay-and-sum beamformer*. It provides the maximum SINR for the case that no directional interferer operating at the same frequency exists [38]. Keeping the magnitudes of the weights constant results in side lobes 13 dB below the main lobe; windowing functions (e.g Hamming, Kaiser, etc) could be applied to reduce the side lobes drastically, but that would increase the width of the main lobe, thus implying a loss in capacity. In order to limit the scope of this study, only equal magnitude weighting is considered in this report.

Furthermore, there are many other methods to synthesize the resulting beam pattern of an antenna array e.g. the Fourier Transform Method, the Schelkunov's Form, the Dolph-Chebyshev synthesis, the Taylor Line Source Synthesis, etc. All these methods are described in detail in [43].

In this way the *array factor* can be defined as:

$$F(\phi_{dir}, \phi) = \mathbf{w}(\phi_{dir})^H \mathbf{a}(\phi), \tag{D.8}$$

it describes the complex amplitude antenna gain of the AA at ϕ when a beam is pointed at ϕ_{dir}, this direction is called beam-pointing direction. In other words, there is no traditional "antenna pattern" as for conventional antennas. All antenna elements receive all signals at all times, and it is the processing of that information in the DSP that "generates" the effective antenna pattern. Since this processing can be done in parallel for several users, it is possible to generate one separate antenna pattern for each user at the same time with the same antenna elements.

Non-Isotropic Elements

In practice, we will not use isotropic elements. The use of non-isotropic elements attenuates the antenna pattern outside the range of the sector. Another advantage is that the gain of the antenna elements can be increased, improving SINR. In the general case, if the field pattern of each array element is $g(\phi)$ and the array elements are identical and oriented in the same direction, the total field pattern of the array is the product of the array factor and the field pattern of each array element. This is called the principle of pattern multiplication [14]. Thus, the complex total amplitude field pattern of the ULA at ϕ when a beam is pointed at ϕ_{dir} is

$$G(\phi_{dir}, \phi) = F(\phi_{dir}, \phi).g(\phi). \tag{D.9}$$

Baumgartner has presented a very illustrative analysis of the impact of the single element antenna pattern on the effective beam in [29].

The Impact of Azimuth Spread

The effectiveness of the beam former depends on the spatial dispersive characteristics of the radio propagation environment (see Section C.3.3). In other words, the CCI reduction through spatial filtering is achieved when the azimuth spread in the radio channel seen from the beam former is much lower compared to beamwidth of the directional beams. A large AS compared to the beamwidth spreads the radiated power of the beam in space, which in practice ruins the shape of the beam (See the discussion presented in Section G.2.1).

With that in mind, let us analyze Figure D.3, which plots the 3 dB beam-

width [5] of the generated beams (assuming zero AS) as a function of number of antenna elements. It can be observed the beamwidth decreases with the number of elements. In principle, if CBF is applied, the beamwidth should be adjusted in such a way that it captures most of the transmitted power, i.e., the beamwidth should be adapted to the degree of azimuth dispersion in the channel (the beamwidth of the synthesized directional beams should be considerably larger than the AS), otherwise, there will be some multipath components of the transmitted signals falling completely out of the radiation pattern of the synthesized beams. Thus, it is concluded that the AS imposes an upper limit to the number of elements.

An AS of 5° suggests the number of elements could be very large, whereas an AS of 20° would restrict it to four. This gives a rough idea about the number of elements in the ULA. Practical implementation reasons should also be taken into account when selecting the number of antennas. This choice is put off until Chapter G.

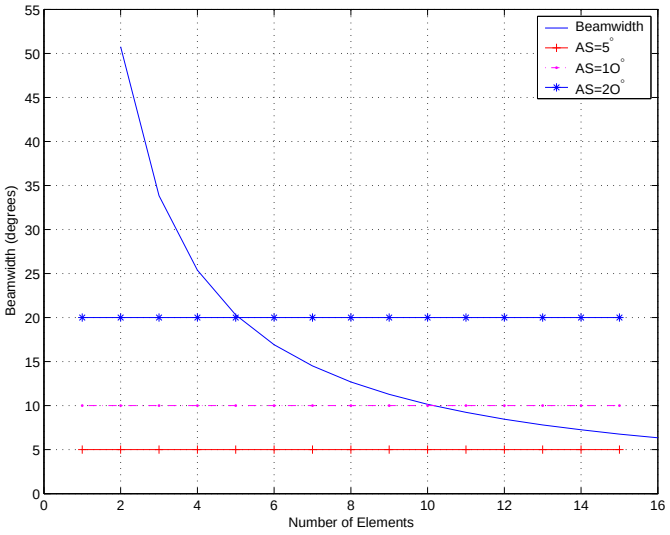

Figure D.3: Beamwidth versus the number of antenna elements.

Considering the previous discussion, let us now take a look at the terminal

[5]The 3 dB or half-power beamwidth is defined as the angle between the two directions in which the radiation intensity is one-half the maximum value in the main lobe. Calculated as $BW_{3\text{dB}} = \arcsin(0.886\lambda/d.M)$ [43].

side and understand why CBF at the UE is not considered here. In a macro cell environment, it is usually assumed that the scatterers surrounding the mobile station are approximately at the same height or higher than the mobile, as already explained, the presence of local surrounding scatterers causes a large AS. Recall that large AS favors diversity techniques, not beamforming.

Besides, the number of antenna elements that can be implemented at the UE is rather limited due to practical restrictions related to power consumption, local processing power, size and antenna isolation, which reduces the spatial filtering gain significantly. Furthermore the human body affects the radiation pattern of each antenna element in a different way, which makes it more difficult to synthesize narrow beams towards the desired azimuth direction, which is likely to change a lot given the user mobility.

Broadband Beamformers

The type of beamforming discussed so far is known as *narrow band* beamforming, since it is only valid under the assumption made in the beginning of this section, which allowed us to consider the signal spectrum to be well characterized by its central frequency f_m, in other words, we are saying the signal has a narrow band or that its bandwidth is small compared to the carrier frequency. Smart antennas need some special considerations when considering wideband systems.

We have seen that the phase shift required by each weight w_m depends on the differential propagation distance between each antenna element and the wavelength of the signal. The phase shift is a function of both the frequency and the desired beam direction while the weights only adjust the desired beam direction. Therefore, it is evident that the weights are optimal for the chosen direction only at this center frequency f_m. However, considering a more realistic (and complex) scenario for wideband systems like UTRA, with a bandwidth of approximately 5 MHz, lower frequency signal components will experience a smaller phase shift for a given propagation distance, while higher frequency signal components undergo a greater phase shift as they travel the same length. The ideal approach would introduce different phase responses for the various frequency components of the

wideband signal, to ensure identical phase shifts.

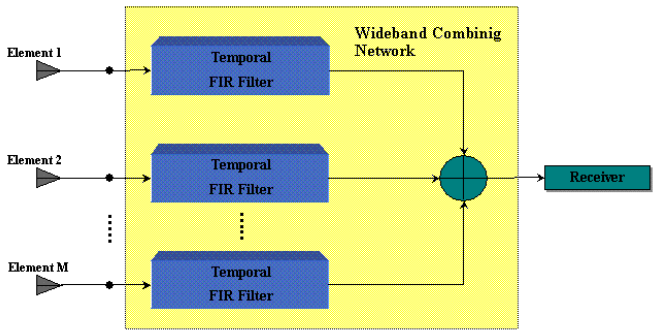

Figure D.4: A broadband beamformer.

This can be accomplished by the so called *broadband beamformer* depicted in Figure D.4, which is capable of processing signals in both spatial and temporal domains. In a broadband beamformer, the weights are substituted by FIR filters which are responsible for the temporal filtering of the signal. More detail on broadband beamformers can be found in [14]. Given the structure of the simulator used (see Sections E.3 and G.2), the design of such filters is not needed.

The discussion presented so far was intended to be as general as possible. However, even though the basic principles remain the same, smart-antenna systems show differences depending on the multiple access technology used and the direction under consideration, UL or DL. In the sequel, we consider the features applicable to UTRA FDD.

D.5.2 Downlink versus Uplink

In the UL, considering that the BS possesses an AA, we can estimate the spatial response of the channel. By spatial response, we mean the spatial covariance matrix ($\mathbf{R}$) of noise and multiple-access interference (MAI), that in the case of spatially uncorrelated noise and MAI, equals [16]

$$\mathbf{R} = \mathbf{I}\sigma + \sum_{u=1}^{U} E\{\mathbf{h}_\mathbf{u}^*.\mathbf{h}_\mathbf{u}^T\}, \tag{D.10}$$

where U is the number of intra-cell interferers, σ is the noise power, $\mathbf{I}$ is the identity matrix, E denotes expectation, $\mathbf{h_u}$ is the Mx1 vector of channel coefficients of the u^{th} user, and $*$ represents complex conjugation.

With this information the complex weights $\mathbf{w}(\phi) = [w_1, w_2, \ldots, w_M]^H$, that maximize the SINR at the combiner output for a desired user d have been formulated by Winters [16] and can be calculated as $\mathbf{w} = \mathbf{R}^{-1}.\mathbf{h_d^*}$. This solution is often called *Optimum Combining* (OC), for it also completely cancels $M-1$ interferers with M antennas [44]. This cancellation is known as *null-steering*, but unfortunately it is only possible for a small number of interfering signals, since for practical reasons the number of antenna elements in the array is limited. Given that in CDMA systems, the number of interferers is much larger than in TDMA or FDMA systems null-steering seems to be impracticable [29, 33, 38].

When this is the case, the interference becomes spatially white (i.e. is approximately equal in all directions) and $\mathbf{R}$ approaches the identity matrix. In this case, OC means where are simply maximizing the power level of the desired user, $\mathbf{w} = \mathbf{h_d^*}$, which is referred to as our old friend, MRC. Moreover, if the incoming signals have little or no AS and $\mathbf{R} = \mathbf{I}$, MRC reduces to forming one beam pattern maximizing the gain in the direction of the desired user, which boils down to conventional beamforming. The problem is then simplified, the only task left is finding the direction of the arriving signal (DoA), in order to steer the beam in that direction. This relation is depicted in Figure D.5.

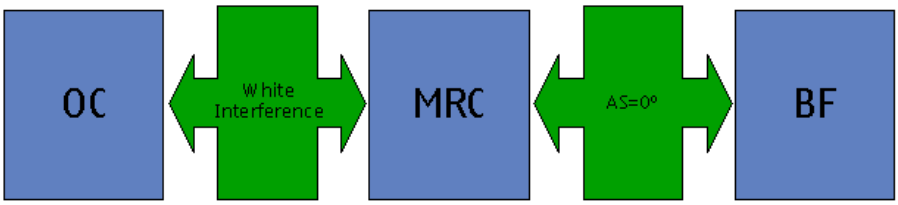

Figure D.5: Relation amongst OC, MRC and CBF.

Now, let us see flip the coin to see its other side, the DL. Here considering that the terminals do not have an antenna array, no knowledge about the spatial

response is available. Thus another strategy to select which beam serves which UE is required. Choosing the correct beam is very important, because the negative impacts of transmitting using the wrong beam are obvious. Can we infer anything from the information obtained from the UL? The answer is yes. Due to the frequency division duplex used in UTRA FDD (many times the coherence bandwidth) the small-scale fading, and consequently, the instantaneous DL channel coefficients will differ and can not be estimated at the BS. However, the large-scale channel variations (path loss and shadowing) are generally considered reciprocal, which means that the signal directions of the different users can be estimated. For this reason, OC or MRC techniques can not be applied for the DL, but CBF can, provided that the angular spreading is reasonably small compared to the antenna beamwidth. Therefore, the rest of this chapter will focus exclusively on DL beamforming. Two different techniques are explained, the *fixed and adaptive beam* approaches. The most noticeable distinguishing factor between them is the way the weighting vector is calculated. But before going into that, a simple discussion about the theoretical capacity gain offered by beamforming is presented.

D.5.3 On the Theoretical Beamforming Gain

Let us briefly consider the expected capacity gain from using this technology. Although beamforming gives inferior performance compared to the more advanced OC and MRC schemes, the expected capacity gain is still substantial. A key parameter used to determine the capacity enhancement is the width of the beams formed with the antenna array. Putting it in a very simple way, the narrower the beam, the less the power radiated in undesired directions causing interference to other users. Therefore, the beamwidth reduction (compared with conventional sector antennas) can be used to approximate the network capacity enhancement. Let us assume that beamforming generates narrow beams, whose beamwidth is B times smaller than that of the conventional sector antenna. Provided that the interference is spatially white, this means that the number of users affected by the interference originated by this beam is divided by B. In consequence, every mobile

experiences on average B times less interference which theoretically results in a B times capacity increase. However, *no capacity gain is expected for the case where all users are positioned at the same azimuth direction.* Hence, we can conclude that the gain *is highly sensitive to the spatial distribution of the users.* Far more advanced analytical studies can be found in the literature, e.g. the work in [45].

D.5.4 Fixed Beams

Fixed beamforming is considered to be a simple yet effective alternative to the complex fully adaptive system. The basic idea is to generate a finite set of pre-determined fixed [6] beam patterns to serve the coverage area. In contrast to the adaptive approach, where each user is served by a dedicated beam, here all users within the coverage area of a beam, "share" this beam as shown in Figure D.6. Compare it with Figure D.7.

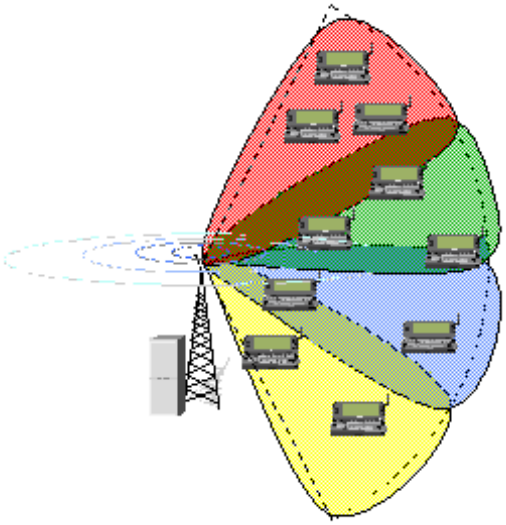

Figure D.6: 120° sector served by four fixed beams.

In UMTS, fixed beams can be used in two different forms. The first possi-

[6]Despite being called fixed beamforming, the weights may be slowly modified to track changes in the environment. The rate of change is very slow when compared to the truly adaptive case.

bility is to split a cell [7] into regions covered by the set of synthesized beams. In this case, the beams are only used to transmit the data channels and a Secondary Common Pilot Channel (S-CPICH) for channel estimation, which represents an undesired pilot overhead. The required common channels (see Section B.4.3) are transmitted using a conventional sector beam, which has to be present, because they have to be heard in the whole cell area. This strategy is commonly referred to as *switched beam method*.

The second technique is known as the *higher order sectorization* (HOS). Here, the area covered by each beam is an effective UMTS cell, since all (common and data) channels are transmitted in each beam. The beam layout is very similar to the previous case, the difference being the absence of the sector beam.

Using the first strategy, we still have only one 120° sector split into four different regions (*cell-portions*). Using the second method, the 120° sector depicted in Figure D.6 would turn into 4 effective cells, each covering an angle of approximately 30°.

Switched Beam Systems

Switched beam systems (SBS) are non-adaptive and usually involve the use of four to eight antenna elements per sector at the BS to create a group of overlapping beams with their main lobes pointed at different fixed directions, creating cell portions, which together cover the entire cell area. This drastically reduces CCI, since a beam much narrower than the conventional sector beam serves the users within its cell portion with increased antenna gain, while the gain towards directions outside the main lobe is much lower.

Recall now, from Sections B.4.2 and B.4.3, that terminals normally use the P-CPICH as the phase reference for channel estimation and that it must be transmitted in a sector beam so that it can be received in the entire cell area. However, the phase-rotation of the signal transmitted through a beam serving an

[7] In this work, cell is used as a synonym for sector. A BS site usually consists of three sectors that cover 120° each.

user is probably different from the phase rotation of the P-CPICH received by the terminal, hence, it can no longer be used as the phase reference. Yet, it is still used for HO measurements. In other words, terminals need to be informed through higher layer protocols to use a different reference, either dedicated pilot signals present in the power-controlled DCH or an S-CPICH. Since a fixed beam usually serves much more than one user, it is preferable to use a S-CPICH as the phase reference for each beam. Nevertheless, the usage of this additional pilot channel represents an undesired overhead, because it represents extra power consumption and interference.

The process of selecting the best beam and informing terminals which reference to use is called *beam switching* and is done in the following manner. The BS continuously measure the average received UL power per beam for each UE and reports this information back to the RNC, which typically picks the beam with the highest SIR (averaged over fast fading) for a given UE. The RNC then informs the BS to transmit the data channel towards this UE using the selected beam. It is important to stress that this process does not include any measurements done by the UE and is considerably faster ($\approx$ 350 ms) than handovers. The beam switching process and wideband power per beam (directional) measurements are discussed in much more detail in [46, 12]. For Release 6, directional measurements needed to support beam switching are defined in [47].

The work in [48] compares the approach described earlier with a much more complex one, which allows the usage of multiple beams and involves the estimation of the *Direction of Arrival* (DoA) of each dominant path of the desired user to select the serving beam(s). It is pointed out that the performance of both methods is very similar (less than 1 dB in the DL mean SINR) and that the latter should only be used if other applications require more accurate DoA information. Besides, a UMTS mobile can not use two different S-CPICHs from the same cell as phase references [6, 46], this restricts the scope of this work to the single-beam reception technique.

A final discussion concerns the scrambling code assignment. Due to the

interference rejection, the utilization of SBS might lead to a situation where the system is no longer interference-limited but hard-limited. The number of users might exceed the amount of codes offered by one OVSF code tree (*code-shortage*). Recall the discussion in Section B.3.2, where we promised to get back to this issue. If this happens, two, three, or even more code trees can be deployed with the utilization of a secondary scrambling code.

As mentioned in Section B.3.2, there are 15 secondary scrambling codes, but their utilization has a negative impact on the system, since the channelization codes scrambled with different codes are no longer orthogonal, which add up to inter-cell interference. However, this negative impact can be diminished by splitting the cell into multiple scrambling code regions, making use of the spatial separation provided by the beams (known as *cell-splitting*). Since the P-CPICH and the other common channels are always scrambled with the primary scrambling code, it is beneficial to have as many beams as possible using the primary scrambling code. An intuitive way of introducing secondary scrambling code is to start using them with beams which are close to the cell border, since the neighboring cell uses a different scrambling code anyway. This subject is discussed further in Chapter G.

Higher Order Sectorization

In this case, the synthesized beams are used to increase the sectorization of a base station site. Each beam behaves just like a regular UMTS cell of a base station, having its own scrambling code, code tree and transmitting all necessary common channels. As seen from a mobile in the system, there are no differences between a logic cell formed by a fixed beam or one served by a sector antenna. This is the greatest advantage of the logic cell method, it can be applied without any modifications to the specifications in Release' 99.

Another advantage of this method is the elimination of the S-CPICH pilot overhead that plagues the SBS. Remember, that here, each beam is a logical cell, thus having all necessary channels. This way, the phase-rotation experienced by the P-CPICH is equal to the one experienced by the user data. However, nothing comes for free, we get rid of the overhead, but there is a degradation of the orthogonality

between signals, since each beam is transmitted under its own primary scrambling code.

It can be understood in a very simple way by looking at Figure D.6 once more. In a SBS, assuming, for example, that the red and green areas are using the same scrambling code, a transmitted signal meant for an UE in the red area, received by a terminal in the green area is seen as intra-cell interference which partially orthogonal [8]. With HOS, the red, green, blue and yellow regions are smaller cells using different scrambling codes, thus this interference becomes inter-cell interference which is much more severe due to the total lack of orthogonality. This degradation may be high compared to the SBS operating in cell-splitting mode [46].

A final comment regards the amount of handovers, since each cell covers a much smaller area compared to a conventional 3-sector case, there is an increased signalling load due to much more frequent handovers. Studies on the impact of handovers were carried out in [46, 29].

D.5.5 Adaptive Beamforming

Adaptive array antenna systems use a variety of signal-processing algorithms to continually monitor their coverage areas, attempting to dynamically adapt to their continuously changing radio environment, which consists of users and interferers. These algorithms have different complexities and may optimize different criteria, e.g. SINR, mean-squared error (MSE) between the array output and the reference signal. Some of the most popular algorithms are the well-known LMS, RLS and MMSE algorithms [14, 49]. They correspond to the adaptive algorithm block, dotted lines, error and reference signals shown in Figure D.2. The utilization of *neural networks* for this purpose has also been reported in [38].

In theory, the CCI reduction achieved by adaptive systems is more substan-

[8] Part of the orthogonality is destroyed by multipath propagation as seen in Sections B.3.2 and C.3.1.

tial than the one obtained with fixed systems, because they can point the main lobe of beam towards a desired user more precisely since the weighting vectors can be dynamically modified, whereas in SBS the best beam (i.e. giving the highest gain in the direction of the user) is selected among N fixed beams.

User-Specific Beamforming

User-specific beamforming (USB) allows for the generation of individual beams towards each mobile. The system adapts the weighting vectors (both phase and magnitude), thus providing an effective antenna pattern that follows the user's motion. It can be seen as an extension of the switched beam method. Figure D.7 illustrates this concept.

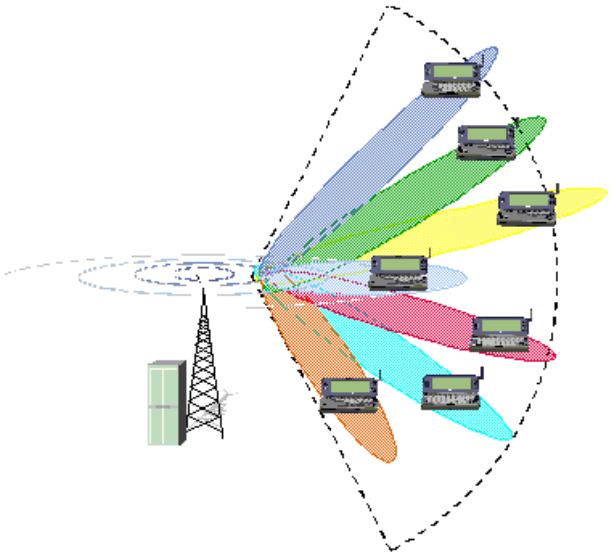

Figure D.7: 120° sector served by user-specific beamforming.

One advantage of this technique is that the radiated power is concentrated in narrow beams with their maximum gains always [9] pointed at the desired users, which reduces the interference, thus leading (in theory) to a higher capacity gain than the fixed beam approach. Another advantage is that beam-switching is not needed as the user moves in the cell, which means less signalling, since a specific

[9]This is due to the "infinite" pointing directions, given the freedom to adapt the weights.

beam tracks the desired user all the time, in other words, within a cell the users will never leave the coverage area of their own beams.

Not everything is perfect though, finding and tracking the weights for the DL in UTRA-FDD involves an extra challenge. Here the issue raised in Section D.5.2 (choosing the correct pointing direction) becomes more critical. The net effect is that beam patterns might not match the desired ones if the same weighting sets are used in both links.

Among the drawbacks, the continuous determination of the transmission weights for all active users is considered to be the most severe due to its is computational cost. Moreover, the terminals can not use the P-CPICH for phase reference and need to be informed through higher layer protocols to use dedicated pilot signals present in the DCH, these pilot signals are transmitted with much less power then the common pilot. Therefore, the channel estimation at these mobiles is poorer than that for mobile on a conventional network. In theory, a S-CPICH could also be transmitted in each beam, but it is intuitive to note the inefficiency of having a common pilot channel being used by just one user. Last but not least, user-specific beamforming is optional, that is, the UEs are not obliged to support it.

D.6 A Concept

It can be said that people usually need high bit rates when they are studying, concentrating, entertaining themselves, i.e. activities that require time and attention. It turns out, that these activities are commonly carried out at at home or inside buildings with very low or no mobility at all, just as sitting on your couch and enjoying a movie while you download it. On the go, we usually "consume" what we have already available, e.g. one's mp3 collection.

The wireless communication industry focused its efforts on outdoor mobile coverage, simply because the wireless industry was developed for mobile voice users,

like people driving their cars between home and work, before the internet boom. Hence, wireless carriers have historically had difficulties penetrating their signal into buildings, houses, etc [4], making it hard to provide high bit rates indoors reliably, due to penetration losses. On the other hand, if we ask ourselves where one finds really high bit rates nowadays, the answer will be conclusive: computer networks, either wired or wireless. Moreover, where are computer networks most commonly available? Inside buildings, houses, offices, etc. Besides, when available, wired networks are unbeatable in terms of throughput, but those also have their drawbacks e.g. setting up the infrastructure, very little (or no) mobility. This is one of the reasons why WLANs despite their inherent lower throughput are currently gaining terrain incredibly fast.

Given this scenario, it is obvious that cellular operators need 3G equipments capable of providing Internet-like capabilities indoors, otherwise, WLANs will have an edge in the competition for the same niche. With that in mind, an intriguing question arises: What can be done to overcome this impairment?

Repeaters have been used to increase coverage in GSM systems for some time and some studies about their applicability in UMTS have been carried out in 3GPP. They do ensure better signals, but do not really increase the capacity. Micro cells are a fine solution and could also be used, but it is important to consider the costs. Besides the capacity of one macro cell is not being increasing, simply a new smaller cell is created within the cell.

In this thesis beamforming has received a lot of attention and it is known to increase the capacity of a cell. Moreover, results in [29] confirm that user-specific beamforming greatly improves the capacity but at very high computational cost. Tracking the position of all desired users is an intensive task, apart from that, the capacity improvement might be degraded due due to imperfect UE position estimation. These reasons explain why the work in [29, 3, 9], among many others, has favored switched beam systems. They offer a good trade-off between performance and complexity.

Why should we bother then? "*Repeater-specific beamforming*" is a concept

that struck the author during the realization of this thesis. As Figure D.8 shows the repeaters would be fixed and would serve indoor users. Since the repeaters are motionless, repeater-specific beams would not imply the added complexity of estimating and tracking the location of users, and the capacity improvements provided by specific beams could be exploited. Indoor UEs would then benefit from stronger repeater provided signal, and would possibly achieve the desired higher bit rates. The difference between this and a conventional receiver is that, we are now concentrating the radiation power in the direction of the repeater, thus reducing CCI and creating a very high quality link between the BS and the repeater.

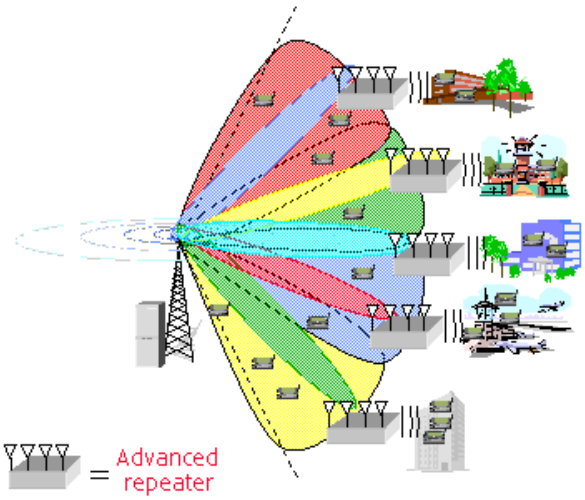

Figure D.8: Repeater-specific beamforming.

If we have an antenna array to generate the repeater-specific beams, we could also use this array to provide "standard" beam switching to the rest of the network. Those repeaters could be placed at key locations chosen by operators, such as offices, airports, or residence buildings willing to pay for this service. This is simply a matter of strategy and planning.

Another advantage of this concept is that it does not require any UE collaboration. Besides, instead of implementing receive diversity at the mobile, repeaters could provide it by having, for example, 2,3,4 antennas, since they would not have the power consumption constraints that terminals have. Moreover, all processing

can be done at RF level, but if we are willing to do some baseband processing, the repeater could even be used to interface completely different technologies, e.g. a WLAN terminal could be connected to a UMTS BS through the repeater, thus turning a possible competitor into an ally.

This way, I conclude that utilizing repeaters plus specific beams seems to be an effective solution for increasing downlink capacity and could compete against WLANs with the advantage of providing in one piece of hardware circuit switched voice [10] and high bit rate data services.

Unfortunately, this concept was not simulated because it would demand considerably deep modifications in the structure of the simulation tool, like the ability to simulate simultaneously indoor and outdoor environments for the same traffic model. It has been presented here as complement to this work and could be further investigated in the future.

D.7 The Big Picture

The purpose of this section is to summarize in a very concise way the concepts introduced in this chapter. The key benefits of antenna array systems are addressed in Table D.1. Figure D.9 foreshadows the simulations carried out in this thesis. The reasons why switched beam systems have been selected are given in Chapter G.

Mode of Operation	**Key Benefits**
Spatial diversity	Protection against fading and average SNR gain.
Beamforming	Interference rejection through spatial filtering

Table D.1: Features and benefits of antenna arrays.

[10] WLANs are capable of providing Voice over IP (VoIP).

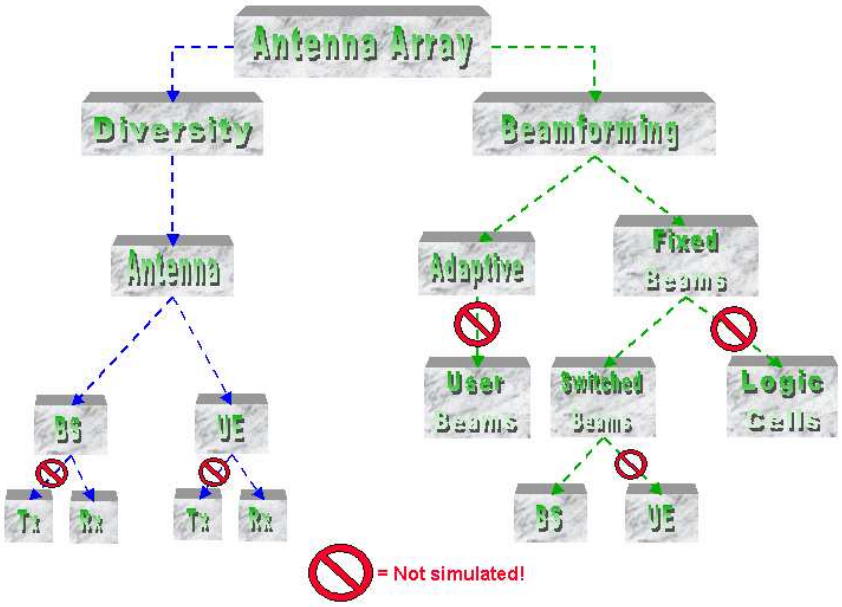

Figure D.9: Array of antennas: getting the big picture.

Part II

Simulations & Results

Apêndice E

System Level Simulations – Reference Cases

This chapter initiates the practical part of this thesis report. Its purpose is to introduce the readers to various methods of assessing the performance of an UMTS network, and to describe the chosen approach, which includes both the tool utilized for generating the results presented at the end of this chapter and the traffic models. These results are used as the comparison basis in the following chapters. Additionally, the default simulation setup and common parameters used throughout the rest of the chapters are presented here.

E.1 Introduction

When it comes to evaluating the performance of cellular systems one can resort to several different approaches, which include theoretical analysis, simulations and field trials. Each of them represents a compromise between level of detail and cost as shown in Table E.1.

Theoretical analysis usually involves low cost and provide rough estimates by means of mathematical models. Typically, these models rely on certain assumptions and simplifications that might not correspond to reality, thus rendering such models very limited in terms of detail. Given the high complexity of UMTS, coming up with a comprehensive theoretical model is an incredibly arduous and time-consuming

task.

Another popular approach, given the amount of processing power available nowadays, is to use computer simulations [1] of cellular networks. Such simulations allow the introduction of more realistic models and even specific algorithms for a more detailed study.

A third option is to conduct field tests in a trial or operational network. For a given network with a specific configuration, this approach yields the most accurate results, simply because everything is automatically being taken into account, design trade-offs, unseen variables, and imperfect implementations. Unfortunately, at the early stage of the development process, an operational network may not be available, and the deployment of a trial network is associated with a high cost. Furthermore, the results tend to be network specific (depending on the network configuration and environment) and may therefore differ from network to network.

Approach	**Cost**	**Level of Detail**
Theoretical modeling	Low	Limited
Static simulations	Moderate	Good
Dynamic simulations	High	Comprehensive
Field trials	Very high	Reality

Table E.1: Methods of evaluation of cellular networks performance.

E.2 Background

As explained earlier, the performance of the radio access network is difficult to investigate analytically due to the high complexity of UMTS. For this reason we resort to network level Monte Carlo simulations to assess the problem. In fact, simulations make it possible to use a high level of detail, saving time and money,

[1] There are basically two kinds of simulators, static and dynamic. The differences between them is clarified in the next section.

especially when compared with field tests.

In order to assess the *system level* performance of an UMTS network it is necessary to simulate several base station sites and hundreds, or even thousands of users. Naturally, a single simulator approach would be preferable but the complexity of such simulator would be huge! Simulating a complete network at chip-level, including all details of the physical layer such as (de-)interleaving, (de-)coding, modulation and so on is far too complex, and the duration of each simulation would be absurd if no super-computers are employed. Therefore, this problem needs to be tackled in another way. The basic idea is rooted in a common engineering principle: *divide and conquer*.

To put matters into perspective, simulators have been divided into two categories:

- *Link* level Simulators
- *System* level simulators

UMTS link level simulators usually operate at chip level ($260\,ns$) and take the whole physical layer into account (including channel coding, modulation, etc.) but the scenarios typically consist of one single base station and just a few mobiles. In most link level simulations, the data of only one mobile is collected. Figure E.1(a) illustrates a typical link level simulation scenario, while Figure E.1(b) depicts a simplified baseband transmitter-receiver structure of a link level simulator. Each block is not detailed here since a thorough description is out of scope and can be found in the literature [6, 13, 31]. Nevertheless, it is instructive to recall that the possible coding options, the interleaving process and the frame structure were mentioned during the description of the DCH in Section B.4.1. Chapter C has been dedicated to the channel modeling, whose simulation specific parameter values are presented in this chapter. Finally, the Rake receiver was introduced introduced in Section D.4.1. This small exercise allows the readers to grasp the intertwinement of the numerous elements that must be taken into consideration when dealing with cellular networks.

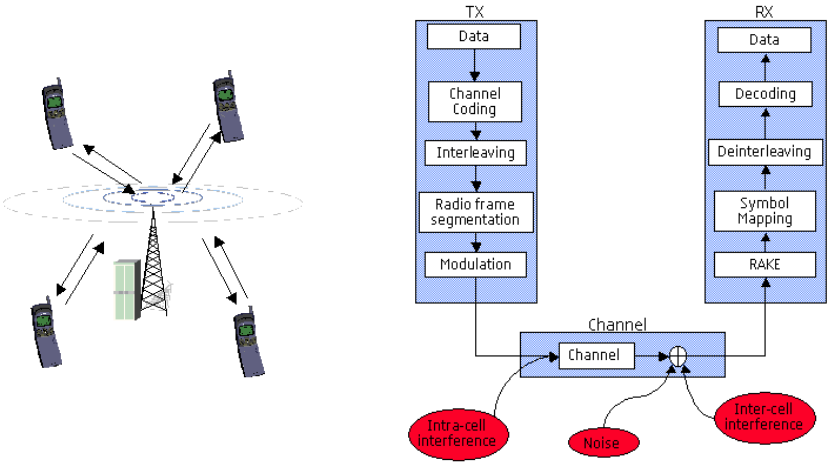

(a) Typical simulation scenario.

(b) Block diagram of the simulator (DL).

Figure E.1: Link Level Simulator.

On the other hand, UMTS system level simulators usually operate at slot level ($667\mu s$) in order to include the effect of the short term control functions, e.g. power control. These simulators model a system, evaluating large areas of an actual network which is populated with hundreds of users and several base station sites. A comparison between Figures E.1(a) and E.2 should help to clarify the difference between the two kinds of simulators. Common outputs of system simulators are e.g. the percentage of served users, the percentage of blocked users, power of each radio channel, total transmitted/received power, etc.

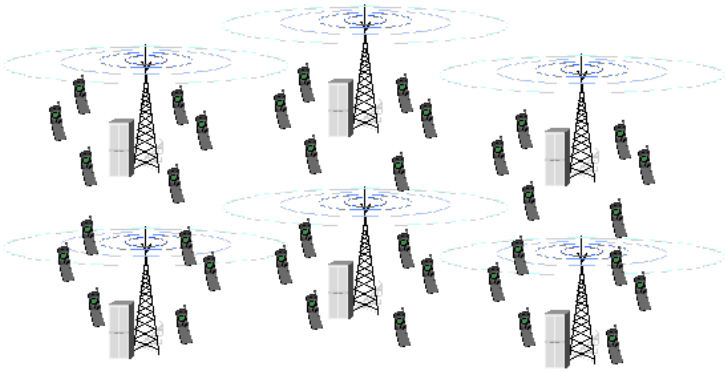

Figure E.2: Typical system level simulation scenario.

Now, that the simulation has been divided into two parts, we need an effi-

cient method of interconnecting them. The basic idea is to perform the computationally heavy link simulations only once to create certain *mapping functions*. In turn, the network simulator uses these mapping functions to convert information such as the Signal-to-Interference Ratio (SIR) into e.g. Block-Error-Probability (BLEP), thus enabling the estimation of the physical layer performance of each radio connection. In other words, system level simulators use *look-up tables* instead of actually simulating the entire physical layer procedures for every user. The look-up tables contain the results of the link level simulations. The generation process of such tables is postponed until Section E.3.3, in order not to disrupt the narrative flow of the chapter.

Now that we have cast our net wider, it is time to investigate system level simulators a little further, because this is the type of simulator used in this project.

E.2.1 System Level Simulators

System level simulators can be further subdivided into three categories: *static*, *quasi-static* and *dynamic* simulators. The second category, i.e. quasi-static, can be considered a combination of the other two.

In static system level simulators, the time dimension is not included. The system is analyzed with a certain number of users distributed in the system, each experiencing certain channel conditions. In order to achieve statistically reliable results, several realizations with independent user distributions and channel conditions are carried out, these realizations are called "snapshots". Simulation results are obtained after averaging the results over a sufficiently large set of "snapshots" (Monte Carlo approach). Since the time dimension is not considered, this kind of simulator is not suitable for analyzing RRM mechanisms, such as the PS (see Section B.5.4), which demand time to be taken into account [29].

By induction, dynamic simulators do consider the time dimension. This kind of simulator is a very good tool for analyzing the performance of radio resource management algorithms. Here a snapshot does not consist of a discrete

time point but several radio frames. During this time period the mobiles move in the system and generate traffic according their specified traffic model [50]. Moreover, the simulator used includes fast fading and fast power control for all mobiles in the system on a per slot basis. Due to the higher time resolution, fully dynamic system level simulators are much more computationally intensive than their static counterparts.

Finally, there is also the so-called quasi-static approach, in which only one time dependent process is observed, while the rest of the mechanisms affecting the system performance are treated as in static simulations.

In what follows, the dynamic system simulator utilized is described. Most of the upcoming issues have been touched on in Chapter C at an intuitive level, but here, as promised earlier, we go a little bit deeper, showing practical aspects related to the implementation in more detail.

E.3 The Simulator – WALLU

The simulation tool used in this project is an advanced dynamic UMTS system level simulator known as WALLU and is being developed by Nokia. Becoming familiar with this really complex tool, aiding the debugging process and testing the implemented features was an extremely time consuming task. In this section this tool is generically described and its simplified flowchart is depicted in Figure E.3 in order to provide readers with a better understanding of the adopted overall simulation strategy.

Due to the complexity of the simulator, an object oriented approach was selected. The sophisticated RRM algorithms (see Section B.5) - such as handovers, load control, admission control, power control and packet scheduling have also been included. The system modeling is highly accurate, hence the most severe drawback of this tool, the long simulation times.

This WCDMA radio network simulator can be used for capacity, coverage

and quality analysis, RRM algorithm development, and to aid WCDMA network planning and optimization in various environments. In this project, capacity analysis has received special attention.

The main characteristics of this simulation tool are: – Time resolution equal to one slot (667 μs). – Path loss, shadowing and fading included. Simulation of both DL intra- and inter-cell interference and of different channel profiles. – Voice, circuit-switched and packet-data are supported. – Accurate simulation of layers 1 to 3, while higher layers are based on simpler models.

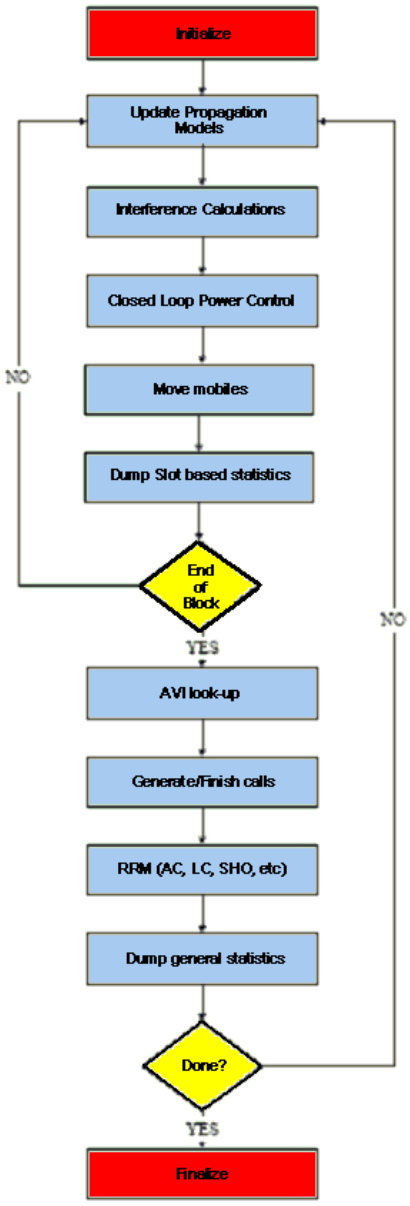

Figure E.3: Simplified flowchart of WALLU.

E.3.1 Radio Propagation

As seen in Chapter C, the transmitted signal is attenuated due to path loss, shadowing and multipath fading. The amount of the attenuation depends greatly on the environment. In what follows the description and the underlying assumptions concentrate in the DL direction, however they are also valid for the UL , unless noted different, due to the principle of reciprocity. Special notes are given where needed. In WALLU the integral path loss of the radio between a BS antenna and that of a mobile separated by d km is modelled according to a standard three-component model. Expressed in decibels, the integral path loss equals:

$$P(d) = P_L(d) + P_S + P_F, \tag{E.1}$$

where $P_L(d)$ is a distance dependent path loss, P_S is a random variable modeling shadowing (large-scale fading), and P_F is a random variable modeling the fading (small-scale fading). The random variables describing the shadowing and fading in one radio link are assumed to be uncorrelated, and independent of the distance (d).

Deterministic Path Loss

Probably the most well-known path loss model is the Okumura-Hata model, which is based on measurements by Okumura in and around Tokyo city and was later approximated by a set of formulae by Hata [51]. The model is valid in the frequency range from 150 MHz to 1000 MHz and takes into account the environment type (large city, medium-small city, suburban, open), the base and mobile antenna heights, and frequency. In the European COST (Cooperation in Science and Technology) 231 project [19], the model was extended to cover also frequencies between 1500 MHz and 2000 MHz in urban/ suburban environments. The path loss model used in WALLU for this project is the so-called COST 231-Hata-Model. It is applicable to built-up macro cell scenarios with quasi-smooth area and distances ranging from 1 km up to 20 km. The basic path loss, L_b (in dB), in urban areas

is [19]:

$$P_L = 46.3 + 33.9 \log_{10} f - 13.82 \log_{10} h_{BS} - a(h_{UE}) + \\ + (44.9 - 6.55 \log_{10} h_{BS}) \log_{10} d + C_m, \tag{E.2}$$

where $a(h_{UE}) = (1.1 \log_{10} f - 0.7)h_{UE} - (1.56 \log_{10} f - 0.8)$, and C_m is an empirical correction factor that equals 0 dB for medium-sized cities, and 3 dB for metropolitan centers.

For $h_{BS} = 30m$ (BS antenna height), $h_{UE} = 1.5m$ (UE antenna height) and carrier frequency $f = 2000$MHz, the model reduces to the following:

$$P_L = 137.74 + 35.22 \log_{10} d + C_m \tag{E.3}$$

Finally, the path loss is plotted as a function of the distance from the BS for $C_m = 0$ in Figure E.4.

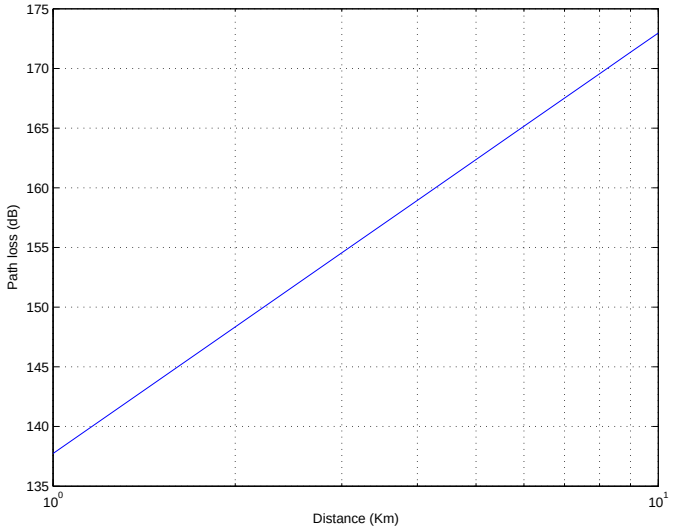

Figure E.4: Path loss predicted by the COST-231-Hata-Model.

Large-Scale Fading

The log-normally distributed shadowing is taken into account by the second term, P_S, in (E.1). Consulting the open literature [25, 52], and studies on the influence on the capacity of an UMTS network carried out both analytically and by means of simulations in [9], a standard deviation of 8 dB has been chosen.

The spatial auto-correlation properties of the shadow fading component are assumed to follow a negative exponential decay according to Gudmmundson's model [20], with a spatial coherence distance[2] of 50 m for macro cells in WALLU.

Finally, the cross-correlation coefficient of shadow fading between the links from one mobile to cells on the same BS site is set via a parameter with default value one, i.e. it is fully correlated. The correlation coefficient of shadow fading between the links from one UE to cells on different BSs is also a fixed parameter with a default value of 0.5. Figures E.5(a) and E.5(b) illustrate both cases. The arrows indicate the sector antenna pointing direction, the dashed arrows represents the strongest signal component of the link between the mobile and the sector antenna.

Results in the open literature have shown that the cross-correlation coefficient here depends on the angle between the vectors from the UE to the two cells, which is intuitively conceivable. However, this model is currently not supported in WALLU and is not expected to have any drastic impact on the capacity, since a value of 0.5 seem to be a good compromise solution [9].

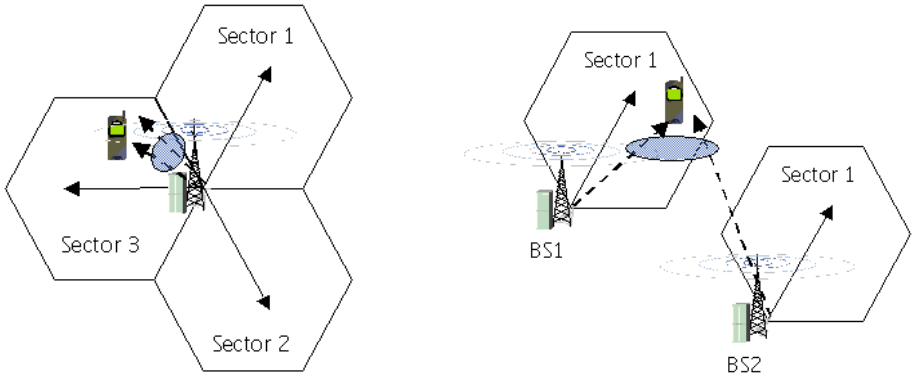

(a) Correlation between sectors=1

(b) Correlation between BS=0.5

Figure E.5: Shadowing Cross Correlation

Small-Scale Fading

As seen earlier in Section C.3, fading of the received signal is caused by

[2]This coherence distance refers to the shadow (large-scale) fading spatial correlation. Not to be confused with the coherence distance D_c (small-scale fading) introduced in Chapter C.

multipath propagation. The wideband channel is simulated with a PDP (see Section C.3.1) in WALLU. For each delay, the received signal consist of a large number of reflections from scattering objects placed on a circle around the MS. Furthermore, it is assumed that there is no LOS component, hence each tap coefficient has a Rayleigh distributed envelope with a Clarke's Doppler spectrum [53, 54] defined as

$$P(\nu) = \frac{1}{\pi} \frac{1}{\sqrt{\left(\frac{v}{\lambda}\right)^2 - \nu^2}} \quad ; \quad |\nu| < \frac{v}{\lambda}, \tag{E.4}$$

where ν denotes the Doppler shift, v is the mobile's speed and λ is the wavelength at the carrier frequency. The term *CLASSIC* is used to identify this Doppler spectrum and it controls the rate of fading due to the l^{th} multipath.

The tap coefficients are assumed to be uncorrelated complex valued stationary random processes because taps are separated by at least one chip-time (T_c). In this case the total channel power (in dB) is given by

$$P_F = 10 \log_{10} \left(\sum_{l=1}^{L} \xi_l \right), \tag{E.5}$$

where ξ_l is central Chi-square distributed with 2-degrees of freedom and denotes the power of the l^{th} path at delay τ_l, and L is the total number of paths. The model is characterized by the number of taps, the time delay relative to the first tap, the average power relative to the strongest tap, and the Doppler spectrum of each tap.

The PDPs for this project have been selected according to the ITU recommendations [21]: Pedestrian-A and Vehicular-A. However, it must be noted that the PDPs used in WALLU are modified versions of the original ITU PDPs, so that the delay between paths would equal at least one chip period ($T_c \approx 0.26\mu$s), i.e. $|\tau_m - \tau_n| \geq T_c \quad \forall \quad m \neq n$, thus all multipath components are resolvable by the Rake receiver. The modified ITU PDPs have been calculated taking into account the root raised cosine (RRC) filters [31] with a roll-off factor of 0.22 at the transmitter and receiver.

The relative average captured power (dB) and the relative delay (T_c) of the channel coefficients for both profiles are given in Table E.2.

Pedestrian A			**Vehicular A**		
Tap	*Rel. Delay*	*Avg. Power*	*Tap*	*Rel. Delay*	*Avg. Power*
1	0	-0.2	1	0	-3.1
2	1	-13.5	2	1	-5.0
3	–	–	3	2	-10.4
4	–	–	4	3	-13.4
5	–	–	5	4	-13.9
6	–	–	6	5	-20.4
Characteristics			**Characteristics**		
Delay	Low rms spread ($\approx$ 45ns).		*Delay*	Medium rms spread ($\approx$ 370ns).	
Freq.	Classic Doppler Spectrum.		*Freq.*	Classic Doppler Spectrum.	
Angle	Low spread ($\approx 2°$).		*Angle*	Low spread ($\approx 2°$).	

Table E.2: Power delay profiles [55, 56].

A limitation of the simulation tool is that the PDP is fixed during a simulation. However, different PDPs can be used simultaneously for each traffic model, i.e. all RT traffic users may be configured to use ITU Pedestrian-A, while e.g. NRT traffic users may use ITU Vehicular-A.

Azimuth Spread

The radio channel azimuthal dispersion observed at the BS is not explicitly modelled in WALLU. For standard simulations with conventional sector antennas at the BS the azimuthal dispersion only have marginal impact on the results, because the AS is much smaller than the 3 dB beamwidth of the sector antenna pattern, and is therefore not important to model. However, for more advanced simulations with smart antenna systems, the azimuthal dispersion starts to become more important. The selected approach for beamforming antenna simulations is described in Chapter G.

E.3.2 UE Performance Modeling

All UEs in the network are assumed to use a standard Rake receiver. The E_b/N_0 is computed for each Rake finger in every slot interval, followed by MRC (see Section D.4.1) to obtain the total E_b/N_0. The effect of using orthogonal channelization codes is included when computing the E_b/N_0 at each finger, since the time-synchronized orthogonal own cell interference is subtracted from the interference term in the denominator. In the following, an expression for the calculation of the E_b/N_0 at each slot for terminal i is given:

$$\frac{E_b}{N_0}(i)_{|slot} = \sum_{l=1}^{R} \frac{P_{\mathrm{RxDPCH}}(s,i).h_{ff}(s,i,l)}{P_{\mathrm{Noise}}^{\mathrm{UE}} + P_{\mathrm{RxTotal}}(i) - P_{\mathrm{own}}(s,i).h_{ff}(s,i,l)} \,.\, G_p \,, \tag{E.6}$$

where

$$P_{\mathrm{RxDPCH}}(s,i) = P_{\mathrm{TxDPCH}}(s,i).\, h(s,i) \,, \tag{E.7}$$

$$P_{\mathrm{RxTotal}}(i) = \sum_{k=1}^{K} \left(P_{\mathrm{TxTotal}}(k).\, h(k,i).\, \sum_{l=1}^{L} h_{ff}(k,i,l) \right) \,, \tag{E.8}$$

$$P_{\mathrm{TxTotal}}(k) = \sum_{u=1}^{\mathrm{Users}_k} P_{\mathrm{TxDPCH}}(k,u) + P_{\mathrm{P-CPICH}}(k) \,, \tag{E.9}$$

$$P_{\mathrm{own}}(s,i) = P_{\mathrm{TxTotal}}(s).\, h(s,i) \,, \tag{E.10}$$

and the notation is given in Table E.3. Note that this expression assumes that the resulting E_b/N_0 value at the output of the Rake receiver can be computed as the sum of the E_b/N_0 values at the output of the different Rake fingers. This is an approximation that assumes that the noise and interference components at the different Rake fingers are totally uncorrelated, which is not totally true but only a good approximation. Nonetheless, as will be explained in the next section, the effect of having partially correlated noised and interference at the Rake fingers is embedded in the look-up tables, which are based on detailed chip level processing.

However, no specific tables were available for SHO. In this case, ideal MRC between the outputs of the different SHO branches is assumed and the E_b/N_0 values corresponding to each branch are summed, in which case (E.6) becomes

$$\frac{E_b}{N_0}(i)_{|slot} = \sum_{s\in \mathbf{A}(i)} \sum_{l=1}^{R} \frac{P_{\mathrm{RxDPCH}}(s,i).h_{ff}(s,i,l)}{P_{\mathrm{Noise}}^{\mathrm{UE}} + P_{\mathrm{RxTotal}}(i) - P_{\mathrm{own}}(s,i).h_{ff}(s,i,l)} \,.\, G_p \qquad \text{(E.11)}$$

Symbol	Definition
G_p	Processing gain defined in Chapter B.
L	The number of multipath components.
R	The number of Rake fingers ($R \leq L$).
K	Total number of cells on the network.
$\mathbf{A}(i)$	Cells in the active set of terminal i during SHO.
s	The user's serving cell.
Users_k	Total number of users served by the k^{th} cell.
$h_{pl}(k,i)$	It represents the distance dependent deterministic path loss from the k^{th} cell to the i^{th} user.
$h_{sf}(k,i)$	It represents the log-normal shadow fading from the k^{th} cell to the i^{th} user.
$h(k,i)$	Path gain from the k^{th} cell to the i^{th} user. It includes the distance dependent deterministic path loss h_{pl}, the shadow fading component h_{pl}, and the transmit and receive antenna gains G_{Tx} and G_{Rx} respectively .
$h_{ff}(k,i,l)$	The path gain describing the fast fading for the l^{th} path of the link from the k^{th} cell to the i^{th} user.
$P_{\mathrm{Noise}}^{\mathrm{UE}}$	Power of the thermal noise at the UE.
$P_{\mathrm{TxTotal}}(k)$	The total wideband transmitted power in the k^{th} cell.
$P_{\mathrm{RxTotal}}(i)$	The total wideband received power by the i^{th} terminal including both own and other cell interference but without thermal noise. It is computed as the sum of the total received power from all the cells in the network.

Symbol	Definition
$P_{\text{own}}(s,i)$	Own cell interference experienced by the i^{th} UE in the s^{th} serving cell excluding fast fading.
$P_{\text{TxDPCH}}(k,u)$	The transmitted power on the DPCH for the u^{th} user in the k^{th} cell.
$P_{\text{RxDPCH}}(s,i)$	Describes the received power on the DPCH of the i^{th} user in the s^{th} cell without fast fading.
$P_{\text{P-CPICH}}(k)$	The power allocated to the primary common pilot channel of the k^{th} cell.

Table E.3: Notation for the E_b/N_0 calculation.

E.3.3 Actual Value Interface

As mentioned earlier, given that the simulation is divided into two parts, a method to interconnect the two simulators has to be defined. Conventionally, the information obtained from the link level tool is linked to the system simulation by using a so-called *average value interface* describing the *Block Error Rate* (BLER) performance as a function of E_b/N_0 values averaged over a very long period (the whole simulation run). By doing this, just the mean characteristics of the effects from multipath fading and interference variations are taken into account. However, this approach is not accurate if there are fast changes in the interference due to, e.g. high bit rate packet users or fast RRM algorithms. This simpler approach works well for static snap-shot simulations, but can not be used in the context of this project.

WALLU uses the so called *actual-value-interface* (AVI) [18] to provide accurate modeling of fast power control and high bit rate packet data. Such look-up tables have been generated and validated in Finland by Nokia researchers after extensive link level simulation campaigns. They represent the *block error rate probability* (BLEP) versus the geometrically averaged (over the transmission block length [3]) Eb/N_0 for a certain set of conditions. Because the generation process of

[3]The block length depends on the traffic type, e.g. 20ms for speech and 10ms for CS data at

the AVI tables is very elucidative, it is described next.

During the link level simulations, E_b/N_0 values are recorded for each slot period. For each block period, the geometrically averaged E_b/N_0 is computed and stored together with the output of the link level simulator, stating whether the block was successfully decoded or not. After the time-consuming link level simulation is finished, the intermediate outcome is a long vector with sets of geometrically averaged E_b/N_0 values per block and information about whether the block was successfully decoded. Then, this information is post-processed, by grouping these pieces of information into E_b/N_0 bins of e.g. 0.1 dB. After this, the corresponding BLEP per bin is calculated as the ratio between the number of unsuccessfully decoded blocks and the total number of processed blocks. In the final reckoning, the AVI table is the outcome of the post-processing of link level simulation results.

Different service profiles have been considered, which use different link level configurations. Therefore, different sets of AVI tables were generated for different bit rates, different spreading factors, different coding schemes (convolutional and Turbo coding) and different interleaving periods (10 ms and 20ms). Moreover, since the link level performance of the receiver depends on the PDP and speed of the terminals, different sets of AVI tables were created taking those factors into account. It is worth mentioning again that no specific AVI tables were created for SHO. One final comment regards the geometry factor defined in (B.3). Previous link level simulations using the G factor have shown that BLER curves are nonlinear functions of it. A difference as large as 3dB in the mean E_b/N_0 value could be seen in DL as function of G. Using averaged AVI tables (averaged over all G values) would result in errors compared to actual AVI curves for each G value. Hence, the tables have been generated for various G factors as well. Table E.4 summarizes all cases that have been used in a concise manner.

As stated before, the manner in which the E_b/N_0 is calculated assumes uncorrelated noise and interference at the output of the different Rake fingers. Although this is an approximation that is done in system level simulations, the

64 kbps.

DL DPDCH Attributes	Values
Spreading factor	8,16,32,128
G factor	$[-3, 12]$ in steps of 3dB
Channel profiles	ITU Ped A and ITU Veh A
Terminal speed	$3, 50$km/h
Channel coding	1/3 Turbo Coding
Interleaving period	10ms

Table E.4: AVI Tables

AVI tables assume that the E_b/N_0 is going to be calculated in this manner, and the effect of correlated noise and interference at the Rake fingers is therefore embedded in the different AVI tables [3].

So far, the purpose and the generation of the AVI have been explained, the next logical step is to understand how they have been put into use by the system level simulator: each time a mobile has received a number of slots corresponding to one block, an equivalent block E_b/N_0 is computed as the geometrical average of the E_b/N_0 values per slot in that given block. The appropriate AVI table (G factor, UE speed, PDP, etc) maps the block E_b/N_0 to an equivalent BLEP. A uniformly distributed number ($\chi \in [0, 1]$) is generated and compared with the BLEP. If $\chi <$ BLEP, the block is labelled as erroneous. Otherwise, it is labelled good.

E.4 Simulation Setup

E.4.1 Network Layout

The network consists of 9 BS with a site-to-site distance of 2.8 km as shown in Figure E.6(a). Given that network *wrap-around* is not used, the collection of statistics is limited to 4 central cells (6, 7, 8 and 14), which are highlighted in blue, the reason for that is the reduced interference levels in the outer cells, hence their results are discarded. Wrap-around would fold the network, somewhat like a soccer

ball, in that case cells 13 and 0 would be neighboring cells.

In all cases, the traffic density is uniform with respect to area in the entire network, i.e. there are no hot spots. Each BS is equipped with 3 sector antennas. The chosen antenna orientation is indicated in Figure E.6(a) by the black arrow looking out over the respective cell. The radiation pattern of the sector antennas is the same for all cells on the network and is shown in Figure E.6(b), and it has been generated according to [22].

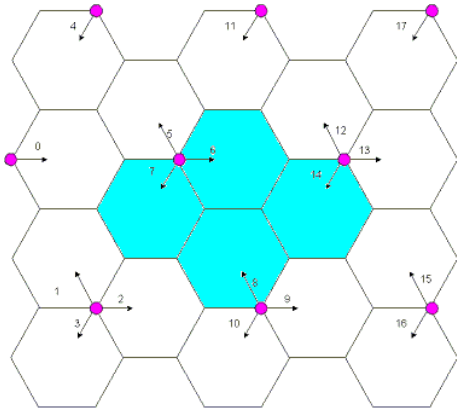

(a) Network layout with 4 center cells highlighted.

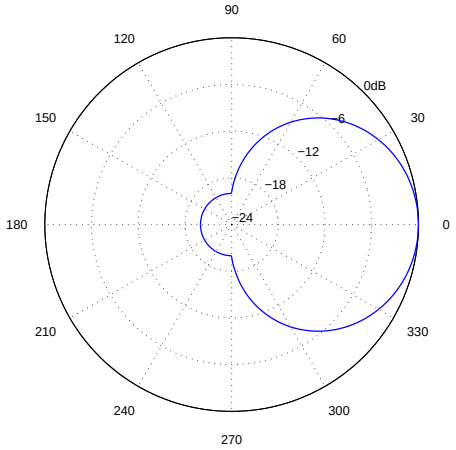

(b) Radiation pattern of the sector antenna

Figure E.6: Simulation setup.

E.4.2 Mobility Modeling

In a real network, the users move around with random speed and directions. For the simulations however, a simplified mobility model has been adopted. When the call is started, a random direction is chosen, and the users moves in this direction during the whole call. The user speed is constant and identical for all users in the network.

E.4.3 Call Properties and Load Settings

In the simulator, when new users are generated, they are uniformly distributed over the simulation area. The users are making calls and transmitting data according to a traffic model which controls the different phases of a call. WALLU supports both RT and NRT packet data models, whose specific details are presented in the next two subsections. Here we outline the call generation process and how the offered traffic is controlled.

Call generation (RT) and arrival of session set-ups to the network (NRT) are both modelled as a Poisson [35] process with a rate of λ calls/s. After being generated, calls necessarily go through two phases before becoming active, so that they do not jeopardize the network stability and the quality of existent connections on the network. These phases are synchronization and admission control. Admission control has been described in Section B.5.3. The synchronization is a very simple operation, a mobile will be synchronized to a BS if its instantaneous SIR exceeds a SIR threshold value for some time. A terminal may try to synchronize to more than one base station. If the SIR is less than a SIR threshold value, the mobile will start to increase its transmit power periodically, after some time if the SIR still does not exceed the SIR threshold value, synchronization is not successful and the call does not become active.

Having specified the call generation, now it is time to discuss how the offered load is controlled and how the network load is measured. The goal is to operate the network close to full load since this project is about capacity enhancing features.

The offered traffic in the network is adjusted with two parameters:

- **MaxNoTerminals**: The maximum number of simultaneous users on the network (users). A user is not calling all the time.
- **CallArrivalRate**: The call arrival rate per user per second (calls/user/s). This is set to a low, such that there will always be a user not calling to whom a call can be assigned.

We have the following relation between the above parameters and λ, the mean number of offered calls per second:

$$\textbf{MeanNoOfferedCalls} = \text{MaxNoTerminals} * \text{CallArrivalRate} \tag{E.12}$$

Adjusting these two parameters we will thus be able to adjust the network load. If we assume that the network is not operating in overload and that there is some prefixed mean call length (usually this would be the case for RT services) then the mean number of calls can be calculated as:

$$\textbf{MeanNoCalls} = \text{MeanCallLength} * \text{MeanNoOfferedCalls} \tag{E.13}$$

However, for NRT services the call length depends amongst other factors on load of the network, the position of the user, etc. At high bit rates a packet call will be shorter than calls with low bit rates. Moreover, the bit rate can vary during the call. So in this case we needed to make educated guesses and some iterations to get the offered traffic right.

E.4.4 Real Time Traffic Model

The traffic class used for circuit switched RT traffic is streaming. Streaming is a technique for transferring data such that it can be processed as a steady and continuous stream. It is becoming increasingly important with the growth of the internet and usually requires a high bit rate DL connection.

For CS streaming services, the traffic model is a constant bit rate model, with 100% activity factor. CS calls are assumed to have a block length of 10ms (15 slots) and a rate 1/3 Turbo encoder [13, 31].

In a real network, the average call lengths is likely to be longer, however, in order to reduce the simulation time, it has been chosen to reduce the mean call length to 20s. Table E.5 summarizes the CS services simulation parameters.

Parameters	Values
Bit rate	64 kbps (fixed)
Spreading factor	32
Call length	20 seconds
Activity factor	100%
Call Arrival	Poisson Distributed
Channel coding	1/3 Turbo Coding
Interleaving period	10ms

Table E.5: RT traffic parameters

E.4.5 Non Real Time Traffic Model

The UMTS traffic class selected for NRT traffic is the interactive and the modelled application is WWW browsing. NRT traffic is carried using Transmission Control Protocol (TCP).

DL NRT data traffic is likely to be one of the biggest sources of throughput in early 3G networks since one of the most commonly used internet services is web browsing. WWW browsing has typically very little throughput in the UL direction (requests for web pages and acknowledgements), whereas in DL all HTML files and graphics must be downloaded.

A packet service session contains one or several packet calls depending on the application. In a WWW browsing session a packet call corresponds to the download of a web page. After the page is received by the terminal, the user spends some time reading the information. This time interval is called *reading time*. It is also possible that the session contains only one packet call.

As previously stated, sessions arrive according to a Poisson process. Each user downloads one packet call, whose file size has been stochastically modelled as shown in Figure E.7(a). The average download file size is 120 kB. Minimum, median and maximum sizes equal 500 B, 30 kB and 1 MB respectively. The packet calls are modelled with start and end phase, which are disabled in the simulations.

TCP slow start and congestion avoidance mechanisms [57] are modelled in the traffic generator [58]. Figure E.7(b) presents the NRT generic model and should help readers visualize the concepts involved.

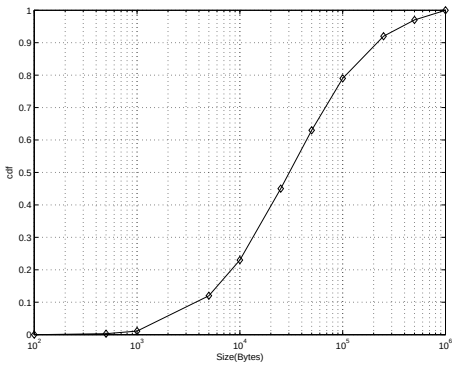

(a) Cdf of the packet call size

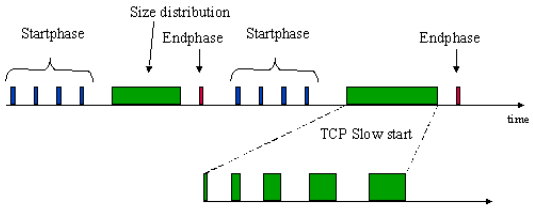

(b) Generic model for NRT traffic. From [58].

Figure E.7: NRT traffic modeling.

Bursty Traffic and Dedicated Channels

There is one last but very important characteristic of NRT traffic, namely its bursty nature, i.e. periods of heavy activity followed by a period of no activity. During a packet call several packets may be generated, which means that the packet call constitutes of a bursty sequence of packets. It is very important to take this phenomenon into account in the traffic model. Why is that so?

It is easy to conceive that for a bursty service transmitted on the the DCH, calls will sometimes be occupying resources that are allocated but not used. When data transmission is over, the DCH resources (channel codes as well as reserved power) are not immediately relinquished. They are usually kept allocated for a few more seconds (between 2 and 5 seconds) depending on the bit rate, and controlled by a network planning parameter, known as *InactivityTimerDownlinkDCH* [4]. Thus, we see that very bursty traffic on dedicated channels consumes a relatively high amount of network resources. When resources are sparse, it is a problem if a lot of

[4]There is an equivalent parameter in the UL, since the DCH is bidirectional. However, the UL is out of the scope of this report.

calls are occupying resources that they do not use.

When a call occupies a DCH with some allocated bit rate, it is said to be in *CELL DCH* mode. When it gets its DCH deallocated due to inactivity, it goes to *CELL FACH* mode, where it can still transmit a little amount of data on the common FACH channel. When it has more data to send, it can submit a new capacity request to get back in *CELL DCH* mode again.

One way to optimize the utilization of resources would be to adapt much faster to the inactivity of bursty services, so that when the call is inactive, the waste would be limited. This can be done by lowering the allocated bit rate in a few steps to some minimum level as soon as inactivity is detected. (Lower bit rates have smaller power and code requirements). Similarly, the bit rate would be increased back to the original level again once the call becomes active. Another way to overcome this problem of too many wasted resources is to lower the inactivity timeout period (*InactivityTimerDownlinkDCH*) to e.g. one second. This means, we simply throw inactive call in *CELL FACH* mode much faster.

Since this approach just involves changing a parameter, it is extremely easy to implement, but the problem is that there is a delay and some signalling involved when allocating/deallocating a DCH, and for services that are active e.g. once every second, the signalling overhead would be significant. In WALLU, however, extra signalling is not a problem, and there is no delay of swapping between *CELL DCH* and *CELL FACH* mode, so simulations were run with short inactivity timeout periods, under the assumption that the monitored performance is similar to what we would get from a proper implementation of a bit rate downgrade/upgrade method. Care has been taken not to set the timer too low, what could mask the higher code demand of NRT traffic. The main parameters can be seen in Table E.6.

E.4.6 RRM Algorithms

RRM algorithms, such as SHO, AC, PC (inner and outer), and PS are simulated. Besides, a resource manager is implemented for each cell to keep track of

Direction	Parameter	Value
UL	Bit rate limited to 16 kbps. Traffic acknowledgements only.	
DL	Radio Link Control (RLC) mode	Acknowledged
	Number of packet calls/session	1
	Start and End phases	Disabled
	TCP slow start	Enabled
	Minimum bit rate	32kbps
	Maximum bit rate	384kbps
	Inactivity timer	1 second

Table E.6: NRT traffic parameters.

the available channelization code resources. If nothing is explicitly stated, the default configuration for these algorithms as well as some other simulation parameter are presented in Table E.7. This simulation tool does not explicitly include any Layer-3 signalling mechanisms and this is estimated to have an effect on the system performance at medium-to-high UE speeds, due to the ignored Layer-3 signalling delays. However, this is not the case for low UE speeds (3 km/h) which are used in the majority of this project.

E.5 Simulation Results

The next subsections present the results of extensive system-level simulations utilizing the parameters introduced earlier. The results shown here for the 3-sector site system will serve as reference for the comparisons made in the subsequent chapters.

In this work, there are no mixed traffic simulation campaigns, that is to say, the offered traffic is either 100% RT or 100% NRT. The more realistic case of mixed traffic is suggested as a possibility for future studies. The aim is to operate the network at full load.

Algorithm	Parameter	Value
SHO	Wadd/Wdrop [6]	2/4 dB
	Max active set size [6]	3
	Tadd [6]	100 ms
	Tdrop [6]	200 ms
AC	$P_{TX\|\text{Target}}$(W/dBm)	10 W/40 dBm
	$P_{TX\|\text{Threshold}}$(W/dBm)	15 W/41.75 dBm
	Maximum BS TX power (sector)(W/dBm)	20 W/43 dBm
PC	Step size: inner loop PC [6]	1 dB
	Step size: outer loop PC [6]	0.5 dB
PS	Scheduling period [6]	200 ms
	Minimum allowed bit rate (DL) [6]	32 kbps
Others	P-CPICH power (W/dBm)	2 W/33 dBm
	Thermal noise power (DL)	-100.8 dBm
	BLER target	5%

Table E.7: Most relevant default parameters.

But first, let us understand what is meant by network load. The load can be measured in different ways. Load is the degree of utilization of a resource. As different resources (codes, power, etc) are needed to transmit data, the load can be specified with respect to a given resource. When a resource is needed and it is not available, blocking occurs. In this project, both power and code loads were used as load measures. When blocking due to power occurs the system is said to be interference limited, when code blocking limits the system capacity, the system is said to be hard-limited.

In addition, for packet switched cases, we look at the ratio of rejected capacity requests to the total number of capacity requests, also called the *capacity rejection ratio*. A request is denied, when the user is not scheduled a bit rate after a maximum amount of time (4 seconds or 6000 slots). This value is a network planning parameter and serves as an NRT traffic parallel for the admission control

blocking probability for RT traffic. In most cases, NRT users will be admitted anyway, because only a DL control channel spreading code (spreading factor 256) is requested. An interesting QoS related information is the mean time a user bit rate allocation request remains in the queue given the network load. If this time is reduced, average response times are lowered and users perceive a better connection, simply because one starts downloading data shortly after requesting it.

E.5.1 Real Time Traffic

The offered load given by **MeanOfferedTraffic** = MeanNoCalls $*$ BitRate, where BitRate = 64 kbps, has been progressively increased until blocking started to occur and the the *carried traffic* saturated. Simulations have been conducted for both PDPs, Pedestrian A (PedA) and Vehicular A (VehA), the latter was also simulated for terminal speeds of 50 km/h (VehA50).

Table E.8 summarizes the information contained in Figures E.8 and E.9. Obviously, not all the simulated scenarios are included in the table, what would make it quite cumbersome. Its sole purpose is to back up the forthcoming discussion, in case readers are avid for some numbers. Code utilization is not included, because this case does not suffer from code blocking.

According to the expectations, despite the larger multipath diversity provided by VehA, the lower time dispersion in PedA preserves better the orthogonality between signals under the same scrambling code and hence allows for a higher absolute capacity per cell. VehA50 results are the poorest ones due to the fast changing nature of the channel, which implies higher variation of the received power, this variation results in higher E_b/N_0 requirements to provide the same quality.

Figures E.8(b), E.9(a), and E.9(b) illustrate the behavior of the system. Power blocking happens more often as the the average total Tx power approaches the target value. Notwithstanding, it should be clear, that even when the average is below the target, instantaneous values can be above it, thus leading to power blocking. Actually, if the AC control is working properly, average values should be

Mean Off. Traf. (kbps)		600	800	1400
Mean Carried (kbps)	Ped A (3km/h)	584.0	639.5	682.0
	Veh A (3km/h)	554.4	604.0	657.4
	Veh A (50km/h)	486.8	523.4	538.2
Avg. Tx Power (W)	Ped A (3km/h)	37.5	38.3	39.0
	Veh A (3km/h)	37.7	38.4	39.0
	Veh A (50km/h)	38.0	38.7	39.2
Blocking (%)	Ped A (3km/h)	4.2	13.7	40.4
	Veh A (3km/h)	7.8	18.5	44.9
	Veh A (50km/h)	13.1	25.9	53.5

Table E.8: Some results for the reference case.

always below but close to 40 dBm when the load is very high.

We can see from Figure E.8(a) that, at first, the carried traffic increases as the offered traffic is incremented. As we approach the pole capacity [6] of the system the curves bend and blocking rates increase visibly without a significant increase in throughput. *The system is clearly interference limited.*

In addition, for comparison purposes, the average throughput, blocking rate and total Tx power of the samples in the flat region of each curve in Figure E.8(a) are calculated and taken as references. One might reasonably argue that commercial systems would never operate at such high blocking levels. Even though this argument is absolutely correct, one of the reasons for doing so is that our goal here is to push the system to its limits. It was decided to wait until the throughput curves were approximately flat to calculate those values. Besides, WALLU currently does not drop users with bad links, they remain in the system, probably demanding high Tx powers, hence taking up resources until their calls are over, which may result in biased blocking rates.

Finally, the average values are [5]:

[5]The presented throughput values take into account users who are in SHO, thus receiving from multiple cells, and exclude erroneously received bits according to the achieved BLER.

PDP	$E\{\text{Carried}\}$ (kbps)	$E\{\text{Blocking}\}$ (%)	$E\{P_{\text{Tx}}\}$ (dBm)
PedA	685.4	48.5	39.2
VehA	658.1	53.0	39.3
VehA50	546.4	60.0	39.4

Table E.9: Reference values for comparison.

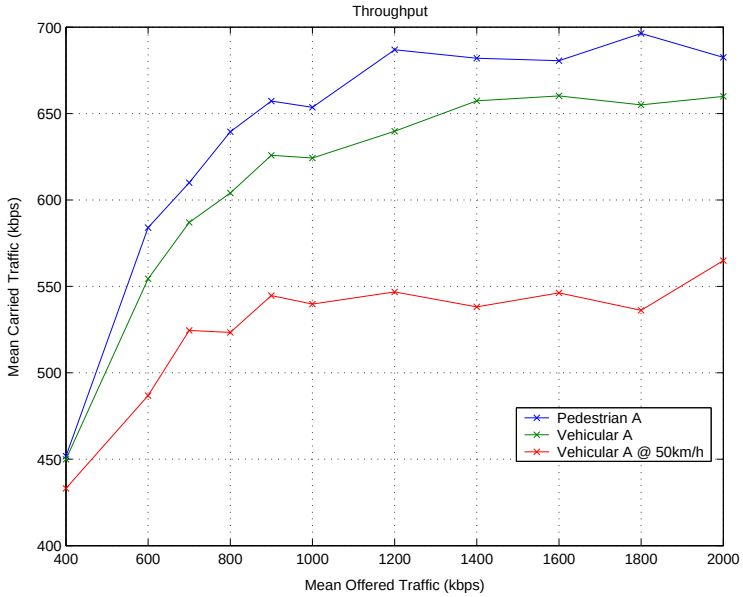

(a) The cell throughput as a function of the mean offered traffic.

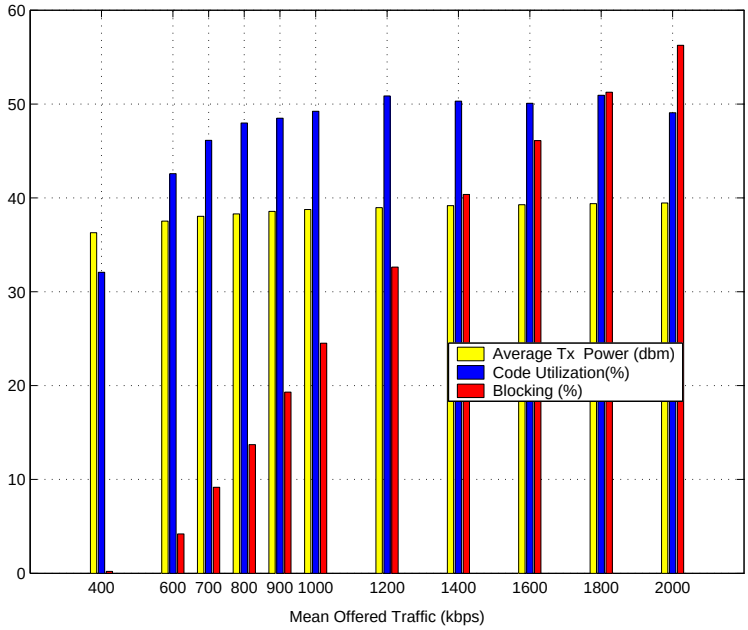

(b) Resource utilization and blocking rate (Pedestrian A).

Figure E.8: Reference case results (RT).

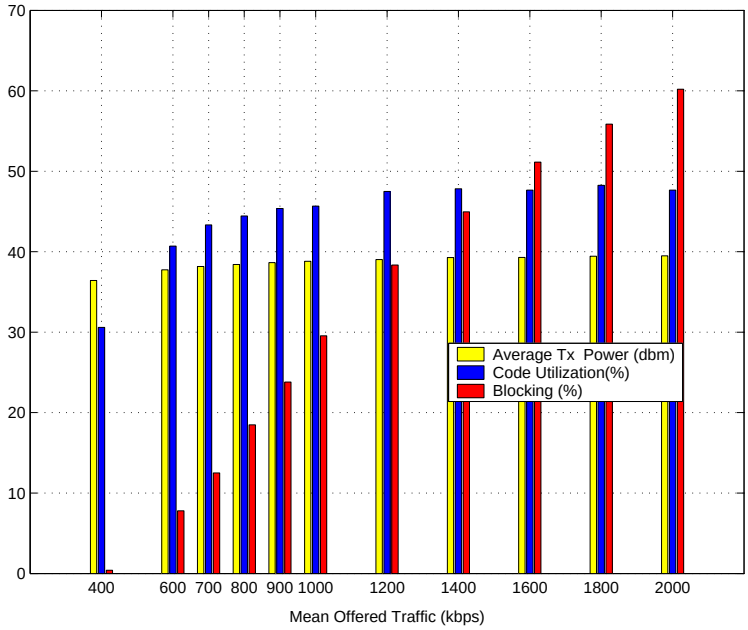

(a) Resource utilization and blocking rate (Vehicular A).

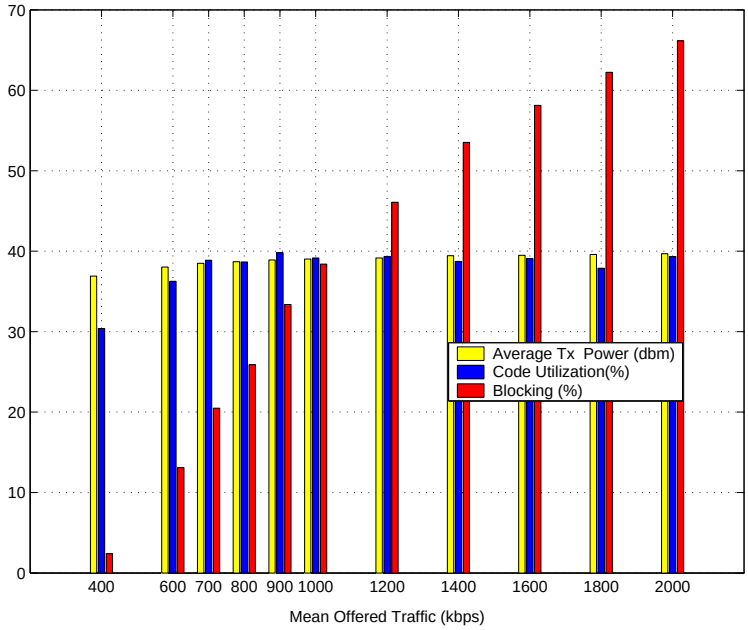

(b) Resource utilization and blocking rate (Vehicular A at 50 km/h).

Figure E.9: Reference case results (RT).

E.5.2 Non Real Time Traffic

The procedure here was similar to the one described in the previous section. However, there is no way to estimate (a priori) the offered traffic, since bit rates and mean call lengths vary as a function of the system's operating point.

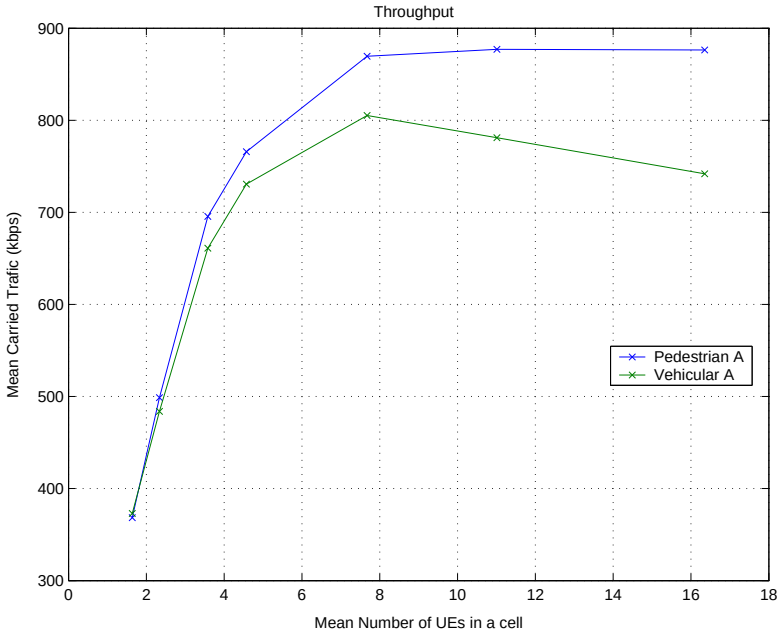

Figure E.10: The cell throughput as a function of the mean number of UEs in a cell.

Figure E.10 depicts the cell throughput as a function of the observed (a posteriori) load. The throughput initially increases with the number of users. The reason is that the low number of users do not download enough data to fill up the capacity of the cell. The capacity is limited to approximately 880 kbps per cell in PedA and 800 kbps in VehA. No NRT simulations have been conducted with mobiles at 50 km/h.

It is interesting to notice that the VehA carried traffic starts decreasing after a while. This is expected to occur with the PedA curve too. The reason for that is simple, as the system becomes more heavily loaded (approaching the interference limit), user scheduled bit rates decrease. Initially, the few users are allocated high bit rates. As the system load is gradually augmented, the PS favors serving more

low bit rate users rather than just a few high bit rate ones as described in Section B.5.4. However, the signalling overhead remains identical per user. Therefore the cell throughput starts to suffer from the large number of signalling channels. This relation can be depicted in a very simple way as shown in Figure E.11.

Observing Figure E.12 one can notice that, as expected, the code utilization now is much higher than that of RT traffic. This is due to the lower activity factor of NRT traffic, which decreases the average transmit power per UE, which in turn increases the number of UEs that can be admitted in the system.

On the other hand, blocking rates are much lower due to the aforementioned request of control channel spreading codes. It is also seen that the system is operating around $P_{TX|\text{Target}}$, what is indicated by the yellow ($P_{TX|\text{Total}}$) and green $P_{TX|\text{NrtInactive}}$ bars. The yellow bar never really reaches ($P_{TX|\text{Target}}$) because some power must reserved for inactive NRT traffic as explained earlier in Section B.5.4. However, their sum is indeed around 39.7 dBm for high loads.

Table E.10 shows the simulated mean value of the active user bit rates for three different loads. The transmitted bit rate distribution (active users only) can be seen for both channel profiles in Figure E.13, where the initial dominance of 384 kbps users is clear. When the load increases, a shift to the lower bit rates can be seen.

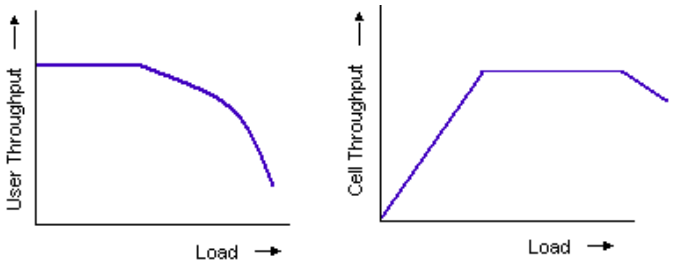

Figure E.11: User and cell throughput vs load.

Finally, Figure E.14 complements the analysis. Given that blocking rates should be seen with care in the NRT traffic case, we resort to the amount of rejected traffic, i.e., capacity requests that after being admitted by the AC, could not be

Mean User Bit Rates			
Relative Load	Low	Medium	High
PedA	244.3 kbps	160.5 kbps	78.1 kbps
VehA	242.1 kbps	151.5 kbps	73.1 kbps

Table E.10: Mean user transmitted bit rates.

scheduled by the PS after 4 seconds. It can be seen that more than 2% of such requests are denied. Moreover, mean queueing times are above 1 second, i.e. 25% of the maximum acceptable time when the mean number of users served by the cell is around 16.

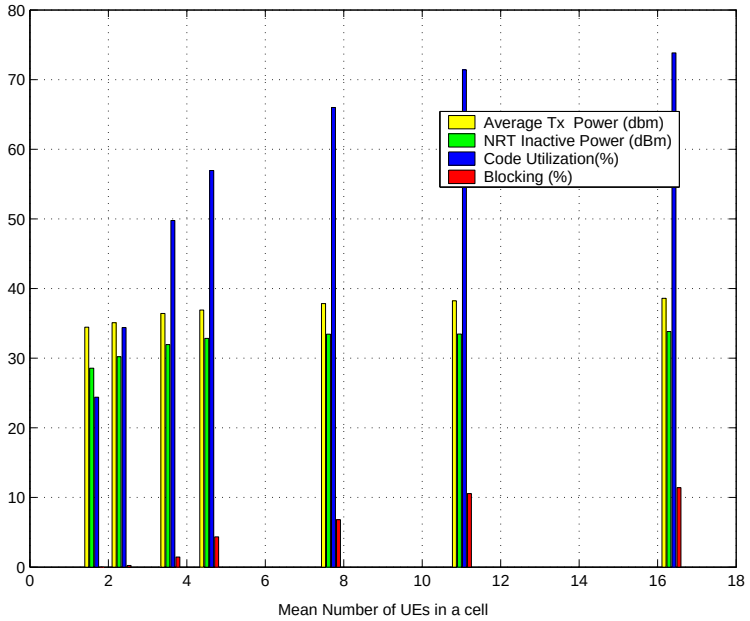

(a) Resource utilization and blocking rate (Pedestrian A).

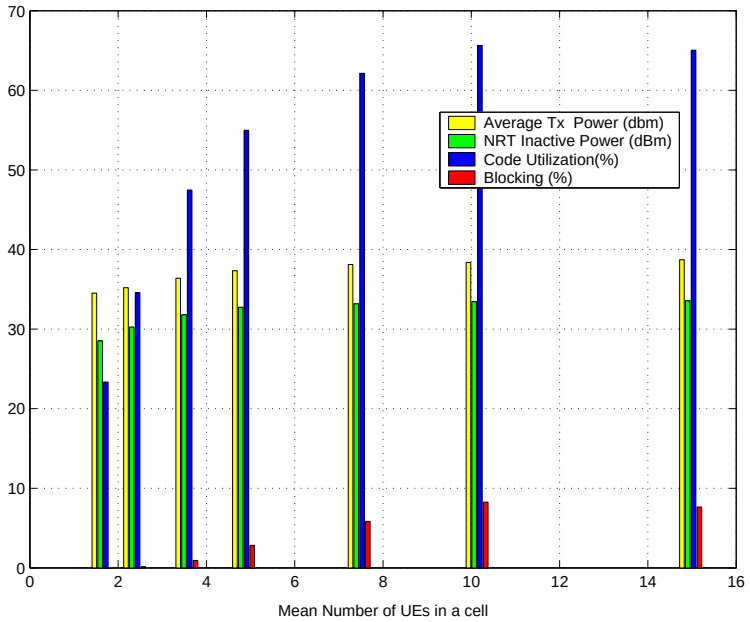

(b) Resource utilization and blocking rate (Vehicular A).

Figure E.12: Reference case results (NRT).

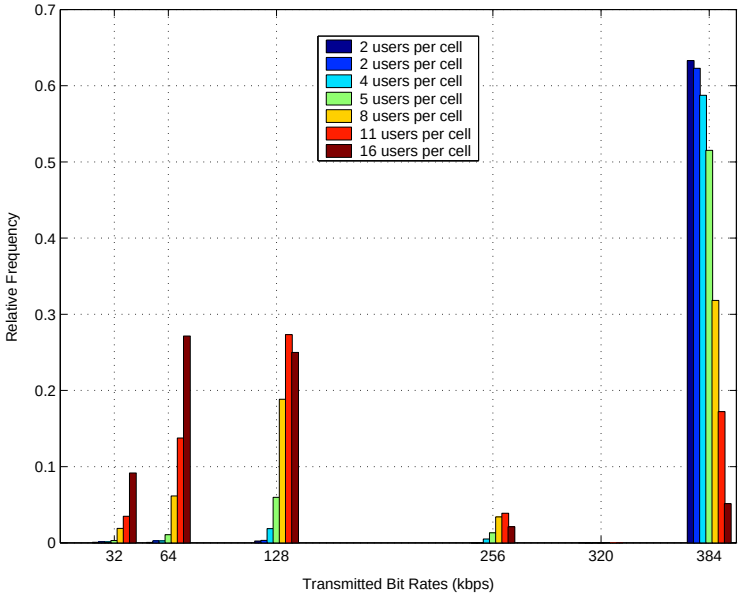

(a) Relative frequency of the DL bit rates at different loads (Pedestrian A).

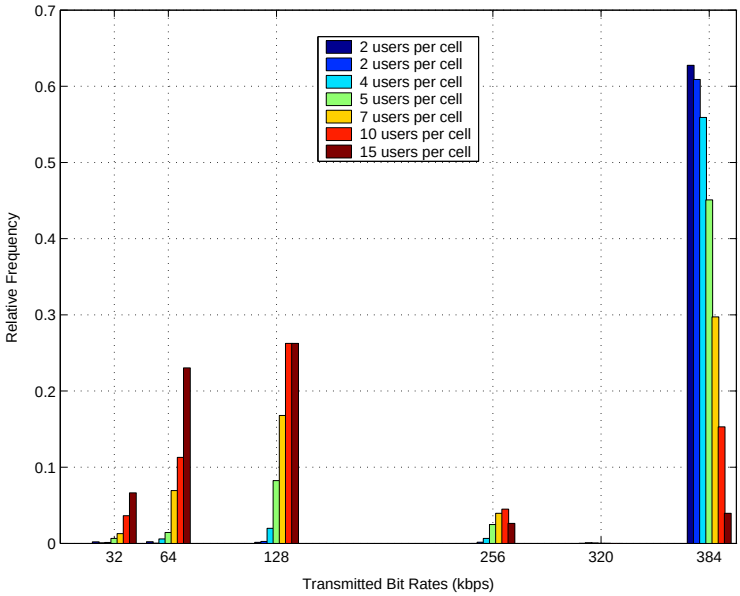

(b) Relative frequency of the DL bit rates at different loads (Vehicular A).

Figure E.13: Reference case results (NRT).

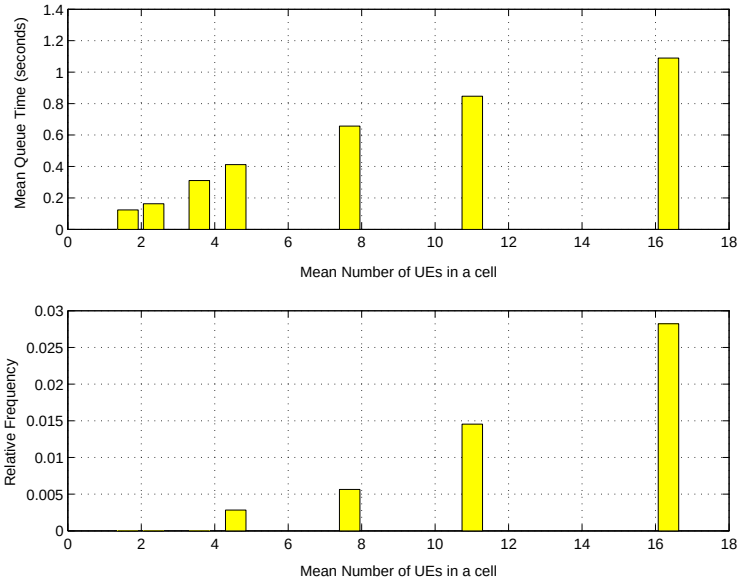

(a) Mean queueing time (above) and frequency of non-scheduled calls as a function of the mean number of UEs in a cell (Pedestrian A).

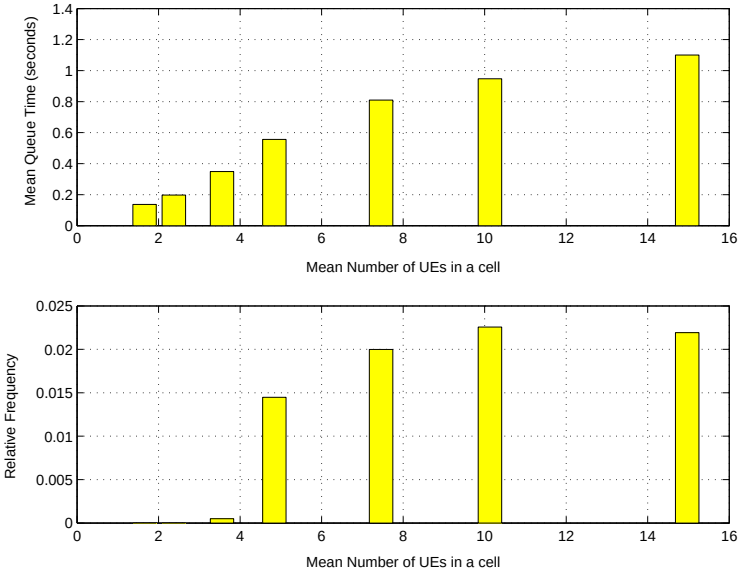

(b) Mean queueing time (above) and frequency of non-scheduled calls as a function of the mean number of UEs in a cell (Vehicular A).

Figure E.14: Reference case results (NRT).

E.6 Concluding Remarks

This chapter introduced various methods of assessing the performance of an UMTS network and described the simulation tool and methodology utilized throughout the rest of this work.

In addition, results which are going to serve as the comparison basis for the upcoming simulation campaigns have been introduced. They indicate that the typical UTRA FDD, macro cell DL capacity is between 550 and 900 kbps per sector per 5 MHz, which is in line with the material presented in Chapters 8 and 12 of [6]. It was seen that in both RT and NRT traffic simulations the system was interference limited. NRT traffic capacity figures were higher than those achieved by RT traffic. One explanation for that is that due to the multiple possible bit rate choices, the system can squeeze more low bit rate users when no capacity is left to serve high bit rate ones. In the RT case, there is no such freedom, the system can not allocate low bit rates even if it has room for such users, for the bit rate is fixed.

Apêndice F

System Level Simulations – Advanced Receiver at the UE

This chapter builds up on the material introduced in Section D.4. Here the DL performance enhancement provided by terminals equipped with advanced receivers is assessed. The results are obtained using the simulation tool described in Chapter E. The main goal is to measure the average system capacity gain in an UMTS cellular network where 100% of the terminals are equipped with such receivers. As before, the analysis is carried out for different traffic classes and channel profiles. Another crucial issue is to observe how the conventional RRM algorithms distribute the extra system capacity among the users.

F.1 Introduction

According to 3GPP Release' 99 specifications, UMTS networks are supposed to support the use of high bit rates, both in UL and in DL. However, the transmission of high bit rates in a cellular environment, however, poses some tough challenges. Among others, cell capacity and link performance in terms of inter-symbol interference can be cited as examples of such difficulties. The capacity results in Section E.5 show an average RT traffic capacity of 700 kbps per cell given the parameters introduced therein. It is straightforward to understand that supporting many high-bit rate users in each cell at the same time, either in RT

traffic or NRT scenarios is no easy task.

According to Release 5 UMTS specifications, the receiver used in the UE is transparent to the UTRAN, that is to say, advanced receiver at the UE can be deployed without further modifications in the rest of the network. Just like smart antennas, the term advanced encompasses many different technologies such as linear minimum mean-square error (LMMSE) chip level equalizers [59], antenna arrays (AA) using either interference rejection combining (IRC) or maximum ratio combining (MRC), etc. As reported in [60], the DL performance can be considerably improved with the use of advanced receivers. In this project, however, the scope of advanced receivers is limited to the Rake receiver at the UE, employing dual antenna MRC.

As stated in Chapter D, there are limitations regarding the number of antennas that can be implemented at the UE. Due to these limitations, the maximum number of antennas at the UE for this study is assumed to be two.

F.2 Simulation Setup

The setup for these simulations is analogous to the one presented in Section E.4. Each cell is covered by a sector antenna like the one described in the aforementioned section and only one scrambling code per cell is used.

The considered PDPs once again follow ITU recommendations [21]. However, there is a distinguishing factor worth mentioning in this case. For 2Rake receivers, two independent radio propagation channels are simulated between each Node-B and each dual antenna UE. Both radio channels have the same deterministic path loss and shadow fading. The average PDP is assumed equal and perfectly time aligned for both antennas, and the fast fading process affecting each propagation path is assumed to be independent from one antenna to the other, see Figure F.1.

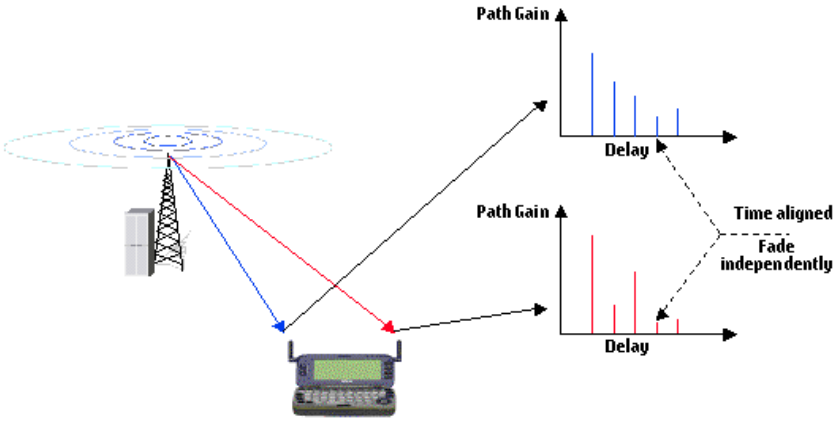

Figure F.1: Illustration of the two independent radio channels.

F.2.1 UE Performance Modeling

Much like, the material presented in the corresponding section in Chapter E, here the way the E_b/N_0 is calculated for terminals with 2Rake receivers is shown. The AVI principle and the calculations on a per slot basis remain valid here. In the following, an expression for the calculation of the E_b/N_0 at each slot for terminal i is given:

$$\frac{E_b}{N_0}(i)_{|slot} = \sum_{m=1}^{M}\sum_{l=1}^{R} \frac{P_{\text{RxDPCH}}(s,i).h_{ff,m}(s,i,l)}{P_{\text{Noise}}^{\text{UE}} + P_{\text{RxTotal}}(m,i) - P_{\text{own}}(s,i).h_{ff,m}(s,i,l)} \cdot G_p, \quad \text{(F.1)}$$

where

$$P_{\text{RxTotal}}(m,i) = \sum_{k=1}^{K}\left(P_{\text{TxTotal}}(k).\, h(k,i).\sum_{l=1}^{L} h_{ff,m}(k,i,l)\right), \quad \text{(F.2)}$$

$M = 2$ is the number of antennas at the UE, $P_{\text{RxTotal}}(m,i)$ is the total power received by the m^{th} antenna of the i^{th} UE, and $h_{ff,m}$ is the path gain describing the fast fading for the l^{th} path of the link between the k^{th} cell and the m^{th} receive antenna of the i^{th} user. The rest of the notation is presented in Table E.3, which is not repeated here for the sake of space. In case of SHO, ideal MRC between the outputs of the different SHO branches is assumed and the E_b/N_0 values corresponding to each branch are summed, similarly to what is shown in (E.6).

Note that this expression assumes that the resulting E_b/N_0 value at the output of the Rake receiver can be computed as the sum of the E_b/N_0 values at the

output of the different Rake fingers. In the analogue expression given in Chapter E, it was pointed out that it assumes that the noise and interference components at the different Rake fingers are totally uncorrelated. As already stated in Section E.3.2, this is not totally true for the case in which the outputs of Rake fingers connected to the same antenna are combined, but the effect of the partially correlated noise and interference is embedded in the AVI tables. However, when combining the outputs of Rake fingers connected to different antennas, it is fair to state that the noise components are totally uncorrelated. As for the interference, this assumption also holds true if the antennas are separated enough to be considered uncorrelated, which is the case in this study.

F.3 Simulation Results

In the following the results of extensive system-level simulations utilizing the parameters introduced earlier and 2Rake receivers at the terminals are presented.

F.3.1 Theoretical Gain

A simple theoretical analysis presented in [3] states that the capacity could be at least doubled if all terminals on a network are equipped with 2Rake receivers and no code restrictions are taken into account.

In this situation, a theoretical SNR average gain of 3 dB is to be expected, providing a link power reduction factor of 2, even if the diversity antennas are fully correlated because the desired signal from the two antenna branches are coherently combined, while the interference is combined non-coherently [6]. In addition, depending on the amount of diversity already present, diversity gains and protection against fading are an extra benefit for the case of uncorrelated or low correlated receive antennas. When extra sources of diversity are already present 2Rake receivers are prevented from adding much diversity gain.

F.3.2 Real Time Traffic

The same procedures described in Section E.5.1 are performed here. It must be pointed out that the capacity gain provided by 2Rake receivers is expected to make the system code limited instead of interference limited, depending on the propagation environment. Hence, both realistic and hypothetical cases, with and without code restrictions have been simulated in order to assess the achievable and full gain provided by dual antenna diversity receivers at the terminals.

In theory, the number of orthogonal codes is not an absolute hard-blocking limitation for the DL capacity because multiple scrambling codes can be taken into use. However, in the real world, nothing comes for free, and as pointed out in Section B.3.2, the uncoordinated introduction of secondary scrambling codes *severely deteriorates* the DL code orthogonality. Unlike the beamforming case described in the next chapter, there is not a straightforward solution to overcome this problem.

Analogously to the previous chapter, the average throughput, blocking rate and total Tx power of the samples in the flat region of each curve in Figures F.2(a) and F.4(a) are presented in Tables F.1 and F.2 for the code restricted and unrestricted cases respectively.

PDP	$E\{\text{Carried}\}$ (kbps)	*Gain* (%)	$E\{\text{Blocking}\}$ (%)	$E\{P_{\text{Tx}}\}$ (dBm)
PedA	1277.8	86.4	39.9	37.8
VehA	1241.4	88.6	40.1	38.8
VehA50	1019.4	86.5	47.3	39.3

Table F.1: Reference values for comparison (Code restricted).

When compared to the results presented in Table E.9, these results show a gain in the order of 86% which is below the expected average gain, specially for the PedA case. So what went wrong here? Figures F.2(b), F.3(a) and F.3(b) contain the answer. It can be seen that blocking rates (red bars) keeps on increasing even though the average P_{Tx} (yellow bar) values are lower than the target value. Looking

at the code utilization the answer becomes clear. The average code utilization is extremely high, specially in the PedA and VehA cases. This gives a clear indication that the system *is no longer interference limited, but code limited*. This is why the full gain is not realized. Let us quench our curiosity and find out what happens without any restrictions.

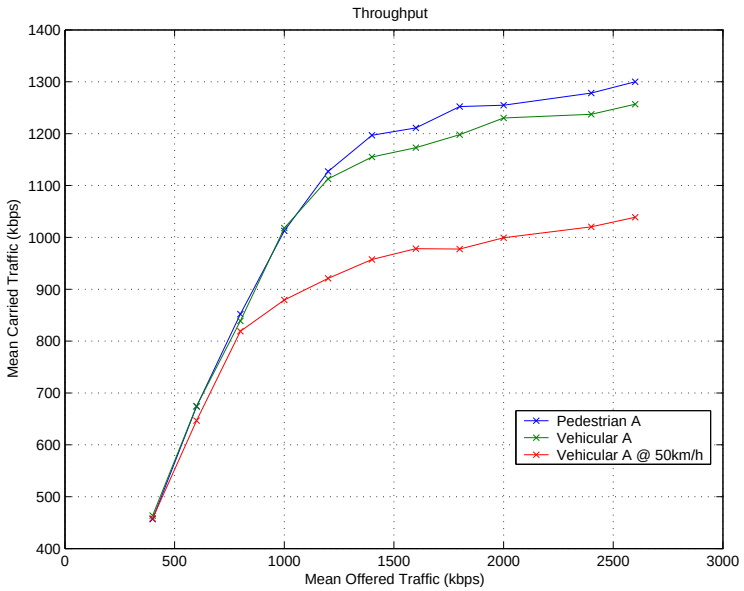

(a) The cell throughput as a function of the mean offered traffic.

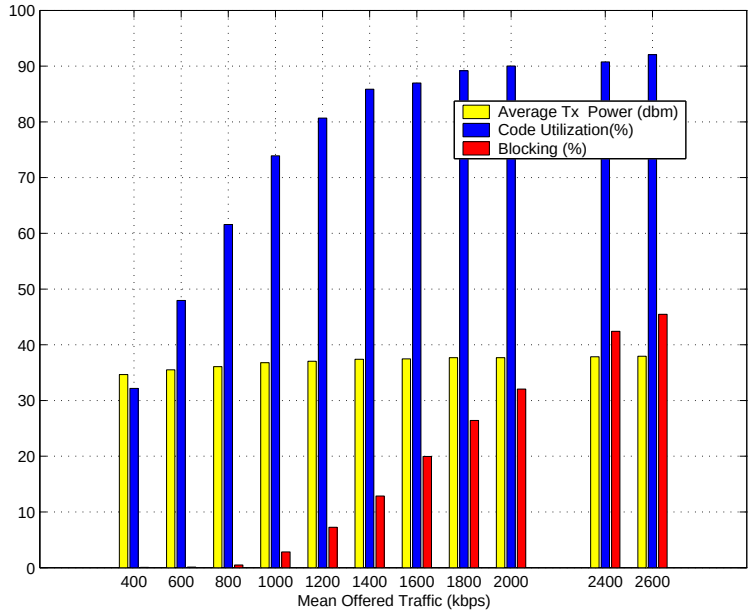

(b) Resource utilization and blocking rate (Pedestrian A).

Figure F.2: 2Rake receiver restricted case results (RT).

Figures F.4 and F.5 depict the behavior of the system in this scenario. The

PDP	$E\{\text{Carried}\}$ (kbps)	*Gain* (%)	$E\{\text{Blocking}\}$ (%)	$E\{P_{\text{Tx}}\}$ (dBm)
PedA	1530.0	123.23	22.4	38.9
VehA	1281.4	94.71	35.7	39.1
VehA50	1023.3	87.28	45.8	39.2

Table F.2: Reference values for comparison (Code unrestricted).

code utilization is always empty because we assume infinite codes. Now, after lifting the limiting factor, it is time to compare the the results presented in Table F.2 with those in Table E.9. We see that the capacity gain is 123.23% for PedA, 94.71% for VehA and 87.28% for VehA50.

VehA50 results do not show much difference, what means, that even with the advent of 2Rake receivers, this propagation environment remains interference limited. In this case, the *achievable* gain and the *full* gain are approximately the same. VehA is quite close to the 100% gain. The interesting part comes now with PedA. It shows a large difference between both cases. The reason for this difference is that PedA has less inherent frequency diversity than VehA, which allows the 2Rake receivers to add much more diversity gain.

It can be concluded that larger code blocking rates is experienced by radio channels with lower time dispersion, because, from an interference point of view, the lower time dispersion preserves better the orthogonality between UEs in the same cell, which increases the capacity. Since the code restrictions are fixed, code blocking has a more severe impact in scenarios facilitating larger absolute capacity. Moreover, if SHO was disabled, capacity gains would have been larger for two main reasons: First, SHO causes an increase in the code blocking rate, due to the higher average code consumption per UE. Second, SHO already provides diversity gain, and the combination of several sources of diversity provides diminishing returns.

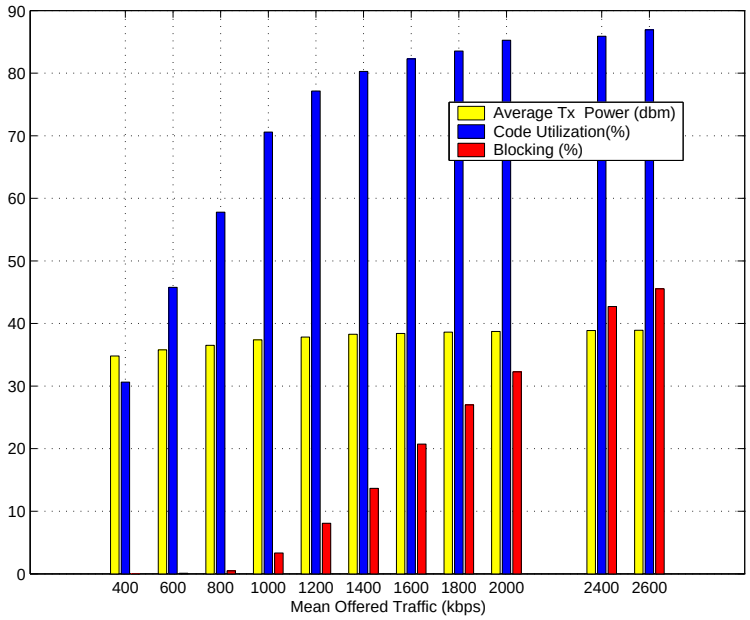

(a) Resource utilization and blocking rate (Vehicular A).

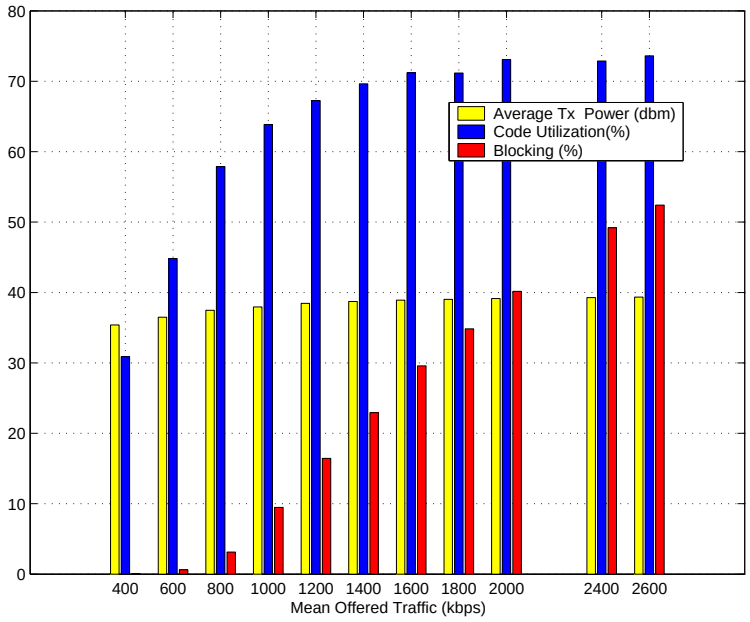

(b) Resource utilization and blocking rate (Vehicular A at 50 km/h).

Figure F.3: 2Rake receiver restricted case results (RT).

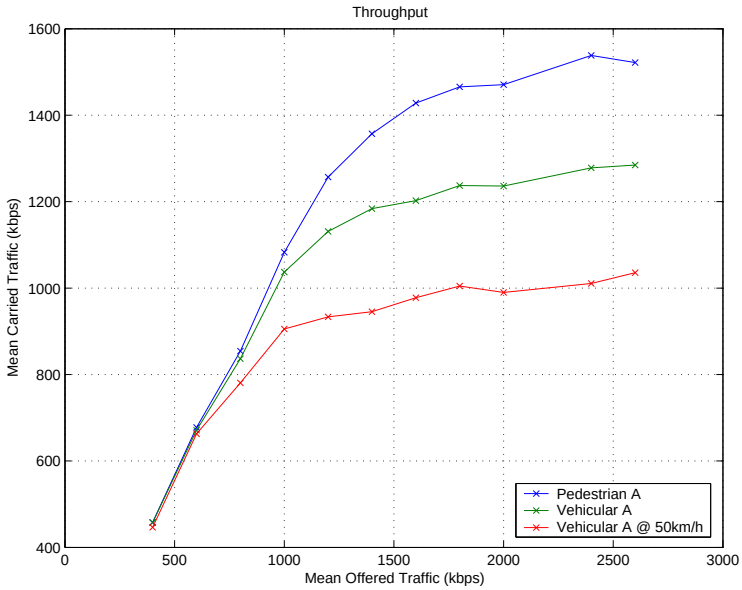

(a) The cell throughput as a function of the mean offered traffic.

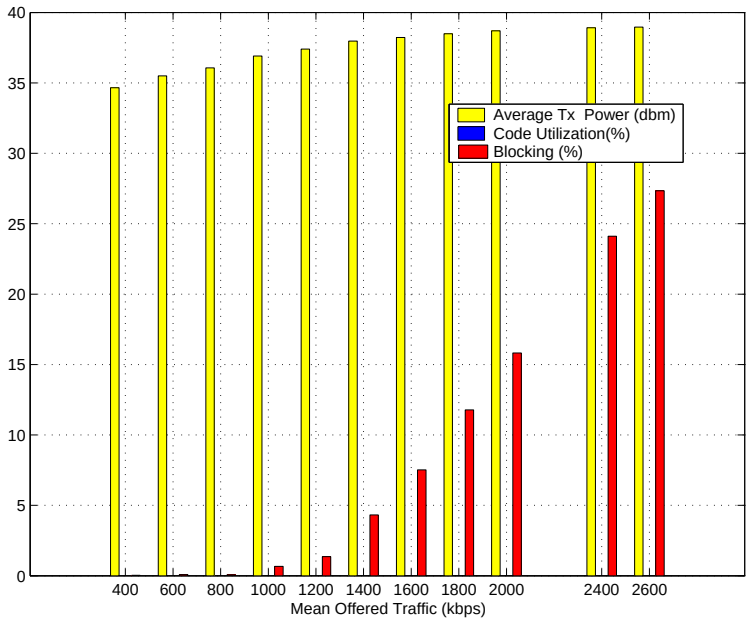

(b) Resource utilization and blocking rate (Pedestrian A).

Figure F.4: 2Rake receiver unrestricted case results (RT).

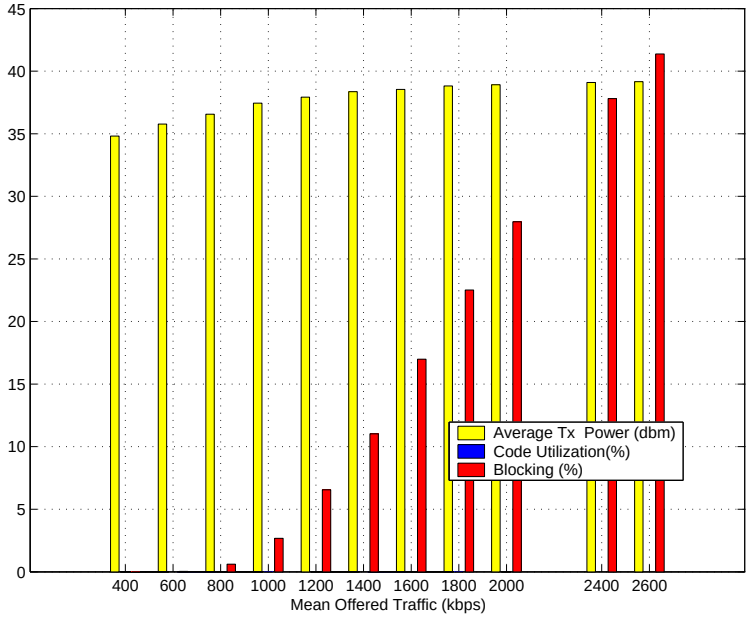

(a) Resource utilization and blocking rate (Vehicular A).

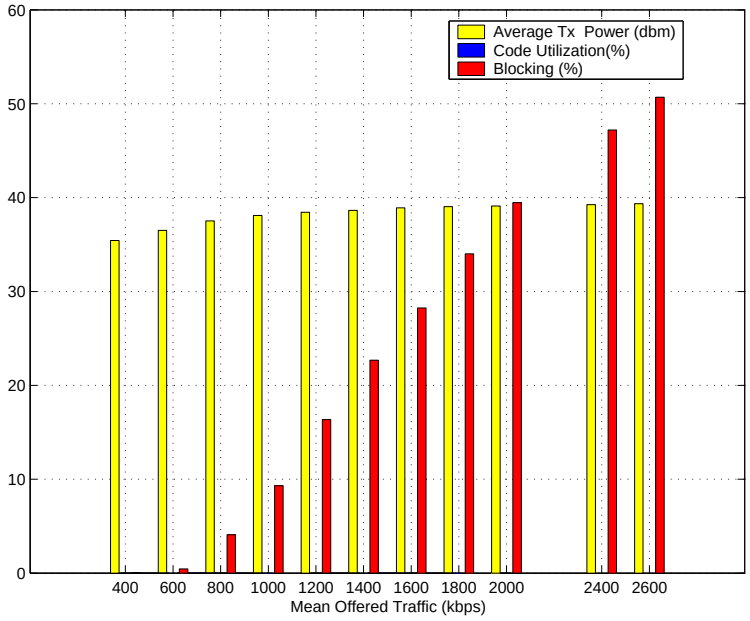

(b) Resource utilization and blocking rate (Vehicular A at 50 km/h).

Figure F.5: 2Rake receiver unrestricted case results (RT).

F.3.3 Non Real Time Traffic

The methodology and discussions presented in E.5.2 remain valid here. Nevertheless the way results are presented changes considerably. In Chapter E, focus was on presenting the behavior of the system. Now, it is desired to compare the performance improvements. Definitely, that was also the main goal of the previous section, however, the RT case is much simpler to analyze. Basically, one looks at the carried traffic for a given operating point, in our case full load, and assesses the capacity gain calculating the ratio between the carried traffic in the system implementing the desired feature and the reference one. NRT traffic model however requires a careful analysis for it tries to conceal its secrets.

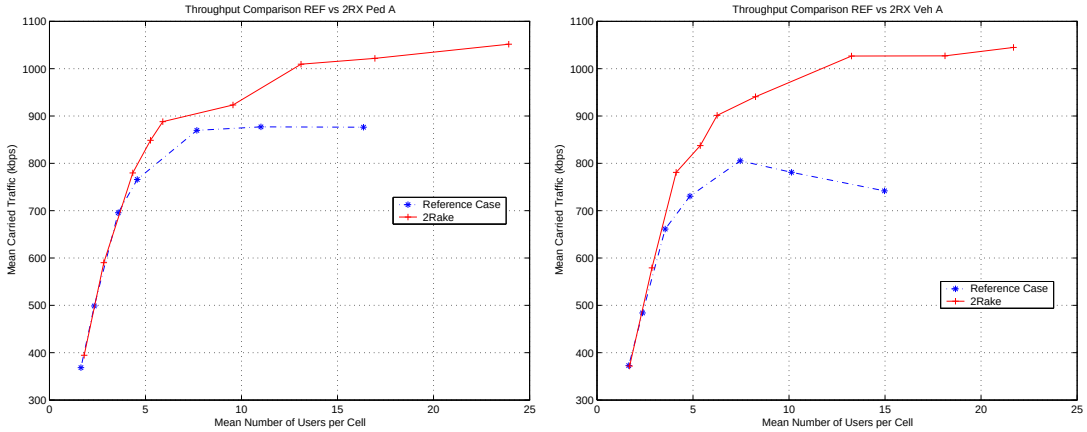

(a) Throughput comparison (Pedestrian A). (b) Throughput comparison (Vehicular A).

Figure F.6: 2Rake versus reference (Throughput).

Let us begin with Figure F.6 which depicts the cell throughput as a function of the observed (a posteriori) load for both PDPs for both systems, the reference and the one with 2Rake receivers at the terminals. When we compare the maximum carried capacity, we see a marginal gain of $19,9\%$ in PedA and $29,75\%$ in VehA. Having seen in the previous section that the system became code limited for RT traffic models with the deployment of 2Rake receivers, it is more than expected to see the same trend here, in light of the discussion in Section E.5.2, NRT traffic models have a higher code utilization. A marginal gain of $29,75\%$ in the maximum capacity would not pay off the investment in more expensive terminals. It would be rather hard to convince either users or operators to purchase such terminals. But,

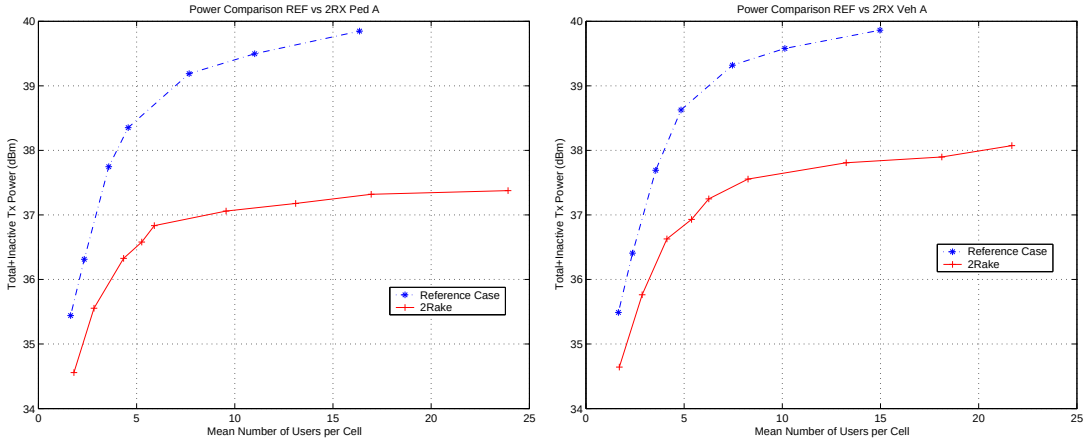

(a) Transmit power comparison (Pedestrian A). (b) Transmit power comparison (Vehicular A).

Figure F.7: 2Rake versus reference (Power).

is this it? The system is no longer interference limited and there is no easy way to overcome this problem, and we have to content ourselves with such an inferior gain?

In addition, we analyze the evolution of transmit power requirements as the load is increased and compare the performance of both systems. The outcome is presented in Figure F.7. The curves show the sums of ($P_{TX|\text{Total}}$) and $P_{TX|\text{NrtInactive}}$, since power must reserved for inactive users and the PS has to abide this restriction. Here, the difference is crystal clear. The reference system reaches its transmit power limit, whereas the system with 2Rake receivers does not, the code limitation does not let that occur. There is a difference of at least 2 dB in both cases. Yet, users can not benefit from that, on the other hand, operators would need less power at their BSs in order to offer the same capacity.

Next, the average value of the user experienced bit rate is investigated as the amount of users in the system is incremented. The goal is to find out wether or not the RRM algorithms, specifically the PS, is capable of providing 2Rake users with higher throughput compared with regular terminals. This is shown in Figure F.8. The curves show the average bit rates packet switched data users enjoy as a function of the average number of users in a cell. There seems not to be a significant difference among both cases. This is due to the packet scheduling strategy, which tries to schedule the highest possible number of users provided that

the power budget and minimal bit rate requirements are respected. In the reference case, as the load increases, the bit rates are lowered because there is no power to provide high bit rate connections. Here, even though power is available, codes are not [1]. The following reasoning should make it clearer. One 384 kbps link requires a code with a SF= 8, while a 32 kbps link uses a SF=64. Therefore, if the PS decided to serve one user with 384 kbps, it would be done in detriment of eight 32 kbps users. The main conclusion is that, since there is still power left in the 2Rake receiver scenario, without any modification in the PS, the system will be able to schedule many more 32 kbps. Once again, operator capitalize on the gain.

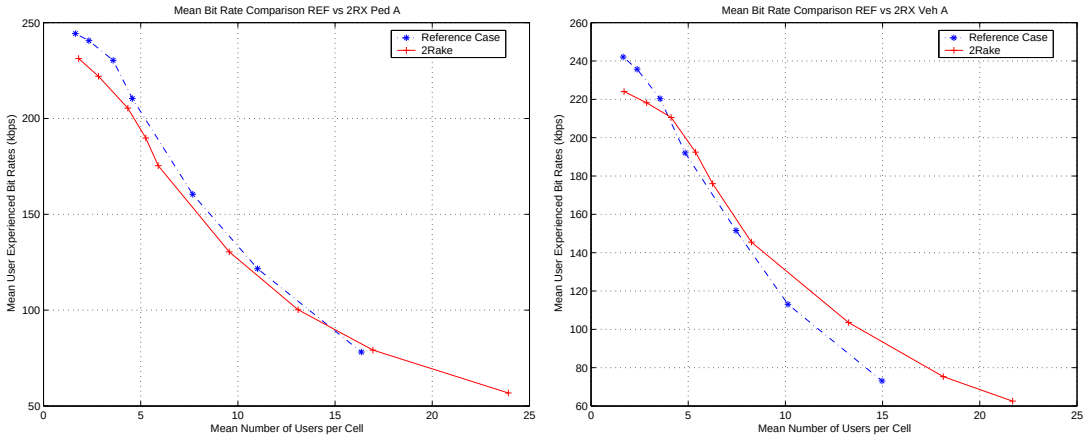

(a) Bit Rate comparison (Pedestrian A). (b) Bit Rates comparison (Vehicular A).

Figure F.8: 2Rake versus reference (Bit Rates).

Finally, Figure F.9 complements the analysis. This time around, users finally see some gain. The amount of rejected capacity requests (below) drops dramatically if all users possess advanced 2Rake mobiles, even if there are many more terminals in a cell. Furthermore, even if the network operator chooses to use the benefit from having UEs with 2Rake receivers in order to admit more UEs in the system, mean queueing times (above) remain substantially lower. Naturally, if the operator opts for a very aggressive strategy, admitting many more users with the same infrastructure, this benefit is expected to disappear as mean queueing time and rejection rates will increase.

[1]Due to the smaller code requirements of VehA, in the region of moderate load, some improvement is seen. Because the BS has both room in the power budget and some codes to schedule

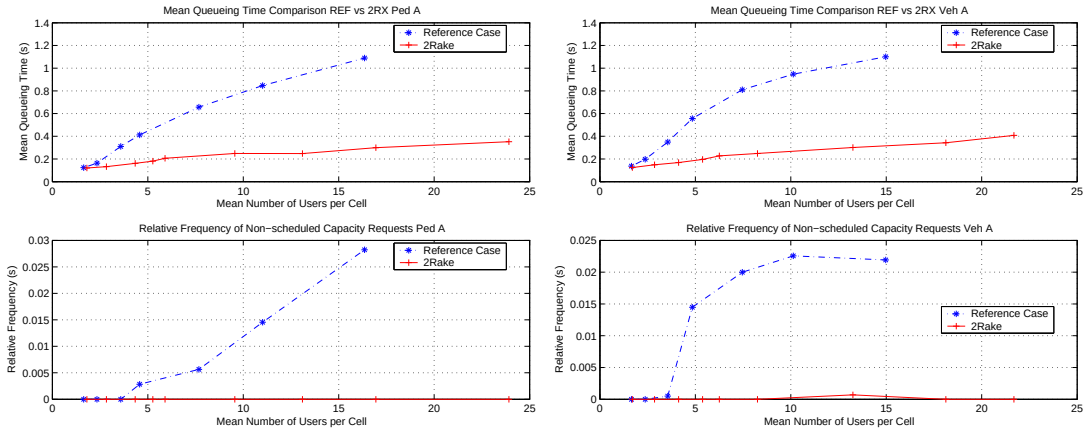

(a) Queueing time comparison (Pedestrian A). (b) Queueing time comparison (Vehicular A).

Figure F.9: 2Rake versus reference (Queueing time).

F.4 Concluding Remarks

This study shows that with the deployment of 2Rake receivers at the UEs, the system becomes code-limited and that the number of CS users that can be served is larger. However, those UEs with 2Rake receivers do not experience any extra quality in the service they receive. Therefore, it is the network operator who obtains the gain in this, since more UEs can be served with the same infrastructure. With that in mind, there is no reason for a user to pay more for such terminals. Operators should subsidize them.

In the case of CS connections, RRM has no freedom to provide better connections to users with 2Rake terminals, but in the NRT scenario, the distribution of the extra capacity depends on the strategy implemented in the PS. It was seen that RRM algorithms automatically capture the gain due to 2Rake receivers, however that did not mean that users experienced a higher throughput. Given the current packet scheduling strategy, the operator enjoys most of the benefits, while users experience shorter queueing times, even if the network load is reasonably increased, what may be perceived as faster response times.

Nevertheless, there is some hope for the users. If the packet scheduling strategy is modified, so that it grants higher bit rates to users with better link

higher bit rates.

budgets, terminals with 2Rake receivers are likely to experience a much better QoS, specially in terms of scheduled bit rates. In addition, extra signalling could be used to make RRM algorithms aware of the type of terminal they are dealing with. Such modifications to RRM algorithms are suggested as future subjects of investigation. Therefore, allowing operators to distribute the extra capacity according to their needs.

Finally, it is important to stress that the presented results are influenced by the underlying assumptions, especially by the utilized AVI tables. The use of different AVI tables generated specifically for 2Rake receivers, would have implied different power requirements per UE, which would have impacted the absolute system capacity. Nonetheless, although different specific performance figures would be reported when different AVI tables were used, the main trends and conclusions described here are expected to remain valid.

Apêndice G

System Level Simulations – Beamforming

This chapter is dedicated to the material introduced in Section D.5.1. The aim of this chapter is to investigate the capacity gain provided by beamforming in the DL of UMTS. As in the previous chapters the results are obtained using the simulation tool described earlier.

The improvement is determined for different traffic models on a network where all sites are equipped with AAs. The choice of the beamforming technique, the beam pattern generation process, the chosen number of beams, as well as some theoretical considerations are explained in the following sections.

The simulation setup selected to evaluate the capacity gain is the same one described in Section E.4, unless noted different. Finally the obtained simulation results are presented and analyzed in Sections G.3 and G.4.

G.1 Introduction

Here we get back to an issue brought up in the very first chapter of this thesis, namely time. Time is not an infinite resource, deadlines must be respected and some choices had to be made. As revealed already in Section D.7, only switched beam systems have been simulated in this work. However, no report would be com-

plete without an explanation about this and other decisions. Hence we begin with a brief comparison of the different beamforming schemes introduced in Chapter D.

The work in [29] compares the system level capacity gains provided by fixed beam and user specific beam systems (FBS and USB)[1] for the DL of an UTRA FDD network. The results therein suggest that the two schemes offer similar gains on an interference-limited network. Given that the architecture of a FBS is far simpler [45], it automatically becomes an attractive solution for increasing the capacity in cellular networks. Moreover, the two fixed beams techniques discussed in the current work, SBS and HOS, had their DL performances compared in [46, 29].

In general, SBS outperforms HOS despite the pilot power overhead due to the transmission of a S-CPICH in every beam. The reason behind it, is a higher orthogonality loss due to the utilization of a different scrambling code in each beam in HOS (See Sections B.3.2 and D.5.4). Thereupon, we restrict ourselves to the capacity evaluation of a SBS.

G.2 Simulation Setup

G.2.1 Beam Generation

The principles of fixed beamforming and smart antennas were presented in Section D.5.1. Equation (D.9), which is repeated here for convenience, $G(\phi_{dir}, \phi) = F(\phi_{dir}, \phi).g(\phi)$, defines the complex antenna gain of the AA. However, complex signals are *not* available in WALLU. Thus, forcing the behavior of beamforming smart antennas to be modelled in the power domain.

From a WALLU implementation point of view, the beamforming antennas are modelled by using different antenna radiation patterns at the BS, depending on the steering direction being used by the different users. As only one set of fixed steering directions is used in this project, the antenna power gain function was

[1] Introduced in Chapter D.

pre-computed according to the material presented in Section D.5.1 and stored in a look-up table.

In addition to the narrow directional beams, a wide sector beam is also needed in the DL in order to provide coverage for the entire cell. Such a beam is required for broadcasting the mandatory common channels such as P-CPICH. It is assumed that the sector beam is formed using only one element of the same antenna array.

For this study, the single element radiation pattern $g(\phi)$ is given by [12]

$$g(\phi) = \begin{cases} \sqrt{\beta}\cos^{\rho}(\phi) & \text{for } -90^\circ \leq \phi \leq 90^\circ \\ \sqrt{\beta/R} & \text{otherwise} \end{cases}$$

where $\beta = 15$dBi is the gain at broadside [2], $R = -33.8$ dB is the front to back ratio and ρ is the directivity factor. In this case, a ρ value of 1.7 generates a

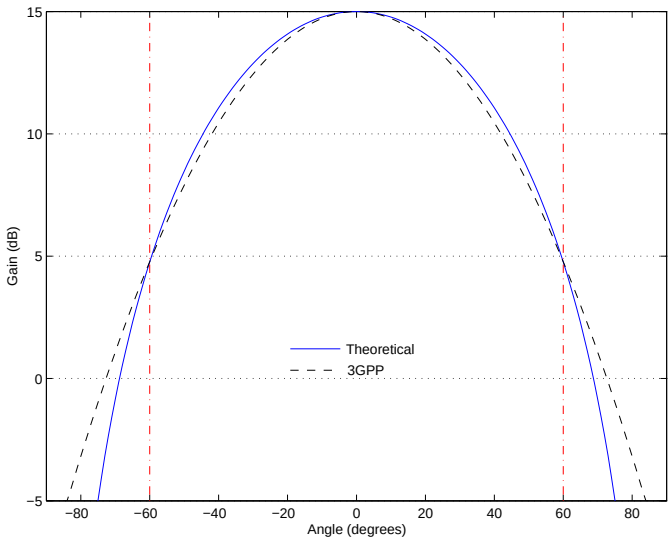

Figure G.1: Theoretical and 3GPP power patterns.

pattern very similar to the 3GPP pattern [22] used in the previous two chapters. Figure G.1 depicts the theoretical power pattern of the antenna element and that of the 3GPP antenna. The power pattern is the magnitude square of $g(\phi)$ and is show by the solid line in the plot. In addition, a plot marked with a dashed line depicts

[2]This value corresponds to a 18dBi gain with a 3dB cable loss.

the UMTS power pattern specified in [22]. It can be seen that the mathematical pattern matches closely that specified by 3GPP, especially in the 120° region of interest delimited by the two vertical red lines.

Number of Antenna Elements

The number of antenna elements specifies the width of the desired beams. A important thing to keep in mind is that using a single beam implies that the expected AS is relatively small compared to the beamwidth of the generated beam patterns as explained earlier in this report.

Here we are faced with a trade-off that limits the beamwidth. As seen previously, the narrower the beam is, the larger is the CCI rejection, which is mapped into more capacity. At the same time, if the beams are too narrow, significant paths might not be captured anymore which will degrade the performance. Apart from that, having very narrow beams increases the sensitivity to DoA estimation errors as studied by Klingenbrunn in [9]. Taking these factors into account, it has been decided to use an AA with $M = 4$ which can cope with larger AS, while still providing substantial capacity improvement.

Azimuth Spread

In all simulations involving beamforming the effect of the AS on the effective power radiation pattern of the directional beam the could not be neglected. Therefore, it has been modelled according to the material presented in [24] and [28].

In those articles the authors observed from field measurements that for typical urban macro cellular environments the pdf of the AoA at an antenna array at the BS has a Gaussian distribution and that the *Power Azimuth Spectrum* (PAS) could be well approximated by a *Laplacian* function [35] with a mediam standard deviation (the azimuth spread, σ_a) of 5° up to 10°, depending on the height of the antenna array. The rms AS decreases the higher the antenna array is [28].

For an FDD system, even though the small-scale fading in the UL and DL is uncorrelated, the PAS at the BS is approximately the same for UL and DL

frequencies, i.e. the same AoA and σ_a in both directions. The effect of the PAS was implicitly modelled in WALLU by an off-line convolution of the PAS and the ideal beamforming antenna radiation patterns. Thus, the effective power antenna gain at ϕ, when the beam-pointing direction is ϕ_{dir} is given by [28]:

$$W(\phi_{dir}, \phi) = \oint |G(\phi_{dir}, \varphi)|^2 . p_A(\varphi - \phi) d\varphi \tag{G.1}$$

$$p_A(\phi) = \frac{1}{\sigma_A \sqrt{2}} \, e^{-\sqrt{2}\frac{|\phi|}{\sigma_A}} \quad \forall \; -180^\circ < \phi < 180^\circ, \tag{G.2}$$

where, $p_A(\phi)$ is the PAS of the radio channel at the BS.

The sector beam is also affected by the azimuth dispersion. The effective power radiation pattern of the sector beam thus equals:

$$S(\phi) = \oint |g(\varphi)|^2 . p_A(\varphi - \phi) d\varphi. \tag{G.3}$$

Figure G.2 shows the influence of different angle spreads on the effective power-gain $W(\phi_{dir}, \phi)$, defined in (G.1). The beam shown here is pointed at $\phi_{dir} = -8^\circ$. It can be seen that the 3 dB width of the main lobe is broadened as the AS in the radio channel increases, thus the directive nature of the beam is gradually lost. Besides, the gain [3] in the pointing direction (ϕ_{dir}) decreases for larger AS values.

Number of Beams

When it comes to digital beamforming, once the number of antenna elements has been defined, one of the very first issues to arise is the number of beams used in one sector.

The limited number of beams in an SBS implementation results in a degradation compared to the USB implementation, due to the reduced antenna gain when the direction of the mobile differs from the actual beam direction. The maximum loss in antenna gain, which occurs approximately in the middle between two fixed beams, is called the *crossover depth* (See Appendix J). One way the reduce the cross-over depth is a proper choice of the beam steering directions, however, for a given N the freedom is limited, under the penalty of ruining the shape of the

[3] Gains have been normalized with respect to the sector beam.

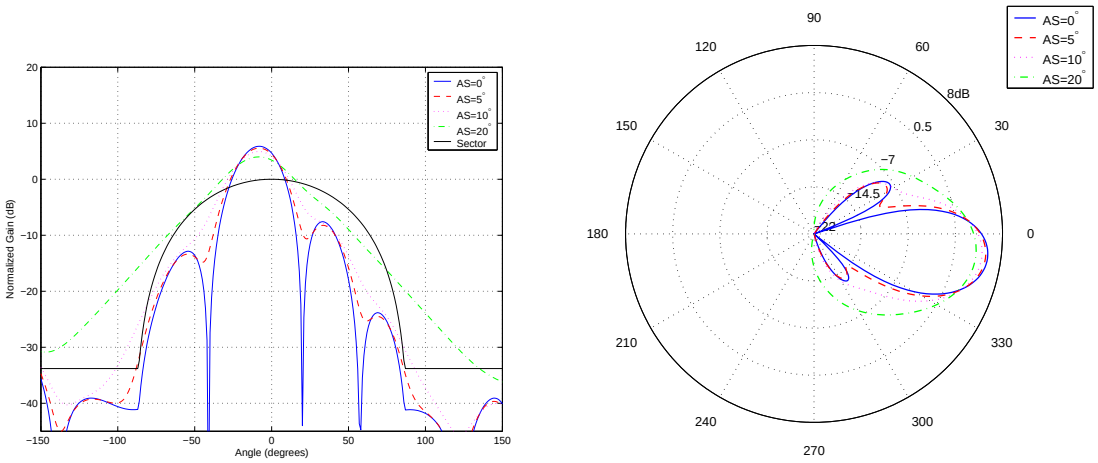

(a) Cartesian plot.

(b) Polar plot.

Figure G.2: Effect of angle spread in the radio channel.

cell. If it is desired to bring the beams even closer, thus reducing the cross-over depths even further, more beams are going to be required to cover the sector.

In [9], the author points out that for a number of beams equal to twice the number of antenna elements, the degradation compared to a USB system is quite small. Considering the required implementation complexity and the marginal gains from having $N > 2M$, he suggests the following relation: $N = 2M$.

In [46, 3], the authors include the *S-CPICH overhead* in the problem of choosing the optimal number of beams. But first, a quick detour to help us understand and quantify this overhead.

As a simple approximation, the ratio between the gain of a directional beam at its steering direction ϕ_{dir} and the that of the sector beam at the same azimuth direction for AS $= 0°$ can be written as

$$\frac{W(\phi_{dir}, \phi_{dir})}{S(\phi_{dir})} = M\,. \tag{G.4}$$

This is because the directional beams are formed in a way that maximizes the gain in a narrow direction, while the sector beam provides coverage for the entire cell.

The transmit power of the S-CPICH signals is then determined in coherence

with the ratio between the gain of the sector beam, carrying the P-CPICH, and that of the directional beams, i.e. the S-CPICH is transmitted with M times less power than the P-CPICH [4]. Thus, with N beams and M antenna elements, the total amount of power required by all secondary pilots is given by

$$P_{\text{TOTAL(S-CPICH)}} = N * \frac{P_{\text{P-CPICH}}}{M} . \tag{G.5}$$

We can see from (G.5), that with $M = 4$ elements and $N = 4$ beams we require an extra amount of pilot power equal to that already dedicated to the P-CPICH. *This extra power, which otherwise would be used for the data channels, is the so-called pilot overhead.*

Now, coming back to the point, the authors of the aforementioned works ponder that the lower the number of beams, the larger cross over depth between the beams, which results into a lower effective antenna gain. On the other hand, increasing the number of beams causes a larger pilot power overhead due to the S-CPICH transmitted in each beam. There is a clear tradeoff between the interference generated by the extra pilot signals and the cross-over depths. Backed by computer simulation results for different numbers of antenna elements, it is suggested that the optimum number of beams can be expressed as $N = M + 2$. They also stress that this result has been obtained assuming a radio channels AS of 5°, and that for larger AS the optimum number of beams would probably become lower, due to a larger overlap between beams.

In this project, one step further has been taken and a simple analytical method, which takes the $P_{TX|\text{Target}}$ (see Section B.5.3), the number of antenna elements, the AS and the P-CPICH power into account, has been devised. Figure G.3 depict the outcome of this study. The interested reader can find a full description of this method in Appendix J. An interpretation of the curves is given next.

The two upper plots show the curves that represent the aforementioned tradeoff for a system with four antennas. The ascending (gain) curves near the performance of a USB sytem, which is taken as a reference as the number of beams

[4] This relation ensures similar coverage for both the P-CPICH and the S-CPICH.

is increased, on the other hand the descending (loss) curves account for the loss incurred by the pilot overhead for three different values of the P-CIPCH power. The

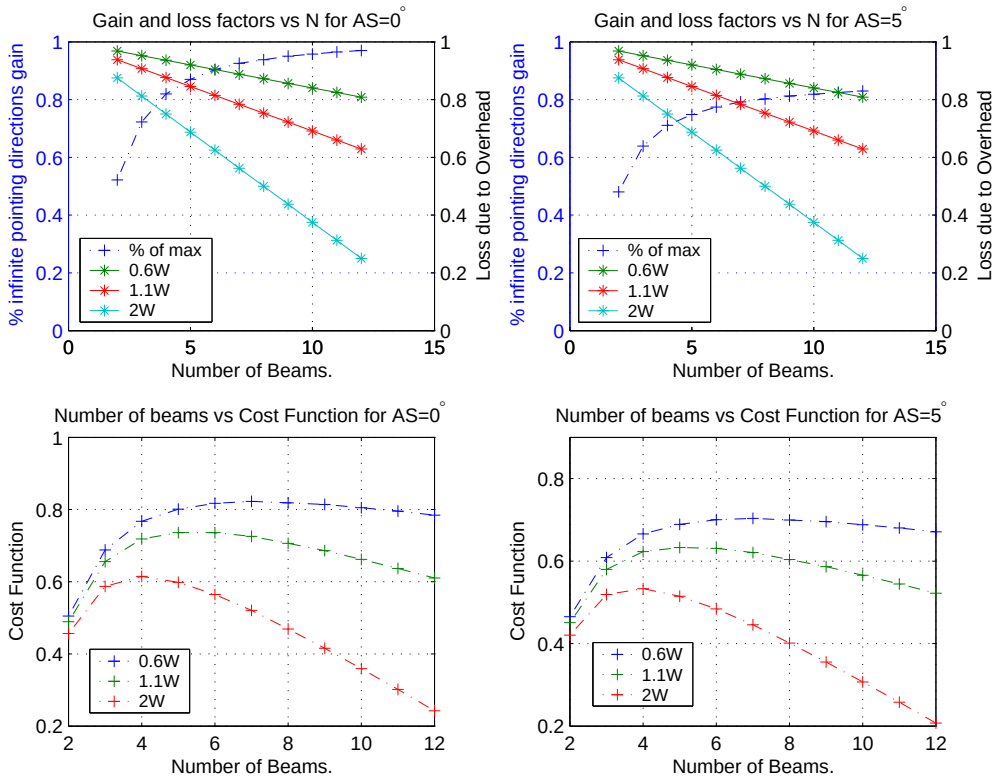

Figure G.3: Gain, loss and cost function versus the number of beams for $M = 4$.

lower plots depict the cost function of this optimization problem, which is defined as the product of the gain and loss curves. We can see that for the configuration utilized in this thesis, that is, 4 antenna elements, 2 W pilot and AS equal to 5°, the cost function reaches its maximum value when $N = M = 4$.

Results have shown a very good match with test simulations and those found in the literature [29, 3]. Therefore, four beams have been selected as the number of beams in all beamforming simulation runs. It is clear that the P-CPICH power strongly impacts this choice and the achievable gains, which is also pointed out in [45]. We can see that the realizable gain decreases as the amount of power dedicated to the primary power channel increases.

Simulations with 4, 5, 6 and 8 beams per sector were carried out. The case with four beams had the best performance and its gain with respect to the

reference case presented in the previous case was taken as the reference. Finally, the ratio $\text{Gain}_{\text{N beams}}/\text{Gain}_{\text{4 beams}}$ was calculated and plotted versus the number of beams along with the theoretical results.

Figure G.4 shows the theoretical and simulated results for the parameter setting utilized in the current work. There is a very good match between both curves. The first point in the curve $\text{Gain}_{\text{4 beams}}/\text{Gain}_{\text{4 beams}}$ does not equal one because it has been normalized to match the maximum value of the 2 W red curve in lower right corner of Figure G.3. Checking the validity of these curves for different number of elements and other pilot settings remains as a future task.

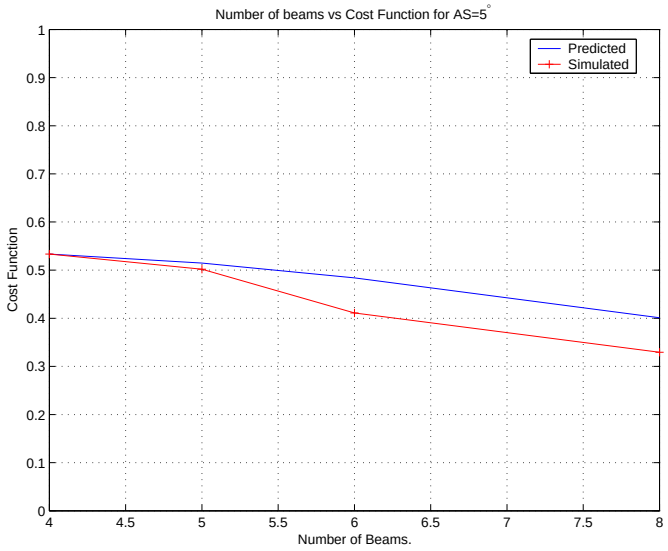

Figure G.4: Theoretical and simulated gains.

Finally, Figure G.5 shows the effective radiation patterns (normalized with respect to the sector beam) of the set of directional beams used in the beamforming simulations carried out for this project. The beams were generated by uniform linear AA of four antenna elements and a AS of 5° and the four beams point at $\phi = [-48°, -14°, 14°, 48°]$. For comparison, a sector beam covering the whole cell is also shown: magenta in G.5(a) and red in G.5(b).

As can be seen, the generated directional beams are much narrower than the sector beam, which facilitates the spatial filtering of the interference.

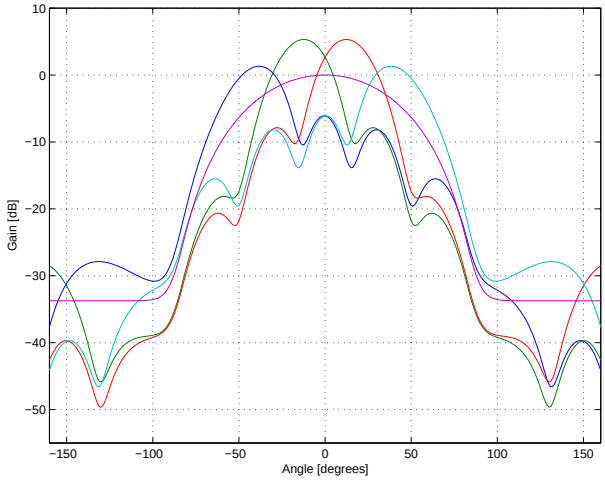

(a) Cartesian Plot.

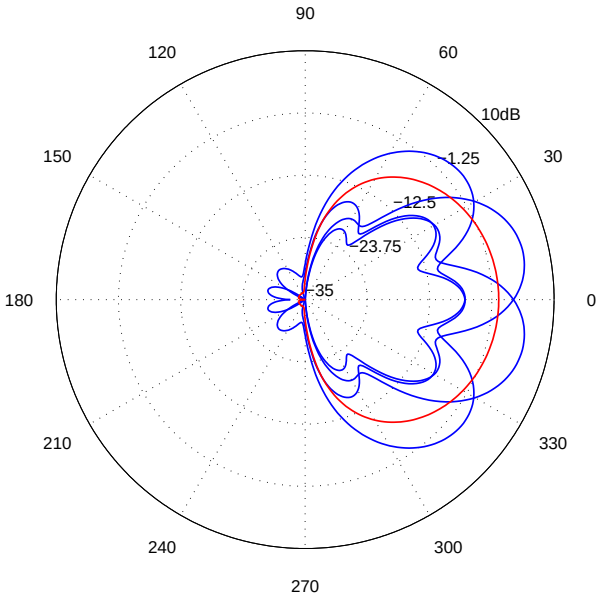

(b) Polar Plot.

Figure G.5: Effective power radiation patterns. $AS = 5°$, $M = 4$

G.2.2 UE Performance Modeling

Once again, following the methodology of the previous chapters, the E_b/N_0 is calculated for terminal i on a network where beamforming is use is presented now:

$$\frac{E_b}{N_0}(i)_{|slot} = \sum_{l=1}^{R} \frac{P_{\text{RxDPCH}}(s,i).h_{ff}(s,i,l)}{P_{\text{Noise}}^{\text{UE}} + P_{\text{RxTotal}}(i) - P_{\text{own}}(s,i).h_{ff}(s,i,l)} \,.\, G_p \,, \tag{G.6}$$

where

$$P_{\text{RxDPCH}}(s,i) = P_{\text{TxDPCH}}(s,\text{beam(i)},i).\, W_s(\phi_{\text{beam(i)}}, \phi_i^s).\, h(s,i) \,, \tag{G.7}$$

$$P_{\mathrm{RxTotal}}(i) = \sum_{k=1}^{K} \left(P_{\mathrm{TxTotal}}(k).\, h(k,i).\, \sum_{l=1}^{L} h_{ff}(k,i,l) \right) , \tag{G.8}$$

$$P_{\mathrm{TxTotal}}(k) = \sum_{n=1}^{N(k)} \left(P_{\mathrm{beam(n)}}(k).\, W_k(\phi_{\mathrm{beam(n)}}, \phi_i^k) \right) + P_{\mathrm{P-CPICH}}(k).\, S_k(\phi_i^k) , \tag{G.9}$$

$$P_{\mathrm{beam(n)}}(k) = \sum_{u=1}^{\mathrm{Users}_{k,n}} P_{\mathrm{TxDPCH}}(k,n,u) + P_{\mathrm{S-CPICH}}(k,n) , \tag{G.10}$$

$$\begin{aligned} P_{\mathrm{own}}(s,i) \;\; = \;\; & \sum_{n \in \mathbf{OS}(i)} \left(P_{\mathrm{beam(n)}}(s).\, W_s(\phi_{\mathrm{beam(n)}}, \phi_i^s).\, h(s,i) \right) + \\ & + X(i).\, P_{\mathrm{P-CPICH}}(s).\, S_k(\phi_i^s).\, h(s,i) , \end{aligned} \tag{G.11}$$

It can be seen that the calculations in this case are significantly more complex than those presented in the two previous chapters, hence beamforming simulations last much longer than the other ones. In case of SHO, ideal MRC between the outputs of the different SHO branches is assumed and the E_b/N_0 values corresponding to each branch are summed, similarly to what is show in (E.6). Table G.1 complements the notation introduced in Table E.3, which once again is not repeated here for the sake of space.

In the next section, we analyze the imperfections in the current model and their possible implications.

Symbol	Definition
$W_k(\phi_{\text{beam(n)}}, \phi_i^k)$	The antenna power gain of the n^{th} beam in the k^{th} cell pointed at $\phi_{\text{beam(n)}}$ towards the the direction ϕ_i^k.
$S_k(\phi_i^k)$	The antenna power gain of the sector beam providing coverage to the entire k^{th} cell in the direction ϕ_i^k.
ϕ_i^k	Azimuth direction of i^{th} UE, referred to the broadside direction of the antenna system in the k^{th} cell
beam(i)	Beam serving the i^{th} UE.
$\phi_{\text{beam(n)}}$	Azimuth direction at which the n^{th} beam is pointed, referred to the broadside direction of the corresponding AA.
$N(k)$	Number of beams synthesized in cell k .
$\text{Users}_{k,n}$	Total number of users served by beam the n^{th} in the k^{th} cell.
$h(k,i)$	Path gain from the k^{th} cell to the i^{th} user. It includes the distance dependent deterministic path loss h_{pl}, the shadow fading component h_{pl} receive antenna gains and G_{Rx}. It is of uttermost importance to notice that it does not include the transmit antenna gain, which is explicitly modelled in previous equations.
$P_{\text{beam(n)}}(k)$	Total transmitted power transmitted through the n^{th} beam in the k^{th} cell.
$P_{\text{TxDPCH}}(k,n,u)$	The transmitted power on the DPCH for the u^{th} user through the n^{th} beam in the k^{th} cell.
$P_{\text{S-CPICH}}(k,n)$	The power allocated to the secondary common pilot channel transmitted on the n^{th} beam in the k^{th} cell.
$X(i)$	Variable that equals one if the i^{th} UE is served under the primary scrambling code. Otherwise, it equals zero.
$\mathbf{OS}(i)$	Set of beams that belong to the scrambling code region in which the UE i^{th} is served.

Table G.1: Complementary notation for the E_b/N_0 calculation.

G.2.3 What Is Missing?

Delay Spread in Different Beams

An important issue, which is not addressed here when using the above channel model, is that the PDP is influenced by the beam direction resulting in a different power delay spectrum than for each beam. The current model assumes the same PDP for all connections, which is just an approximation, which becomes exact if the AS equals zero.

This claim can be understood in the following manner. If the AS is extremely large compared with the beamwidth of the synthesized directional beams, there will be some multipath components of the transmitted signals falling completely outside the radiation pattern of the synthesized beam. Therefore, they should not be included in the PDP that characterizes the radio channel between the BS and the UE. In the case analyzed in this project (AS = 5^o), the approximation is considered to be valid for the transmission of the desired signal, since the AS is much smaller than the beamwidth of the directional beams.

Correlation of Slow Fading and Azimuth Spread

In principle each communication link in WALLU should have its own value for the AS. Measurements have shown that the local AS is a time variant random variable, which is negatively correlated with shadow fading [17]. This means that mobiles in deep shadow fades will at the same time experience a reduced antenna gain, thus reducing the network capacity.

However, in order to simplify the simulations it is simply assumed that the AS is a fixed constant input parameter to the simulator e.g. $5°$. Nevertheless, an effort to evaluate the impact of different AS values on the effective radiation patterns has been presented in Section G.2.1 and Appendix J.

Finally, this approximation is not expected to affect the results significantly, but is an interesting topic for future research, so that the exact impact of this phenomenon is fully understood.

Loss of Capacity due to Code Splitting

The capacity gain obtained from using SA is likely to be sufficiently high so channelization code shortage becomes the limiting factor (See Section B.3.2), instead of the actual interference level at the radio interface (MAI). This limitation can be solved by deploying a secondary scrambling code, which means that an extra channelization code tree becomes available.

Unlike the 2Rake case, the loss due to poorer orthogonality can be reduced with beamforming by splitting the cell into multiple scrambling code regions. In this case, the spatial isolation between beams using different scrambling codes helps compensate for the lack of code orthogonality. This is the cell-splitting concept discussed earlier in Section D.5.4. Figure G.6 clarifies this idea.

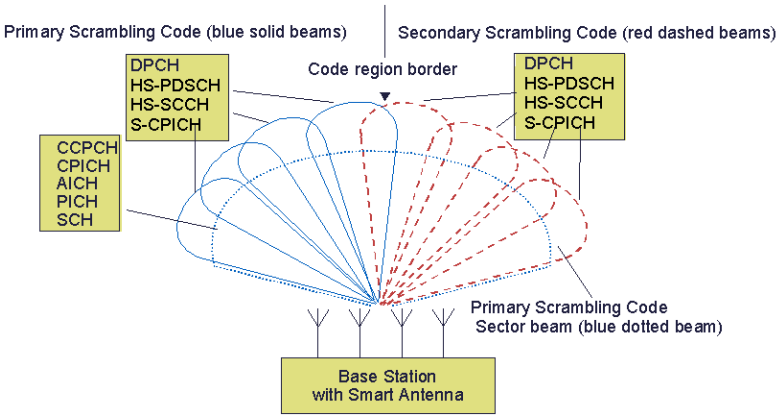

Figure G.6: Cell Splitting. Extracted from [46].

Here half of the beams are using the primary scrambling code (blue) and the remaining beams are using the secondary scrambling code (red). Depending on the load per beam, the code region border could be adjusted, so e.g. 6 beams are using the primary while 2 beams are using the secondary. Now, it is very important to comprehend that the "red beams" will have slightly lower throughput per beam than the "blue beams". Why? This is because the signals transmitted on the sector beam interfere more with the signals transmitted under the secondary scrambling code. The "blue beams" and the sector beam are using channelization codes from the same code tree, and therefore have a better orthogonality.

This means that ideally, only the primary scrambling code should be deployed as long as there is a sufficient amount of channelization codes available. Once channelization codes associated with the primary scrambling code are used up, a second scrambling code should be introduced. Hence, an adaptive code assignment scheme is in principle the preferred option, depending on the channelization code tree load.

Here comes the imperfection, not exactly in the modeling, but actually in the implementation. The variable $X(i)$ in (G.11) should be set to zero for all terminals served by beams using the secondary code, i.e. the "red beams". Yet, implementing, debugging and testing the SA feature in WALLU took way longer than anyone had foreseen. Unfortunately, at this point, time was running out, the actual writing of this thesis started to take precedence. It was then decided to use a fixed value of $X(i) = 1$ in all simulations, even in the presence of a secondary scrambling code, because cell splitting was not fully tested. Now the question is, how does that affect the results?

On one hand it could be seen as a super efficient implementation of an adaptive code assignment scheme, where a secondary is not introduced until it is absolutely necessary and its use is confined to the absolute minimal number of beams. On the other hand, the "red beams" are going to have the same performance as the blue ones, which might represent a positive bias in the capacity results.

It has been shown in [3] that for a four-element configuration, there is a marginal penalty of 4% (Vehicular A) and 8% (Pedestrian A) associated with cell-splitting due to the lack of orthogonality between signals under different scrambling codes. This penalty is larger for Pedestrian A because the relative orthogonality was already partly destroyed by the time dispersiveness of the Vehicular A radio channel. Moreover, Figure 6.12 on page 102 in [29] shows that never more than two beams out of four need to use the secondary scrambling code.

In consequence, this bias is considered to be marginal for the tested configuration. This, however, does not mean that further tests should not be carried out in the future to evaluate the precise impact of this simplification.

G.3 Simulation Results

G.3.1 Real Time Traffic

The same steps described in Section E.5.1 are followed here. However, due to the complexity of the calculations presented in Section G.2.2, beam forming simulations take an obscene amount of time. Shortening the length of the simulations was not desired in order to keep statistical reliability of the results. Consequently, it was decided to run Vehicular A simulations only, the not attractive alternative was ruling out NRT simulations. Furthermore, unlike the simulations in Section F.3, not much difference in the gain is expected, since it is independent of the amount of diversity already present.

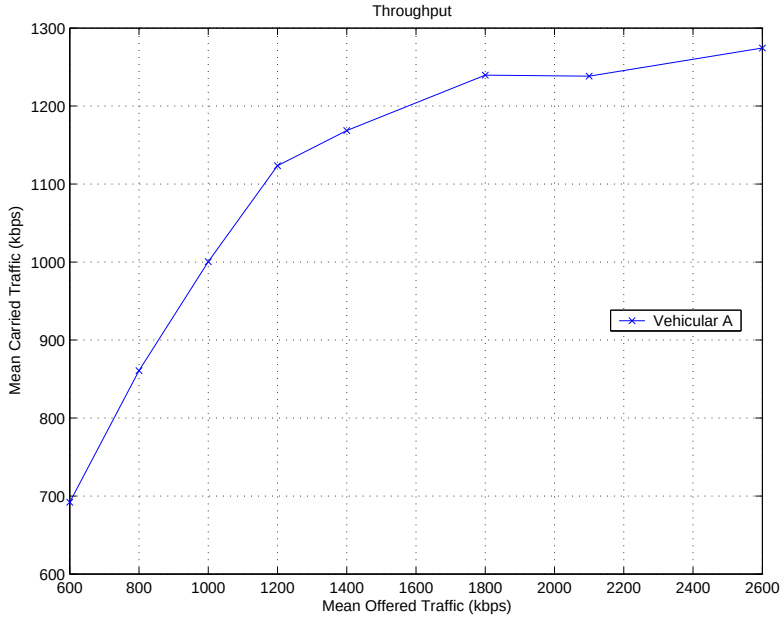

Figure G.7: The cell throughput as a function of the mean offered traffic.

Table G.2 summarizes the achieved results presented in Figures G.7 and G.8. Compared to the reference case, we see a capacity gain of 90%. In these simulations, a secondary scrambling code was deployed, thus the number of available channelization is twice as large. The average code utilization (blue bar) remains above 40% in the high load region, what indicates that had a secondary scram-

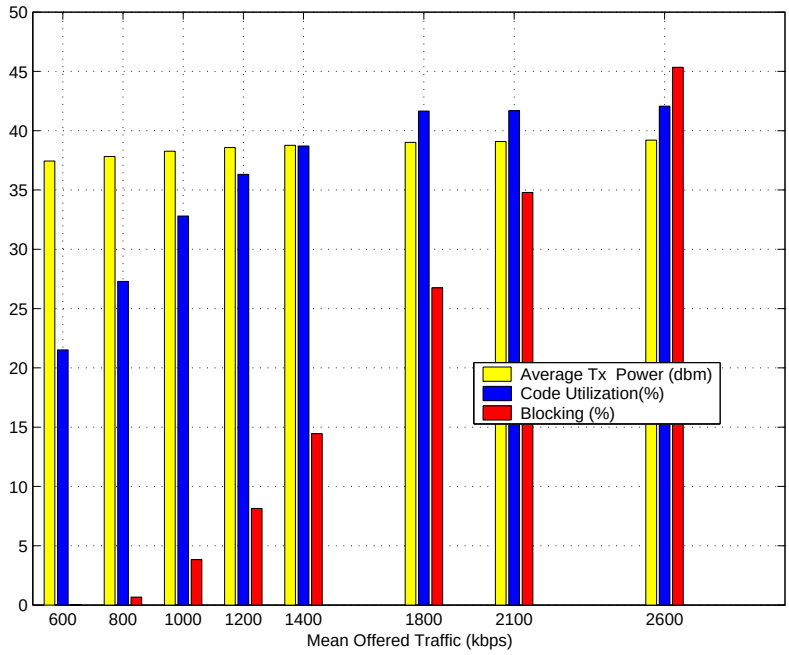

Figure G.8: Resource utilization and blocking rate (Vehicular A).

bling code not been deployed, *the system might have experienced code blocking (i.e. greater than 80% average code utilization), but would have remained predominantly interference limited.*

Results (S-CPICH 4 Beams)				
PDP	$E\{\text{Carried}\}$ (kbps)	*Gain* (%)	$E\{\text{Blocking}\}$ (%)	$E\{P_{\text{Tx}}\}$ (dBm)
VehA	1250.4	90	30.3	39.12
Upper Bound (No-S-CPICH 8 Beams)				
PDP	$E\{\text{Carried}\}$ (kbps)	*Gain* (%)	$E\{\text{Blocking}\}$ (%)	$E\{P_{\text{Tx}}\}$ (dBm)
VehA	2100	219	42.6	39.2

Table G.2: Reference values for comparison.

However, to be positive that the full gain from deploying SA in the DL direction will be capitalized, two scrambling codes are required. If only one one scrambling code is present, the gain from introducing SA *is likely to be limited by channelization code shortage*, depending on the power delay profile of the channel, SHO settings, etc. Remember that channels with low temporal dispersion favors

more capacity in the DL, and that code utilization is sensitive to SHO settings.

Finally, a simulation without the S-CPICH overhead was carried out, in this case, the number of beams per sector was $N = 2M = 8$, as reported in [9]. The result is included in Table G.2. The goal here was to obtain an upper bound for the full gain. Compared to the reference case, we see a gain of 219%.

Obviously, we must look at this number with care for two reasons. First, there is no miraculous way to avoid the overhead. Recall now, from Section D.5.4 that in SBS, terminals use either the dedicated pilot present in the DCH or the S-CPICH for channel estimation. By omitting the overhead, we imply that the dedicated pilots are used. In this case the link performance deteriorates due to the degradation of the channel estimates for power controlled channels. This can be explained by the fact that the BS lowers the transmit power as a consequence of the spatial interference filtering gain. Unfortunately no AVI tables were available for this case, hence the optimistic results. The gain will certainly be reduced. Second, in this simulation, a mean code utilization of 70% was observed, even in the presence of a secondary scrambling code. This means that the loss due to code splitting in this case, which is not present in the current implementation as discussed earlier, might not be negligible as there will be more users served by the secondary scrambling code. Comparing the performance of SBS for different S-CPICH overheads, i.e. as a function of the P-CPICH allocated power, with that of the same system using the dedicated pilots for channel estimation is suggested as an interesting topic for future research.

G.3.2 Non Real Time Traffic

The methodology introduced in E.5.2 is repeated in this section. Besides, we stick to the comparison line used earlier in Section F.3.3.

We begin with Figure G.9(a) which depicts the cell throughput as a function of the observed (a posteriori) load for both systems, the reference and the one with SA. When we compare the carried capacity of both systems at the same operating

point, that is, close to the target level, we see a gain of 58.15%. Now, an intriguing question is, why this gain is lower than the one achieved by the RT traffic model. This time, code blocking is not the answer, because a secondary scrambling code was deployed, and the observed code utilization, despite being moderate, was not the limiting factor.

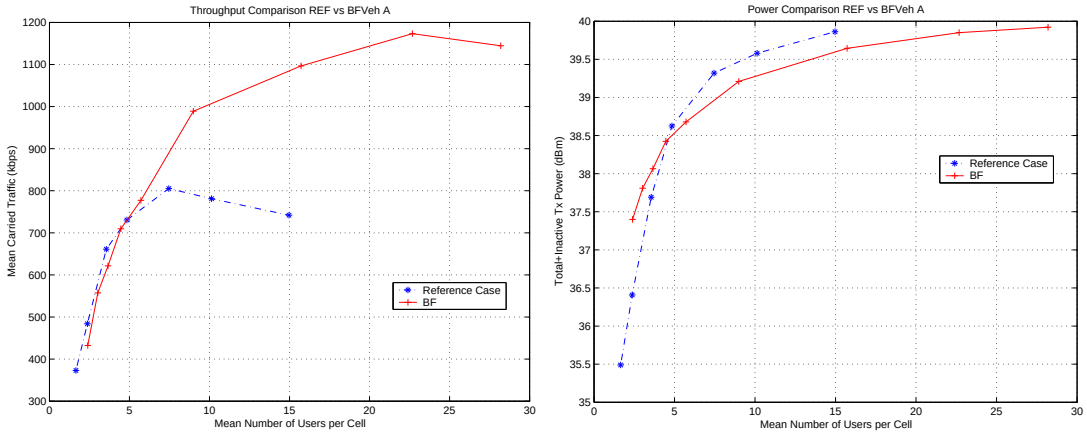

(a) Throughput comparison. (b) Transmit power comparison.

Figure G.9: Beamforming versus reference.

The system now is interference limited. Figure G.9(b) shows that the target level is reached here, just like in the reference case, but with a greater number of users per cell.

Now, it is time to answer the question raised previously. The reason for this difference was explained in Section D.5.3, which is restated here for convenience. The full capacity gain is only achieved if the spatial interference is approximately white, i.e. approximately the same in all directions, while no capacity gain is expected for the case where all users are positioned at the same azimuth direction. Therefore, the capacity gain due to spatial filtering is very sensitive to the spatial distribution of interference.

Now, in systems with non-uniform bit rate distribution, the spatial interference is likely to deviate from the spatial white assumption. The purpose of Figure G.10 is to compare the normalized amount of power transmitted per beam in the RT case with the NRT one. Moreover, a test simulation with a higher number of low bit rate users (16 kbps RT) was carried out too. Beams number 2 and 3

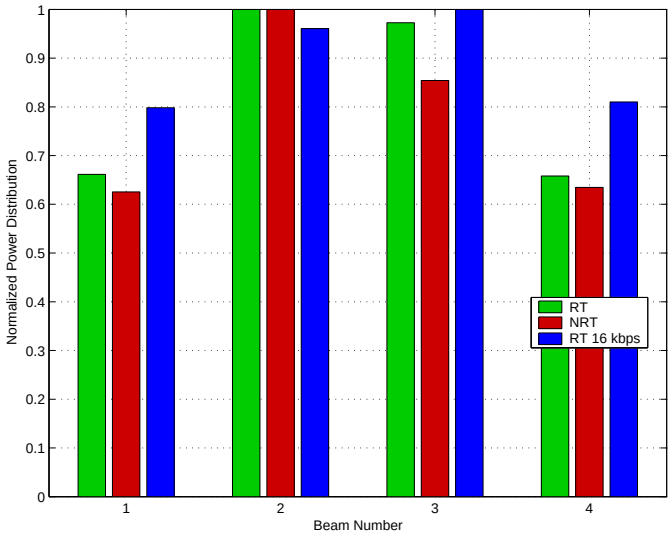

Figure G.10: Normalized power distribution (RT vs NRT).

are the ones serving the central region of the cell, that is why the are transmitting with more power than the outermost ones, beams 1 and 4. For each case, the beam transmitting with the largest amount of power was picked as the reference. This comparison clearly indicates that the spatial interference is not strictly white in neither case, but in the NRT case, this "violation" is more severe, thus the lower gain, whereas the 16 kbps shows the smallest variation.

Next, the average value of the user experienced bit rate is analyzed as the amount of users in the system is incremented. This is shown in Figure G.11(a). The curves show the average bit rates packet switched data users experience as the cell load is augmented. Again, due to the packet scheduling strategy no extraordinary difference between both cases is visible. However, in the region of moderate load, some improvement is seen, because the BS has both some room in the power budget and codes to schedule higher bit rates. If the system is pushed to its limits, the tendency is end up scheduling many more 32 kbps than it was possible in the reference case.

As in the previous Chapter, Figure G.11(b) complements the analysis. When SA antennas are deployed, users experience a reduction in the amount of rejected capacity requests (below) even for a larger number of terminals in a cell. Further-

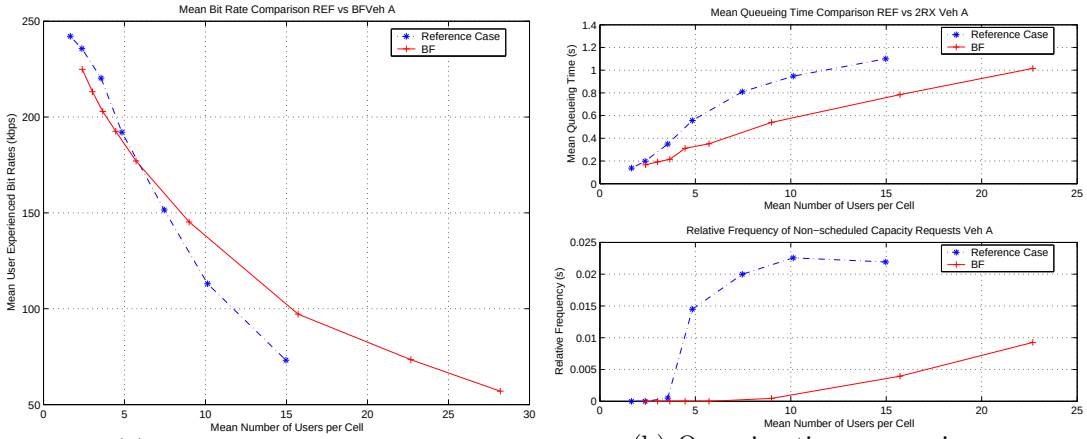

(a) Bit Rates comparison.

(b) Queueing time comparison.

Figure G.11: Beamforming versus reference.

more, mean queueing times (above) remain lower, even though the improvement is not as large as the one observed with 2Rake receivers. This a consequence of admitting more users into the system, since the code restriction is relaxed through the deployment of a secondary scrambling code.

G.4 Concluding Remarks

In this chapter, the application of SBS for downlink capacity enhancement has been studied. The first part discusses general issues related to the simulation of SBS. In order to study the performance of beamforming arrays in a realistic simulation environment, a channel model including time and azimuth dispersion is introduced. An analytical study of the optimal number of beams as a function of the pilot overhead and the AS of the channel is presented. The second part presents various network simulation results using fixed beamforming for both RT and NRT traffic models.

It is concluded that the significant capacity improvements achieved with DL beamforming may result in code shortage, which occurs when the users in the cell require more channelization codes than available. In that case, and additional scrambling code can be allocated due to spatial filtering properties of SA. In the case of packet switched traffic, results indicate a small improvement in the user ex-

perienced bit rates in the region of moderate load compared to the reference system for the same average number of users in a cell. Notwithstanding, system performance with NRT traffic needs further attention, since the employed traffic models and selected scheduling strategies for cells with beamforming capabilities may impact the performance figures. Operators should have the freedom to distribute the extra capacity as they see fit.

In addition, it is stressed that absolute capacity figures are strongly influenced by the utilized AVI tables. If different AVI tables the were employed, the reported values would change. Nevertheless, the presented trends and phenomena are expected to remain the same qualitatively.

Finally, the author suggests further investigations to assess precisely the impact of the imperfections in the space-time model of the radio channel cited in Section G.2.3. Considering that the S-CPICH overhead negatively impacts the gain offered by SBS, comparing the performance improvement for different S-CPICH overheads, i.e. as a function of the P-CPICH allocated power, with that of the same system using the dedicated pilots for channel estimation is also pointed out as an interesting topic for future research.

Apêndice H

System Level Simulations – Putting It All Together

The penultimate chapter of this thesis is the obvious sequel to its predecessors. It studies the joint deployment of the schemes analyzed in Chapter F and Chapter G. As in the previous chapters the results are obtained using the simulation tool described earlier.

The main goal is to measure the capacity gain when 100% of the terminals are equipped with 2Rake receivers and a beamforming AA is employed at the BS. A brief analysis is carried out for both traffic models (RT and NRT).

The simulation setup selected to evaluate the capacity gain is the same one described in Section E.4, unless noted different. Finally the obtained simulation results are presented and analyzed in Sections H.3 and H.4.

H.1 Introduction

Its has been shown that the 2Rake scenario investigated in Chapter F becomes code-limited when there is only one scrambling code per cell, thus the full gain provided by the deployment of such receivers can not be realized in scenarios that favor more capacity. This limitation became even more severe for NRT traffic due to its higher code requirements. What is worse, there is no easy of of introduc-

ing an extra scrambling code due to the acute loss of orthogonality. That chapter ended without solving this dilemma.

In the beamforming case described in Chapter G, the code splitting strategy turned out to be an effective method to overcome channelization code limitations as indicated in [3] due to spatial filtering properties of beamformers, which make it possible to spatially isolate regions with different scrambling codes.

Now, imagine a system that combines the use beamforming at the BS and 2Rake receivers at the UEs. It will enjoy both the spatial filtering gain from SA and the full benefits from 2Rake receivers at the UE. The two techniques are independent, but in a way, they complement each other.

H.2 Simulation Setup

The setup for these simulations is analogous to the one presented in Section E.4. Beamforming related parameters have been taken from the previous chapter in order to allow fair comparisons, that is, beam patterns, number of antenna elements and number of beams per cell remain the same.

H.2.1 UE Performance Modeling

In this case, the E_b/N_0 is calculated by combining the expressions introduced in Sections F.2.1 and G.2.2. In the following, an expression for the calculation of the E_b/N_0 at each slot for terminal i is given:

$$\frac{E_b}{N_0}(i)_{|slot} = \sum_{m=1}^{2}\sum_{l=1}^{R} \frac{P_{\mathrm{RxDPCH}}(s,i).h_{ff,m}(s,i,l)}{P_{\mathrm{Noise}}^{\mathrm{UE}} + P_{\mathrm{RxTotal}}(m,i) - P_{\mathrm{own}}(s,i).h_{ff,m}(s,i,l)} \,.\, G_p, \quad \text{(H.1)}$$

where

$$P_{\mathrm{RxTotal}}(m,i) = \sum_{k=1}^{K} \left(P_{\mathrm{TxTotal}}(k).\, h(k,i).\sum_{l=1}^{L} h_{ff,m}(k,i,l) \right), \quad \text{(H.2)}$$

and $h_{ff,m}$ is the path gain describing the fast fading for the l^{th} path of the link between the k^{th} cell and the m^{th} receive antenna of the i^{th} user.

Apparently, this expression is identical to (F.1). The difference is in the calculations of $P_{\mathrm{RxDPCH}}(s,i)$, $P_{\mathrm{TxTotal}}(k)$, and $P_{\mathrm{own}}(s,i)$, which are now computed according to (G.7), (G.9), and (G.11) respectively. Equations are repeated here for convenience. The notation is given in Tables E.3 and G.1.

$$P_{\mathrm{RxDPCH}}(s,i) = P_{\mathrm{TxDPCH}}(s,\mathrm{beam(i)},i).\, W_s(\phi_{\mathrm{beam(i)}},\phi_i^s).\, h(s,i)\,,$$

$$P_{\mathrm{TxTotal}}(k) = \sum_{n=1}^{N(k)} \left(P_{\mathrm{beam(n)}}(k).\, W_k(\phi_{\mathrm{beam(n)}},\phi_i^k)\right) + P_{\mathrm{P-CPICH}}(k).\, S_k(\phi_i^k)\,,$$

$$\begin{aligned} P_{\mathrm{own}}(s,i) \;\; = \;\; & \sum_{n\in \mathbf{OS}(i)} \left(P_{\mathrm{beam(n)}}(s).\, W_s(\phi_{\mathrm{beam(n)}},\phi_i^s).\, h(s,i)\right) + \\ & + X(i).\, P_{\mathrm{P-CPICH}}(s).\, S_k(\phi_i^s).\, h(s,i)\,. \end{aligned}$$

In case of SHO, ideal MRC of the outputs of the different SHO branches is assumed and the E_b/N_0 values corresponding to each branch are summed, analogously to what is show in (E.6). The AVI principle and comments related to MRC combining presented in Section F.2.1 continue valid here.

H.3 Simulation Results

It can be see from the E_b/N_0 calculations presented earlier that for the case when both features are combined the beamforming related computations are carried out twice for each terminal what led to unbelievably time consuming simulations.

Considering that the behavior of an UMTS network implementing the features described in the two previous chapter already was extensively studied for gradually incremented loads, and the long computational times required by the current case, it has been decided to run two simulations only, one for each traffic model with a very high offered load. The goal is to evaluate the absolute maximum capacity provided by the combination of both techniques.

In the following the results of system-level simulations for the combined case are presented.

H.3.1 Real Time Traffic

The same procedure described in Section E.5.1 is followed here to calculate the mean offered traffic, which was set to 4000 kbps. Given that only Vehicular A simulations were carried out in Chapter G, here, simulations are performed for the same channel profile. The capacity improvements is likely to be even more substantial for Pedestrian A due its inherent lower frequency diversity compared to Vehicular A, which allows the 2Rake receivers to add much more diversity gain.

In order to be coherent with the previous chapter, only 2 scrambling codes were deployed. Considering that 4 beams are synthesized in every sector, up to 4 scrambling codes could have been introduced. Despite seeing a mean code utilization of 95.04%, which indicates code blocking occurred, the simulation output showed that power blocking was present as well, as $E\{P_{\text{Tx}}\} = 39$ dBm in Table H.1 proves. Now, if we had simulated the Pedestrian A profile, two codes certainly would not have been enough. The mean carried traffic was above 2800 kbps, which represents an impressive improvement of 326%.

Results (S-CPICH 4 Beams + 2Rake)				
PDP	$E\{$Carried$\}$ (kbps)	*Gain* (%)	$E\{$Blocking$\}$ (%)	$E\{P_{\text{Tx}}\}$ (dBm)
VehA	2806.4	326%	60.3	39.1

Table H.1: Reference values for comparison.

Now, let us take this gain of 326% as a multiplicative factor equal to 4.26, where 1 is the capacity of the reference system. This factor is greater than the product of the corresponding individual factors 1.9 (BF) and 1.94 (2Rake unrestricted) presented in Sections F.3.2 and G.3.1. Why? One possible explanation is that the higher average number of 64 kbps users in the cells made the interference much closer to the ideal spatially white assumption, thus increasing the beamforming gain. If we assume the gain coming from the 2Rake was kept constant (no reason for it to change), then the one due to SA went up to a factor of 2.19 (4.26/1.94). Thus, it seems that *the combination of both techniques not only solved the code*

limitation of the 2Rake solution, but also improved the benefit of beamforming.

Nevertheless, the author strongly suggests further investigation, because the losses due to code splitting were not taken into account. In this case, it is likely that half of the beams is using the secondary scrambling code, while the other half, the primary, consequently causing a certain degradation.

H.3.2 Non Real Time Traffic

The situation here is a little more complicated to analyze given only one simulation run. The observed gain in throughput was 104.37%, corresponding to a multiplicative factor of 2.04, which approximately matches the product (1.582 x 1.298) of the gain factors presented in Sections F.3.3 and G.3.2. Mean queueing time was around 1 second and the capacity rejection ratio remained fairly lower than that in the reference network. However, the system was code limited and it becomes hard to make a comprehensive judgment of the results. It remains as an interesting task for the future.

H.4 Concluding Remarks

The combination of both techniques makes the channelization code shortage problem even more severe, given that the capacity is greatly improved. Notwithstanding, the possibility to allocate the scrambling codes on a beam basis opens for a solution to this problem. Under conditions that favor more absolute capacity, this solution is likely to require the use of more than two scrambling codes.

Furthermore, results for RT traffic showed an impressive mean carried traffic improvement of 326% when compared to the reference system, which was surprisingly more than the product of the gains offered by each feature individually, thus, suggesting that the combination of both techniques introduced the means to overcome the code limitation of the 2Rake solution, and the added benefit of improving the performance of beamforming by making the interference whiter. Unfortunately,

NRT results were not conclusive.

Finally, it is important to stress that the presented results are influenced by the underlying assumptions, especially by the utilized AVI tables. The use of different AVI tables generated specifically for 2Rake receivers, would have implied different power requirements per UE, which would have impacted the absolute system capacity. Nonetheless, although different specific performance figures would be reported when different AVI tables were used, the main trends and conclusions described here are expected to remain valid.

Apêndice I

Conclusions and Future Work

And so, we come to the end.

Finally, in compiling and reminiscing about my efforts in putting together this thesis, I realize it has taken me over one year to get to this point and to finally be able to write these last lines. In retrospect, becoming familiar with this interesting and totally new to me field of mobile communications was one of the most rewarding and challenging aspects of the project. Tackling a thesis like this has been a fascinating mixture of technological skill, planning, determination, and even creative spark.

Above all, I believe that the essence of a thesis project of this nature can be summed up in one word: research. There is the constant need to explore, investigate, and contemplate. There is the need to be self-motivated, to work towards a goal, overcoming many obstacles along the way.

A good question now would be, "What was the main thing which I have learned or gained from the project?" Answering this question and paving the avenues for future work is the purpose of this chapter.

I.1 Introduction

This thesis evaluated performance enhancements provided by advanced antenna structures for the the Frequency Division Duplex mode of the Universal Mobile Telecommunication System. The downlink DCH performance was evaluated using dynamic system level simulations, and to some extent, theoretical calculations.

The problem was tackled in a systematic manner. The ultimate goal was to build up, chapter by chapter, the necessary preconditions to accomplish the objectives of this project. The organization of this last chapter essentially follows the process I went through over the course of this thesis.

I.2 UMTS

Chapter B was the first step. It introduced the UMTS system architecture followed by a short description of its physical layer. After all, it was needed to understand and become familiar with the system considered in all upcoming chapters.

I.3 Radio Channel

Before, venturing into the more complex field of smart antennas, it was necessary to understand the fundamental problems and limitations imposed by the mobile radio channel. Simply put, Chapter C was the time to know the enemy.

I.4 Antenna Arrays

It was time to learn about some possible solutions capable of mitigating the limitation of the radio channel. In Chapter D, various antenna development

stages are summarized in an increasing order of "intelligence". It was seen that antenna arrays are basically designed to operate in two modes of operation, namely diversity and beamforming. The former provides protection against fading and an average SNR gain, whereas the latter offers interference suppression through spatial filtering.

I.5 Reference System

The stage was set. The goal now was to get results. Chapter E introduced various methods of assessing the performance of an UMTS network, described the simulation tool and the methodology utilized throughout the rest of this work. The network consisted of 9 BS equipped with three-sector antennas with a site-to-site distance of 2.8 km.

In addition, results which served as the comparison basis for the upcoming simulation campaigns were presented. They indicated that the system was interference limited, irrespective of the traffic model and that NRT traffic demanded much more codes than than its RT counterpart. Finally, it was found that, given the selected parameters, the macro cell DL capacity was between 550 and 900 kbps per sector per 5 MHz, depending on the dispersive characteristics of the radio channel and the type of service.

I.6 2 RX Diversity

In Chapter F, AA were used in the diversity mode at the terminals, while nothing else changed at the BSs. Dynamic system level simulations assuming a 100% penetration of terminals with dual antenna Rake (2Rake) receivers were performed.

This study showed that the deployment of 2Rake receivers at the UEs, made the system code instead of interference-limited with one scrambling code per cell.

This limitation was more severe for NRT traffic due to its higher code requirements. Unfortunately, there is no easy way of introducing an extra scrambling code in this case, without seriously degrading the orthogonality between signals transmitted with different scrambling codes.

Considering the code limitation, an average gain of 86% was observed in all scenarios for CS traffic. It was also seen that UEs with 2Rake receivers do not experience any extra quality in the service they receive. Simulating a hypothetical case, where the code limitation was removed, Pedestrian A, Vehicular A, (all UEs at 3km/h) and Vehicular A (UEs at 50km/h) showed gains of 123.23%, 94.71%, and 87.28% respectively. Given the difference between the achieved gains in the restricted and unrestricted cases, it could be concluded that code blocking is more severe when the absolute cell capacity is larger, i.e. for Pedestrian A.

It was also pointed out that RRM algorithms automatically capture the gain due to 2Rake receivers in the packet switched domain (NRT). However, that did not mean that users experienced a higher throughput. Given the current packet scheduling strategy, the operator enjoys most of the benefits. Users, however, did experience shorter queueing times, and the rejection rate of capacity requests was dramatically reduced.

If the packet scheduling strategy is modified, so that it grants higher bit rates to users with better link budgets, terminals with 2Rake receivers are likely to experience a much better QoS, specially in terms of scheduled bit rates.

I.7 Beamforming

The next logical step was to investigate the beamforming mode of antenna arrays. This is precisely what is done in Chapter G. Where antenna arrays elements are employed at the BS. In this chapter, the application of switched beam systems (SBS) for downlink capacity enhancement has been studied. An analytical study of the optimal number of beams as a function of the secondary pilot overhead and the

azimuth spread of the channel is presented. It shows that the S-CPICH overhead negatively impacts the maximum gain offered by SBS.

By forming a narrow beam towards each desired user, the resulting spatial filtering can significantly improve the capacity. The improvement is determined by the effective antenna beamwidth, which is determined by the number of elements and the azimuth spread. Results presented in this work assume four elements and a azimuth spread of five degrees.

In a scenario with 4 beams per sector, 2 W P-CPICH, thus yielding 4 W dedicated to pilot channels (P-CPICH + 4 S-CPICH) out of a total of 10 W, capacity gains of 90% and 58.15% were achieved for RT and NRT traffic models respectively (Vehicular A only). Furthermore, an outstanding gain of 219% (RT traffic) was seen when the S-CPICH overhead was removed and 8 beams were synthesized.

In the case of packet switched traffic, results indicated a small improvement in the user experienced bit rates in the region of moderate load compared to the reference system for the same average number of users in a cell.

It is concluded that the significant capacity improvements achieved with DL beamforming may result in code shortage, which occurs when the users in the cell require more channelization codes than available. In that case, and additional scrambling code can be allocated due to spatial filtering properties of SA.

I.8 Beamforming and 2 RX Diversity Combined

In Chapter H, a brief analysis of the capacity gain offered by the combination of terminals equipped with 2Rake receivers and a beamforming AA employed at the BS is presented. In the simulations it was assumed that all terminals on the network were equipped with such receivers and the beamforming configuration was identical to the one employed in Chapter G.

Moreover, results for RT traffic showed a striking capacity gain of 326% when compared to the reference system. This result was surprisingly more than the expected product of the gains offered by each feature individually. It suggests that the combination was beneficial for both techniques. Their combination introduced a means to overcome the code limitation of the 2Rake solution, and the added benefit of improving the performance of beamforming by making the interference whiter. Unfortunately, NRT results were not conclusive.

I.9 Future Work

Topics for posterior studies have been suggested throughout this report, yet they are recollected here to provide some food for thought.

Unfortunately, the concept of Repeater Specific Beams introduced in Section D.6 could not be simulated for it requires deep modifications in the structure of the simulation tool, but it seems to be an interesting topic for further investigations, although challenging from an implementation point of view.

Regarding all simulation chapters, one aspect of this work is the lack of mixed traffic simulation campaigns. Carrying out a similar exercise for the more realistic case of mixed traffic is suggested as a natural extension of this project.

One of the strongest conclusions presented in Chapters F– H is that currently the operators take full advantage of the capacity gains provided by the features analyzed therein. If it is desired to share part of this extra capacity, the applied scheduling policy should be modified. Such modifications to RRM algorithms are an strategic field of research, because it gives operators much greater freedom to distribute the extra capacity according to their needs.

Another potential follow-up of the work conducted in Chapter G is evaluate the impact of the imperfections in the space-time model of the radio channel cited in Section G.2.3, specifically the one related to code splitting. A thorough test of the validity of the theoretical analysis of the optimal number of beams, which is

fully described in Appendix J is another candidate.

Last but not least, the concept presented in Chapter H deserves a lot more attention, specially the NRT case. For such study, it would be convenient to utilize specific AVI tables for terminals possessing 2Rake receivers.

Apêndice J

Optimizing the Number of Beams

A simple way to calculate the optimum number of beams in an SBS with a pilot signal per beam (S-CPICH) is presented here. The ideas discussed here are related to the tasks carried out in Chapter G, thus the same naming convention is employed here. The calculations consider the tradeoff between the interference generated by the extra pilot signals and the cross-over depths. This tradeoff is affected by the radio channel's azimuth dispersion, since it reduces the spatial filtering gain.

In a SBS, as opposed to an USB system, only a limited number of fixed beams is available. While in USB system, users are served by individual beams in their respective directions, thus always experiencing the maximum gain, assuming small errors in the estimation of direction of terminals. In a SBS due to the limited number of beams, users will experience reduced antenna gains if their direction differs from the actual fixed beam pointing direction. The worst case occurs halfway two consecutive beams, the so-called cross-over depth, which is show in Figure J.1. The higher the cross-over depths between beams, the higher the capacity degradation compared to a system with infinite pointing directions. It is, then desired to reduce this degradation as much as possible.

If it is desired to bring the beams closer, thus reducing the cross-over depths, more beams are going to be required to cover the same region. On the other hand, with a fixed grid of beams, the higher the number of beams, the more pilot power

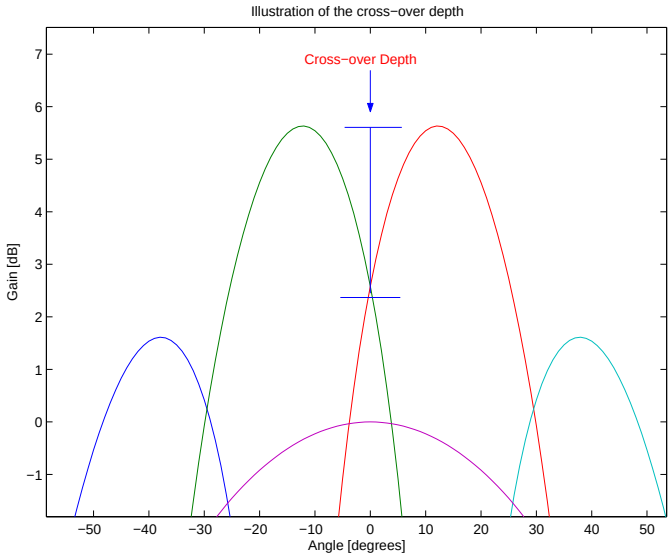

Figure J.1: Cross-over depth.

is transmitted into the air interface, which has a double fold negative impact on the capacity, because it generates interference and eats up from the total power pool, leaving less power available to be distributed among the system users. A tradeoff between the two aforementioned effects is to be found in order to calculate the number of beams that maximizes the sector capacity.

How can we do it? Let us consider a uniform linear antenna array of M elements. A fixed grid of N beams is synthesized and that the beam maxima ϕ_{dir} are equally spaced in the sine space, with azimuth directions given by [43]:

$$\phi_{\text{dir(i)}} = \arcsin(\lambda/N.\Delta x).i$$

for $i = \pm 1/2, \pm 3/2, \ldots \pm (N-1)/2$ for N even or $i = 0, \pm 1, \pm 2, \ldots \pm (N-1)/2$ for N odd, where Δx is the spacing between antenna elements. Without loss of generality, let us assume we do not pack the beams closer together, hence we can only reduce the cross-over depth by increasing the number of beams.

The UEs are always connected to the best beam. Thus, the power antenna gain at ϕ can therefore be written as

$$\text{Best Gain}(\phi) = \max\{W(\phi_{\text{dir(i)}}, \phi), \ldots, W(\phi_{\text{dir}((\text{N}-1)/2)}, \phi)\}$$

.

At times, Best Gain(ϕ) will equal the gain at the cross-over depth; however, this situation represents the worst case loss. From a network capacity point of view, it is more relevant to consider the average performance of SBS compared to USB, taken over the whole 120° sector which is given as

$$\psi = E\left\{\frac{\text{Best Gain}(\phi)}{W_{\text{USB}}(\phi)}\right\}, \tag{J.1}$$

where $W_{\text{USB}}(\phi)$ is the power antenna gain in the direction ϕ in the case of infinite pointing directions. Hence, (ψ) is a variable between 0 and 1 that approaches unity asymptotically as the number of beams increases, meaning we are nearing the performance of an USB system.

Now, let us take a look at the other side of the coin. Assuming a power based radio resource management strategy, which aims at keeping the effective transmitted power close to $P_{TX|\text{Target}}$, the impact of the pilot overhead, which is due to the transmission of a S-CPICH on each beam can then be defined as

$$\xi = \frac{P_{TX|\text{Target}} - P_{\text{P-CPICH}} - P_{\text{TOTAL(S-CPICH)}}}{P_{TX|\text{Target}} - P_{\text{P-CPICH}}}, \tag{J.2}$$

where $P_{\text{TOTAL(S-CPICH)}}$ has been defined in (G.5). Thus, ξ is a factor between 0 and 1, which equals unity when there is no S-CPICH pilot overhead and zero when there is no capacity left due to the S-CPICHs.

As in every optimization problem, a cost function must be defined, in this case, this role is played by Υ defined as

$$\Upsilon = \psi.\xi.\kappa\,. \tag{J.3}$$

The last term κ in the equation is dealt with now. In order to take the impact of the AS into account, the normalizing factor κ was introduced. It has been shown in Section G.2 that the gain in the pointing direction (ϕ_{dir}) decreases for larger AS values. When $W_{\text{USB}}(\phi)$ is calculated for $AS = 0°$, its maximum value ($\max\{W^{0°}_{\text{USB}}(\phi)\}$) is taken as a reference. Moreover, it was seen that the 3 dB width of the main lobe is broadened as the AS in the radio channel increases, thus the directive nature of the beam is gradually lost, hence the 3 dB beamwidth of a

single beam pointing at broadside [1] ($\Theta^{0^\circ}_{3\,dB}$) is taken a second reference. When the optimization is carried out for a different value (σ) of the AS, κ is defined as the product of the ratios

$$\kappa = \frac{\max\{W^{\sigma}_{\mathrm{USB}}(\phi)\}}{\max\{W^{0^\circ}_{\mathrm{USB}}(\phi)\}} . \frac{\Theta^{0^\circ}_{3\,dB}}{\Theta^{\sigma}_{3\,dB}} . \tag{J.4}$$

Therefore, κ is a factor between 1 and 0, which equals unity when there is no AS.

The maximization of Υ was carried out for a 120° sector assuming $M = [4, 6, 8]$ antennas, $P_{TX|\mathrm{Target}} = 10$ W and $P_{\mathrm{P-CPICH}} = [0.6, 1.1, 2]$ W. The AS assumes the following values $[0^\circ, 5^\circ, 10^\circ, 20^\circ]$, corresponding to a macro cellular urban propagation environment.

Figure J.2 shows ξ (loss curves) and the product $\psi \,.\, \kappa$ (% of maximum gain) for different AS and P-CPICH power values and $M = 4$.

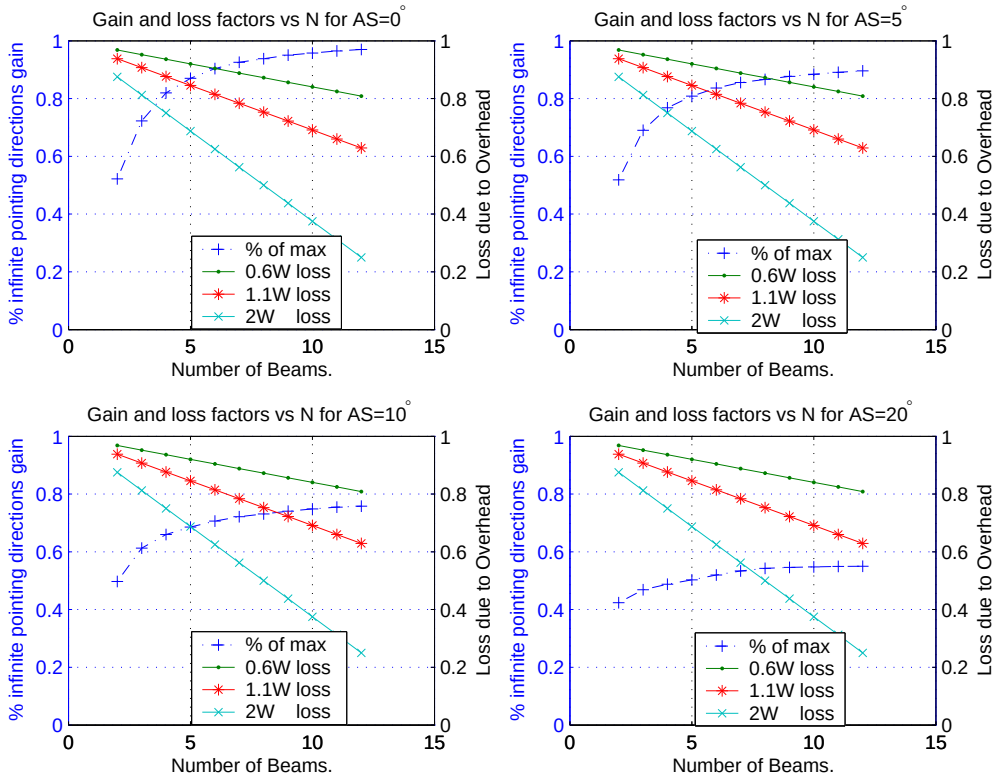

Figure J.2: The values of ξ and $\psi \,.\, \kappa$ for $M = 4$ and multiple AS values.

[1] This is an simplification for the 3 dB beamwidth changes as a function of ϕ_{dir}.

Figures J.3, J.4 and J.5 depict Υ versus the number of beams for different AS and P-CPICH power values for $M = 4$, $M = 6$ and $M = 8$ elements respectively.

All plots are normalized with respect to the maximum achievable gain for that specific number of elements, hence a given value of Υ in Figure J.3 represents a smaller absolute gain than that of the same value in Figure J.5. This can be explained by the fact that 8 elements generate beam patterns with approximately half the beamwidth of those generated by 4 elements, thus providing two times more interference reduction, which, in turn corresponds to a capacity gain. A value of $\Upsilon = 1$ for $M = 8$ would be equivalent to $\Upsilon = 2$ for $M = 4$.

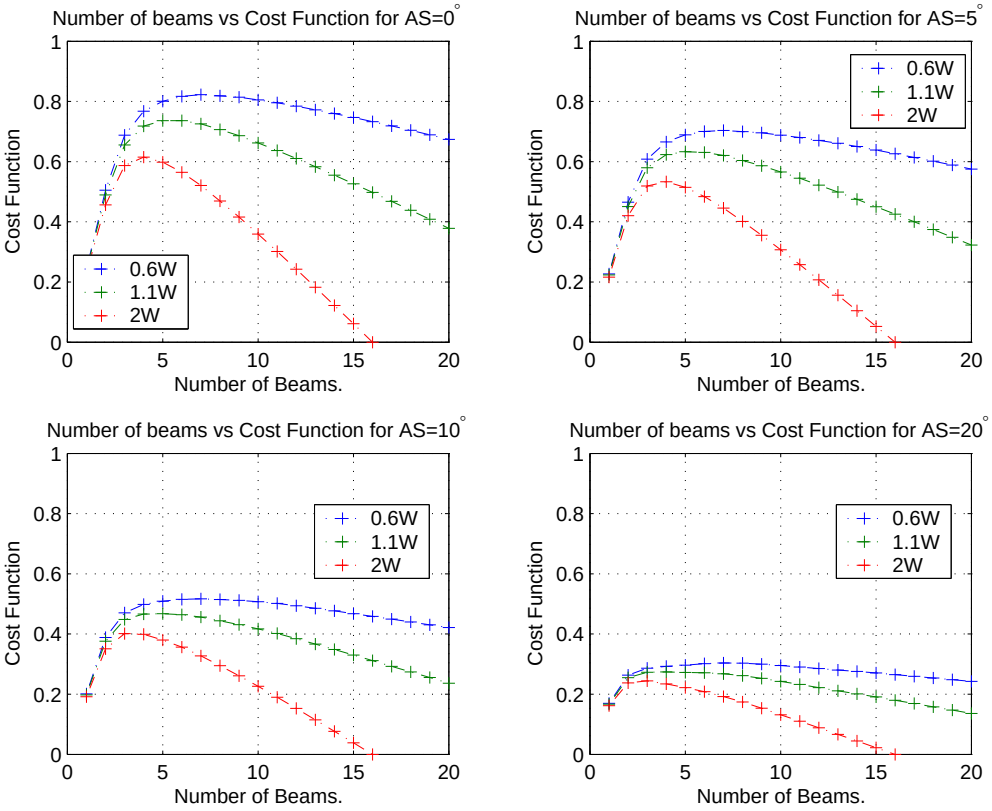

Figure J.3: Υ versus the number of beams for $M = 4$.

The most intuitive conclusion is that, the higher M is, the higher the optimal number of beams (ONoB) becomes. The abscissa for which Υ is maximum indicates the ONoB . Moreover, a higher AS involves a lower ONoB, since the effective radiation patterns are smoothed and the cross over depth between beams becomes less dominant. Furthermore, for a larger number of antenna elements, the expected

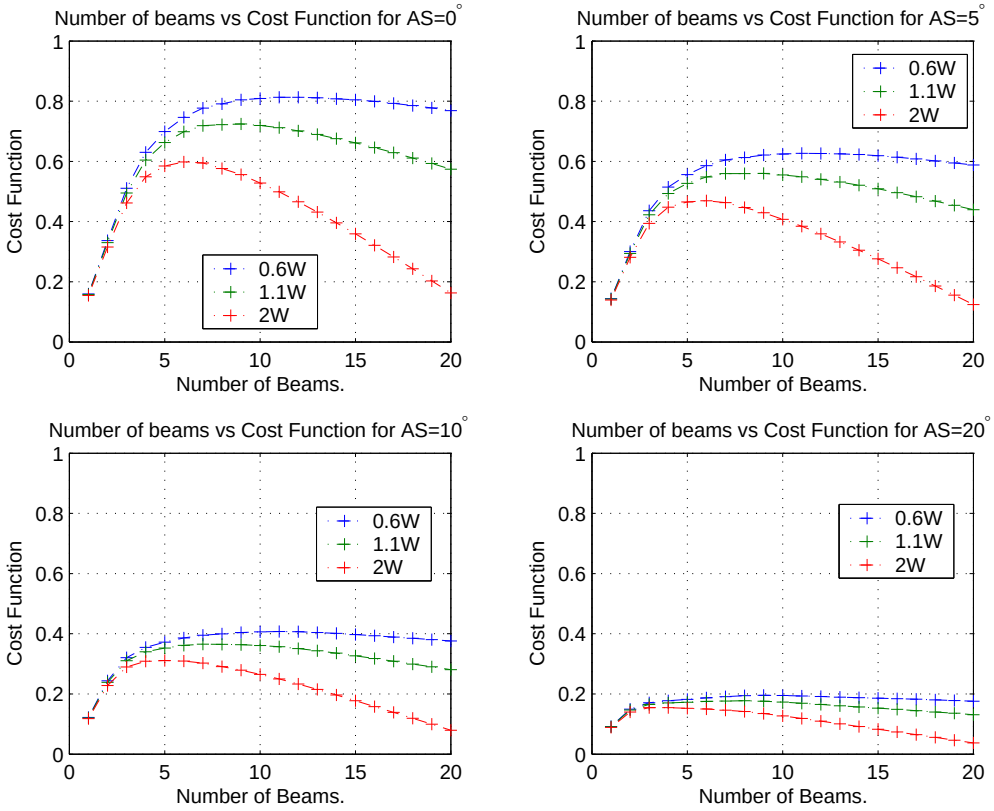

Figure J.4: Υ versus the number of beams for $M = 6$.

gain becomes much more sensitive to the AS, because the directional beams become narrower and the degradation caused by large AS values becomes more severe.

Finally, readers should notice the impact of the amount of power dedicated to the pilot channel. The beamforming gain for a fixed AS and M becomes smaller as more power is utilized by the pilot channels. This is seen in all figures, the maximum gain achieved by the 2 W configuration is always less than that obtained by the other settings. The reason is the double fold negative impact discussed earlier.This impact is shown by ξ, which becomes steeper the more power is allocated to the primary pilot, thus worsening the overhead. It can be seen from the 0.6 W curves, that there is not much difference in the gain if the chosen number of beams N varies from $N = M + 2$ to $N = 2M$ beams. The 2 W curves have their peaks much more well defined even for high AS values.

Table J.1 summarizes the results for an AS equal to five degrees, given that

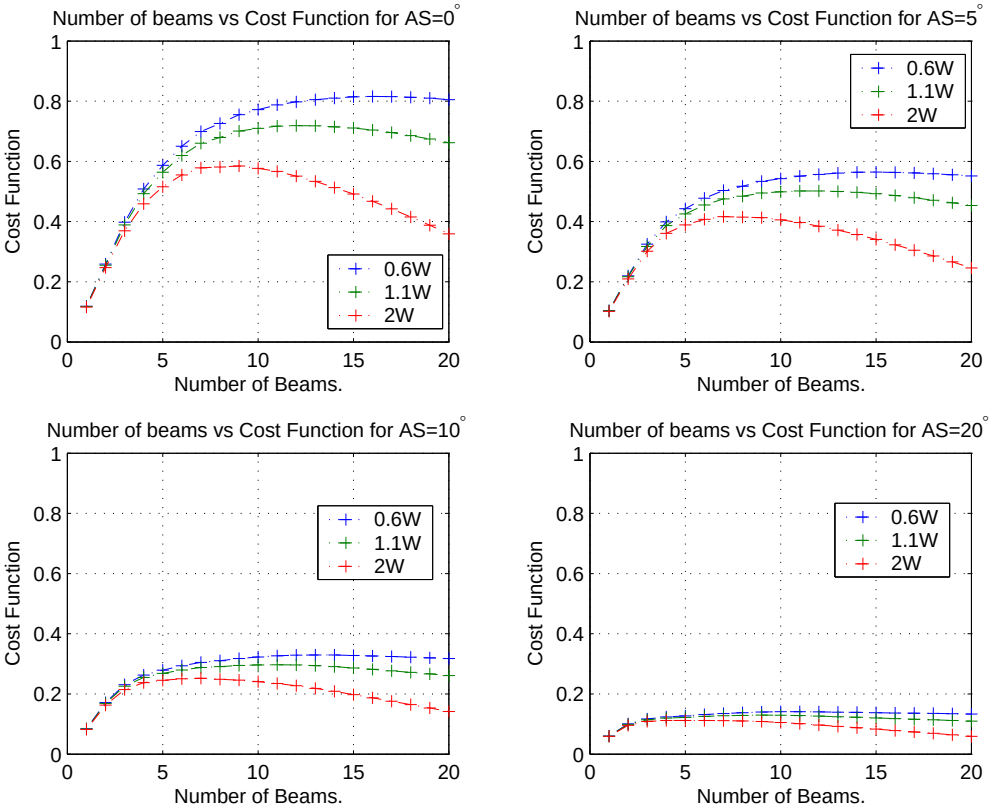

Figure J.5: Υ versus the number of beams for $M = 8$.

is the value utilized throughout this work.

—	**Pilot Power (P-CPICH)**		
Elements	0.6 W	1.1 W	2 W
$M = 4$	6-9	4-7	4
$M = 6$	8-13	7-10	6
$M = 8$	14-18	9-14	8

Table J.1: Optimal number of beams for different configurations.

Interestingly, results in the open literature match quite well the numbers given by the Υ function. The results presented herein can be seen as a generalization of those presented in [46, 29, 3, 9]. Some test simulations for N equal to 4, 5 and 6 beams have also been carried out for this project and the results are presented in the body of this thesis. Please refer to Chapter G.

Apêndice K

Abbreviations

2

2G 2nd Generation

3

3G 3rd Generation

3GPP 3rd Generation Partnership Project

A

AA Antenna Array

AC Admission Control

AoA Angle of Arrival

AoD Angle of Departure

AS Azimuth Spread

AVI Actual Value Interface

AWGN Additive White Gaussian Noise

B

BER Bit-Error Rate

BF Beamforming

BLEP Block Error Probability

BLER Block Error Rate

BPSK Binary Phase Shift Keying

BS Base Station

C

CBF Conventional Beamforming

CCI Co-Channel Interference

CDMA Code Division Multiple Access

CIR or C/I Carrier to Interference Ratio

CPICH Common Pilot Channel

CS Circuit Switched

D

DCH Dedicated Channel

DL Downlink

DoA Direction of Arrival

DoD Direction of Departure

DPCCH Dedicated Physical Common Control Channel

DPCH Dedicated Physical Channel

DPDCH Dedicated Physical Data Channel

DSCH Downlink Shared Channel

DSP Digital Signal Processor

DTX Discontinuous Transmission

E

ETSI European Telecommunication and Standards Institute

F

FACH Forward Access Channel

FDD Frequency Division Duplex

G

GGSN Gateway GPRS Support Node

GMSC Gateway Mobile Switching Center

GSM Global System for Mobile Communications

H

HC Handover Control

HLR Home Location Register

HO Handover

HOS Higher Order Sectorization

HSDPA High Speed Data Packet Access

I

ILPC Inner Loop Power Control

IP Internet Protocol

ITU International Telecommunications Union

ISI Intersymbol Interference

L

LC Load Control

M

MAC Medium Access Control

MAI Multiple-Access Interference

MRC Maximum Ratio Combining

MSC Mobile Switching Center

N

NRT Non-Real Time

O

OC Optimum Combining

OLPC Outer Loop Power Control

OSVF Orthogonal Variable Spreading Factor

P

PC Power Control

P-CPICH Primary Common Pilot Channel

PDF Probability Density Function

PDP Power Delay Profile

PN Pseudo Noise

PS Packet Scheduler

Q

QoS Quality of Service

QPSK Quaternary Phase Shift Keying

R

RAB Radio Access Bearer

RACH Random Access Channel

RF Radio Frequency

RLC Radio Link Control

RM Resource Manager

RNC Radio Network Controller

RRM Radio Resource Management

RT Real Time

Rx Receiver

S

SA Smart Antennas

SBS Switched Beam Systems

S-CPICH Secondary Common Pilot Channel

SF Spreading Factor

SGSN Serving GPRS Support Node

SHO Soft handover

SINR Signal to Interference plus Noise Ratio

SIR Signal to Interference Ratio

SNR Signal to Noise Ratio

STTD Space Time Transmit Diversity

T

TCP Transmission Control Protocol

TTI Transmission Time Interval

Tx Transmitter

U

UE User Equipment

UL Uplink

ULA Uniform Linear Array

UMTS Universal Mobile Telecommunication System

USB User Specific Beam

USIM UMTS Subscriber Identity Module

UTRA Universal Terrestrial Radio Access (3GPP)

UTRAN UMTS Terrestrial Radio Access Network

V

VLR Visitor Location Register

W

WCDMA Wideband Code Division Multiple Access

WLAN Wireless Local Area Network

Referências Bibliográficas

[1] VERDÚ, S., "Wireless Bandwidth in the Making", *IEEE Communications Magazine*, pp. 53–58, jul 2000.

[2] VERDÚ, S., "Minumum Probability of Error for asyncronous gaussian multiple-access channels", *IEEE Transactions on Information Theory*, v. 32, pp. 85–96, jan 1986.

[3] MORENO, J. R., *System Level Performance Analysis of Advanced Antenna Concepts in WCDMA*. Ph.D. dissertation, Aalborg University, Department of Communication Technology, 2003.

[4] AL., T. S. R. E., "Wireless Communications: Past Events and a Future Perspective", *IEEE Communications Magazine*, , 2002.

[5] 3^{rd} GENERATION PARTNERSHIP PROJECT. http://www.3gpp.org.

[6] HOLMA, H., TOSKALA, A., *The WCDMA for UMTS Radio Access for Third Generation Mobile Communications*. 3 ed. England, John Wiley & Sons, Ltd, 2004.

[7] 3^{rd} GENERATION PARTNERSHIP PROJECT, *Radio Resource Management Strategies*. http://www.3gpp.org, Mar 2002. TR.25.922, Version 5.0.0.

[8] MOULY, M., PAUTET, M.-B., *The GSM System for Mobile Communications*. France, Cell & Sys, 1992.

[9] KLINGENBRUNN, T., *Downlink Capacity Enhancement of UTRA FDD Networks — Using Fast Power Control, Soft Handover Transmit Diversity*

and Adaptive Antennas. Ph.D. dissertation, Aalborg University, Center for Person Kommunikation, 2001.

[10] RAMIRO-MORENO, J., PEDERSEN, K. I., MOGENSEN, P. E., "Radio Resource Management for WCDMA Networks Supporting Dual Antenna Terminals", *IEEE Personal Communications*, pp. 36–48, feb 1998.

[11] Peréz-ROMERO, J., SALLENT, O., Agustí, R., *et al.*, "A Downlink Admission Control Algorithm for UTRA FDD", pp. 18–22, 2002.

[12] PEDERSEN, K. I., MOGENSEN, P. E., "Directional Power Based Admission Control for WCDMA Systems using Beamforming Antenna Array Systems". In: *IEEE Trans. on Vehicular Technology*, v. 51, pp. 1294–1303, Nov 2002.

[13] HAYKIN, S., *Communications Systems*. 4 ed. John Wiley & Sons, Inc, 2001.

[14] JR, J. C. L., RAPPAPORT, T. S., *Smart Antennas for Wireless Communications*, Prentice Hall Communications Engineering and Emerging Technologies Series. Upper Saddle River, NJ 07458, Prentice Hall, PTR, 1999.

[15] ZAHID, K. A., *Space-Time Processing for the Wideband CDMA System*. M.Sc. dissertation, Virginia Polytechnic Institute and State University, 2001.

[16] WINTERS, J. H., "Optimum Combining in Digital Mobile Radio with Cochannel Interference", *IEEE Transactions on Communicatio Theory*, , 1984.

[17] MOGENSEN, P. E., PEDERSEN, K. I., LETH-ESPENSEN, P., *et al.*, "Preliminary Measurement Results from an Adaptive Antenna Array Testbed for GSM/UMTS", *IEEE Vehicular Technology Conference (VTC)*, , 1997.

[18] HÄMÄLÄINEN, S., SLANINA, P., HARTMAN, M., *et al.*, "A Novel Interface Between Link and System Level Simulations", *Proceedings of ACTS Summit 1997*, pp. 599–604, Oct 1997.

[19] 231, C. A., *Digital Mobile Radio towards Future Generation Systems*, n. EUR 18957. Office for official publications of the european communities.

[20] GUDMUNDSON, M., "Correlation Model for Shadow Fading in Mobile Radio Systems", *Electronics Letters*, pp. 2145–2146, 1991.

[21] M.1225, I. R., "Guidelines for valuation of radio transmission technologies for IMT-2000", *ITU-R*, p. 60, 1997.

[22] 3^{rd} GENERATION PARTNERSHIP PROJECT, *Feasibility Study for Enhanced Uplink for UTRA FDD*. http://www.3gpp.org, March 2004. TR 25.896 V6.0.0.

[23] RAPPAPORT, T. S., *Wireless Communications Principles & Practice*, Prentice Hall Communications Engineering and Emerging Technologies Series. Upper Saddle River, NJ 07458, Prentice Hall, PTR, 1999.

[24] PEDERSEN, K. I., MOGENSEN, P. E., FLEURY, B. H., "Spatial channel characteristics in outdoor environments and their impact on BS antenna system performance", *48th IEEE Vehicular Technology Conference*, v. 2, n. 8, pp. 719–723, May 1998.

[25] PAULRAJ, A. J., D.GESBERT, PAPADIAS, C., *Smart Antennas for Mobile Communications*, v. Encyclopedia for Electrical Enginnering. John Wiley Publishing Co, 2000.

[26] AL, C. B. D. E., "Smart Antennas in Wireless Communications: Base-Station Diversity and Handset Beamforming", *IEEE Antennas and Propagation Magazine*, v. 42, n. 5, pp. 142–151, Oct 2000.

[27] VENTOLA, M., TUOMAALA, E., RANTA, P. A., "Performance of Dual Antenna Diversity Reception in WCDMA Terminals", , 2003.

[28] PEDERSEN, K. I., MOGENSEN, P. E., FLEURY, B. H., "A Stochastic Model of the Temporal and Azimuthal Dispersion Seen at the Base Station in Outdoor Propagation Environments", *IEEE Transactions On Vehicular Technology*, v. 49, n. 2, pp. 719–723, March 2000.

[29] BAUMGARTNER, T., *Smart Antennas Strategies for the UMTS FDD Downlink*. Ph.D. dissertation, Teschnischen Universität Wien, Fakultät für Elektrotechnik und Informationstechnik, 2003.

[30] PALOMAR, D. P., *A Unified Famework for Communications through MIMO Channels*. Ph.D. dissertation, Universisat Politècnica de Catulanya, 2003.

[31] PROAKIS, J. G., *Digital Communications*, McGraw-Hill Series in Electrical and Computer Engineering. 4 ed. McGraw-Hill, 2001.

[32] 3^{rd} GENERATION PARTNERSHIP PROJECT, *Requirements for support of radio resource managment (FDD)*. http://www.3gpp.org, March 2003. TS 25.133 V3.13.0, (Release 1999).

[33] PAULRAJ, A. J., NG, B. C., "Space-Time Modems for Wireless Personal Communications", *IEEE Personal Communications*, pp. 36–48, feb 1998.

[34] RAPPAPORT, T. S., *Wireless Communications Principles & Practice*. In: *Prentice Hall Communications Engineering and Emerging Technologies Series* [23], p. 104, 1999.

[35] PAPOULIS, A., *Probability, Random Variables, and Stochastic Processes.*, Electrical Enginnering. 2^a ed. McGRAW-HILL, 1984.

[36] PAULRAJ, A. J., PAPADIAS, C., "Space-Time Modems for Wireless Personal Communications", *IEEE Signal Processing Magazine*, pp. 49–83, Nov 1997.

[37] THE INTERNATIONAL ENGINEERING CONSORTIUM, *Smart Antenna Systems*. http://www.iec.org.

[38] CHRYSSOMALLIS, M., "Smart Antennas", *IEEE Antennas and Propagation Magazine*, v. 42, n. 3, pp. 129–136, Jun 2000.

[39] COOPER, M., GOLDBURG, M., "Intelligent Antennas: Spatial Division Multiple Access", *Annual Review of Communications*, pp. 999–1002, 1996.

[40] 3^{rd} GENERATION PARTNERSHIP PROJECT, *Physical Channels and mapping of transport channels onto physical channels (FDD)*. http://www.3gpp.org, Sep 2002. TS 25.211 V4.6.0.

[41] ALAMOUTI, S., "A simple transmit diversity technique for wireless communications", *IEEE Journal on Selected Areas on Communications*, v. 16, n. 8, Oct 1998.

[42] ALEXIOU, A., "Comparison of Multiple Antenna Techniques for UMTS Downlink Capacity Enhancement", *IEEE Trans. on Vehicular Technology*, , 2001.

[43] MAILLOUX, R. J., *Phased Array Antenna Handbook*. Artech House,Inc, 1994.

[44] WINTERS, J. H., "Smart Antennas for Wireless Systems", *IEEE Personal Communications*, pp. 23–27, feb 1998.

[45] ALLEN, B., BEACH, M., "On the Analysis of Switched-Beam Antennas for the W-CDMA Downlink", *IEEE Transactions on Vehicular Technology*, v. 53, n. 3, pp. 569–578.

[46] PEDERSEN, K. I., MOGENSEN, P. E., RAMIRO-MORENO, J., "Application and Performance of Downlink Beamforming Techniques in UMTS", *IEEE Communications Magazine*, pp. 134–143, oct 2003.

[47] 3^{rd} GENERATION PARTNERSHIP PROJECT, *Physical Layer Measurements*. http://www.3gpp.org. TS 25.215 V.5.4.

[48] LI, H.-J., LIU, T.-Y., "Comparison of Beamforming Techniques for W-CDMA Communication Systems", *IEEE Transactions on Vehicular Technology*, v. 52, n. 4, Jul 2003.

[49] DINIZ, P. S. R., *Adaptive Filtering: Algorithms and Practical Implementations*. Kluwer Academics Publisher, 2002.

[50] HÄRING, L., CHALISE, B. K., CZYLWIK, A., "Dynamic System Level Simulations of Downlink Beamforming for UMTS FDD", *Globecom 2003*, pp. 492–496, 2003.

[51] HATA, M., "Empirical formulae for propagation losses in land mobile radio services", *IEEE Transactions on Vehicular Technology*, v. 29, pp. 317–325, 1980.

[52] PARSONS, J. D., *The Mobile Radio Propagation Channel*. Pentech Press.

[53] CLARK, R., *A Statistical Theory of Mobile Reception*, v. 49. BSJT.

[54] JAKES, W., *Microwave Mobile Communications*. John Wiley & Sons, 1974.

[55] 3^{rd} GENERATION PARTNERSHIP PROJECT, *Selection procedures for the choice of radio transmission technologies for the UMTS*. http://www.3gpp.org, April 1998. TR 101.112 V3.2.0.

[56] PEDERSEN, K. I., *Overview of the macro cell propagation models in WALLU*. Nokia. Internal Document, 2003.

[57] STEVENS, W., *RFC 2001 - TCP Slow Start, Congestion Avoidance, Fast Retransmit, and Fast Recovery Algorithms*. Network Working Group, 1997.

[58] AMEIGEIRUS, P. J., LOPEZ, I., WIGARD, J., *et al.*, "Traffic Models for Packet Data Services in 3G Wireless Networks", *4th International Symposium on Wireless Personal Multimedia Communications (WPMC)*, , 2001.

[59] HEIKKILA, M. J., KOMULAINEN, P., J.LILLEBERG, "Interference suppression in CDMA downlink through adaptive channel equalization", *IEEE Vehicular Technology Conference,*, , Sep 1999.

[60] HOLMA, H., *A STUDY OF UMTS TERRESTRIAL RADIO ACCESS PERFORMANCE*. Ph.D. dissertation, Helsinki University of Technology, 2003.

[61] LAMPORT, L., *LaTeX: A Document Preparation System*. Addison-Wesley, 1986.

[62] JEROEN WIGARD, RAYMOND KWAN, I. S. P. A., *Traffic Models for Simulating NRT Data and Streaming*. Nokia. Internal Document, July 2001. Version 1.0.2.